NASA TECHNICAL NOTE

NASA TN D-4856

NASA TN D-4856

AERODYNAMIC CHARACTERISTICS OF TWIN-PROPELLER DEFLECTED-SLIPSTREAM STOL AIRPLANE MODEL WITH BOUNDARY-LAYER CONTROL ON INVERTED V-TAIL

by Richard J. Margason and Garl L. Gentry, Jr.

Langley Research Center
Langley Station, Hampton, Va.

NATIONAL AERONAUTICS AND SPACE ADMINISTRATION • WASHINGTON, D. C. • NOVEMBER 1968

NASA TN D-4856

AERODYNAMIC CHARACTERISTICS OF TWIN-PROPELLER DEFLECTED-SLIPSTREAM STOL AIRPLANE MODEL WITH BOUNDARY-LAYER CONTROL ON INVERTED V-TAIL

By Richard J. Margason and Garl L. Gentry, Jr.

Langley Research Center
Langley Station, Hampton, Va.

NATIONAL AERONAUTICS AND SPACE ADMINISTRATION

For sale by the Clearinghouse for Federal Scientific and Technical Information
Springfield, Virginia 22151 – CFSTI price $3.00

AERODYNAMIC CHARACTERISTICS OF TWIN-PROPELLER DEFLECTED-SLIPSTREAM STOL AIRPLANE MODEL WITH BOUNDARY-LAYER CONTROL ON INVERTED V-TAIL

By Richard J. Margason and Garl L. Gentry, Jr.
Langley Research Center

SUMMARY

This report presents stability and control data for a small deflected-slipstream short take-off and landing (STOL) airplane model which had an inverted V-tail equipped with boundary-layer control. The results of the static wind-tunnel investigation are promising and indicate that with further development, an inverted V-tail with boundary-layer control can be designed which would produce the longitudinal and directional trim required for an engine-out situation with no control input by the pilot. The data also show that the lateral control required for an engine-out situation can be obtained from a spoiler with the attendant lift loss.

The airplane can be trimmed with both engines operating with or without the boundary-layer control on the tail when the flaps are retracted (0° flap deflection); however, when the flaps are deflected (45° flap deflection), the boundary-layer control is needed to obtain trim up to a thrust coefficient of 2.10. The rudder is capable of producing large increments of yawing moment without changing directional stability and without causing cross coupling with rolling moment for both the flaps-retracted and the flaps-deflected configuration. Both flap configurations (flaps retracted and flaps deflected) with and without the boundary-layer control on the tail have positive dihedral effect and are directionally stable through most of the test ranges of angles of attack and sideslip.

INTRODUCTION

Recent experience in developing a small deflected-slipstream short take-off and landing (STOL) airplane has shown a need for additional stability and control data on this type of configuration. Several wind-tunnel investigations of a powered model of a twin-propeller deflected-slipstream STOL configuration were conducted to provide some of this information. The results of the longitudinal stability and control investigation are presented in reference 1, and the results of the lateral control investigation, in reference 2. A T-tail configuration was used in both investigations.

The present wind-tunnel investigation was undertaken to evaluate an inverted V-tail with boundary-layer control similar to the tail on the counterinsurgency (COIN) airplane proposed by the Martin Company to the Department of the Navy. This type of tail was designed in the late fifties by Hans Multhopp. (See ref. 3.)

The present investigation was conducted in the 17-foot (5.18-meter) test section of the Langley 300-MPH 7- by 10-foot tunnel and its purpose was primarily to study two items: (1) the effectiveness of the inverted V-tail with boundary-layer control on the elevator for improvement of longitudinal stability and control and (2) the effectiveness of the inverted V-tail with boundary-layer control for yaw control, especially with an engine failure.

The model in reference 1 was rebuilt by extending the two engine nacelles as booms to support an inverted V-tail. Boundary-layer control was installed on the tail to simulate an airplane whose engine exhaust is ducted through each of the booms and expelled under the movable surfaces of the inverted V-tail to make possible high tail lift coefficients. These coefficients are obtained by deflecting the elevators upward to produce a large down load at the tail. In the event of an engine failure, blowing would stop on the side with the engine out and blowing on the side with the engine operating would continue. A yawing moment at the tail would thereby be generated which would oppose the yawing moment due to loss of thrust from one engine.

The longitudinal and lateral-directional data are presented at several thrust coefficients with flap deflections which represent a cruise configuration (0^{o} flap deflection) and a take-off and landing configuration (45^{o} flap deflection). The effects of tail momentum coefficient, tail incidence, and elevator deflection on the longitudinal aerodynamic characteristics are presented. Also presented are the lateral-directional stability characteristics and the effects of tail momentum coefficient, rudder deflection, and loss of power from one engine on the lateral-directional data. A brief analysis was made to evaluate the effectiveness of the tail in providing directional control when power is lost from one engine.

SYMBOLS

The longitudinal data (lift, drag, and pitching-moment coefficients) in this report are referred to the stability axis. The lateral-directional data (rolling-moment, yawing-moment, and side-force coefficients) are referred to the body axis. The thrust coefficient is referred to the thrust axis, which is parallel to the longitudinal body axis. All the data are referred to a moment center located chordwise at the wing quarter-chord line and vertically 2.13 inches (5.41 cm) below the wing-chord plane. (See fig. 1.)

The units used for physical quantities defined in this paper are given in both the U.S. Customary Units and the International System of Units (SI). Factors relating these two

systems of units are presented in reference 4. The symbols used are defined as follows:

b wing span, 5.00 feet (1.52 meters)

C_D drag coefficient, $\frac{\text{Drag}}{qS}$

C_L lift coefficient, $\frac{\text{Lift}}{qS}$

C_l rolling-moment coefficient, $\frac{\text{Rolling moment}}{qSb}$

C_{l_β} effective dihedral parameter based on increment of C_l between $\beta = 0^o$ and -5^o, $\frac{\partial C_l}{\partial \beta}$

C_m pitching-moment coefficient referred to model moment center at wing quarter-chord line (c/4), $\frac{\text{Pitching moment}}{qSc}$

C_n yawing-moment coefficient, $\frac{\text{Yawing moment}}{qSb}$

C_{n_β} directional-stability parameter based on increment of C_n between $\beta = 0^o$ and -5^o, $\frac{\partial C_n}{\partial \beta}$

C_T propeller thrust coefficient based on free-stream velocity and wing area, $\frac{T}{qS}$

$C_{T,s}$ propeller thrust coefficient based on slipstream velocity and propeller-disk area, $\frac{T}{q_s N S_p}$

C_Y side-force coefficient, $\frac{\text{Side force}}{qS}$

C_{Y_β} side-force parameter based on increment of C_Y between $\beta = 0^o$ and -5^o, $\frac{\partial C_Y}{\partial \beta}$

C_μ tail momentum coefficient, $\frac{F}{qS_t}$

c	wing chord, 1.29 feet (0.39 meter)
c_t	tail chord, 1.00 foot (0.31 meter)
D	propeller diameter, 2.00 feet (0.61 meter)
F	jet momentum force on tail, pounds (newtons)
i_t	tail incidence, degrees
l_{be}	length of blowing slot on one side of tail, also length of elevator on one side of tail, 1.77 feet (0.54 meter)
l_t	tail length, distance between wing quarter-chord line and tail quarter-chord line, 3.08 feet (0.94 meter)
N	number of propellers
q	free-stream dynamic pressure, $\frac{\rho V^2}{2}$, pounds/foot^2 (newtons/meter^2)
q_s	slipstream dynamic pressure, $q + \frac{T}{NS_p}$, pounds/foot^2 (newtons/meter^2)
S	wing area, 6.46 feet^2 (0.60 meter^2)
S_p	propeller-disk area, $\frac{\pi D^2}{4}$, feet^2 (meters^2)
S_t	tail area, feet^2 (meters^2)
T	propeller thrust, pounds (newtons)
V	free-stream velocity, feet/second (meters/second)
x	distance measured along airfoil chord line from leading edge, feet (meters)
y_l	distance measured perpendicular from airfoil chord line to airfoil lower surface, feet (meters)

y_u distance measured perpendicular from airfoil chord line to airfoil upper surface, feet (meters)

α angle of attack, degrees

β angle of sideslip, degrees

δ deflection of movable surface, with subscript to denote surface deflected, degrees

ρ air density, slugs/foot^3 (kilograms/meter^3)

Subscripts:

e elevator

f flap

r rudder

s spoiler

v vane

MODEL AND APPARATUS

A three-view drawing and photographs of the model are presented in figures 1 and 2, respectively. The wing had an unswept NACA 4415 airfoil section, a 15.50-inch (39.37-cm) chord, a span of 5 feet (1.52 meters), and an aspect ratio of 3.87. The wing contour was formed with faired wooden blocks fastened to a metal spar which supported the fuselage strongback, the two engine nacelles, the high-lift flap system, and the twin booms which in turn supported the inverted V-tail. The fuselage strongback served as a mount for a strain-gage balance which was sting supported.

The empennage consisted of two inverted NACA 4415 airfoils forming an inverted V mounted on the twin booms. There was an internal plenum chamber in the trailing edge with a row of slot nozzles that emitted a sheet of air under the control surfaces. Details of the tail profile, the plenum chamber, and the blowing slot are presented in figure 3. The plenum chamber was supplied by cold dry compressed air which was brought on board the model through a thin-wall metal tube bent to follow the sting support and form a limber

connection across the strain-gage balance. This air-supply line did not cause any zero shifts and did not change the sensitivity of the strain-gage balance. The mass flow of air was controlled by varying the pressure of the compressed air.

The double-slotted high-lift flap system consisted of a 20-percent-wing-chord vane with a St. Cyr 156 airfoil section and a 40-percent-wing-chord flap with a modified Rhode St. Genese 35 airfoil section over the forward 30 percent of its chord faired into the wing airfoil section over the rear 70 percent of its chord. The flap and vane ordinates, as well as the flap and vane positions when deflected, are given in figure 4.

The three-blade propellers were made of balsa covered with glass-fiber cloth and were driven by water-cooled variable-frequency electric motors operated in parallel from a variable-frequency power supply which kept the motor speeds matched within 20 rpm. The speed of rotation of each propeller was determined by a stroboscopic indicator which received the output frequency of small alternators connected to each motor shaft. For all the tests, the right propeller rotated in a clockwise direction and the left propeller rotated in a counterclockwise direction when viewed from the rear of the model. The speed of rotation was maintained at 6000 rpm during the tests. The thrust coefficient was varied primarily by changing the wind-tunnel speed.

The motors were mounted inside aluminum-alloy nacelles by means of strain-gage beams so that the propeller thrust could be measured. The total normal force, longitudinal force, pitching moment, rolling moment, yawing moment, and side force were measured by a strain-gage balance mounted to the fuselage at the wing quarter-chord line. Unless otherwise noted, all moment data are taken about the moment reference center shown below the wing quarter-chord line in figure 1.

TEST AND CORRECTIONS

The investigation was made in the 17-foot (5.18-meter) test section of the Langley 300-MPH 7- by 10-foot tunnel. For the powered tests, the free-stream dynamic pressure was varied from about 1.0 to 5.5 lb/ft^2 (48 to 263 N/m^2), depending on the desired thrust coefficient. The slipstream dynamic pressure was relatively constant at about 6.0 lb/ft^2 (287 N/m^2) for all thrust coefficients. For the propeller-off tests, a free-stream dynamic pressure of about 6.0 lb/ft^2 (287 N/m^2) was used. The Reynolds number (based on wing chord and slipstream velocity) over the wing for all conditions was approximately 0.58×10^6. Since errors due to blockage, slipstream contraction, and tunnel-wall effects have been found to be small for models of this size in the 17-foot test section (ref. 5), no corrections for these errors have been applied to the data.

The propeller thrust data have been presented as the conventional thrust coefficient, that is, thrust nondimensionalized by the product of free-stream dynamic pressure and

wing area ($C_T = T/qS$). In all cases, a thrust coefficient of zero was obtained by removing the propellers from the model. Since the motor rotation speed was held constant, the thrust varied as the angle of attack of the model increased; as a result, the thrust coefficients are not constant for a particular range of angle of attack. For convenience, the average values of the thrust coefficient near zero angle of attack for the data presented in this report (used as reference values throughout the report) are listed in the following table:

δ_f, deg	$C_{T,s}$	C_T	C_μ
0	0	0	0
	.13	.14	.02
	.31	.43	.05
45	0.31	0.43	0.05
	.46	.83	.10
	.69	2.10	.21
	.84	5.10	.40

It is often desirable to use the propeller thrust coefficient based on slipstream velocity and propeller-disk area. Figure 5(a) is a plot of the relation between these two thrust coefficients for the model tested.

Also shown in the table are the values of the tail momentum coefficient C_μ used with each thrust coefficient. These values represent the basic C_μ range. The schedule of the thrust coefficients and the corresponding tail momentum coefficients used in this investigation is presented in figure 5(b). This schedule is based on the engine-exhaust mass flow which could be obtained from a Pratt and Whitney T-74 turboprop engine operating at sea level at a velocity of 50 knots (93 km/hr). The tail momentum coefficient for the model was determined from the measured static gross thrust of each internal plenum chamber nondimensionalized by the product of free-stream dynamic pressure and tail area. This area was measured normal to the tail surface, the span being equal to the length of both plenum chambers, 3.54 feet (1.08 meters), and the chord being equal to 1.00 foot (0.31 meter).

RESULTS AND DISCUSSION

The results of a wind-tunnel investigation of a model of a twin-propeller deflected-slipstream STOL airplane are presented in the following figures:

Longitudinal Data

Effect of tail boundary-layer control.- One of the primary reasons for incorporating blowing boundary-layer control under the elevator was to increase the down load capability of the tail by increasing its maximum lift coefficient so that sufficient longitudinal control would be available to trim the diving moments produced by the flaps. The longitudinal aerodynamic characteristics showing the effect of tail boundary-layer control are presented in figures 6 to 12.

In figure 6, the longitudinal characteristics as a function of tail momentum coefficient are presented for several elevator deflections on the flaps-retracted configuration at

a thrust coefficient of zero and an angle of attack of 0^{o}. For a given elevator deflection, increasing the tail momentum coefficient results in an increased down load at the tail, which in turn produces an increment of nose-up pitching-moment coefficient and reduces the lift coefficient. For a given tail momentum coefficient, the down load is increased by negative deflections of the elevator, as would be expected. However, at higher tail momentum coefficients, there is an increase in elevator control effectiveness. (The increment of pitching moment due to a change in elevator deflection is increased.) In addition, the boundary-layer control makes the elevator effective to much higher deflections. For a given value of tail momentum coefficient, the net drag depends on elevator deflection. At low elevator deflections, there is a reduction in the net drag on the model because of the jet thrust at the tail; but at higher elevator deflections, the net drag increases because of the drag due to the increased lift on the tail. These same trends can be seen in the results presented in figure 7, which shows the longitudinal characteristics as a function of tail momentum coefficient for several elevator deflections on the flaps-deflected configuration at a thrust coefficient of 2.10 and an angle of attack of 0^{o}.

The effect of the variation of tail momentum coefficient on the aerodynamic characteristics of the flaps-deflected configuration at a thrust coefficient of 2.10 through a range of angle of attack is presented in figure 8. These data show that the effects (decreased lift and increased nose-up pitching moment with increase in C_{μ}) found at an angle of attack of 0^{o} hold throughout the entire angle-of-attack range of the tests.

The data in figures 9 to 12 present the aerodynamic characteristics for the model configuration with the flaps deflected through the basic schedule of thrust and tail momentum coefficients. The nominal values of these coefficients are presented in the section on tests and corrections and plotted in figure 5(b), which represents the basic C_{T}, C_{μ} schedule for the data in this report. The variation in thrust coefficient from one run to another (for example, fig. 9(c)) is caused by fluctuations in test conditions, such as thrust and free-stream dynamic pressure. In addition to the data for the basic C_{μ} range, data for zero C_{μ} and for the configuration with the tail off are also presented in these figures. These data illustrate the nose-up pitching-moment increment produced by the tail without boundary-layer control and the increased increment produced by the tail with boundary-layer control.

Effect of tail incidence ($\delta_{e} = 0^{o}$).- The effect of tail incidence on the longitudinal aerodynamic characteristics of the flaps-retracted configuration ($\delta_{f} = 0^{o}$) at several thrust coefficients is presented in figures 13 to 15 for zero tail momentum coefficient and in figures 16 and 17 for the basic range of tail momentum coefficient. These data (part (b) of figs. 13 to 17) show that the model is stable and can be trimmed by utilizing tail incidence through nearly the full range of lift coefficient for the values of thrust coefficient presented. These data also show at zero elevator deflection that the boundary-layer

control has little effect on the longitudinal aerodynamic characteristics of the flaps-retracted configuration over the range of tail momentum coefficient used. (Compare figs. 14 and 15 with figs. 16 and 17, respectively.)

The effect of tail incidence on the longitudinal aerodynamic characteristics of the flaps-deflected configuration ($\delta_f = 45^o$) at several thrust coefficients is presented in figures 18 to 22 for zero tail momentum coefficient and in figures 23 to 25 for the basic range of tail momentum coefficient. The data for the flaps-deflected configuration without boundary-layer control (figs. 18 to 22) show that trim can be obtained to at least 0.9 of the maximum lift coefficient at each thrust coefficient with the tail incidences presented. These data also show that the model is stable up to a thrust coefficient of 0.83 (figs. 18 to 20), that the model is neutral at a thrust coefficient of 2.10 (fig. 21), and that the model is unstable at a thrust coefficient of 5.10 (fig. 22). The data for the flaps-deflected configuration with boundary-layer control (figs. 23 to 25) show that trim can be obtained up to the maximum lift coefficient at each thrust coefficient with the tail incidences of the tests. These data also show that the stability is essentially unchanged by boundary-layer control on the tail. However, at a thrust coefficient of 2.10, the tail with boundary-layer control (fig. 25(b)) produces much larger nose-up increments of pitching moment than the tail without boundary-layer control (fig. 21(b)). As a result, a trimmed stable configuration with boundary-layer control on the tail can be obtained at all thrust coefficients presented by shifting the moment center forward.

Effect of elevator deflection.- The effect of elevator deflection on the longitudinal aerodynamic characteristics is presented for the flaps-retracted configuration ($\delta_f = 0^o$, basic C_μ range, $i_t = 0^o$) in figures 26 to 28 and for the flaps-deflected configuration ($\delta_f = 45^o$, basic C_μ range) in figures 29 to 32 ($i_t = 0^o$) and in figures 33 to 36 ($i_t = 10^o$). The data for the flaps-retracted configuration ($\delta_f = 0^o$, part (b) of figs. 26 to 28) show that with elevator deflections between 0^o and 10^o, the model can be trimmed up to lift coefficients as high as 1.80 with high stability levels ($\partial C_m/\partial C_L \leq -0.15$). For the flaps-deflected configuration ($\delta_f = 45^o$), the 0^o tail incidence (part (b) of figs. 29 to 32) provides slightly higher levels of stability and provides trim to slightly higher lift coefficients than the 10^o tail incidence (part (b) of figs. 33 to 36). For thrust coefficients between 0 and 0.83, both tail incidences were capable of providing trim up to lift coefficients of approximately 4.0 with high stability levels ($\partial C_m/\partial C_L \leq -0.14$). At the highest thrust coefficient presented ($C_T = 2.10$) the 0^o tail incidence (fig. 32(b)) provided trim to a lift coefficient of at least 5.00 with a stability level of approximately $\partial C_m/\partial C_L = -0.10$, whereas the 10^o tail incidence (fig. 36(b)) provided trim to a lift coefficient of 4.80 with neutral stability. Trim throughout the angle-of-attack range of the tests can be obtained from elevator deflections which ranged between 0^o and 15^o for the 0^o tail incidence or which ranged between -15^o and approximately 5^o for the 10^o tail incidence. As shown in figures 29 to 32, the elevator can be deflected up to -50^o to provide for longitudinal control after trim has been achieved.

These data show that the inverted V-tail with boundary-layer control is capable of providing trim, stability, and control for the model up to a lift coefficient of at least 5.0.

Lateral-Directional Data

Lateral-directional stability.- The variations of effective dihedral parameter C_{l_β}, directional-stability parameter C_{n_β}, and side-force parameter C_{Y_β} are presented through an angle-of-attack range in figure 37 for the flaps-retracted configuration ($\delta_f = 0^o$) and in figure 38 for the flaps-deflected configuration ($\delta_f = 45^o$). These parameters were obtained by using increments of lateral and directional moments and side force measured at sideslip angles of 0^o and -5^o through a range of angle of attack. These parameters were then compared with slopes obtained from variable-sideslip runs at angles of attack of 0^o and 12^o. The slopes were measured between angles of sideslip of -5^o and 5^o. Since this check showed a lack of consistency in the side-force parameters for the flaps-deflected configuration at thrust coefficients of 0.83 and 2.10, the side-force parameter was omitted for both angle-of-attack runs and sideslip runs at these coefficients. This inconsistency was a result of the low level of side force and the low sensitivity of the strain-gage balance in side force. The quantities being measured were smaller than the range of measurement accuracy of the balance in side force.

The flaps-retracted configuration (fig. 37) is directionally stable with the tail on up to angles of attack of 20^o to 25^o and exhibits positive dihedral effect through the entire angle-of-attack range. The flaps-deflected configuration (fig. 38) has a positive dihedral effect throughout the range of angle of attack, and its directional stability is appreciably increased at angles of attack above 10^o for thrust coefficients equal to 0.83 and 2.10. This increase is apparently due to a favorable sidewash induced by the propellers in the region near the tail at these higher thrust conditions.

Effect of tail boundary-layer control.- The effect of tail boundary-layer control on the aerodynamic characteristics of the flaps-deflected configuration ($\delta_f = 45^o$) as a function of sideslip angle for several thrust coefficients at angles of attack equal to 0^o and 12^o is presented in figures 39 to 42. For all but the highest thrust coefficient of the tests ($C_T = 2.10$), the lateral stability and directional stability are essentially constant over the full test range of sideslip angle. At the highest thrust coefficient (fig. 42), these stabilities are constant only between sideslip angles of approximately -5^o and 5^o. The data for the highest thrust coefficient show an increase in directional stability at these small sideslip angles.

Effect of rudder deflection.- The effect of rudder deflection on the aerodynamic characteristics through a range of sideslip angle at an angle of attack of 0^o for several thrust coefficients is presented in figures 43 to 45 for the flaps-retracted configuration ($\delta_f = 0^o$, basic C_μ range, $i_t = 0^o$) and in figures 46 to 49 for the flaps-deflected configuration

($\delta_f = 45^o$, basic C_μ range, $i_t = 0^o$). Data are presented for 0^o rudder deflection (0^o deflection of control surfaces) and for 15^o rudder deflection (the right control surface deflected 15^o and the left control surface deflected -15^o). The data for both model configurations show that rudder deflection provided a large increment of yawing moment ($\Delta C_n/\Delta\delta_r$ between -0.006 and -0.010) without significantly changing the slope of the yawing-moment variation with sideslip angle. However, some nonlinear variation was found at sideslip angles outside the range from 5^o to -5^o with the flaps-deflected configuration at the highest thrust coefficient of the tests ($C_T = 2.10$). The data show little cross-coupling effect of yaw with roll due to rudder deflection. Lift and drag coefficients show little change as a result of rudder deflection. A small nose-up pitching-moment increment is caused by the rudder deflection. This change in pitching moment could be alleviated by reducing the negative deflection on the left side and by increasing the positive deflection on the right side.

Effect of loss of power from one engine ($\delta_f = 45^o$).- On a twin-engine airplane without cross-shafting or automatic control, the loss of power from one engine at STOL flying conditions – high thrust, low speed, and flaps deflected – causes large asymmetric moments and a loss in lift which can be serious enough to prevent a safe take-off or landing. If, for example, the right engine fails, there will be a loss of thrust and slipstream on the right side of the airplane. The loss of thrust will cause a positive yawing moment. The loss of slipstream will bring about a reduction in lift on the right wing, which in turn will cause a positive rolling moment and a reduction in the nose-down pitching moment generated by the right wing. The effect of loss of power from the right engine for the flaps-deflected configuration ($\delta_f = 45^o$, $i_t = 0^o$, $\delta_e = 0^o$) is seen in figures 50 to 52 by comparing data obtained when both engines were operating with data obtained when only the left engine was operating. These data show the expected incremental changes in lift and in the three moments. For example, with the tail off at a nominal thrust coefficient of 2.10 and an angle of attack of 0^o (fig. 52), the following increments were measured: lift coefficient (-1.00), pitching-moment coefficient (0.36), rolling-moment coefficient (0.18), and yawing-moment coefficient (0.14). To illustrate the effect of the power loss, the following example is given of an airplane similar to the model with the inverted V-tail at 0^o tail incidence. Assume it has a wing loading of 36 lbm/ft^2 (176 kg/m^2) and that it is flying at 20 percent above stall speed with a nominal thrust coefficient of 2.10. If one engine fails and the airplane maintains a constant angle of attack, the operating lift coefficient is reduced from 4.10 to 3.10, which represents a requirement of increase in speed from 51 knots (94 km/hr) to 58 knots (107 km/hr) to maintain altitude.

In order to keep the airplane under control with the right engine out, the moments must be trimmed. The lateral trim can be obtained in one of two ways; either restore lift on the right wing or reduce lift on the left wing. Since the original lift loss was a result

of the loss of slipstream on the right wing, a lateral control which could restore lift on that wing would require some additional power source, such as boundary-layer control or some other form of jet flap. The alternate method of obtaining lateral trim is to reduce the lift on the left wing. As indicated in reference 2, this reduction can most effectively be achieved with spoilers. Use of this device results in a loss of total lift and requires a further increase in speed to maintain altitude. Another method of reducing lift on the left wing is to reduce the thrust of the left engine. This method, however, would make the required speed increase much more difficult to achieve.

The data presented in figures 53 to 55 show primarily the lateral-directional trim and control provided by the rudder and spoiler control surfaces to oppose the moments caused by the loss of power from the right engine of the flaps-deflected configuration ($\delta_f = 45^o$, $i_t = 0^o$). Figures 54(d) and 56 show a spoiler deflection which trims the rolling moment. Deflection of the spoiler to achieve lateral trim for the engine-out condition at a nominal thrust coefficient of 2.10 results in an estimated loss of lift coefficient from 3.10 to 2.45. This loss results in a further requirement in the example stated earlier of an increase in speed from 58 knots (107 km/hr) to 66 knots (122 km/hr) to maintain altitude.

The summary plot (fig. 56) for pitching moment presents the longitudinal control ability of the inverted V-tail for the flaps-deflected configuration with the right engine out at angles of attack and sideslip of 0^o. As previously indicated, blowing boundary-layer control on the right half of the inverted V-tail is stopped when the right engine is out. The data show that the tail with zero control-surface deflection and partial span blowing provides enough pitching moment to more than trim the nose-down moment generated when the tail is off. This result indicates that a smaller tail could be used to provide longitudinal trim for this model.

The summary plot (fig. 56) for yawing moment shows that the tail with zero control-surface deflection and partial span blowing provides a small increment which reduces the asymmetric yawing moment but does not provide trim. This moment can be trimmed in two ways. A conventional horizontal- and vertical-tail assembly would use a rudder deflection. A rudder deflection can be used with the inverted V-tail. The data in figure 56 show that when the surfaces are deflected 15^o to serve as a rudder, trim is easily attained. However, if this inverted V-tail requires a rudder deflection to trim yawing moment, it provides little improvement over more conventional tail designs for directional control.

The second method of providing trim is unique to tail configurations which use boundary-layer control because trim can be obtained without a rudder deflection. The sketches of the tail panels show the force vectors which are produced by the tail.

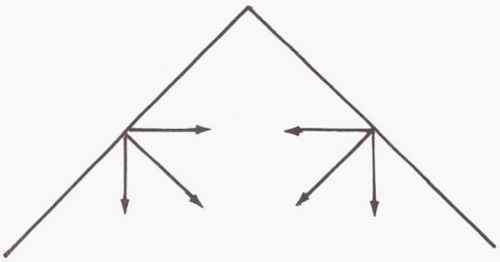

Sketch (a)

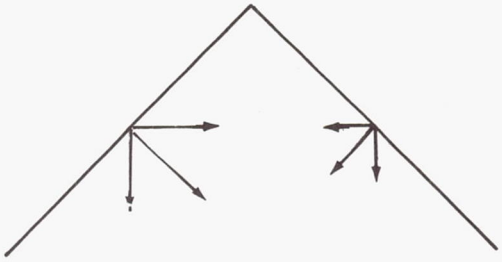

Sketch (b)

Sketch (a) represents the down load with blowing on both sides of the tail. The resultant force is downward and produces only the increment of nose-up pitching moment required for longitudinal trim. Sketch (b) illustrates failure of the right engine and the reduction in resultant force produced by the right side of the tail surface because blowing on the right side has stopped. The resultant of the side-force components gives a force to the right which causes a negative yawing-moment increment to trim the positive yawing moment generated by the loss of thrust. Combination of the down load components gives a reduced nose-up pitching-moment increment, as compared with sketch (a), to trim the reduced nose-down moment generated by the wing. The summary plot (fig. 56) for yawing moment shows that the tail with zero control-surface deflection and partial span blowing (diamond symbol) is not effective enough to provide trim.

This situation would be different if a larger yawing moment could be generated by partial span blowing on the tail (similar to that illustrated in sketch (b)). A larger yawing moment can be accomplished only if the change in down load at the tail caused by eliminating the boundary-layer control on one side is larger than that obtained in the data presented for this wind-tunnel test. This larger change can be achieved by increasing the tail momentum coefficient or by increasing the negative elevator deflection or by a combination of both.

The pitching-moment data from figure 7(b) were used to make an estimate of the effectiveness of each of these changes. The yawing moment contributed by the tail with one engine out was computed as one-half of the pitching-moment contribution for the entire tail with boundary-layer control minus one-half of the pitching-moment contribution for the entire tail without boundary-layer control. This relation is true since the tail dihedral angle is 45° and for the engine-out situation, one side of the inverted V-tail has boundary-layer control and the other side does not. This calculation neglects changes in carryover lift between the two tail surfaces, changes in sidewash velocity, and changes in slipstream wake over the tail; but it is felt that the calculation gives an indication of the effect of partial span blowing on yawing moment. The results of these calculations are presented as faired curves in figure 57 for the flaps-deflected ($\delta_f = 45^{\circ}$) configuration with a nominal thrust coefficient of 2.10 (right engine out) and for angles of attack and sideslip equal to zero. The tail-off data point presents the asymmetric yawing moment caused by the right

engine being out; this is the moment (C_n = 0.185) which must be trimmed by the tail at this thrust coefficient. Two tail-on data points at zero elevator deflection are also presented to show their correlation with the computed data. The tail-on data point for a tail momentum coefficient of zero shows that the tail alone provides an increment of -0.04 in yawing moment; a tail momentum coefficient of 0.21 increases this increment of yawing-moment coefficient to -0.06, compared with a computed value of -0.085. The computed values should be interpreted as being slightly optimistic. The curves show that there is a minimum tail momentum coefficient required before the yawing moment is trimmed by asymmetric blowing. They also show that increasing the tail momentum coefficient above the minimum required for trimmed yawing moment shifts the elevator deflection required from high negative angles toward zero or positive angles. These data (fig. 57) indicate that several combinations of elevator deflection and tail momentum coefficient exist which can provide directly a trimmed yawing moment with one engine out for this model configuration.

Since some combination of increased blowing and elevator deflection is required for a self-trim capability in yawing moment with an engine out, the pitching moment described previously would become even more nose-up. This result indicates the size of the tail could be reduced or that the moment center could be shifted aft to reduce the tail length in order to obtain a tail which will produce pitching-moment trim for all conditions and sufficient yawing moment due to asymmetric blowing to compensate for engine-out yawing moment. Although these data demonstrate the feasibility of the inverted V-tail with boundary-layer control, further development is required to achieve the desired longitudinal and directional trim for a particular configuration in an engine-out situation with no control inputs by the pilot.

CONCLUSIONS

The results of a wind-tunnel investigation of the static aerodynamic characteristics of a model of a twin-propeller deflected-slipstream STOL airplane configuration with an inverted V-tail equipped with boundary-layer control indicate the following conclusions:

1. The model with the flaps retracted (0^o flap deflection) was longitudinally stable and had satisfactory control characteristics with or without boundary-layer control on the inverted V-tail.

2. The model with the flaps deflected (45^o flap deflection) and without boundary-layer control on the tail could be trimmed with at least neutral longitudinal stability up to a thrust coefficient of 2.10. When boundary-layer control was used on the tail, larger control increments were obtained.

3. Both flap configurations (flaps retracted and flaps deflected) with and without boundary-layer control on the tail have positive dihedral effect and are directionally stable through most of the test ranges of angles of attack and sideslip.

4. The rudder is capable of producing large increments of yawing moment without changing directional stability and without causing cross coupling with rolling moment for both the flaps-retracted and the flaps-deflected configuration.

5. The lateral control required for an engine-out situation can be obtained from a spoiler with the attendant lift loss.

6. The results are promising and indicate that with further development, an inverted V-tail with boundary-layer control can be designed which would produce the longitudinal and directional trim required for an engine-out situation with no control input by the pilot.

Langley Research Center,
National Aeronautics and Space Administration,
Langley Station, Hampton, Va., July 18, 1968,
721-01-00-18-23.

REFERENCES

1. Margason, Richard J.; Hammond, Alexander D.; and Gentry, Garl L.: Longitudinal Stability and Control Characteristics of a Powered Model of a Twin-Propeller Deflected-Slipstream STOL Airplane Configuration. NASA TN D-3438, 1966.

2. Margason, Richard J.; and Hammond, Alexander D.: Lateral Control Characteristics of a Powered Model of a Twin-Propeller Deflected Slipstream STOL Airplane Configuration. NASA TN D-1585, 1964.

3. Fink, Donald E.: Martin COIN Design Has Inverted V-Tail. Aviat. Week Space Technol., vol 80, no. 15, Apr. 13, 1964, pp. 82-88.

4. Mechtly, E. A.: The International System of Units – Physical Constants and Conversion Factors. NASA SP-7012, 1964.

5. Staff of Powered-Lift Aerodynamics Section, NASA Langley Res. Center: Wall Effects and Scale Effects in V/STOL Model Testing. AIAA Aerodynamic Testing Conference, Mar. 1964, pp. 8-16.

Geometry	
Wing:	
Airfoil section	NACA 4415
Chord, ft (m)	1.29 (393)
Span, ft (m)	5.00 (1.524)
Area, sq ft (sq m)	646 (.600)
Aspect ratio	3.87
Tail:	
Airfoil section (mounted inverted)	NACA 4415
Chord, ft (m)	1.00 (.305)
l_t / wing chord	2.39
Tail dimensions projected to horizontal plane:	
Span, ft (m)	2.77 (844)
Area, sq ft (sq m)	2.77 (257)
Aspect ratio	2.77
Tail dimensions projected to vertical plane:	
Span, ft (m)	1.39 (424)
Area, sq ft (sq m)	2.77 (.257
Tail dimensions normal to tail surface:	
Length of the blowing slot and of the elevator, l_{be}, ft (m)	1.77 (.540)
Area based on l_{be} and used for computing C_μ (for each tail panel), sq ft (sq m)	1.77 (.164)
Propellers:	
Diameter, ft (m)	2.00 (610)
Hub diameter, ft (m)	.33 (101)
Number of blades (each)	3

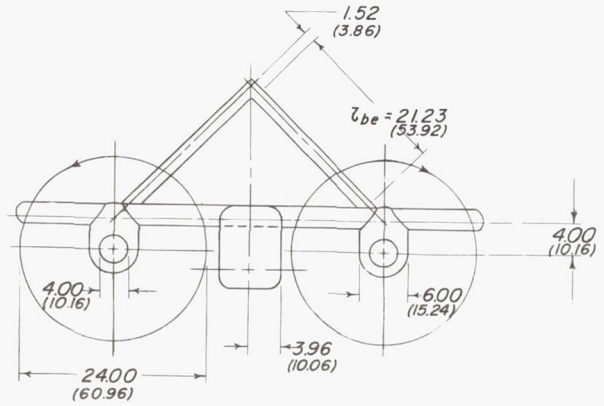

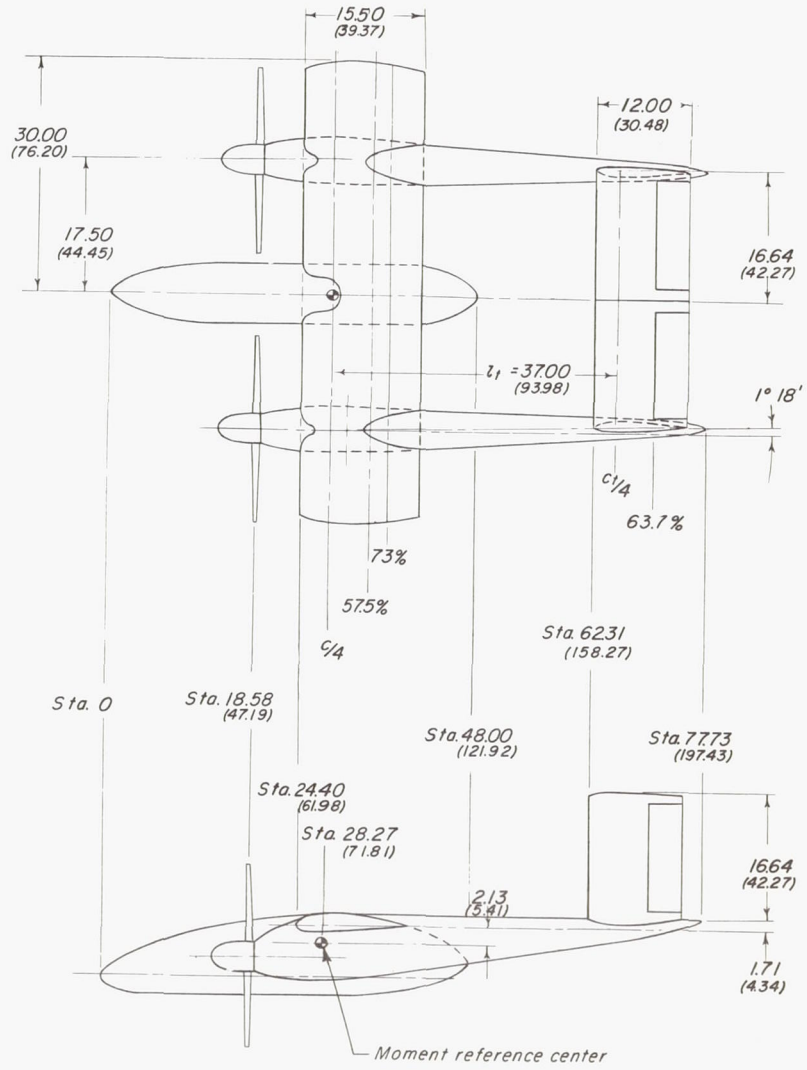

Figure 1.- Three-view drawing of model and table of geometric characteristics. All dimensions are in inches (centimeters) unless otherwise noted.

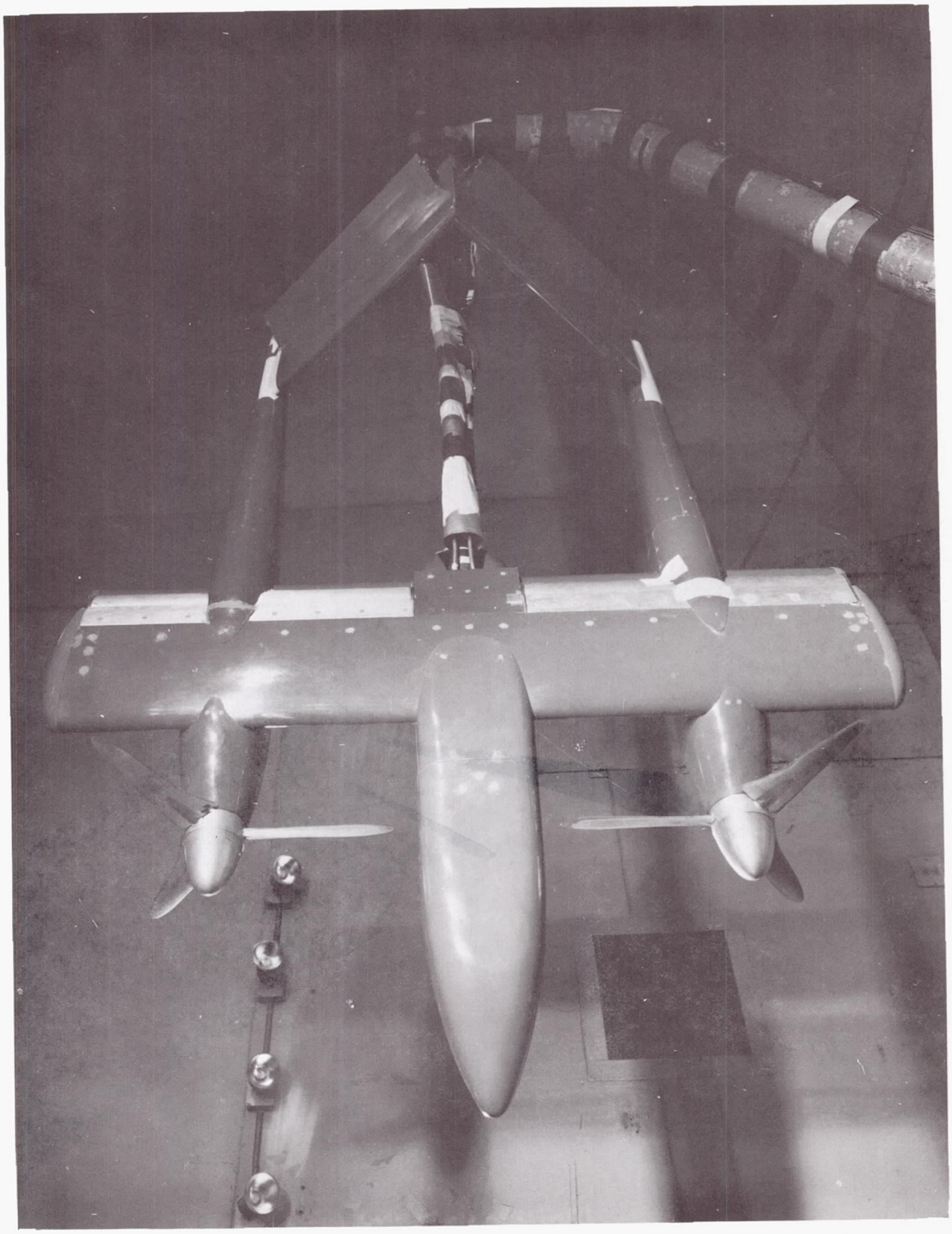

L-64-1928

(a) Top quarter front view.

Figure 2.- Model in wind tunnel.

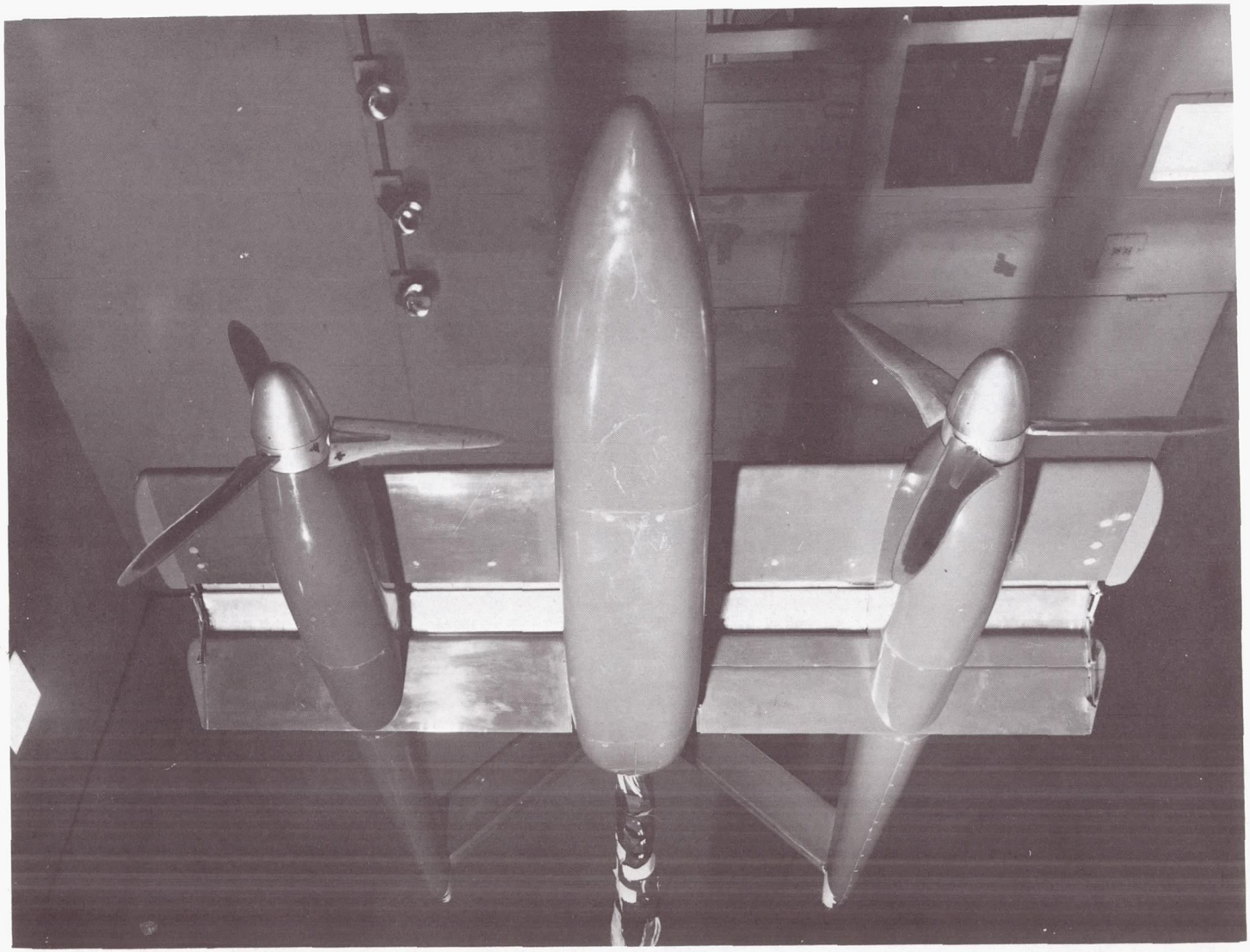

L-64-1926

(b) Lower quarter front view.

Figure 2.- Continued.

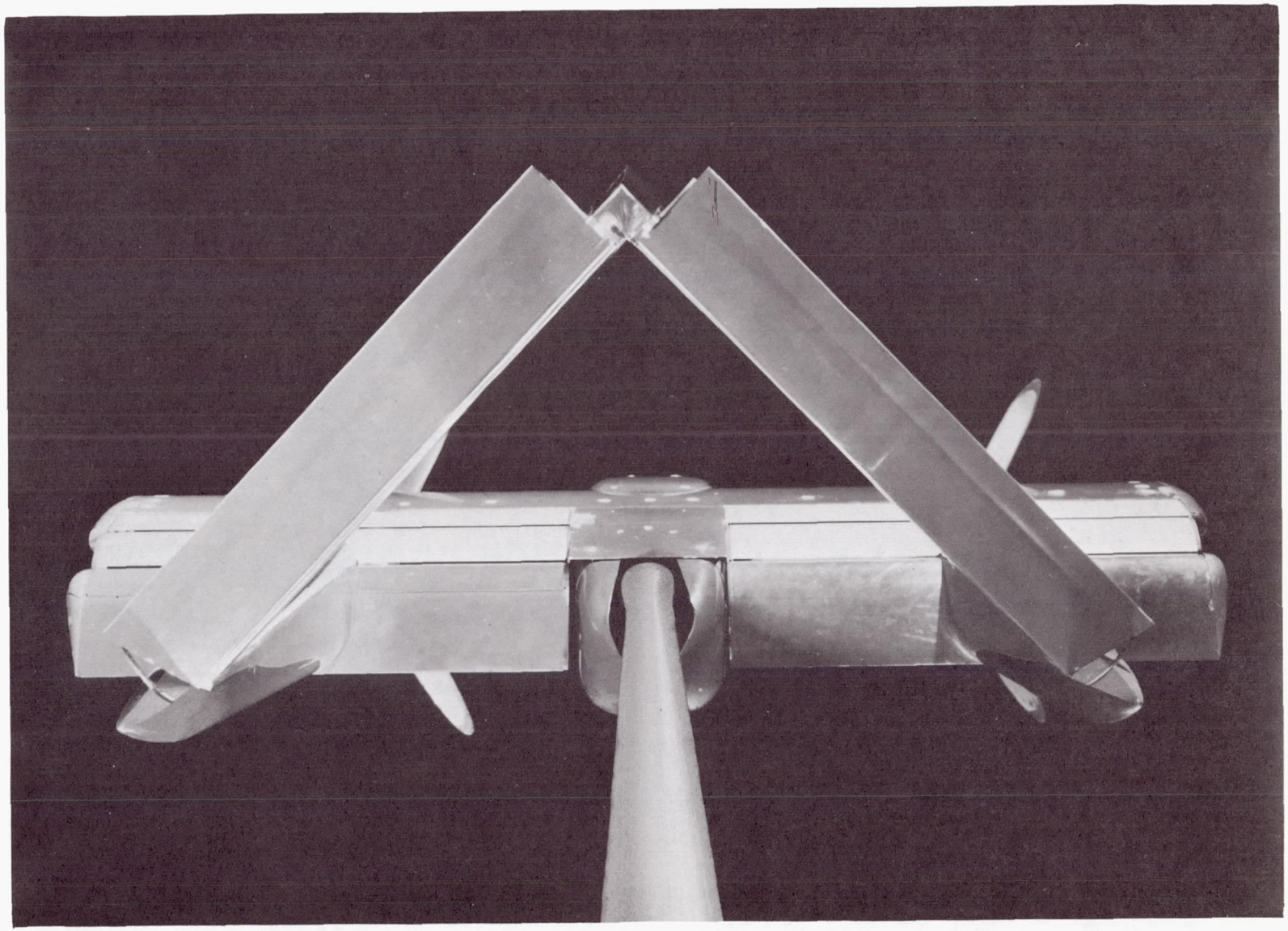

L-64-1927.1

(c) Rear view.

Figure 2.- Concluded.

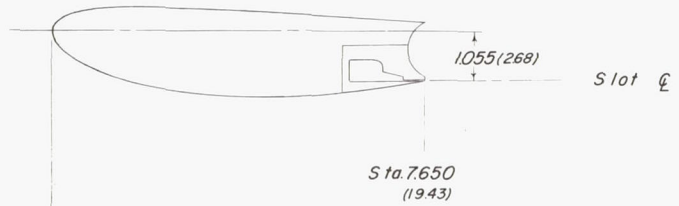

(a) Tail profile without elevator showing cross section of plenum chamber.

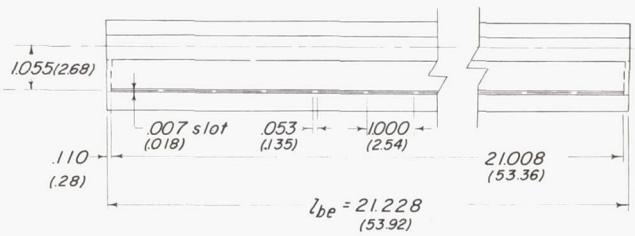

(b) Trailing-edge view of tail without elevator showing location of boundary-layer-control slot.

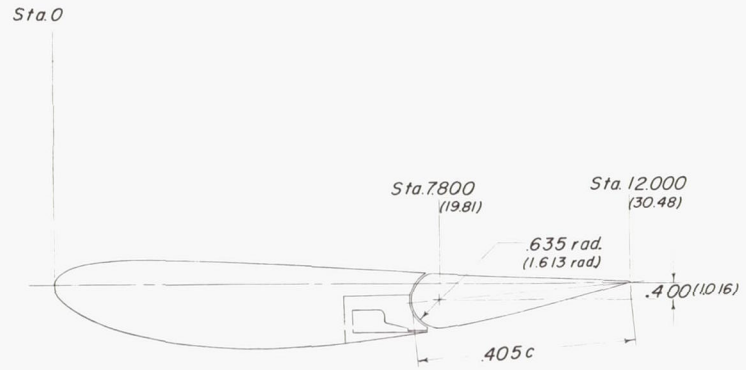

(c) Tail profile with elevator undeflected (NACA 4415 airfoil).

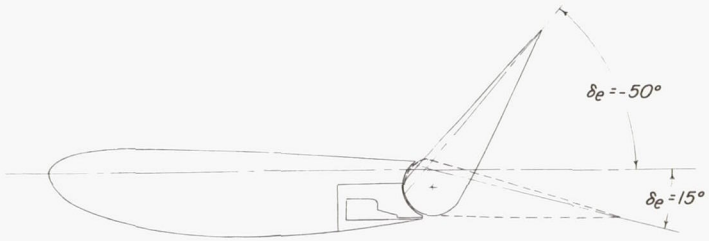

(d) Tail profile with elevator deflected.

Figure 3.- Detailed drawing of inverted V-tail sections with control surfaces and blowing assembly. All dimensions are in inches (centimeters) unless otherwise noted.

VANE ORDINATES ST. CYR 156 SECTION		
x/c	y_u/c	y_l/c
0	0	0
.0125	.0381	-.0268
.0250	.0522	-.0339
.0500	.0739	-.0409
.0750	.0905	-.0446
.1000	.1039	-.0448
.1500	.1269	-.0409
.2000	.1440	-.0300
.3000	.1630	-.0140
.4000	.1660	.0010
.5000	.1600	.0180
.6000	.1440	.0300
.7000	.1170	.0320
.8000	.0830	.0300
.9000	.0484	.0180
.9500	.0274	.0107
1.0000	.0065	0

(a) Plain wing (NACA 4415 airfoil).

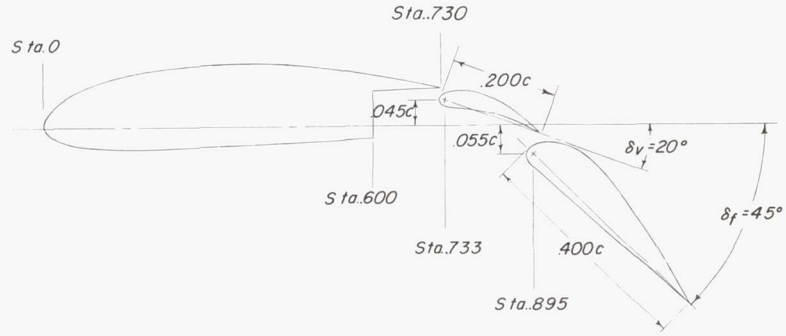

FLAP ORDINATES		
x/c	y_u/c	y_l/c
0	0	0
.0125	.0460	-.0290
.0250	.0645	-.0387
.0500	.0919	-.0435
.0750	.1145	-.0460
.1000	.1306	-.0468
.1500	.1516	-.0444
.2000	.1621	-.0420
.3000	.1677	-.0373
.4275	.1532	-.0312
.5000	.1387	-.0278
.6275	.1065	-.0217
.7500	.0769	-.0159
.8750	.0435	-.0100
1.0000	.0040	-.0040

(b) Flap deflected 45°.

Figure 4.- Geometric characteristics of wing section showing flap deflection. All dimensions are given in fraction of wing chord unless otherwise noted.

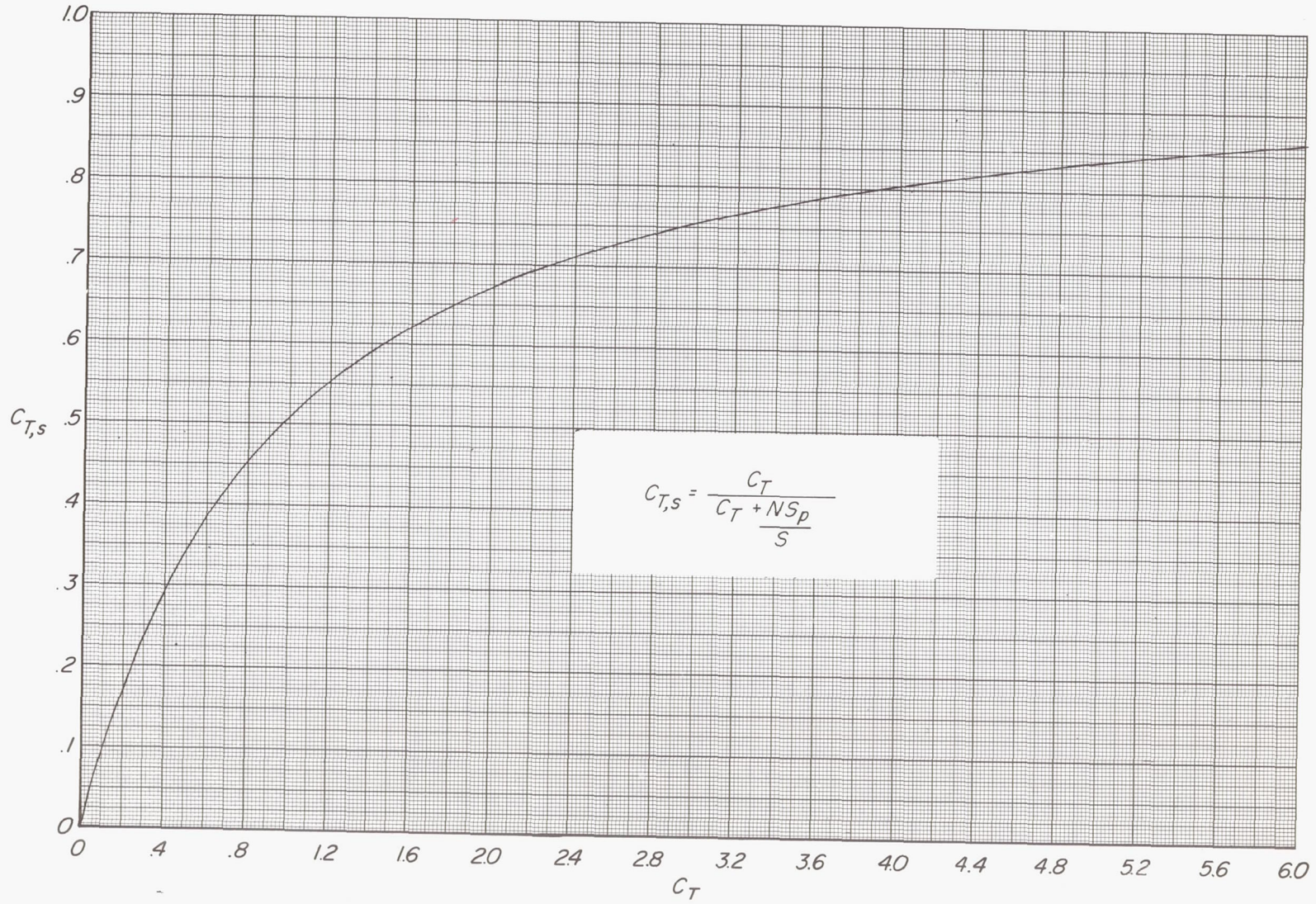

(a) Slipstream thrust coefficient as a function of free-stream thrust coefficient.

Figure 5.- Relationships of slipstream thrust coefficient and tail momentum coefficient to free-stream thrust coefficient.

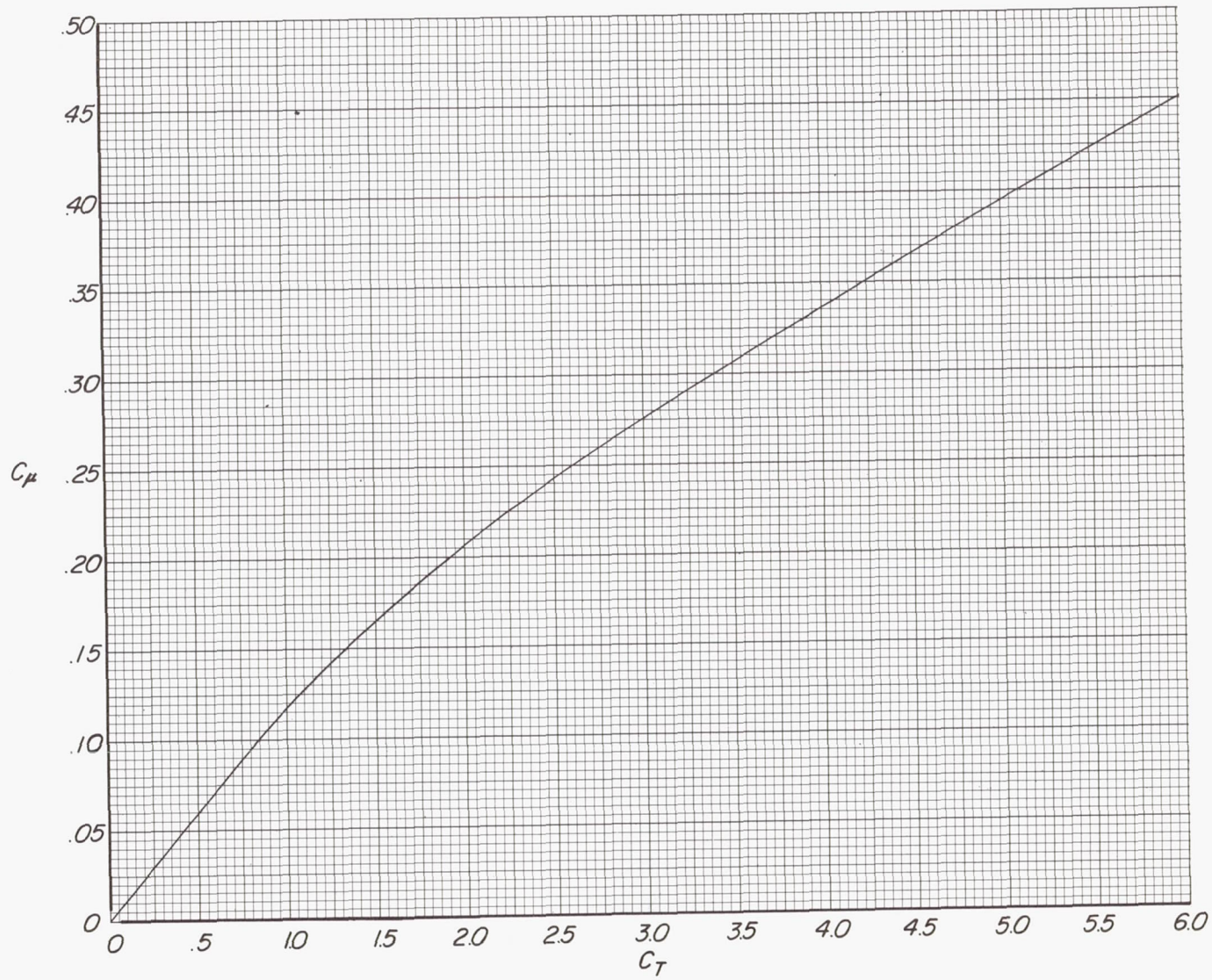

(b) Schedule of free-stream thrust coefficients and corresponding tail momentum coefficients.

Figure 5.- Concluded.

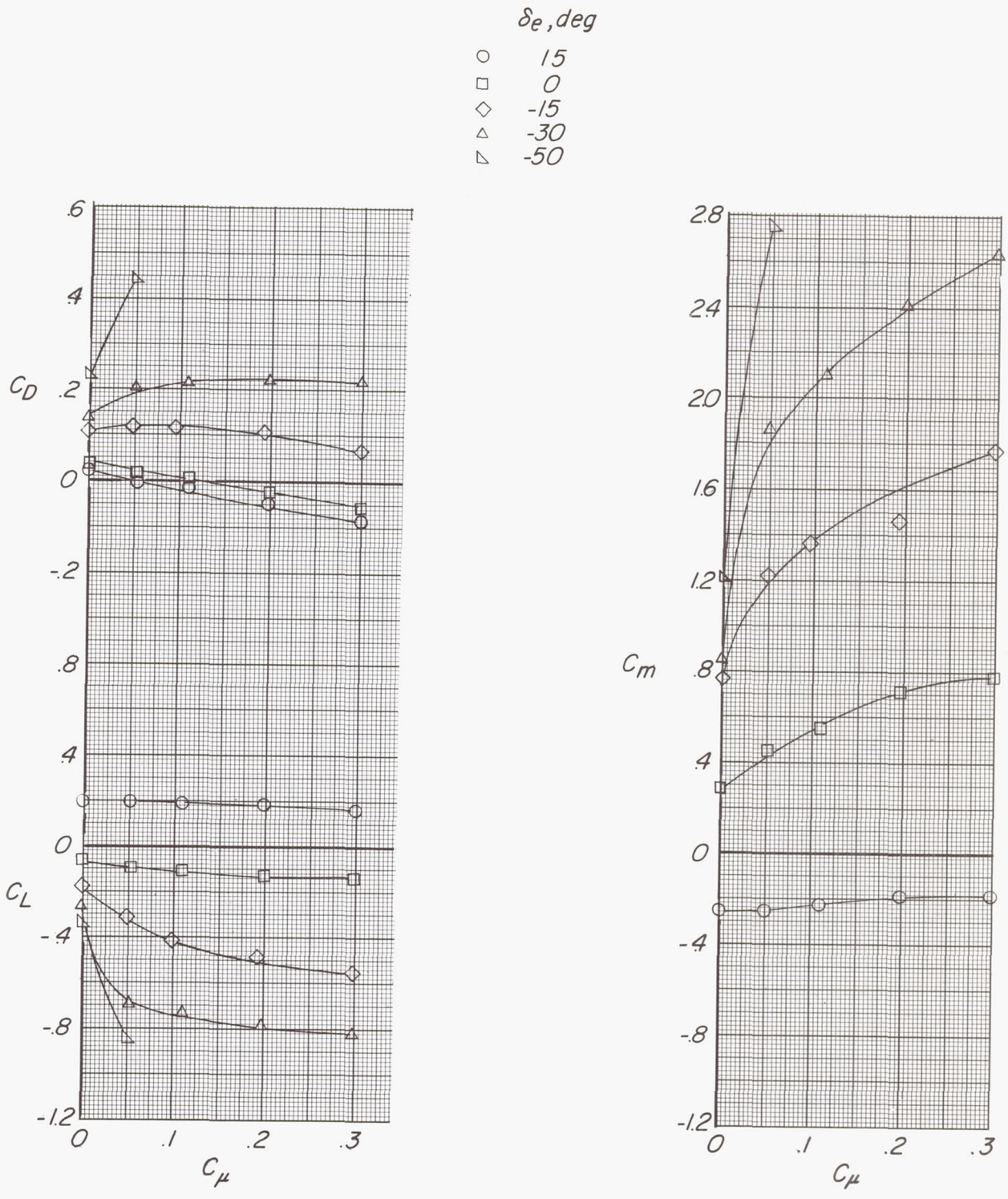

Figure 6.- Effect of tail momentum coefficient on longitudinal aerodynamic characteristics for several elevator deflections. $\delta_f = 0^o$; $C_T = 0$; $\alpha = 0^o$; $\beta = 0^o$; $i_t = 0^o$.

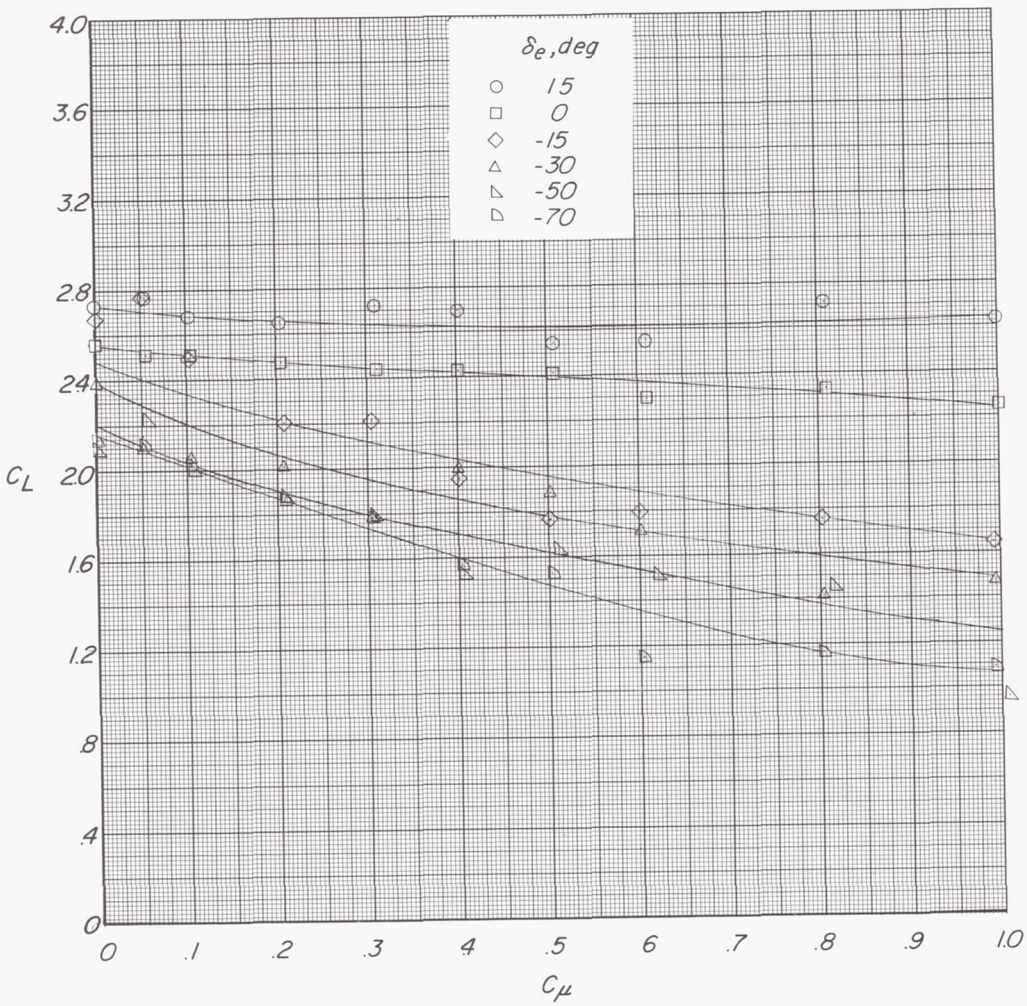

(a) Variation of C_L with C_μ.

Figure 7.- Effect of tail momentum coefficient on longitudinal aerodynamic characteristics for several elevator deflections. $\delta_f = 45^0$; $C_T = 2.10$; $\alpha = 0^0$; $\beta = 0^0$; $i_t = 0^0$.

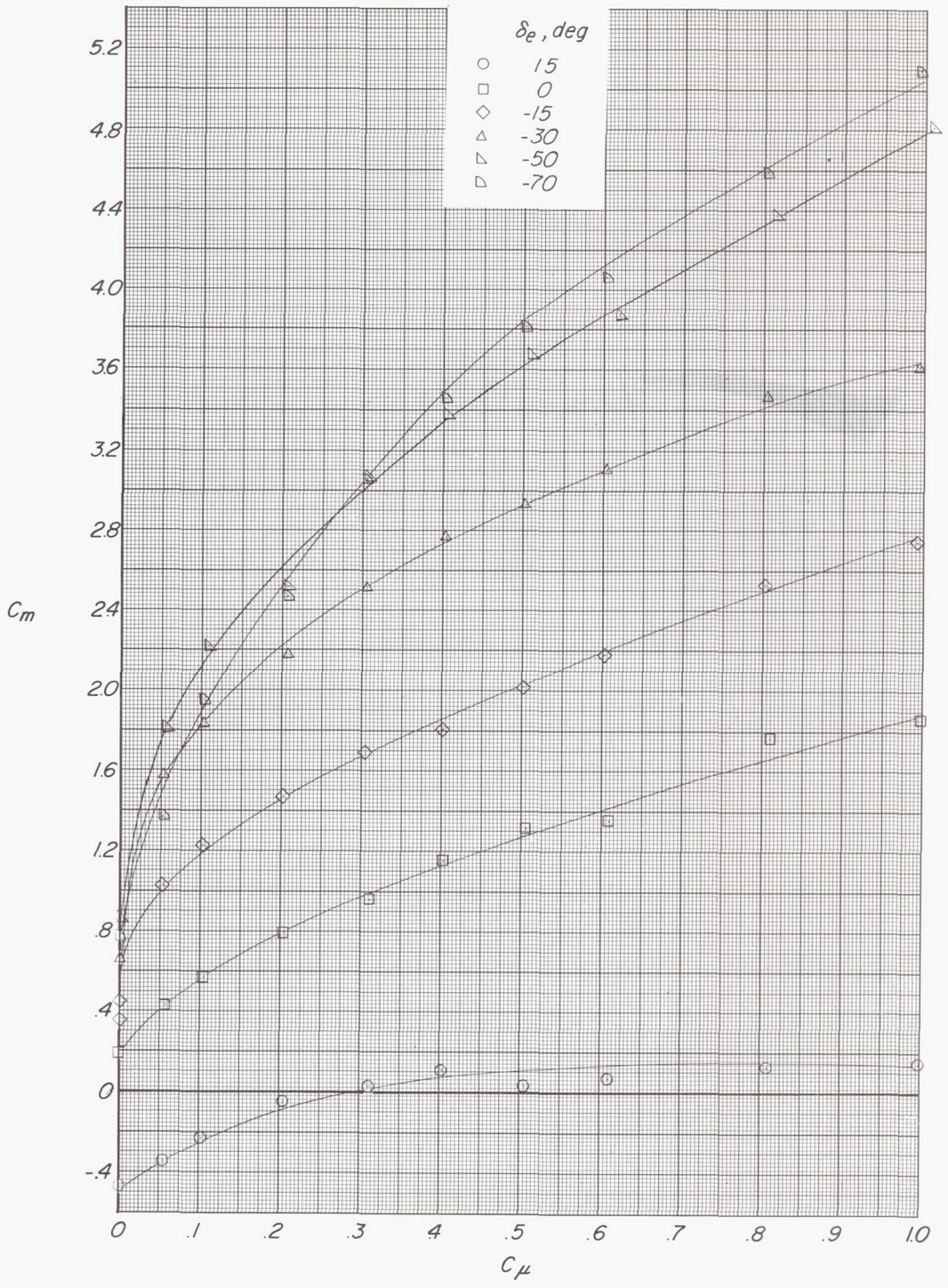

(b) Variation of C_m with C_μ.

Figure 7.- Continued.

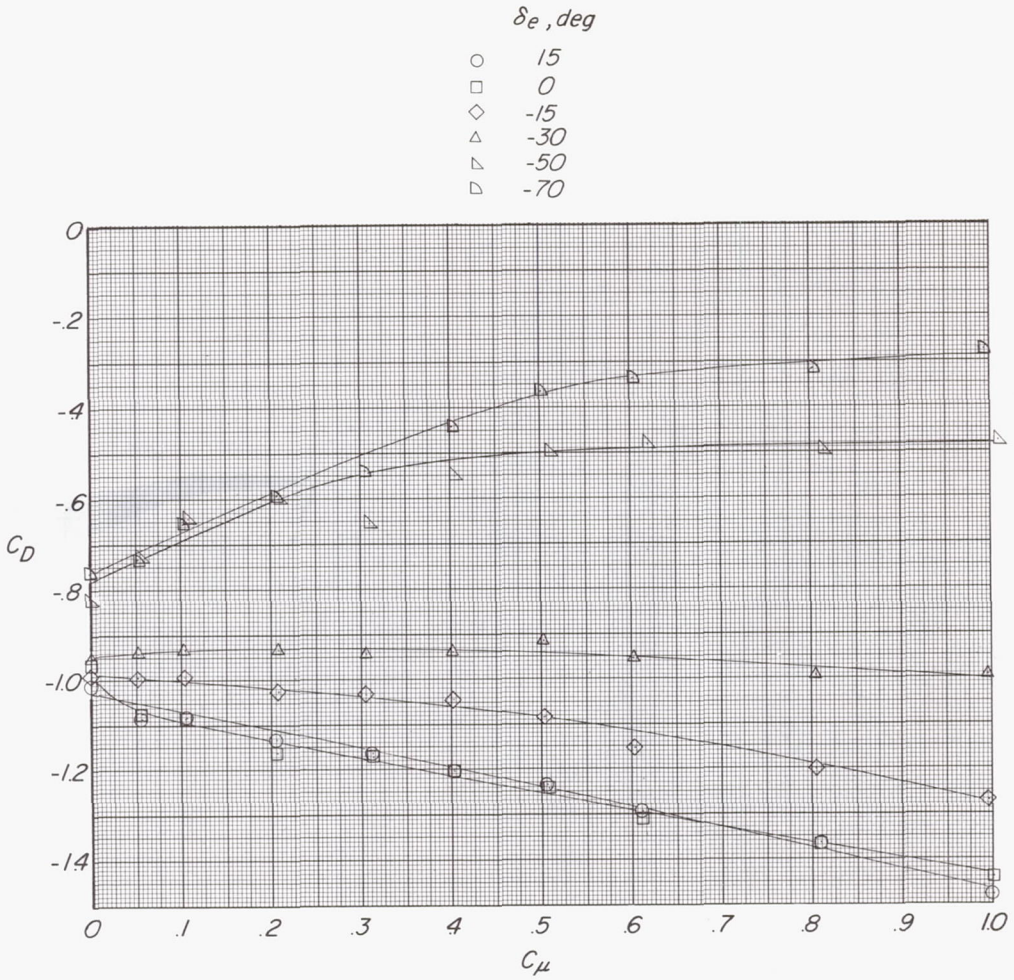

(c) Variation of C_D with C_μ.

Figure 7.- Continued.

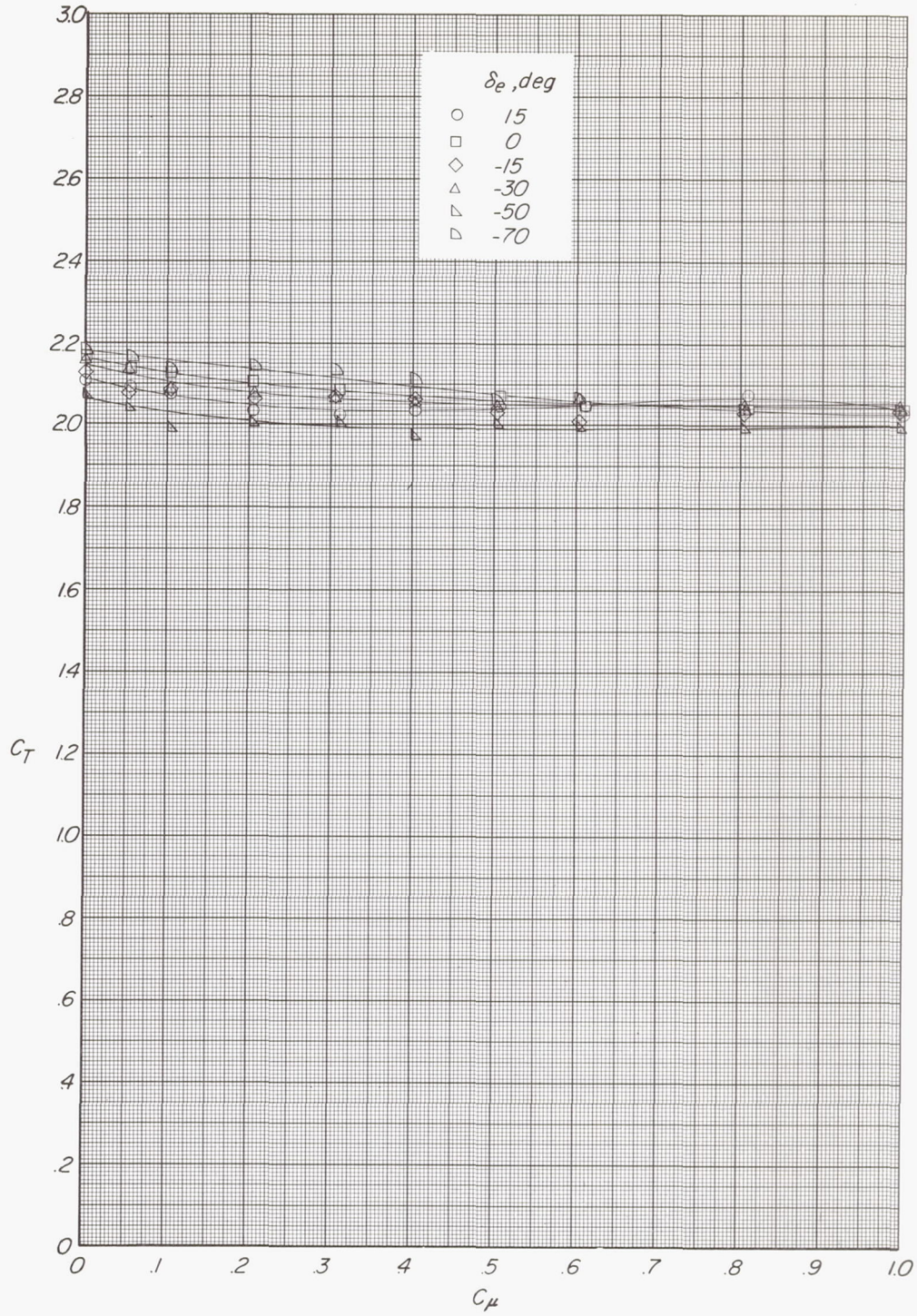

(d) Variation of C_T with C_μ.

Figure 7.- Concluded.

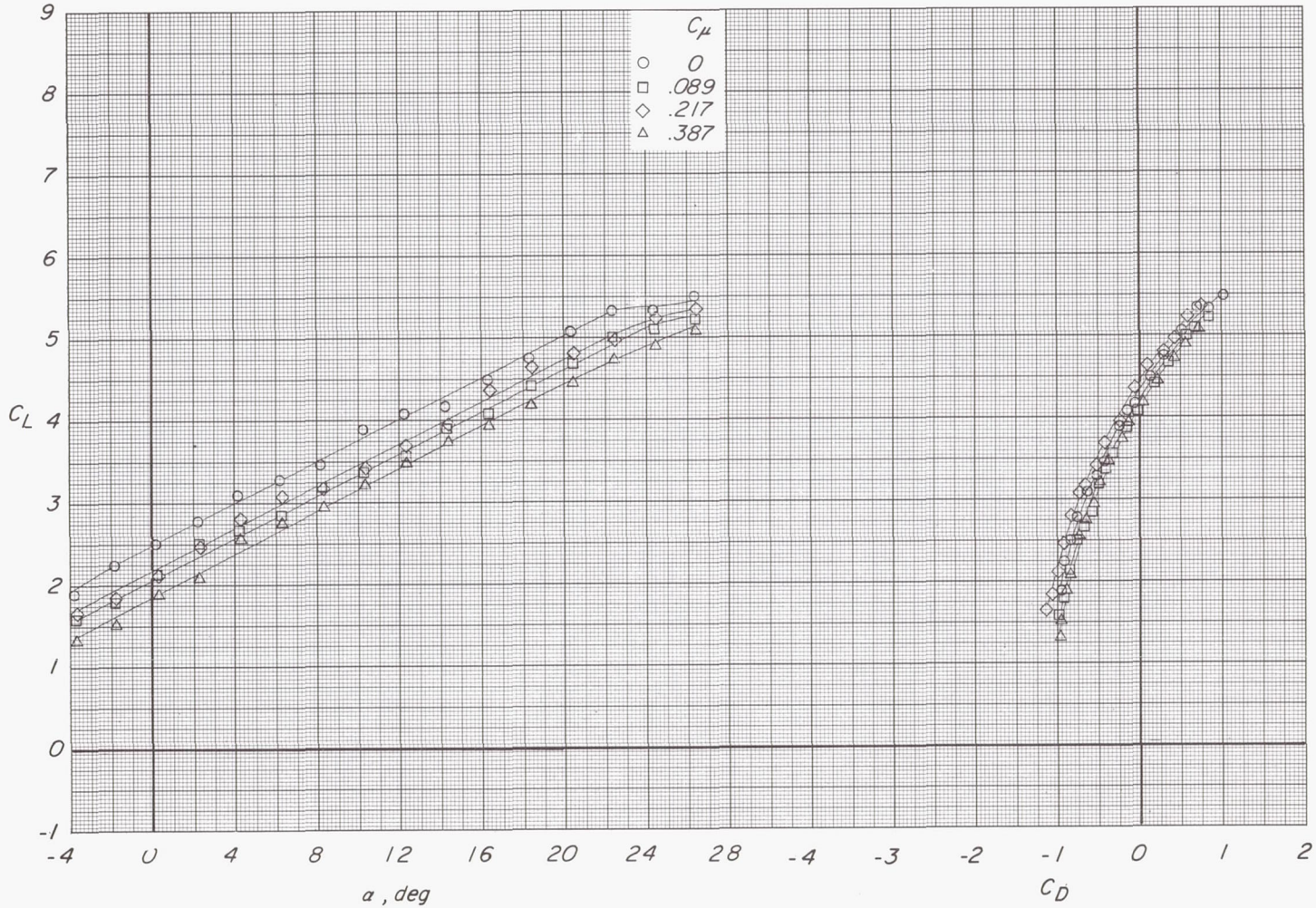

(a) Variation of C_L with α and C_D.

Figure 8.- Effect of tail momentum coefficient on longitudinal aerodynamic characteristics. $\delta_f = 45^0$; $C_T = 2.10$; $i_t = 0^0$; $\delta_e = -15^0$.

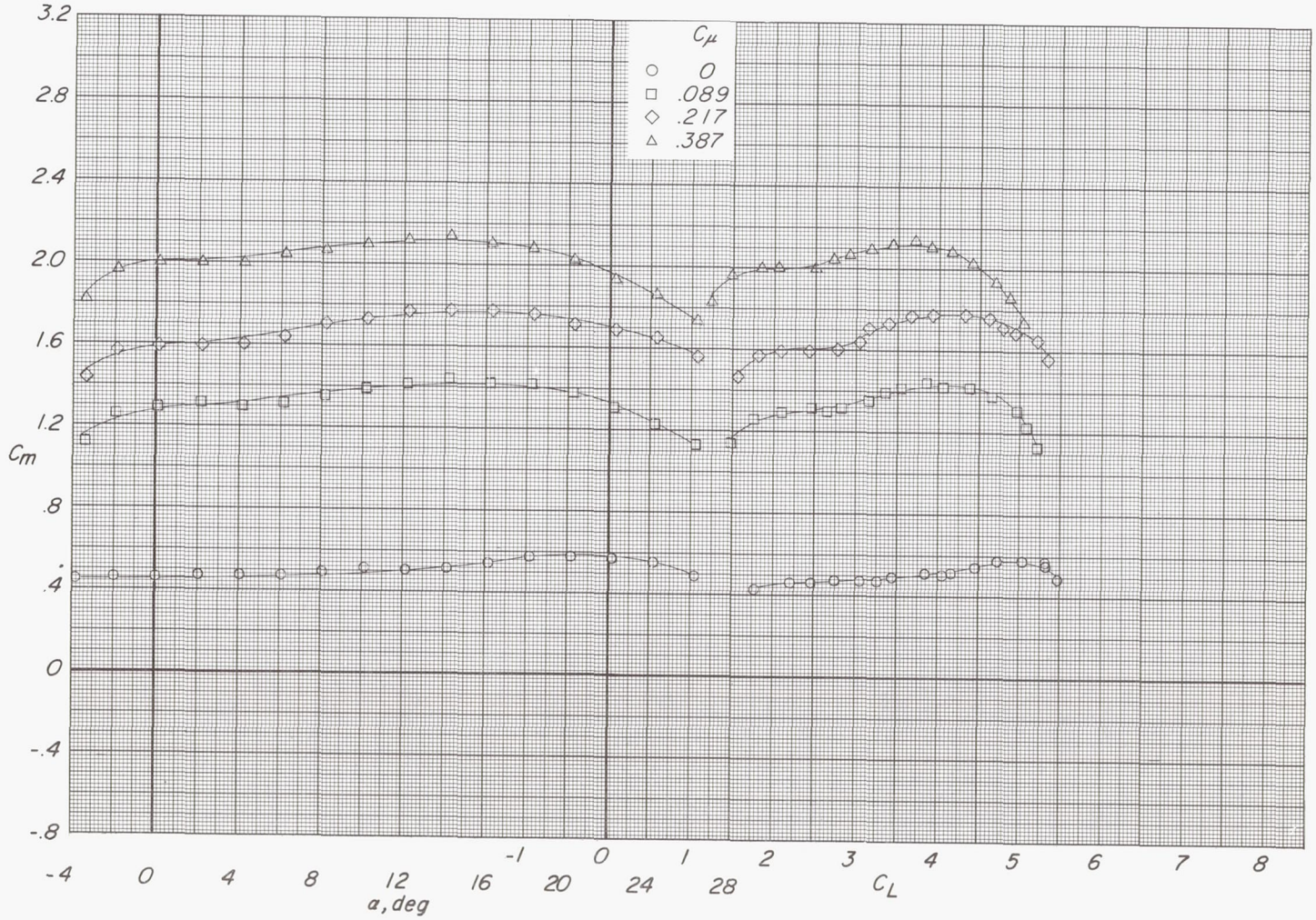

(b) Variation of C_m with α and C_L.

Figure 8.- Continued.

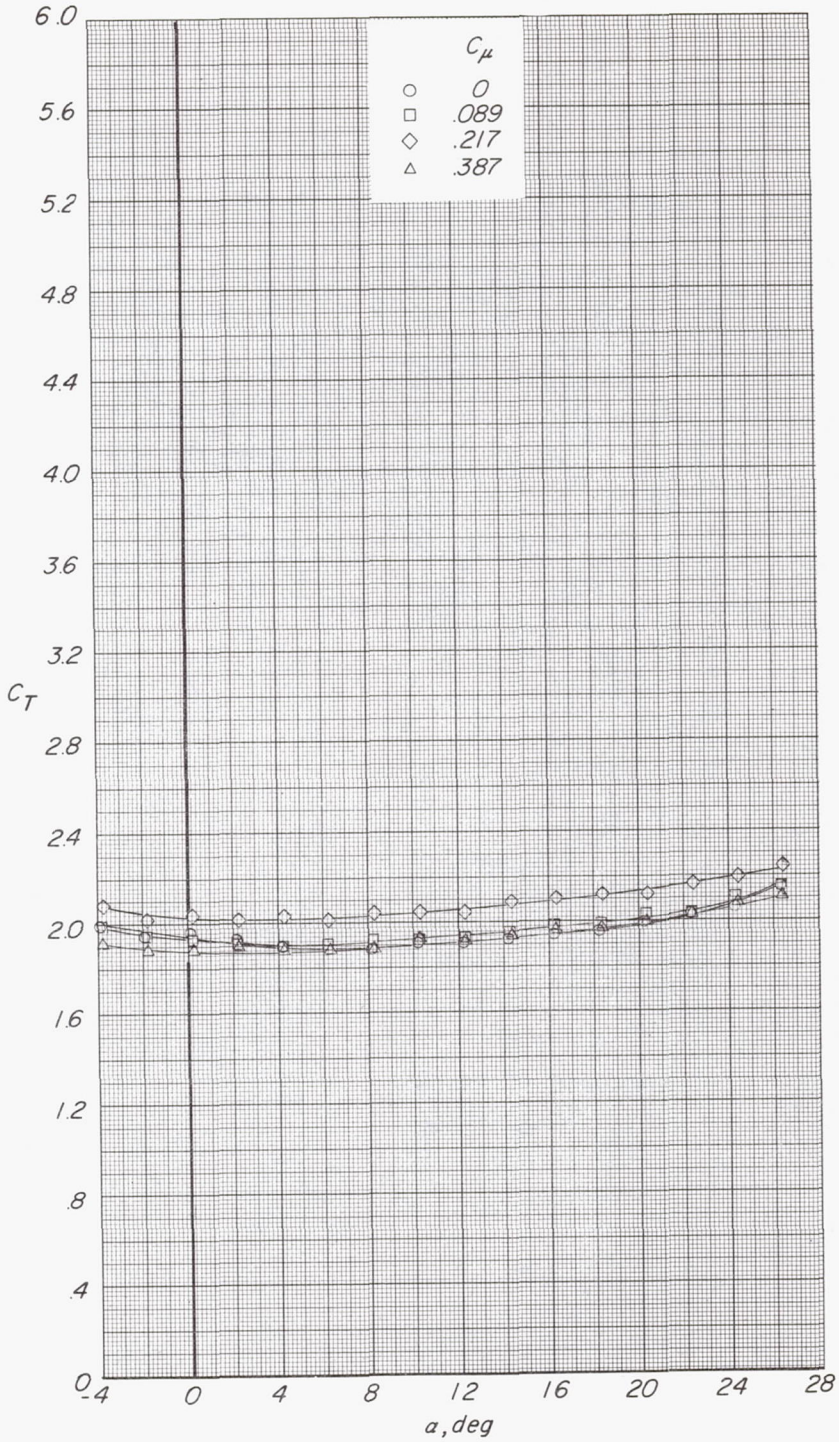

(c) Variation of C_T with α.

Figure 8.- Concluded.

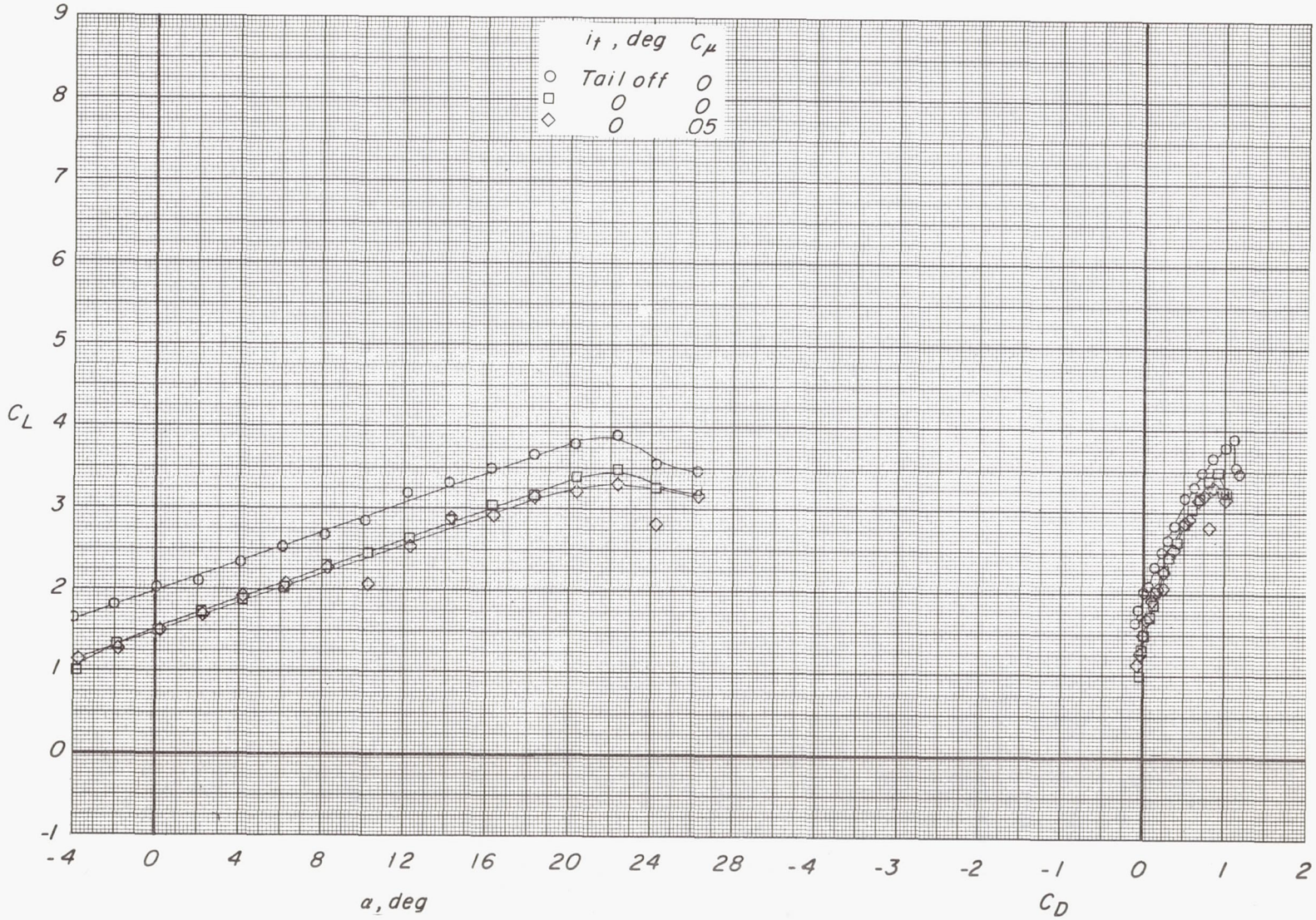

(a) Variation of C_L with α and C_D.

Figure 9.- Effect of tail and tail momentum coefficient on longitudinal aerodynamic characteristics. $\delta_f = 45^0$; $C_T = 0.43$; $i_t = 0^0$; $\delta_e = 0^0$.

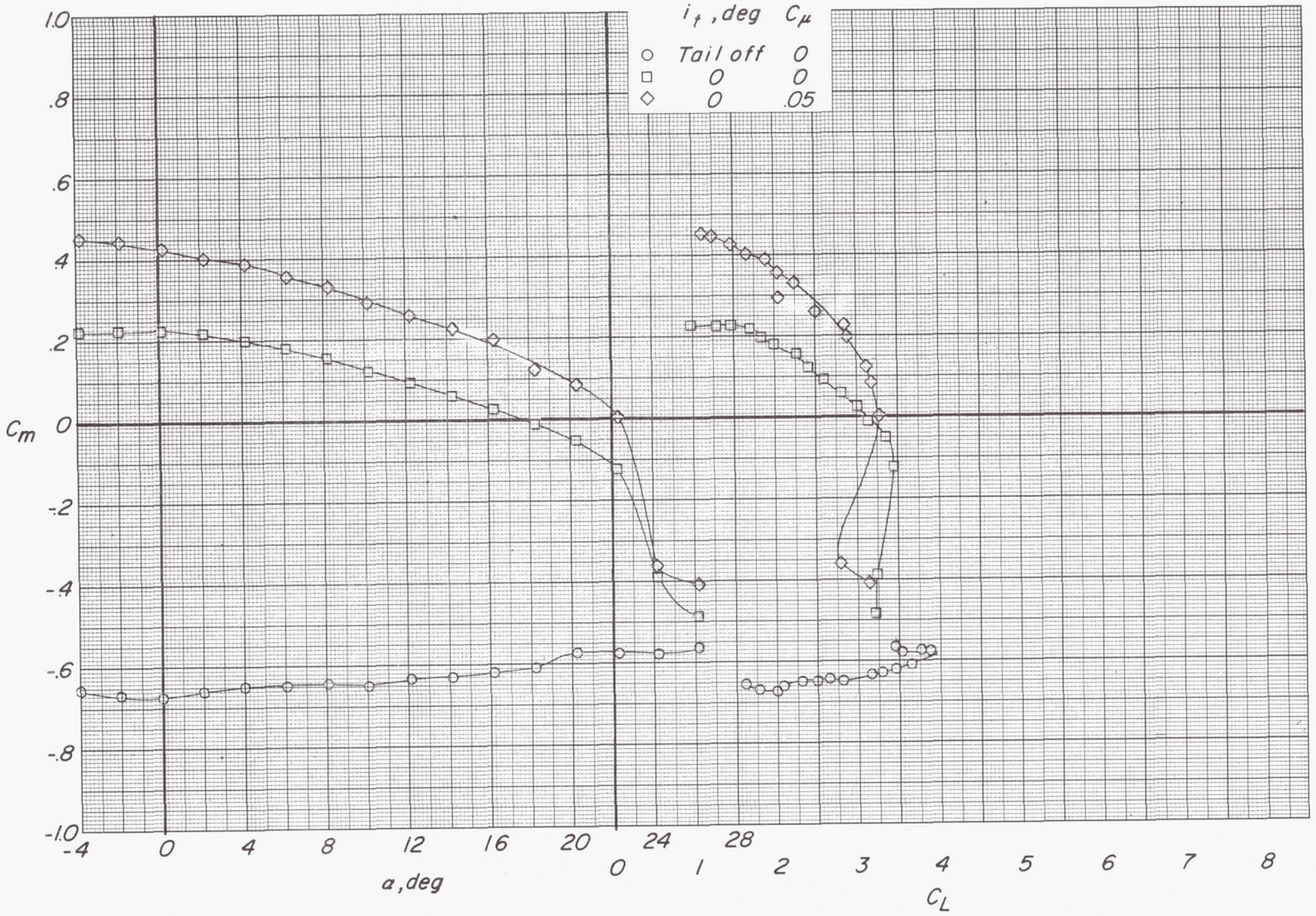

(b) Variation of C_m with α and C_L.

Figure 9.- Continued.

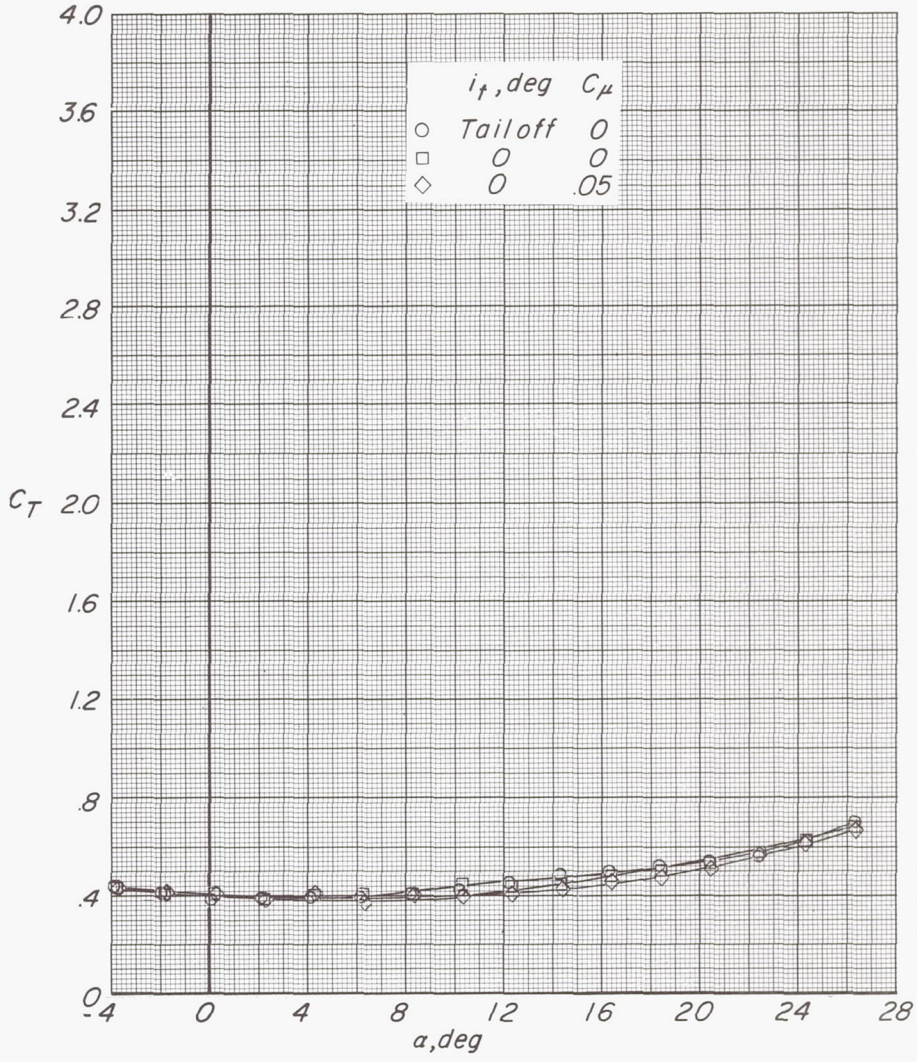

(c) Variation of C_T with α.

Figure 9.- Concluded.

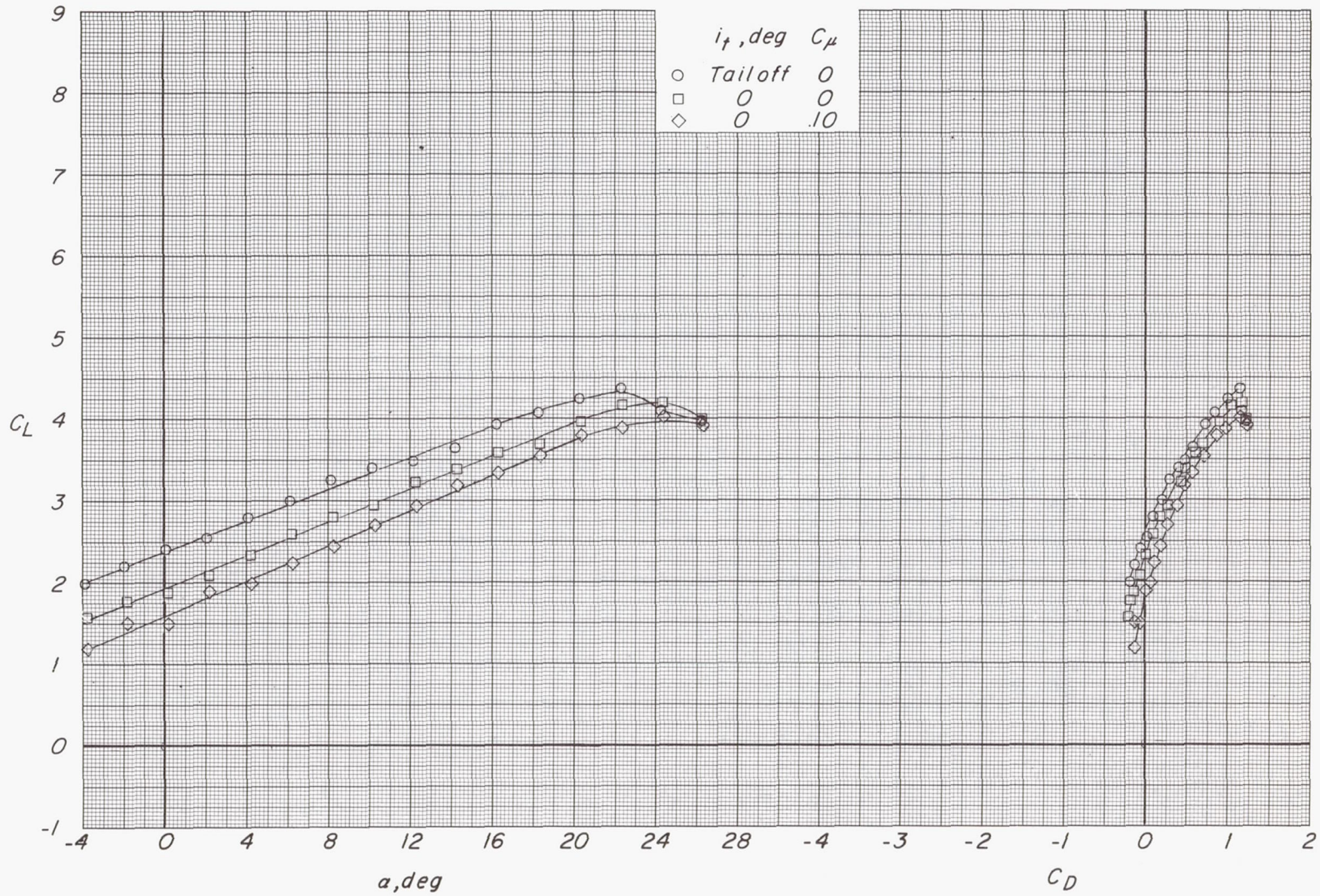

(a) Variation of C_L with α and C_D.

Figure 10.- Effect of tail and tail momentum coefficient on longitudinal aerodynamic characteristics. $\delta_f = 45^0$; $C_T = 0.83$; $i_t = 0^0$; $\delta_e = 0^0$.

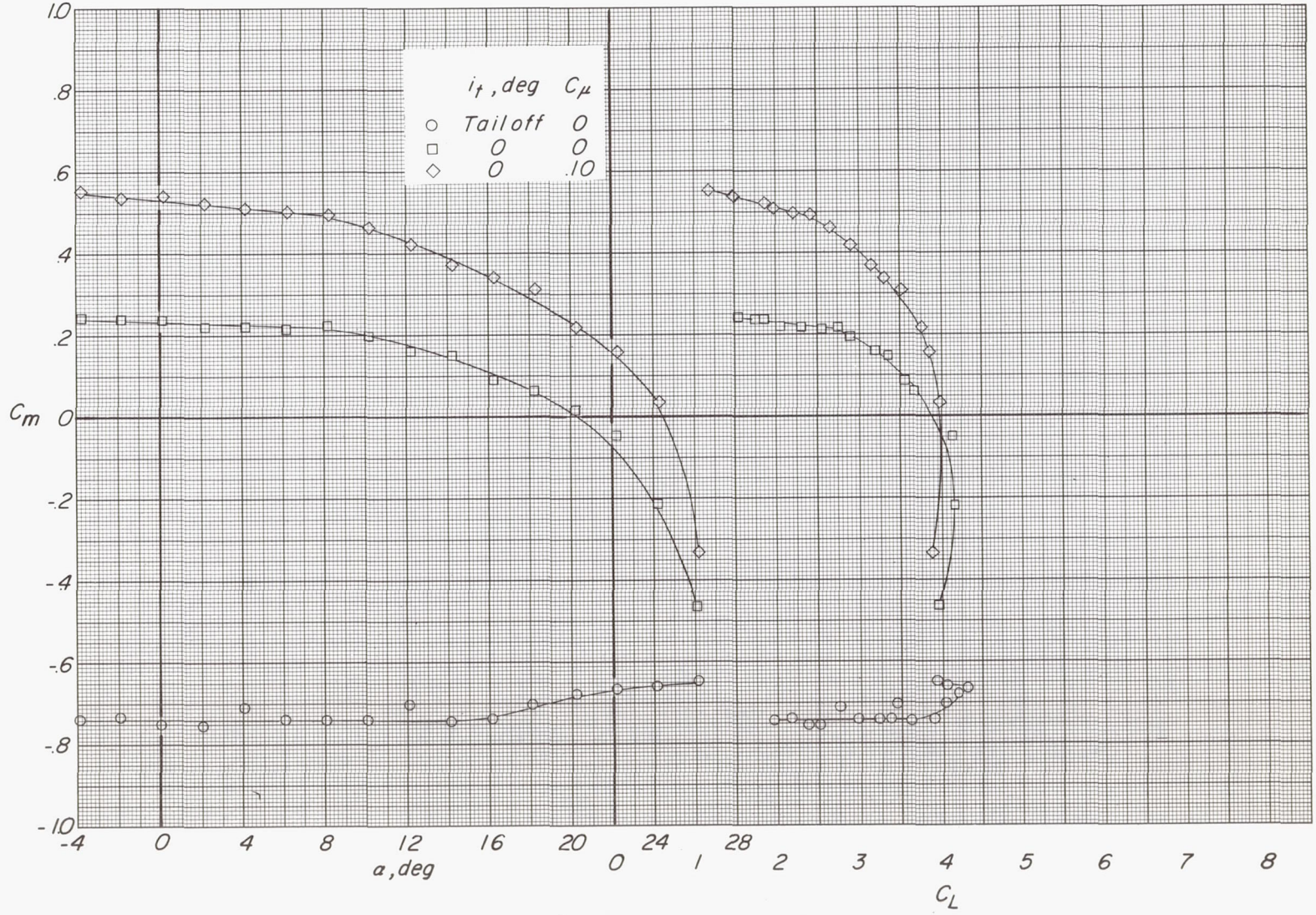

(b) Variation of C_m with α and C_L.

Figure 10.- Continued.

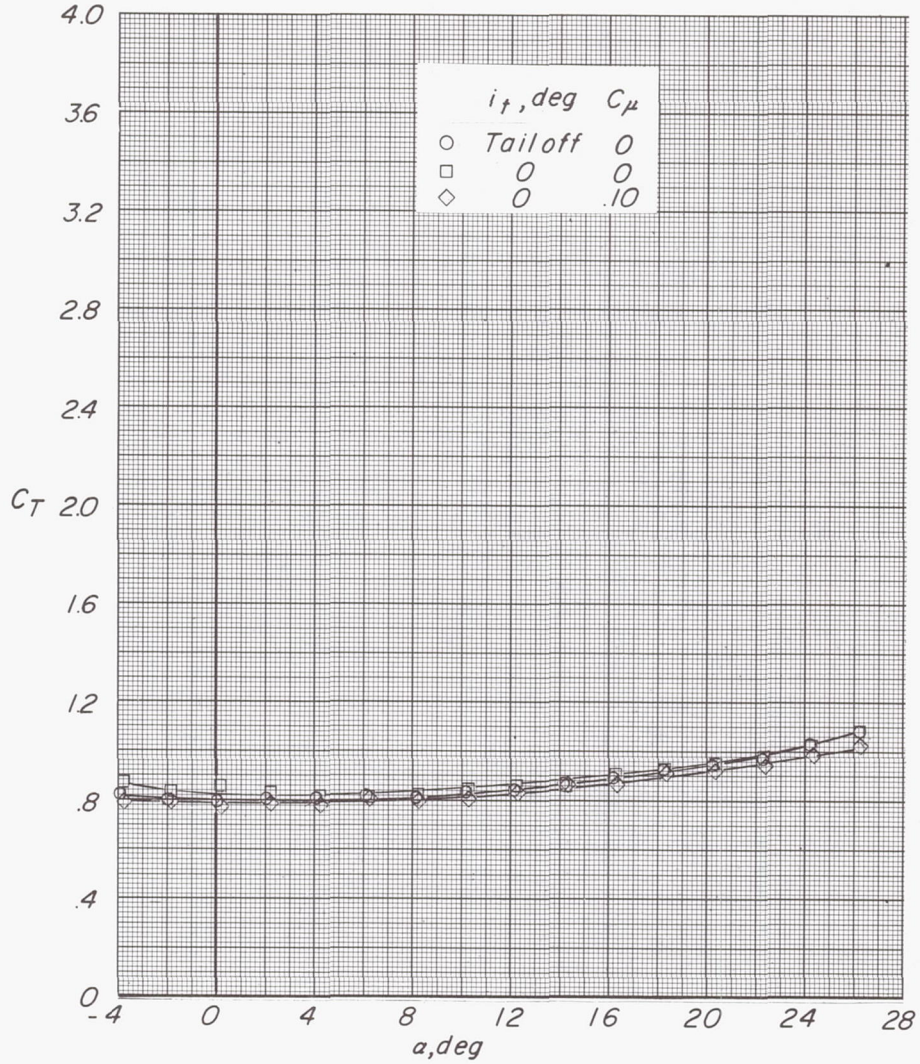

(c) Variation of C_T with α.

Figure 10.- Concluded.

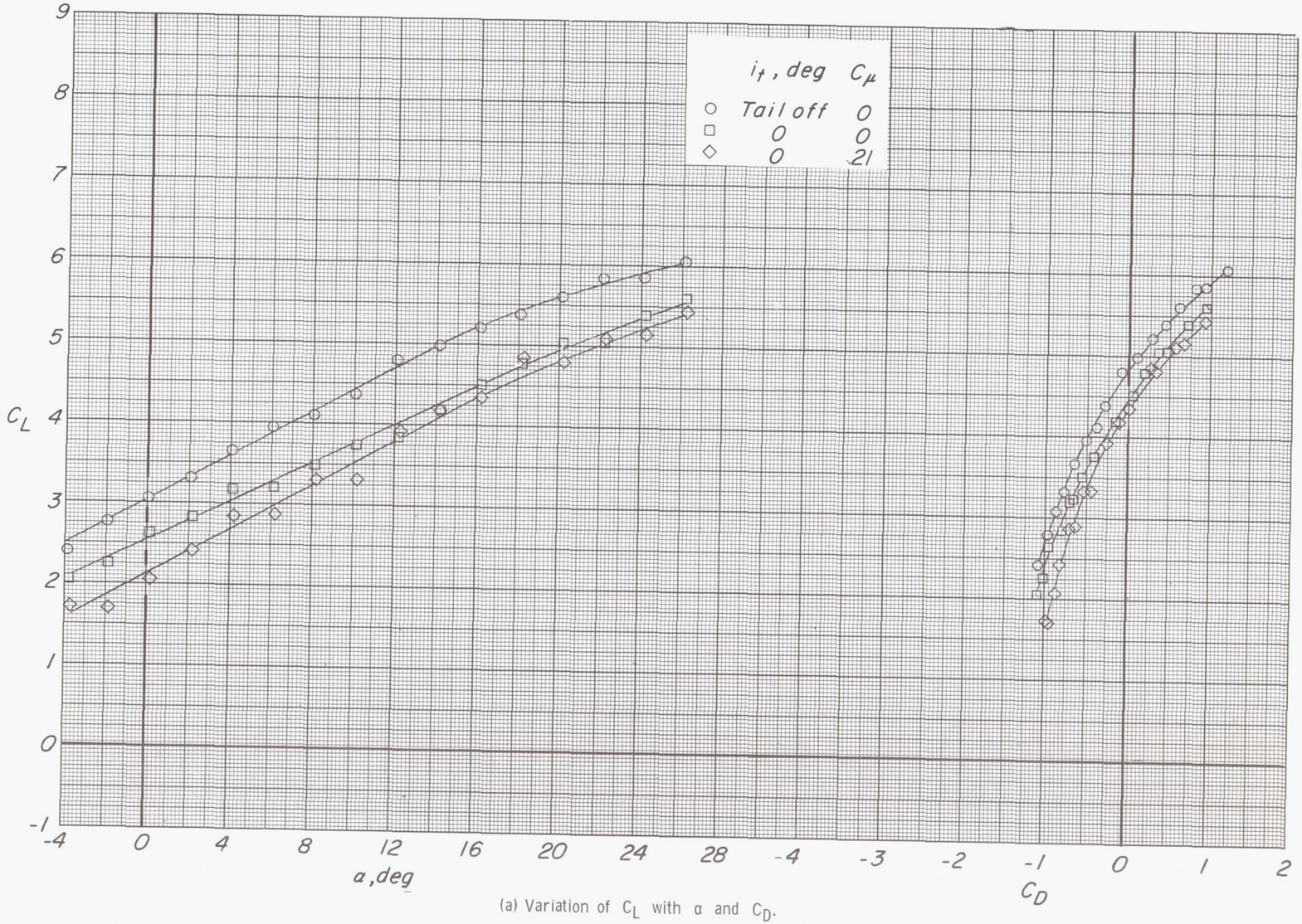

(a) Variation of C_L with α and C_D.

Figure 11.- Effect of tail and tail momentum coefficient on longitudinal aerodynamic characteristics. $\delta_f = 45^0$; $C_T = 2.10$; $i_t = 0^0$; $\delta_e = 0^0$.

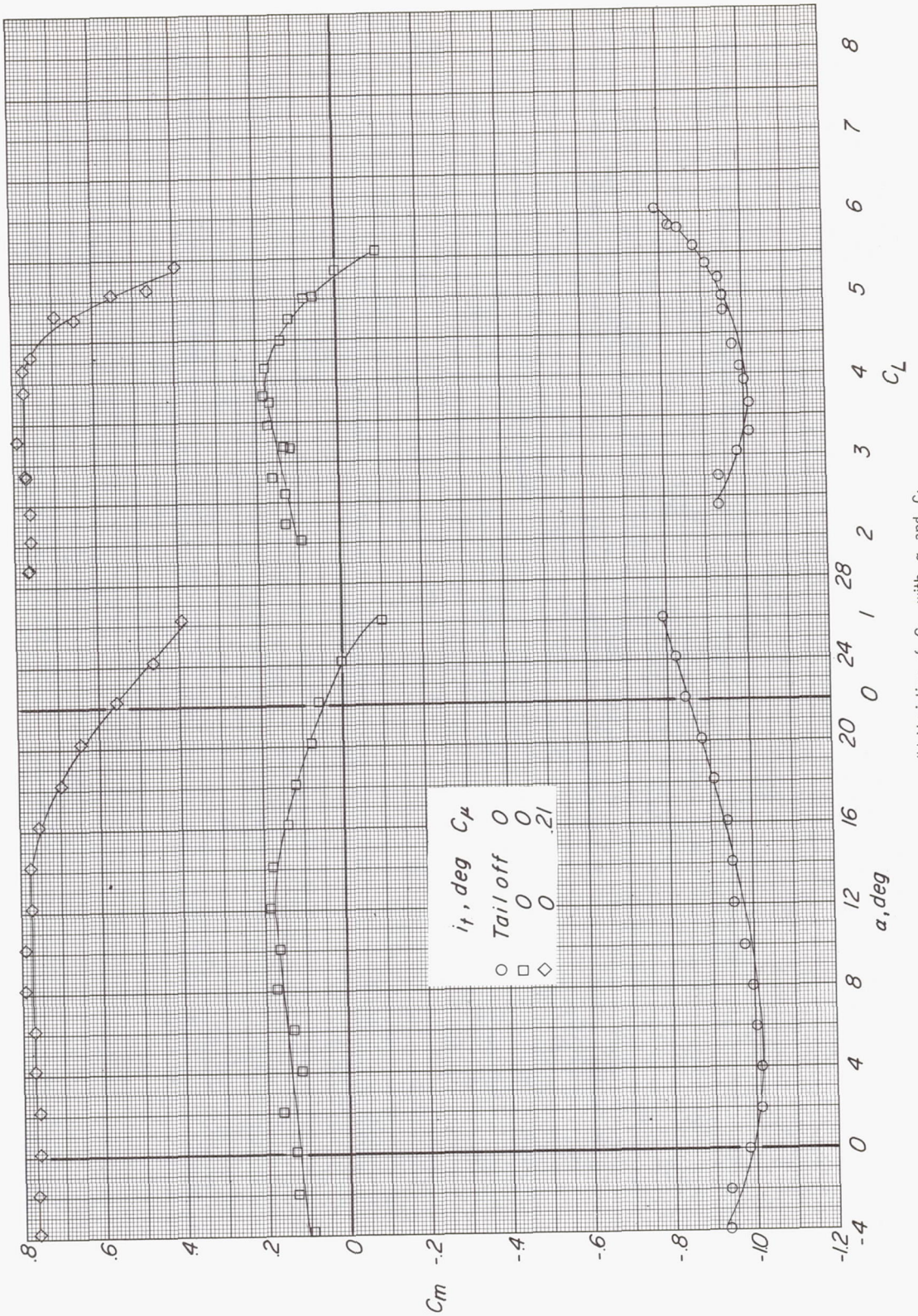

(b) Variation of C_m with α and C_L.

Figure 11.- Continued.

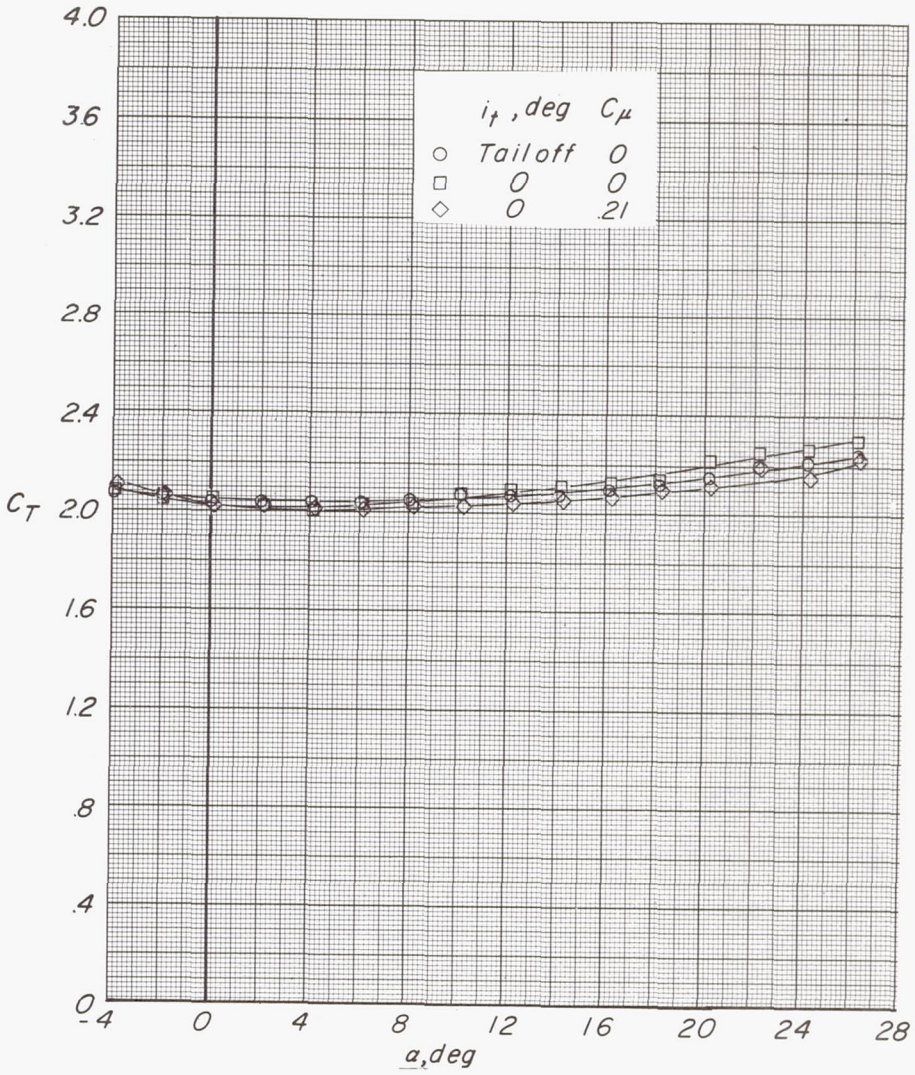

(c) Variation of C_T with α.

Figure 11.- Concluded.

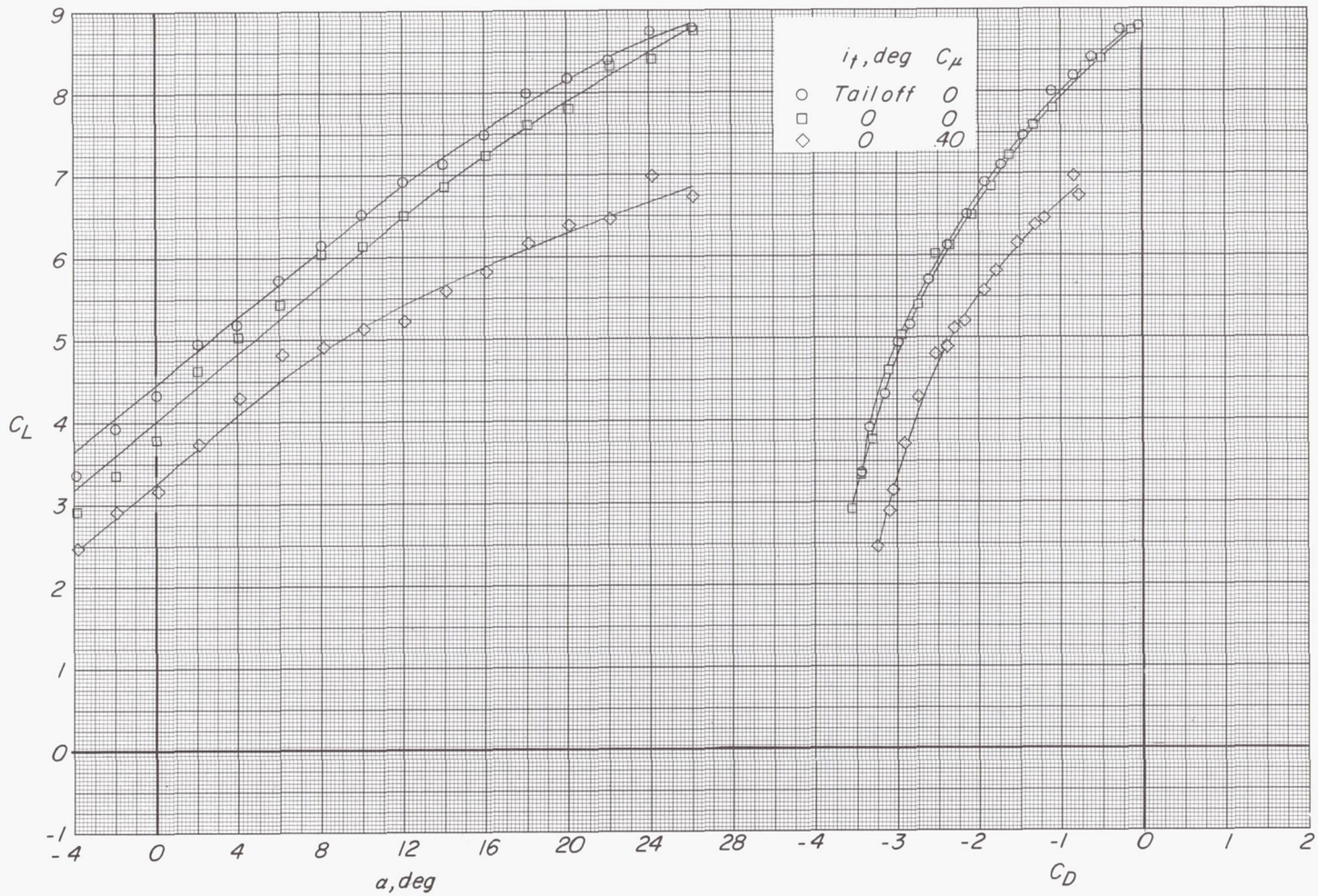

(a) Variation of C_L with α and C_D.

Figure 12.- Effect of tail and tail momentum coefficient on longitudinal aerodynamic characteristics. $\delta_f = 45^0$; $C_T = 5.10$; $i_t = 0^0$; $\delta_e = 0^0$.

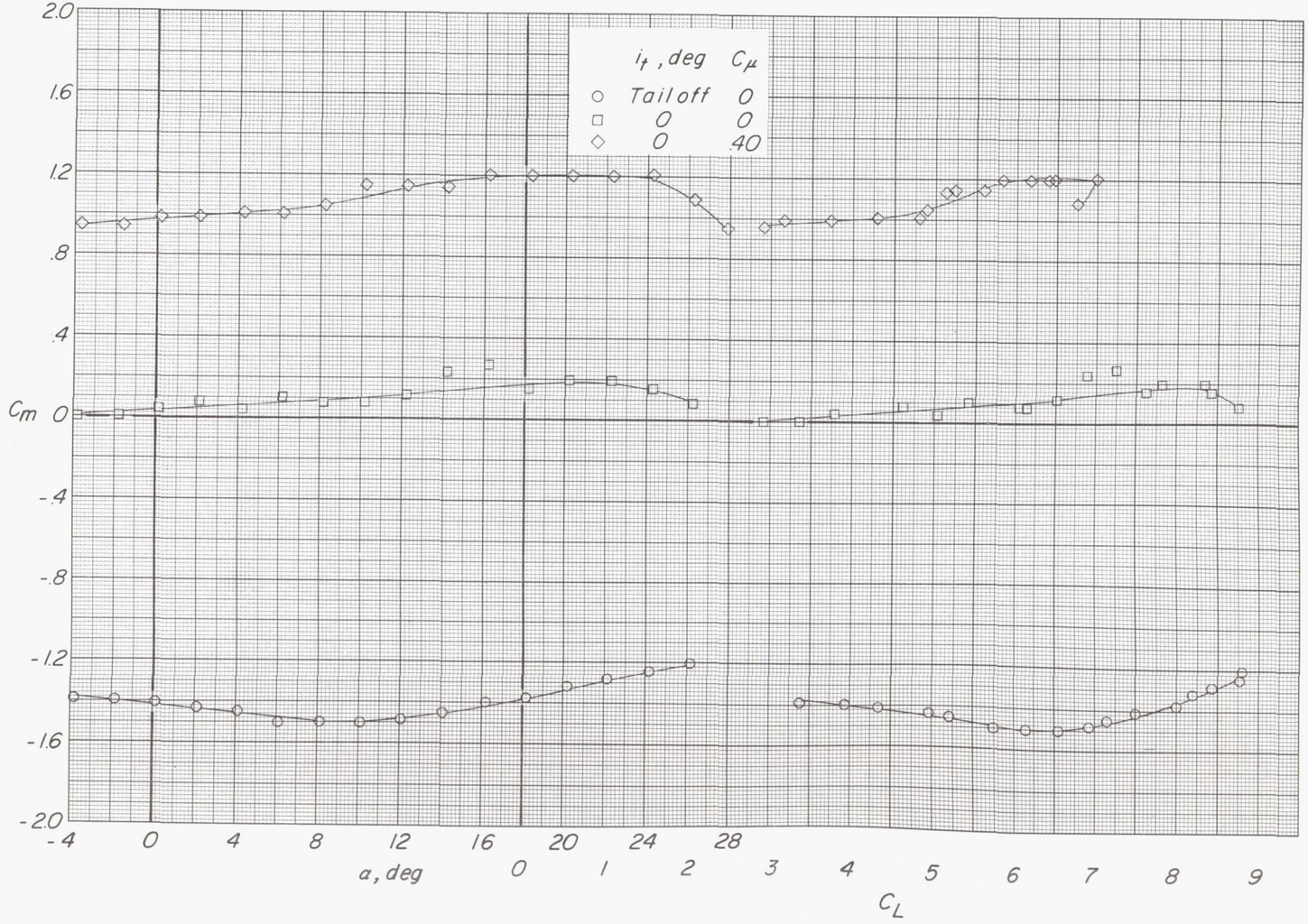

(b) Variation of C_m with α and C_L.

Figure 12.- Continued.

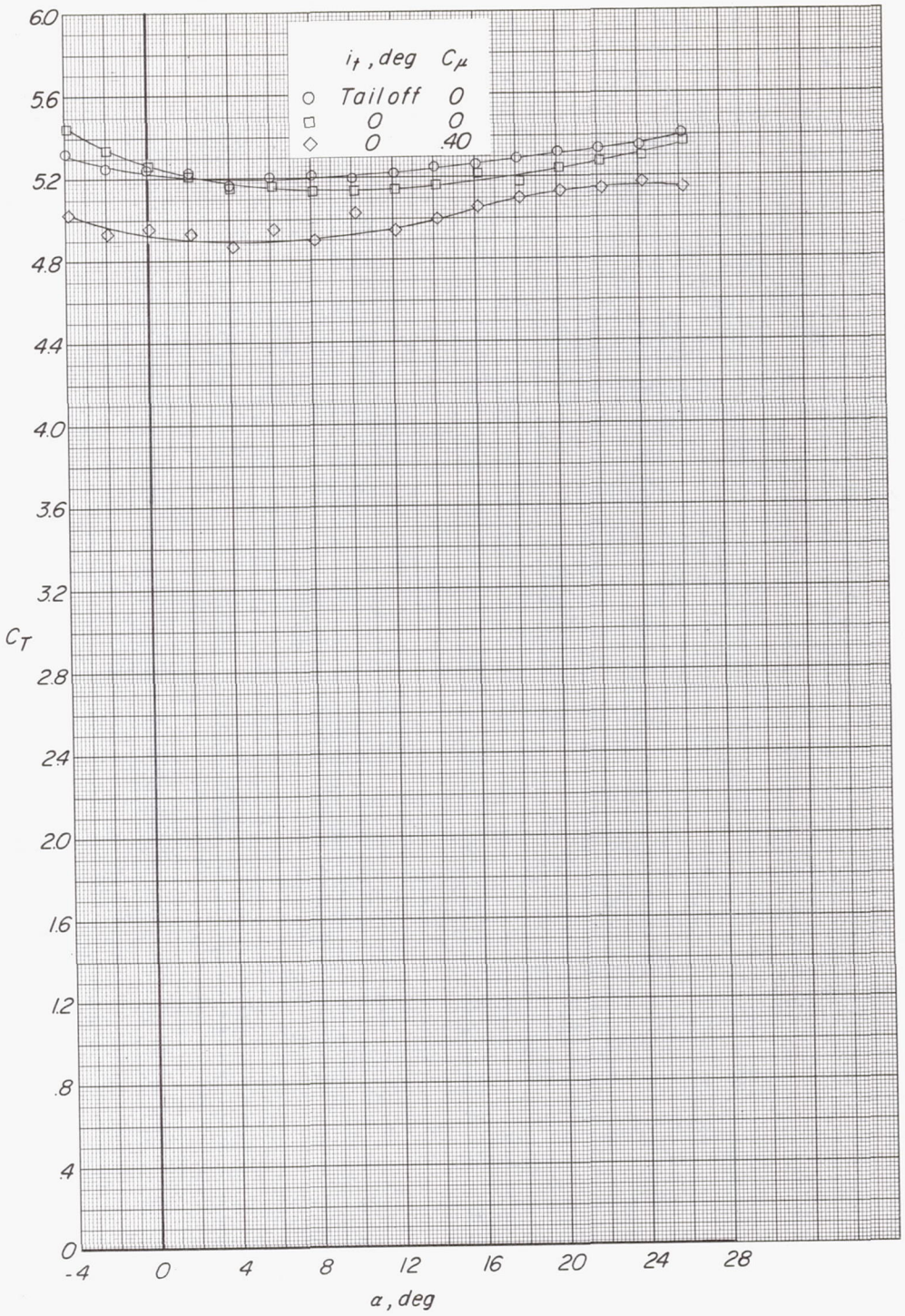

(c) Variation of C_T with α.

Figure 12.- Concluded.

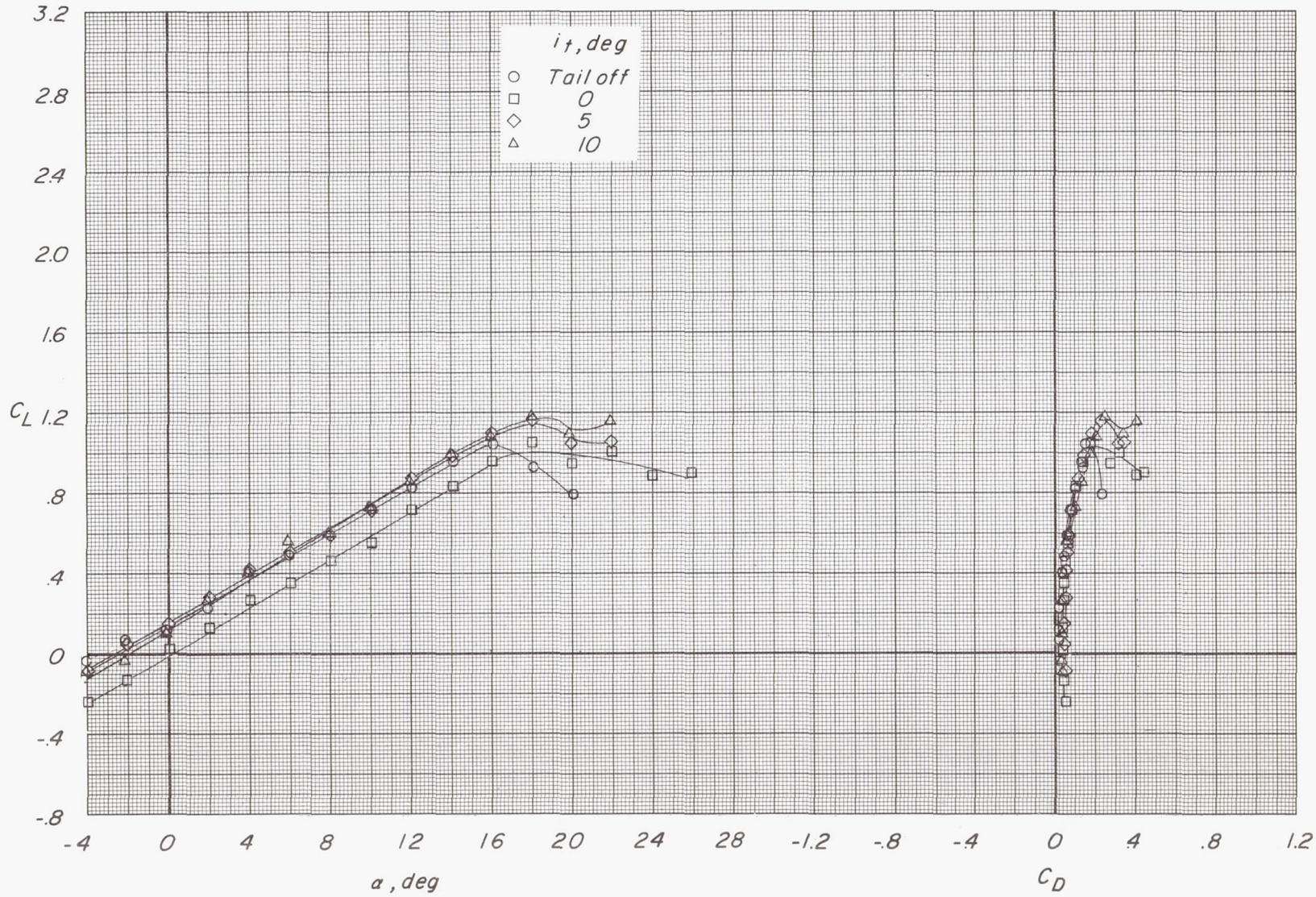

(a) Variation of C_L with α and C_D.

Figure 13.- Effect of tail incidence on longitudinal aerodynamic characteristics. $\delta_f = 0^0$; $C_\mu = 0$; $C_T = 0$; $\delta_e = 0^0$.

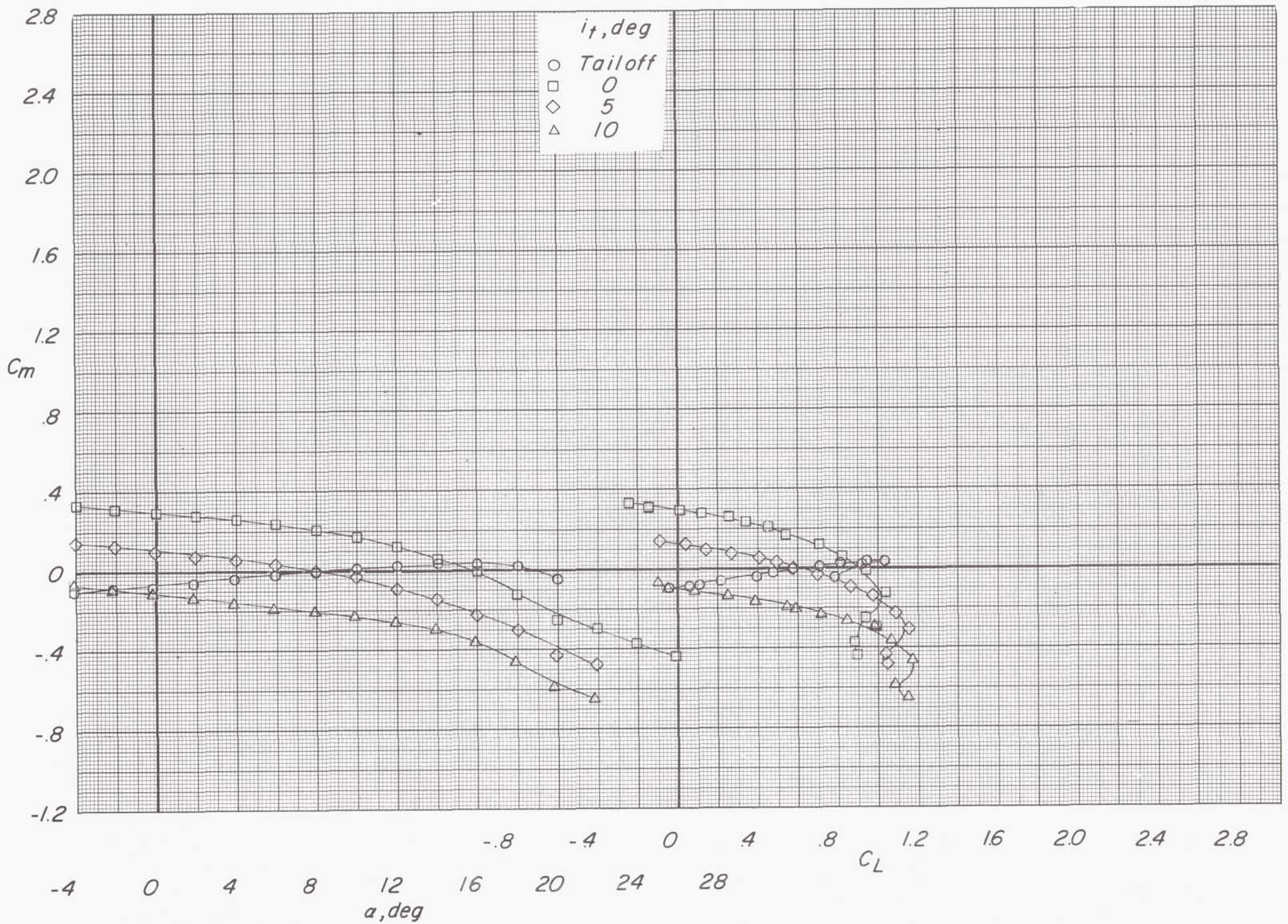

(b) Variation of C_m with α and C_L.

Figure 13.- Concluded.

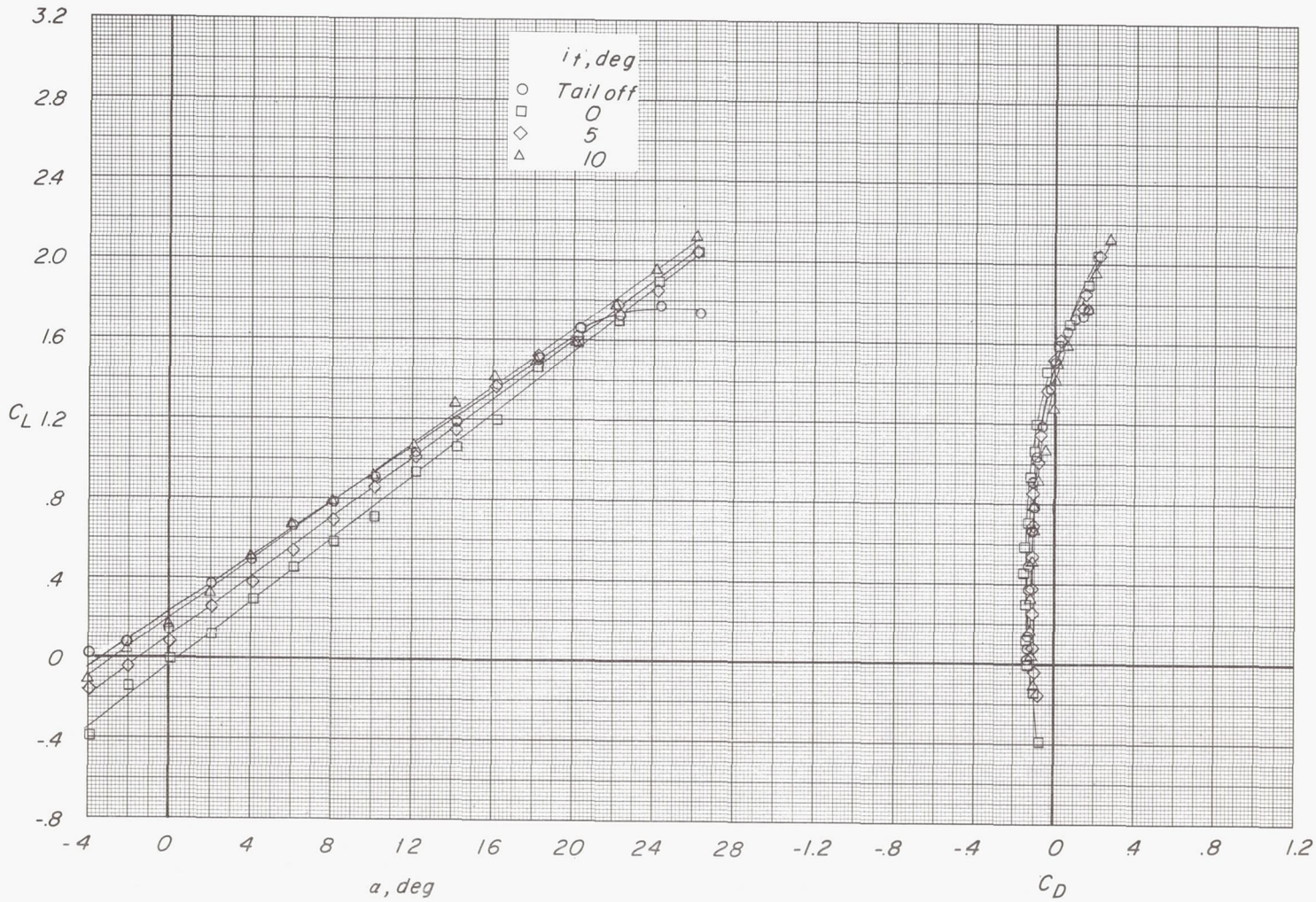

(a) Variation of C_L with α and C_D.

Figure 14.- Effect of tail incidence on longitudinal aerodynamic characteristics. $\delta_f = 0^o$; $C_\mu = 0$; $C_T = 0.14$; $\delta_e = 0^o$.

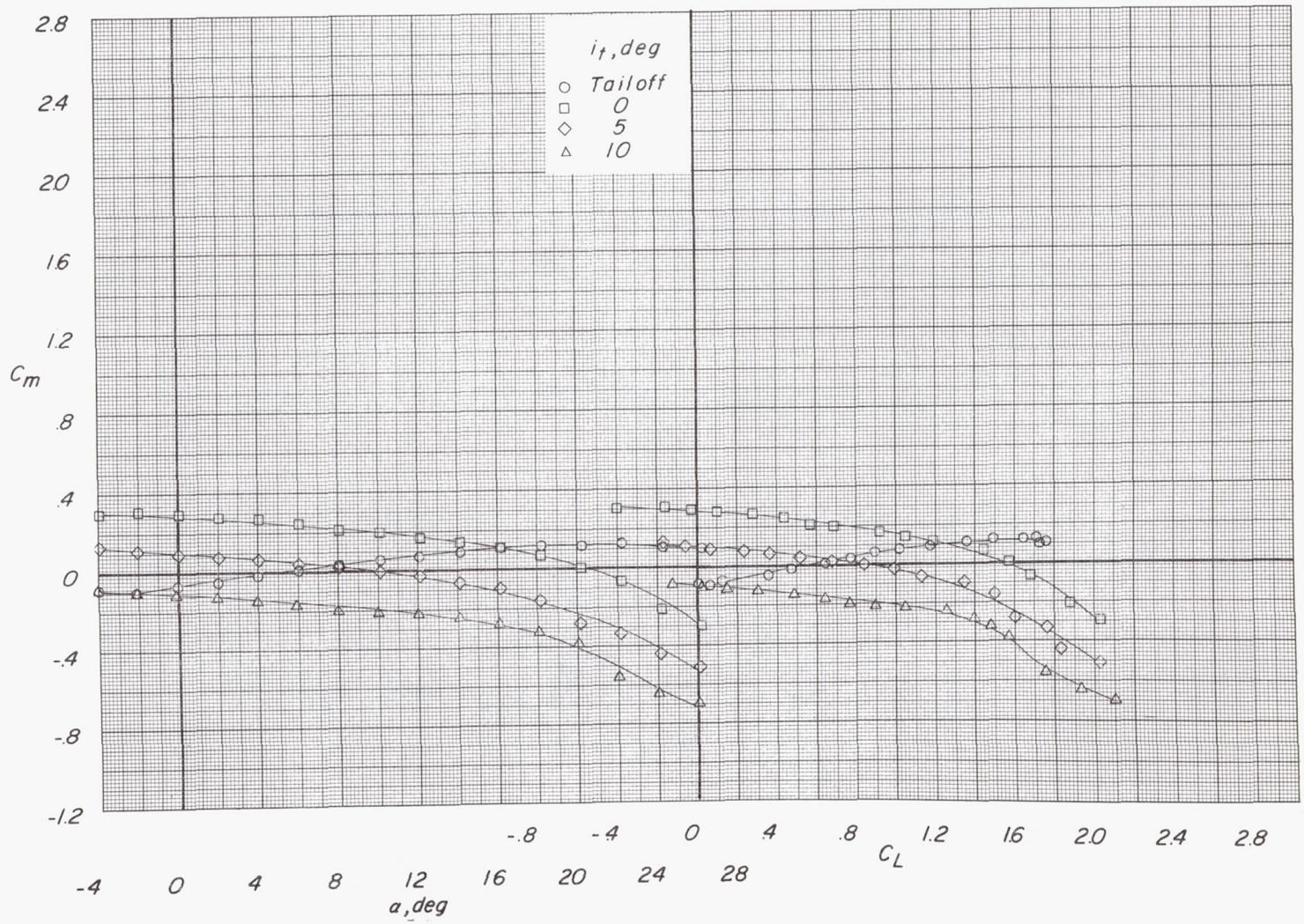

(b) Variation of C_m with α and C_L.

Figure 14.- Continued.

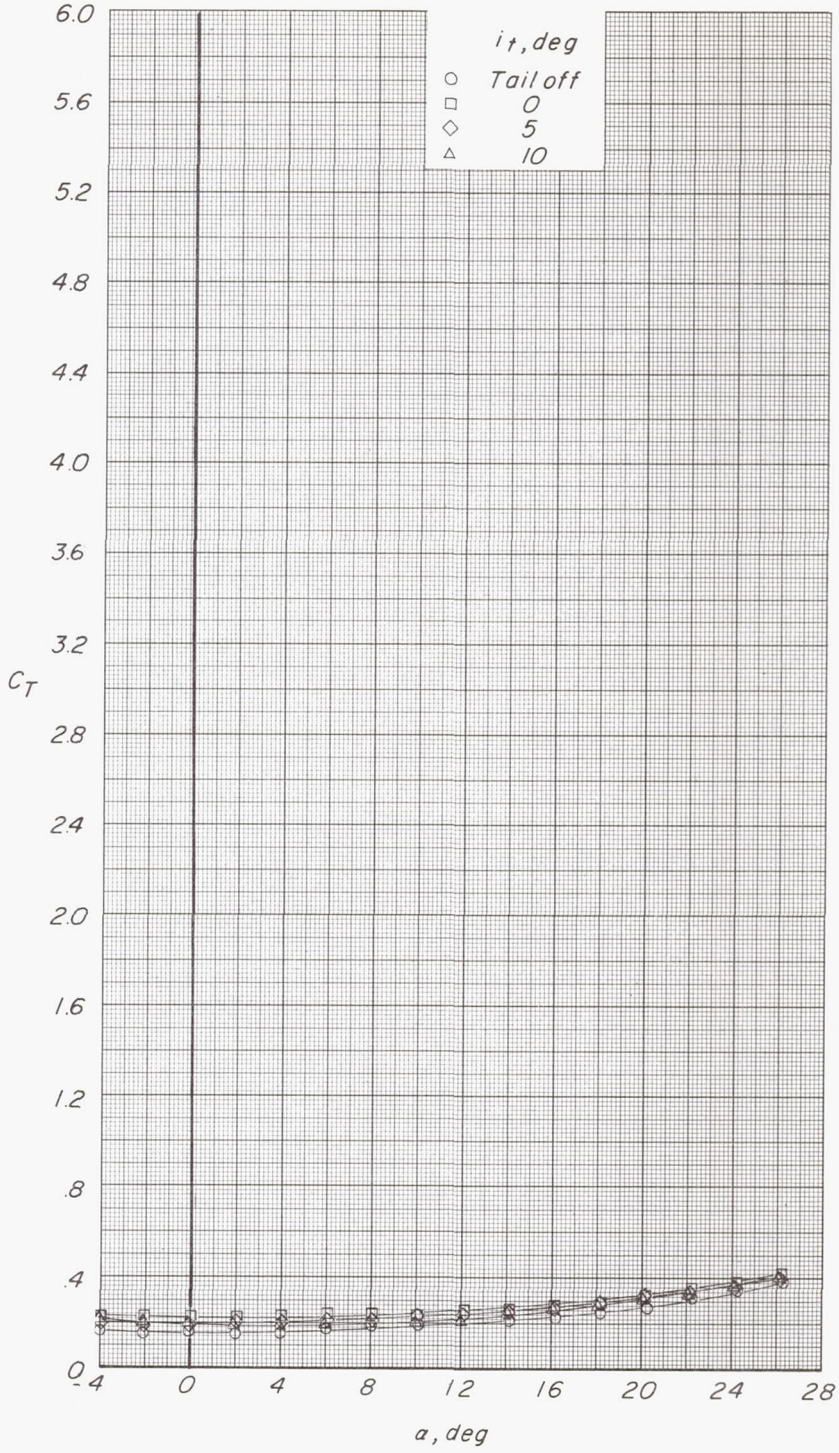

(c) Variation of C_T with α.

Figure 14.- Concluded.

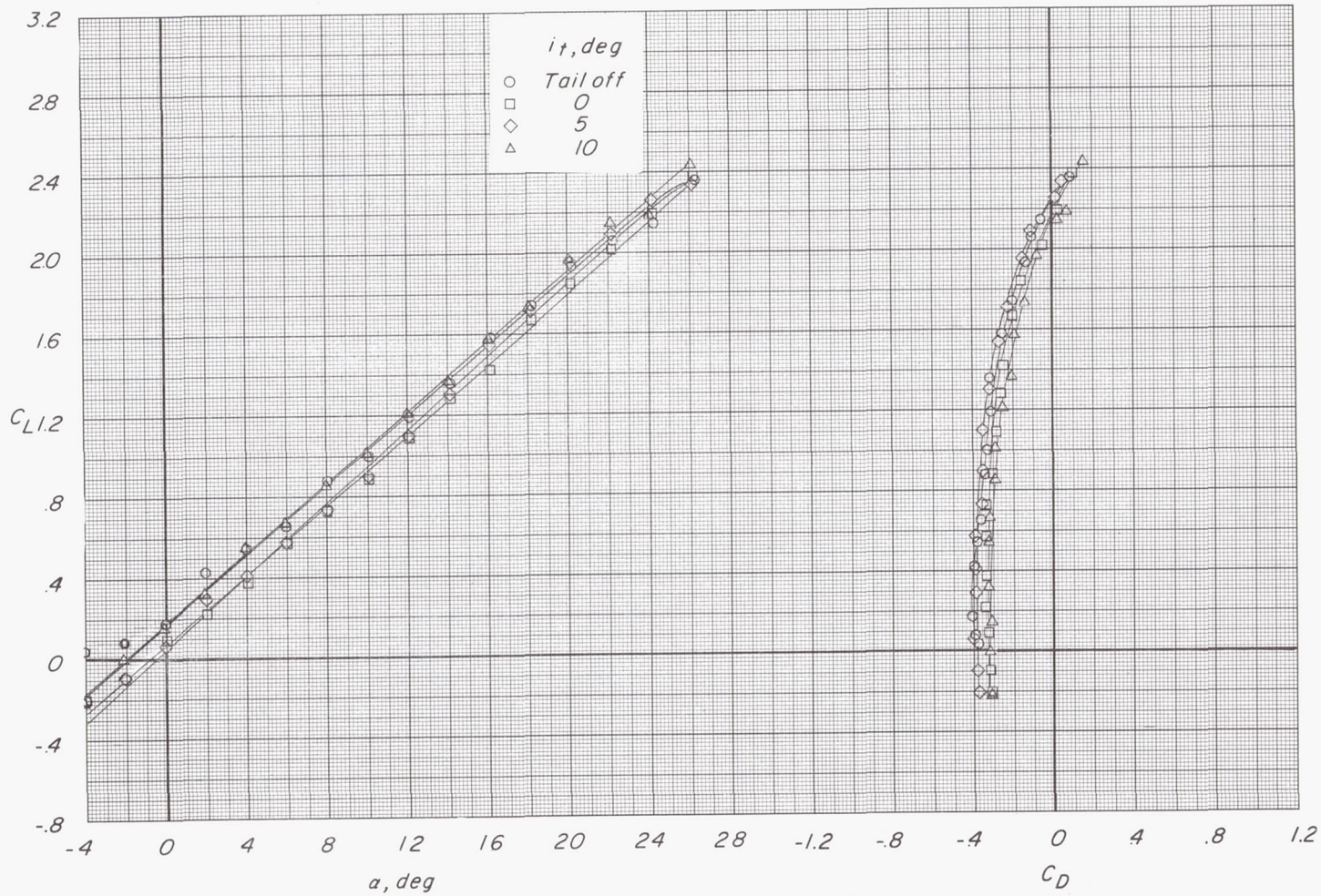

(a) Variation of C_L with α and C_D.

Figure 15.- Effect of tail incidence on longitudinal aerodynamic characteristics. $\delta_f = 0^o$; $C_\mu = 0$; $C_T = 0.43$; $\delta_e = 0^o$.

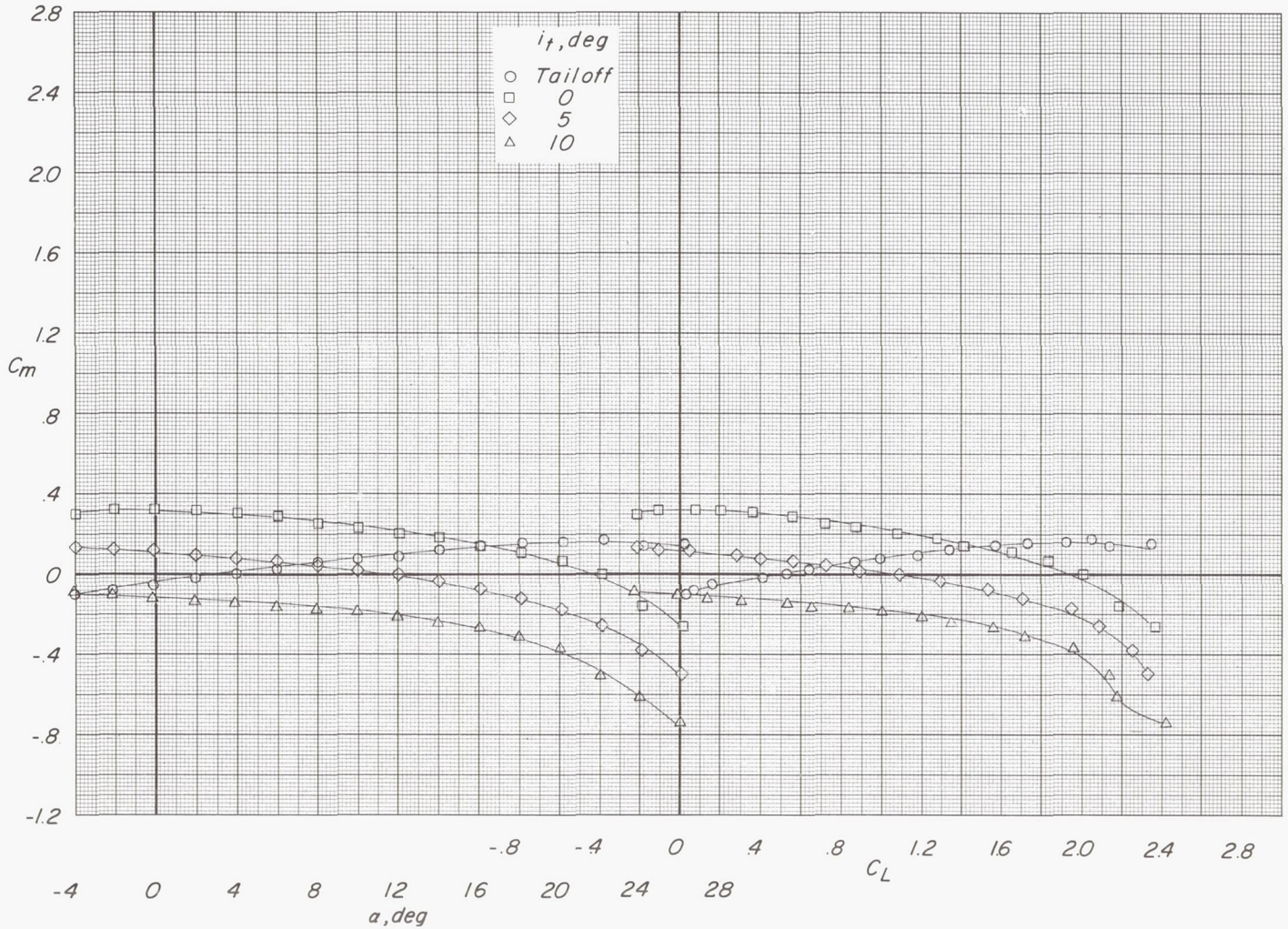

(b) Variation of C_m with α and C_L.

Figure 15.- Continued.

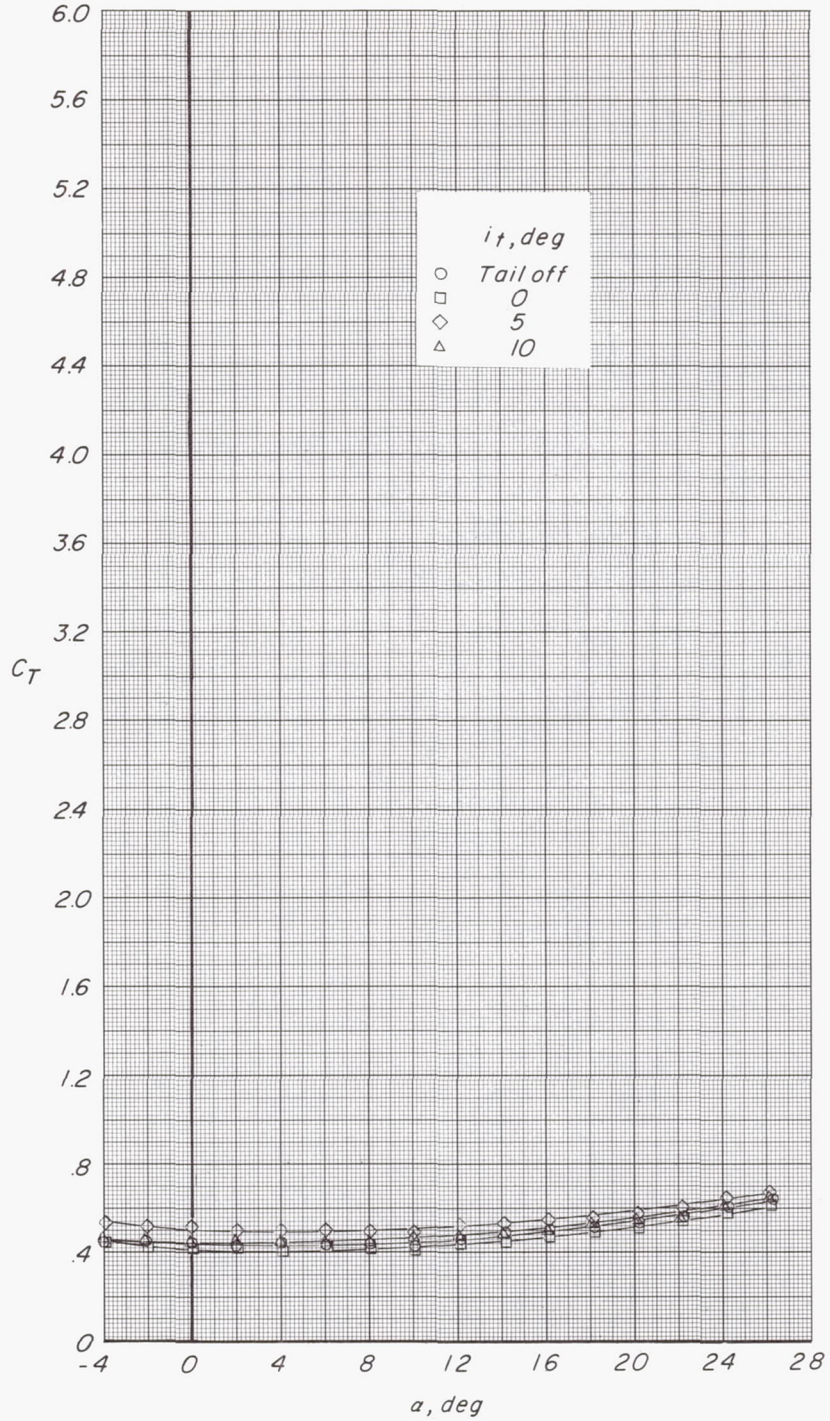

(c) Variation of C_T with α.

Figure 15.- Concluded.

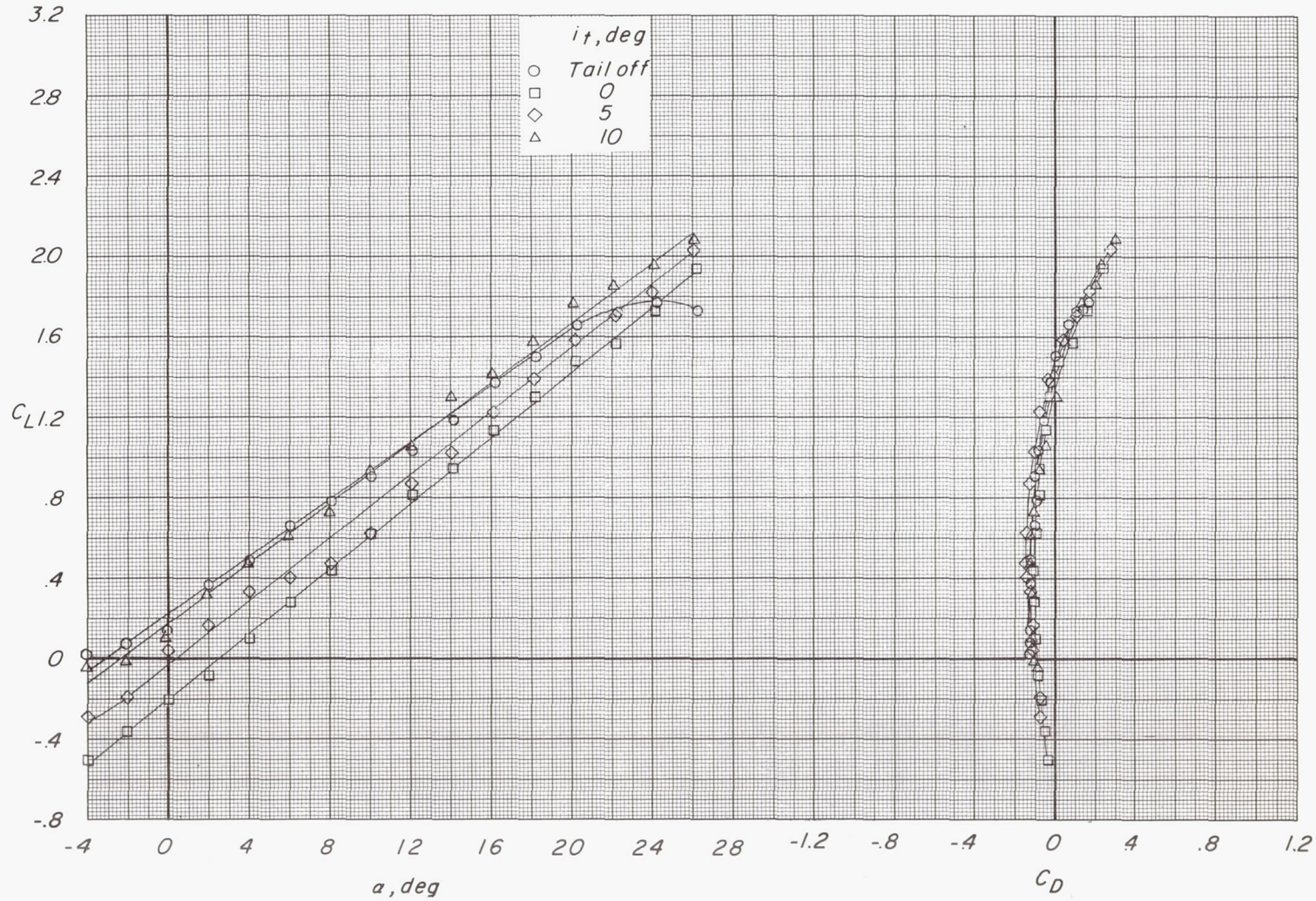

(a) Variation of C_L with α and C_D.

Figure 16.- Effect of tail incidence on longitudinal aerodynamic characteristics. $\delta_f = 0^o$; $C_\mu = 0.02$; $C_T = 0.14$; $\delta_e = 0^o$.

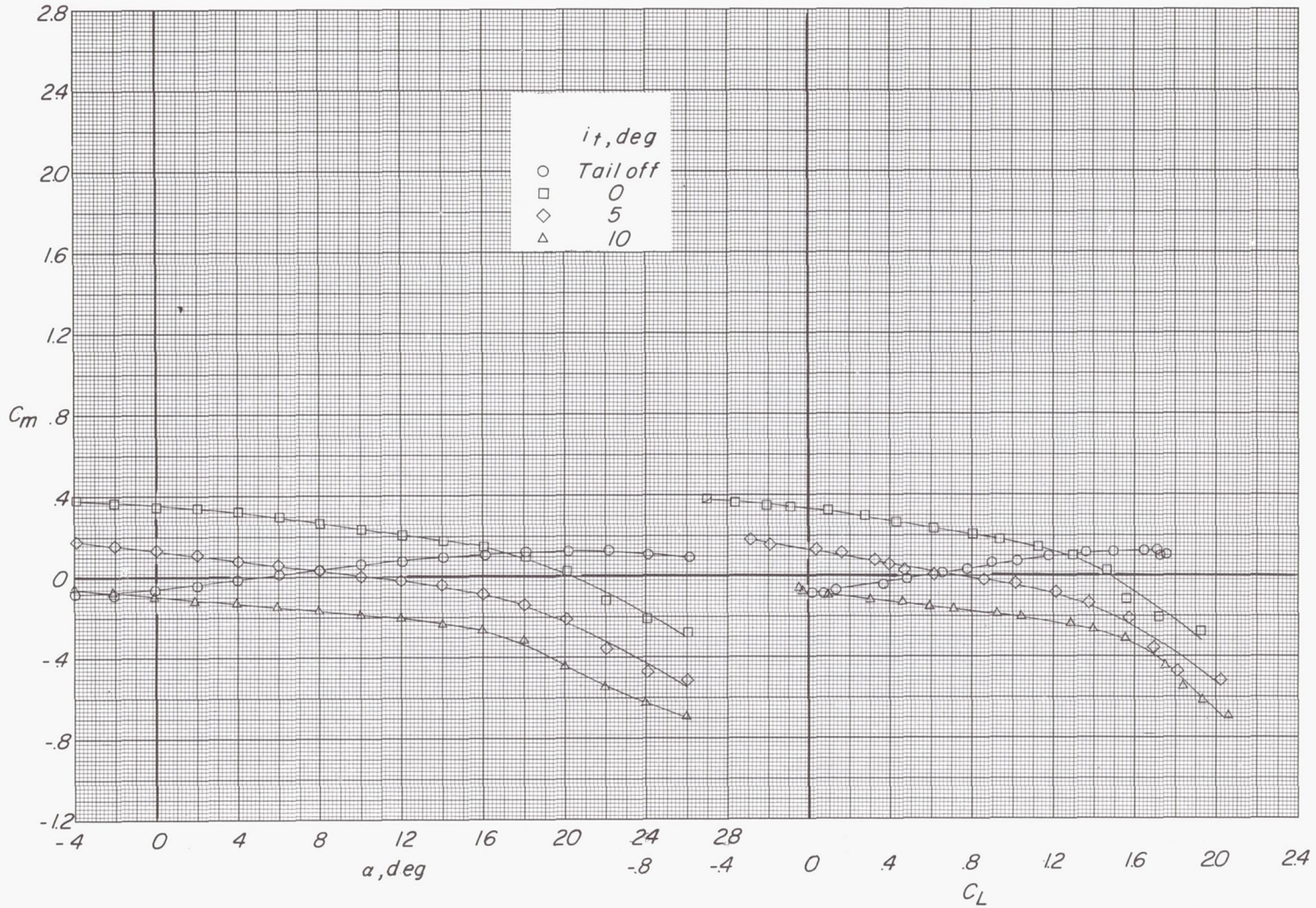

(b) Variation of C_m with α and C_L.

Figure 16.- Continued.

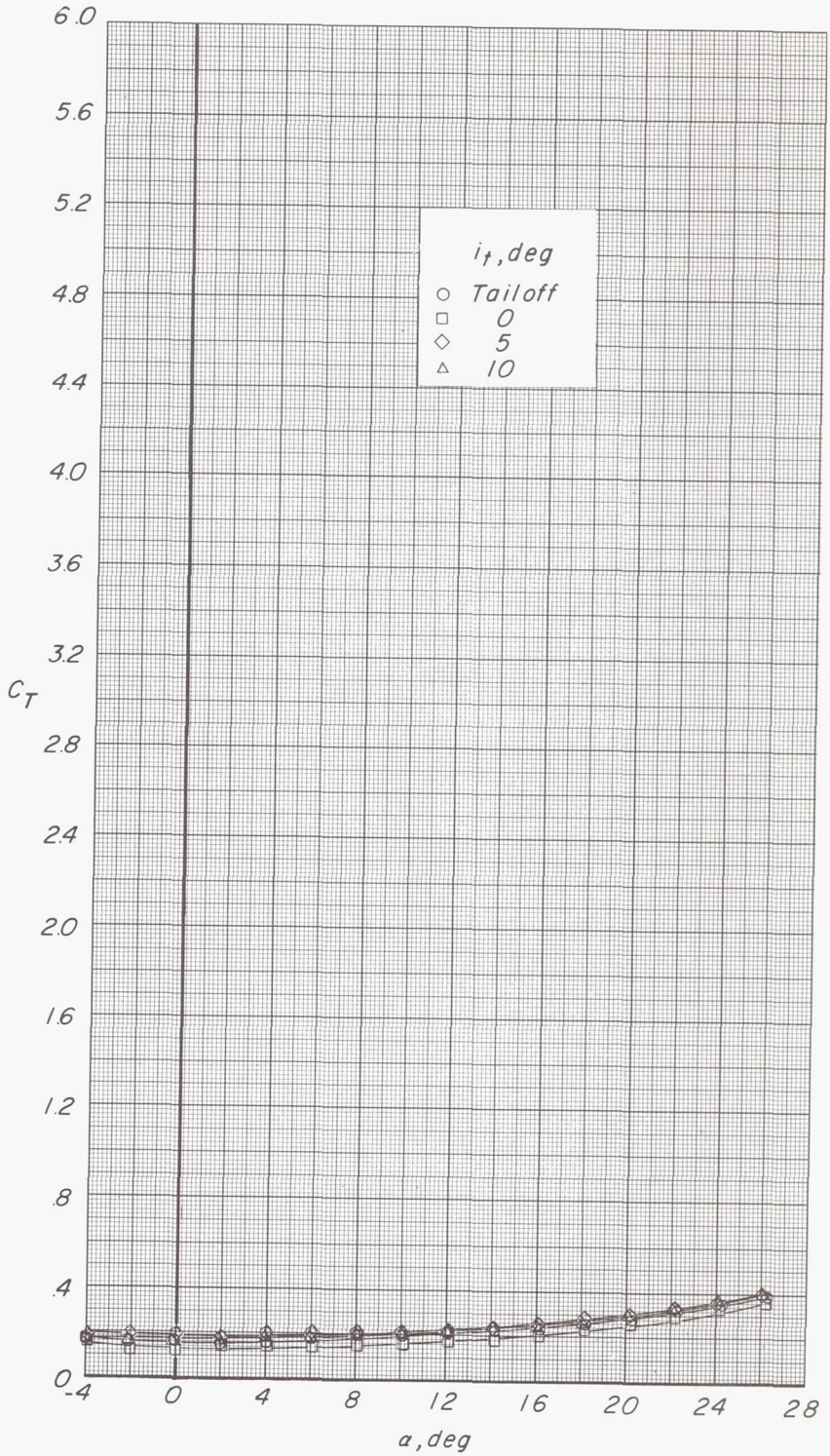

(c) Variation of C_T with α.

Figure 16.- Concluded.

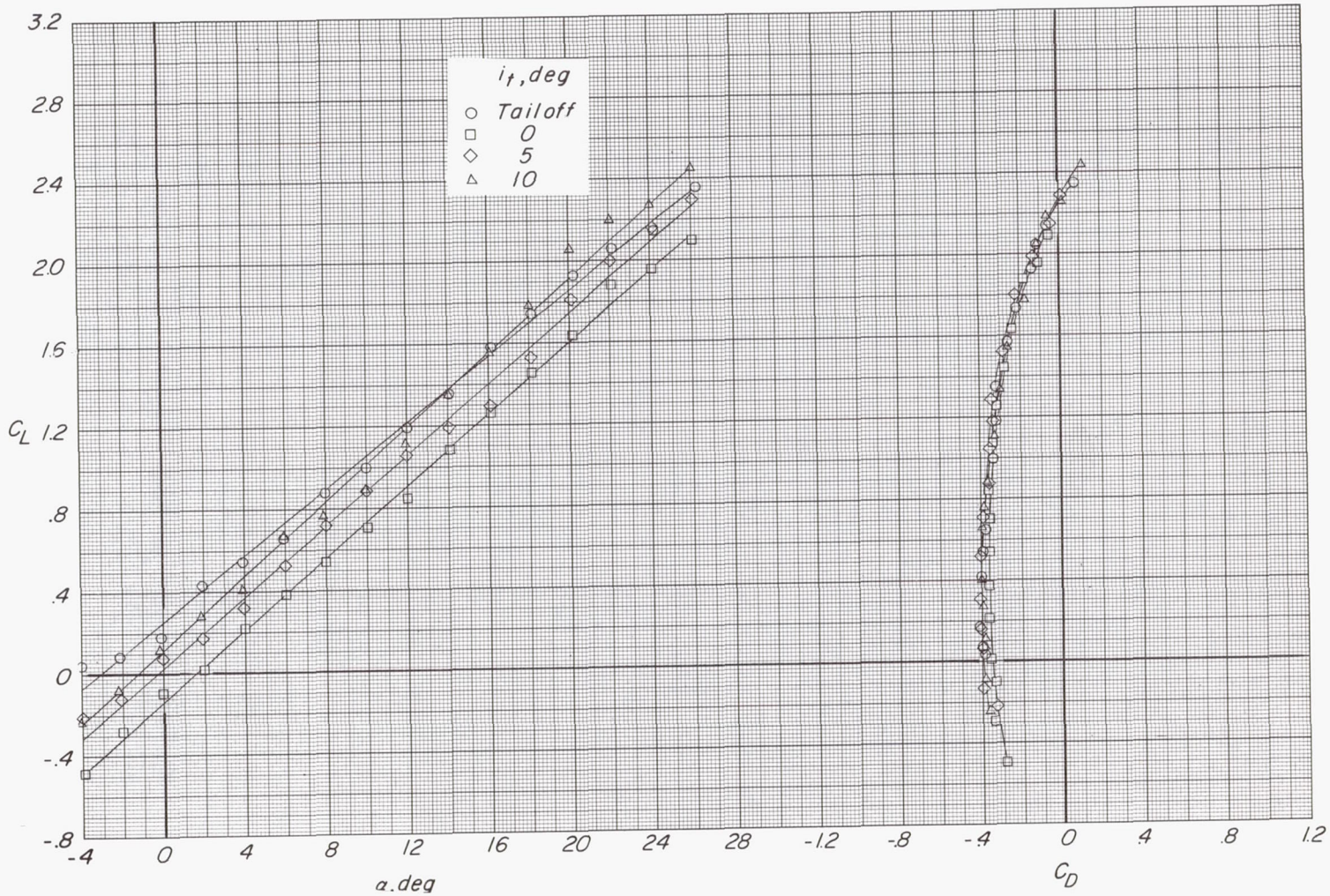

(a) Variation of C_L with α and C_D.

Figure 17.- Effect of tail incidence on longitudinal aerodynamic characteristics. $\delta_f = 0^0$; $C_\mu = 0.05$; $C_T = 0.43$; $\delta_e = 0^0$.

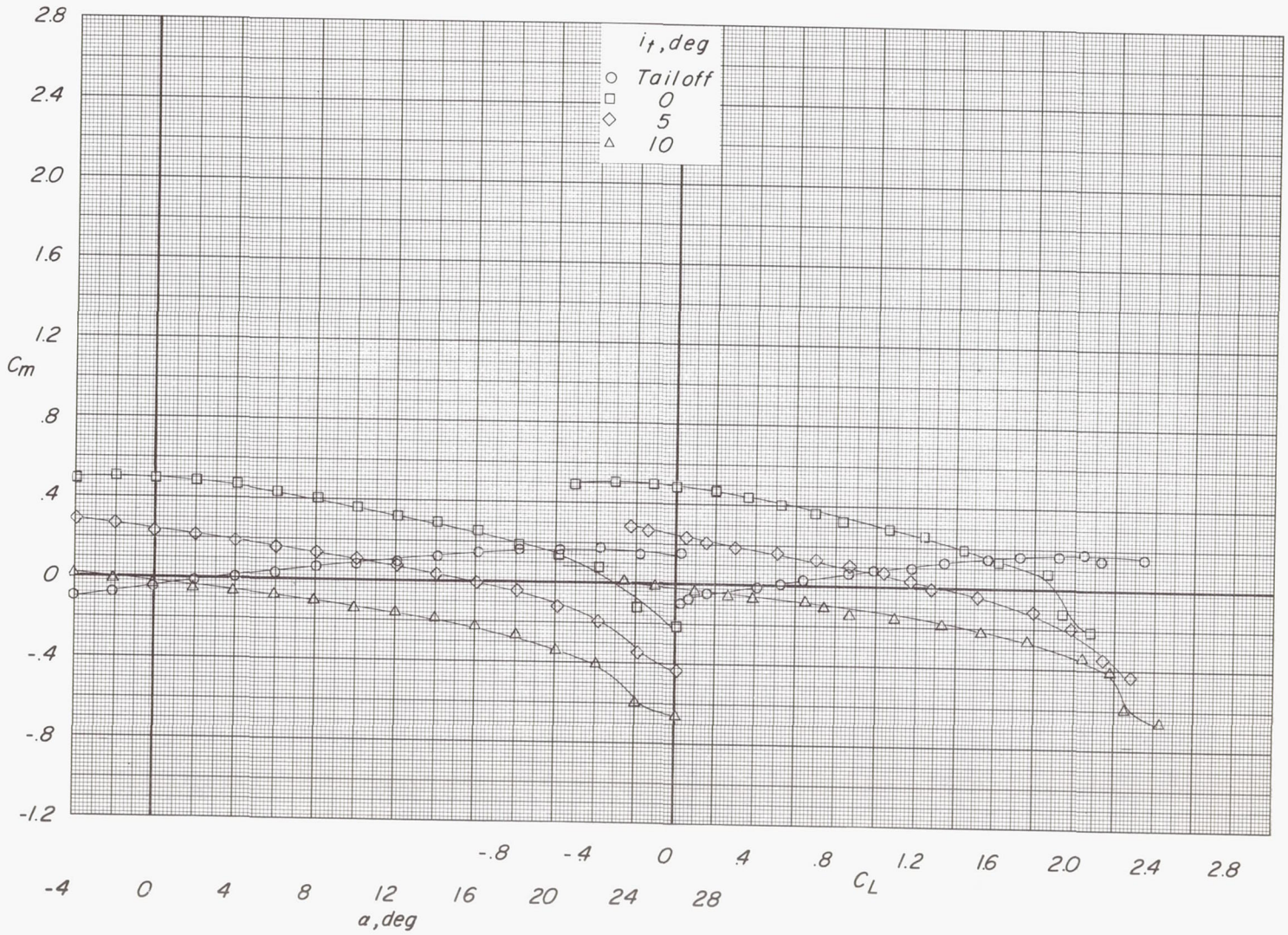

(b) Variation of C_m with α and C_L.

Figure 17.- Continued.

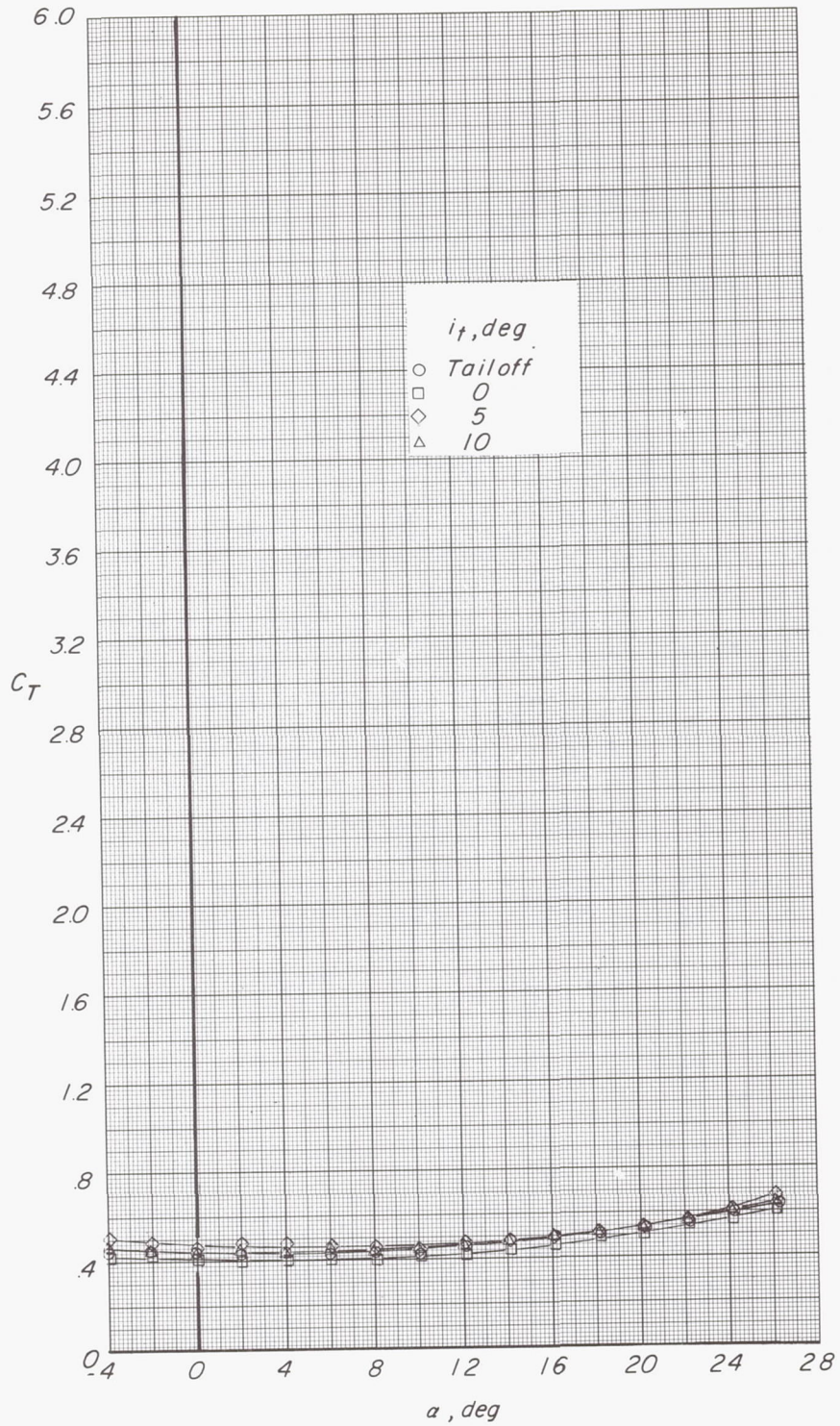

(c) Variation of C_T with α.

Figure 17.- Concluded.

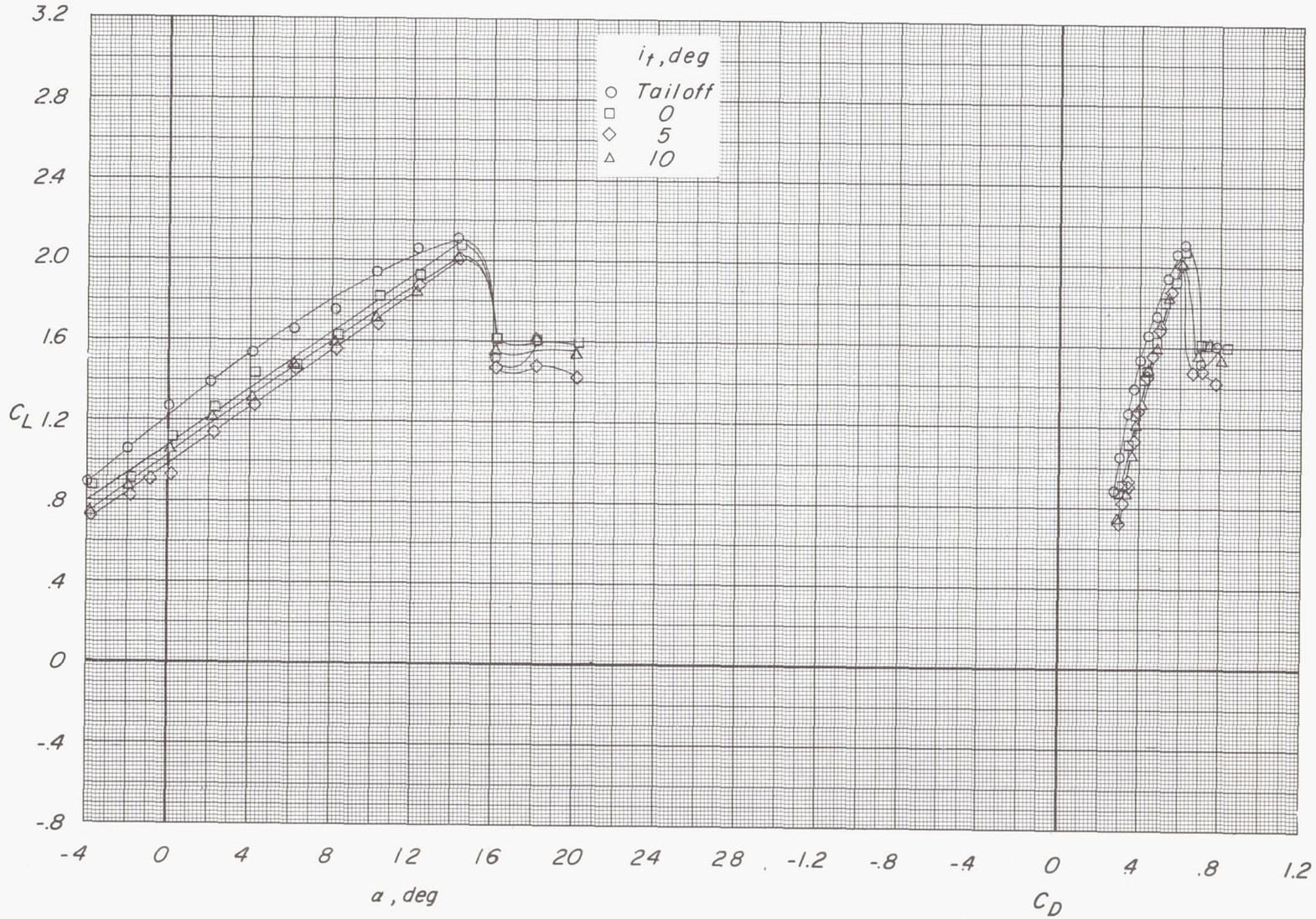

(a) Variation of C_L with α and C_D.

Figure 18.- Effect of tail incidence on longitudinal aerodynamic characteristics. $\delta_f = 45^o$; $C_\mu = 0$; $C_T = 0$; $\delta_e = 0^o$.

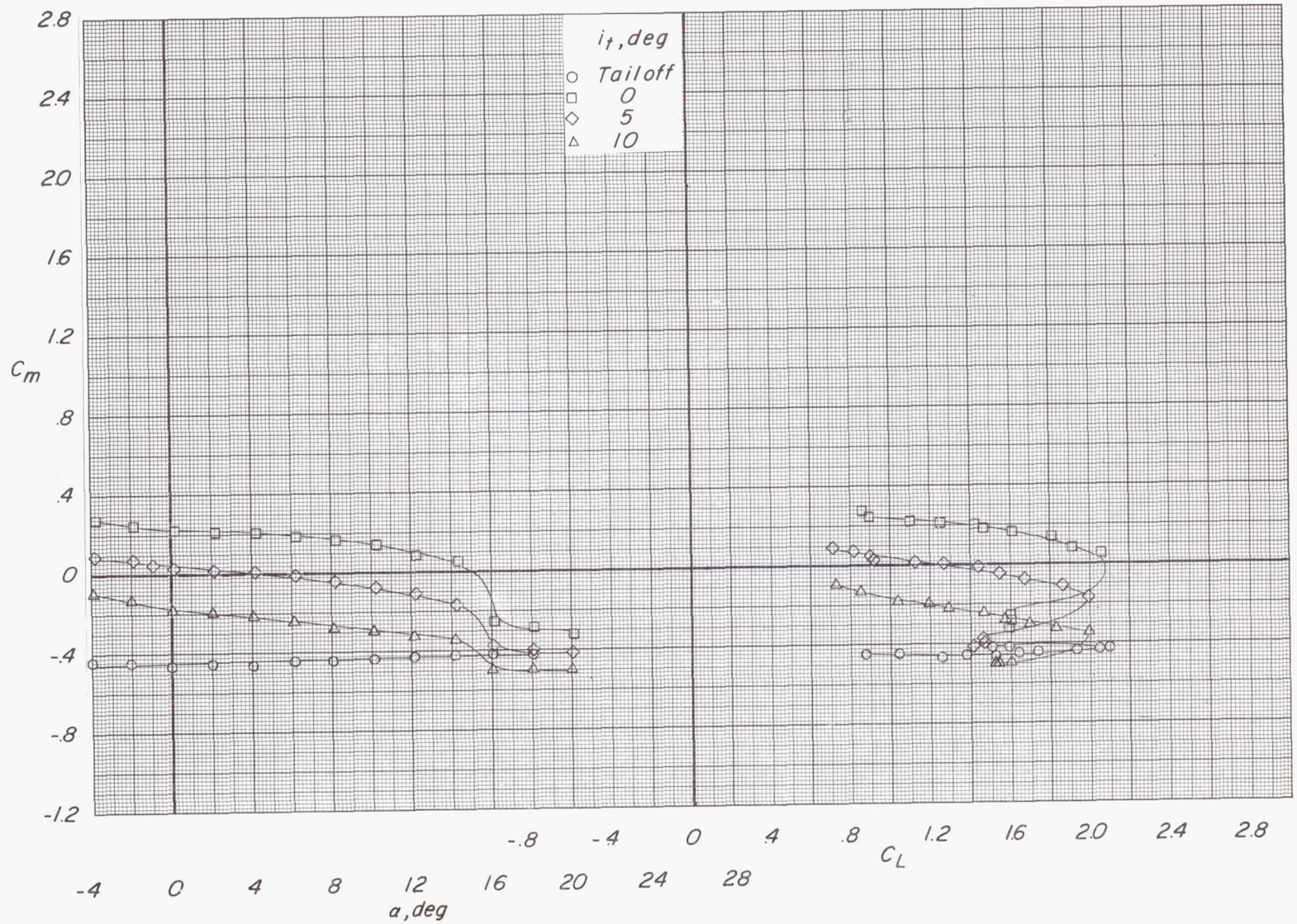

(b) Variation of C_m with α and C_L.

Figure 18.- Concluded.

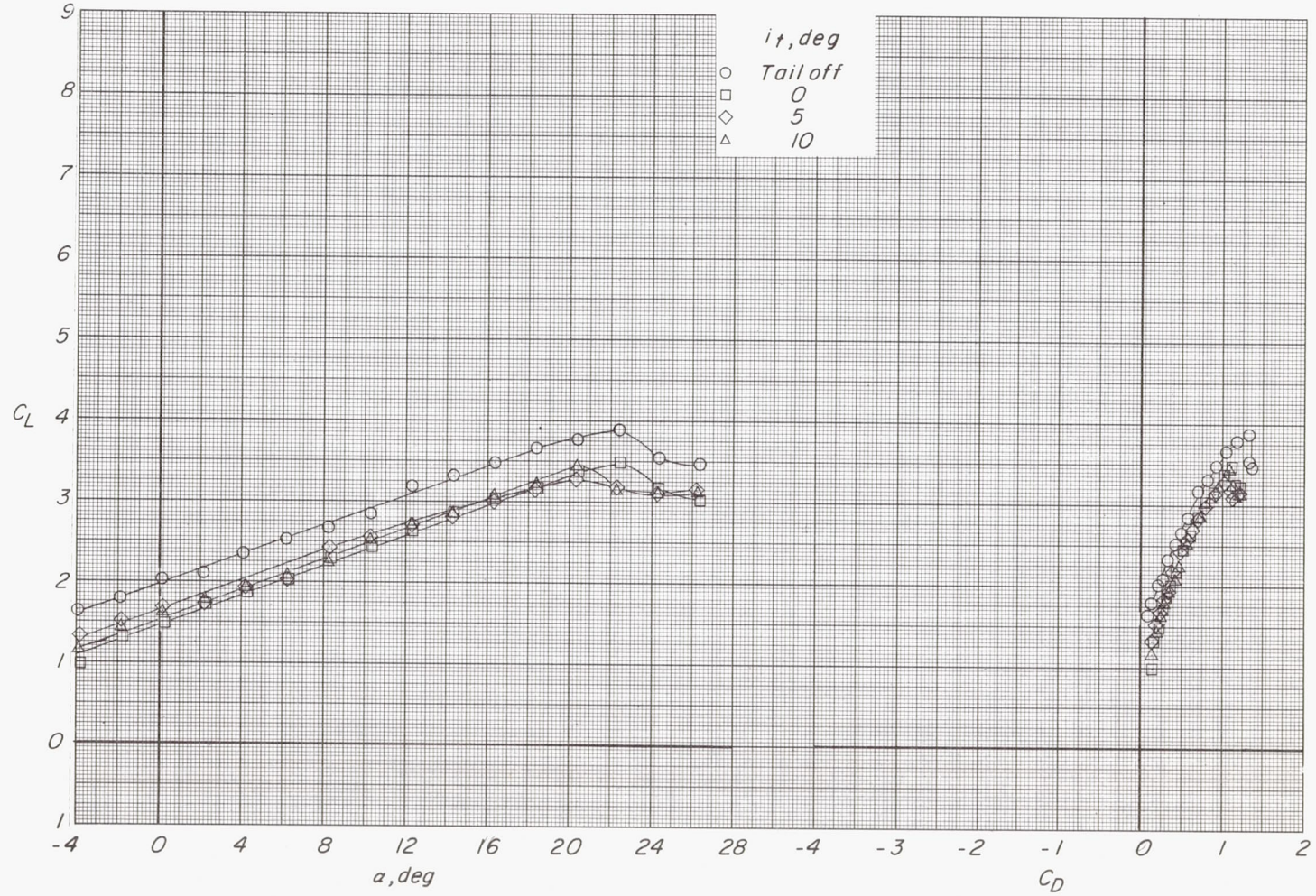

(a) Variation of C_L with α and C_D.

Figure 19.- Effect of tail incidence on longitudinal aerodynamic characteristics. $\delta_f = 45^o$; $C_\mu = 0$; $C_T = 0.43$; $\delta_e = 0^o$

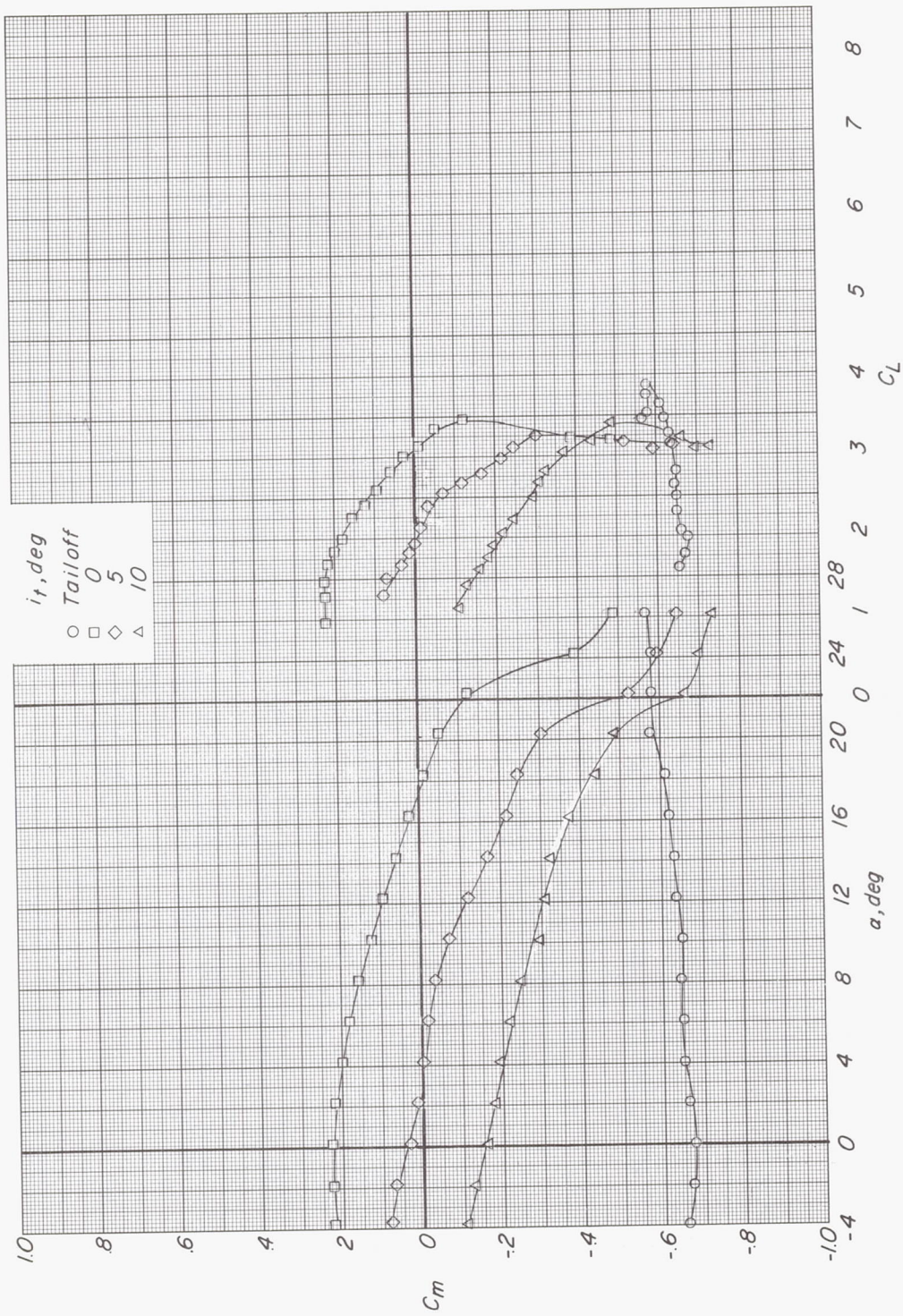

(b) Variation of C_m with α and C_L.

Figure 19.- Continued.

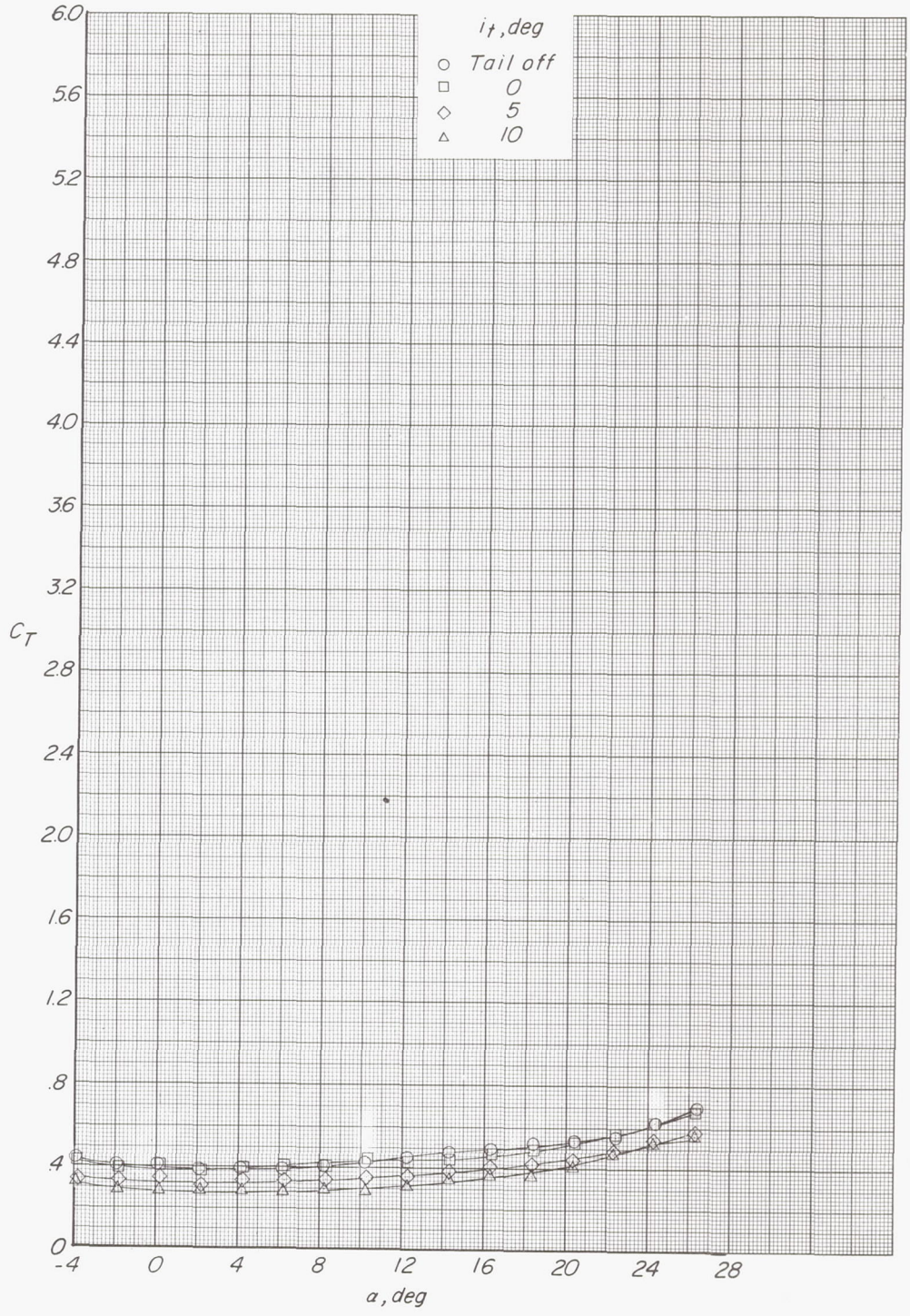

(c) Variation of C_T with α.

Figure 19.- Concluded.

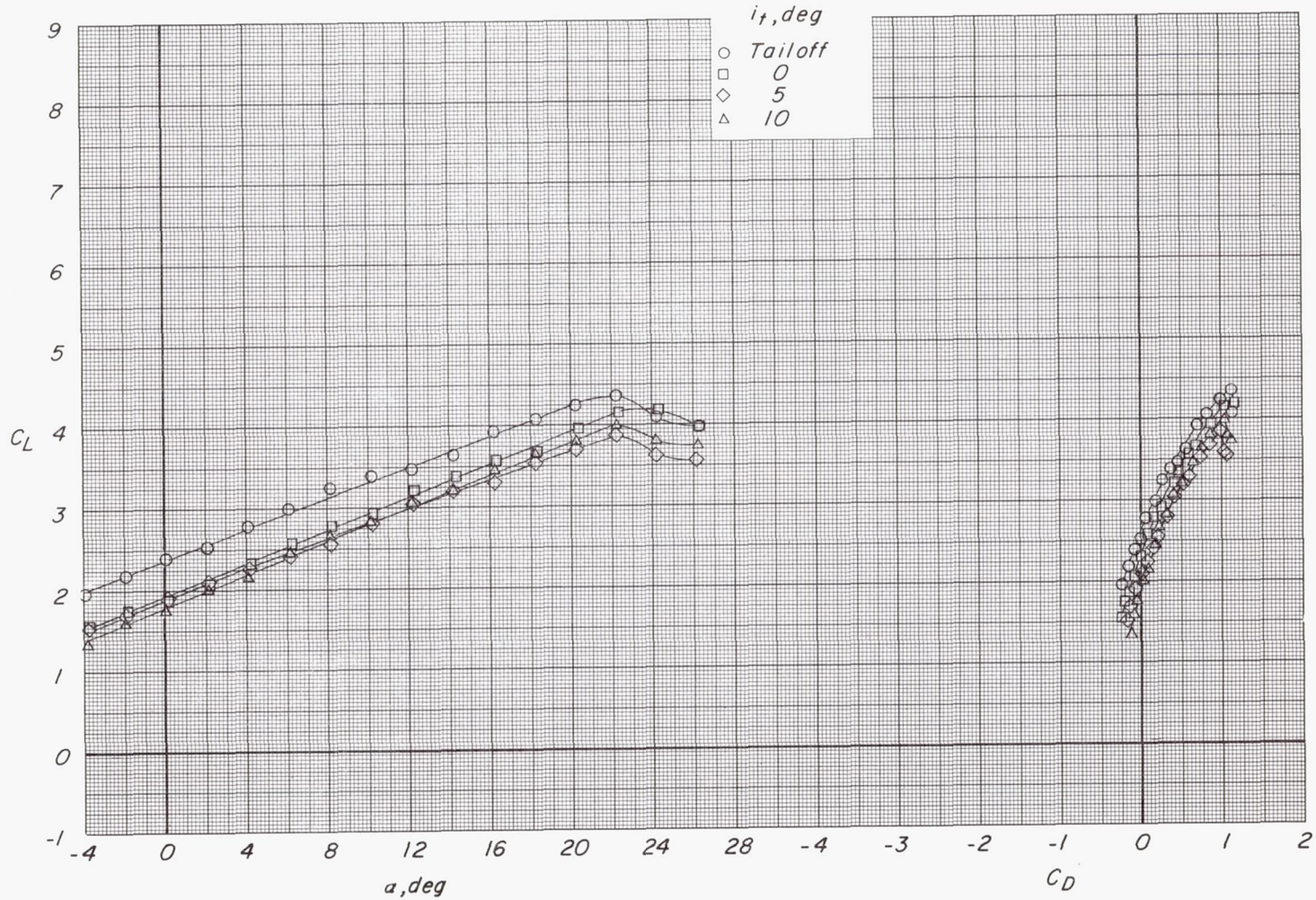

(a) Variation of C_L with α and C_D.

Figure 20.- Effect of tail incidence on longitudinal aerodynamic characteristics. $\delta_f = 45^0$; $C_\mu = 0$; $C_T = 0.83$; $\delta_e = 0^0$.

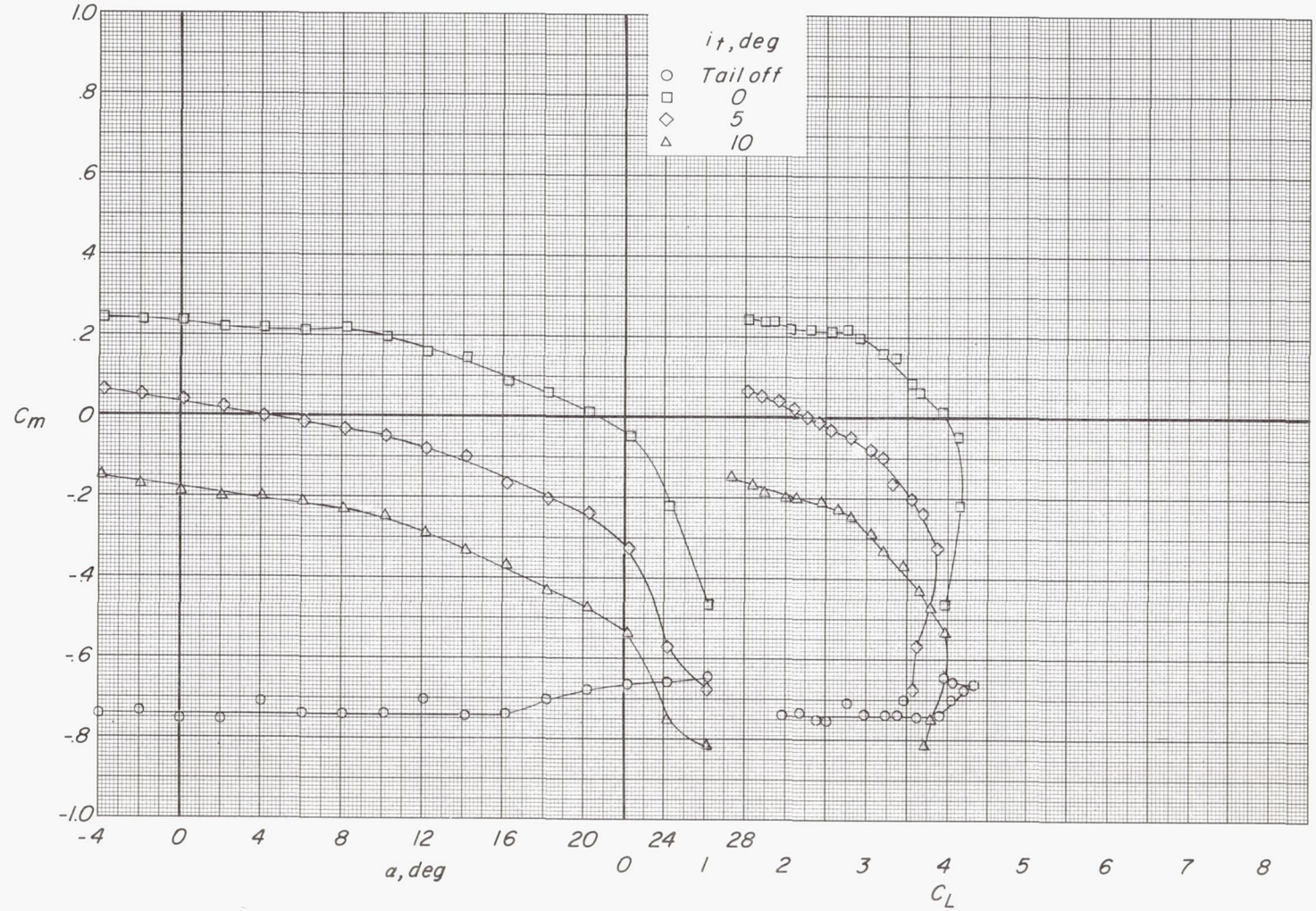

(b) Variation of C_m with α and C_L.

Figure 20.- Continued.

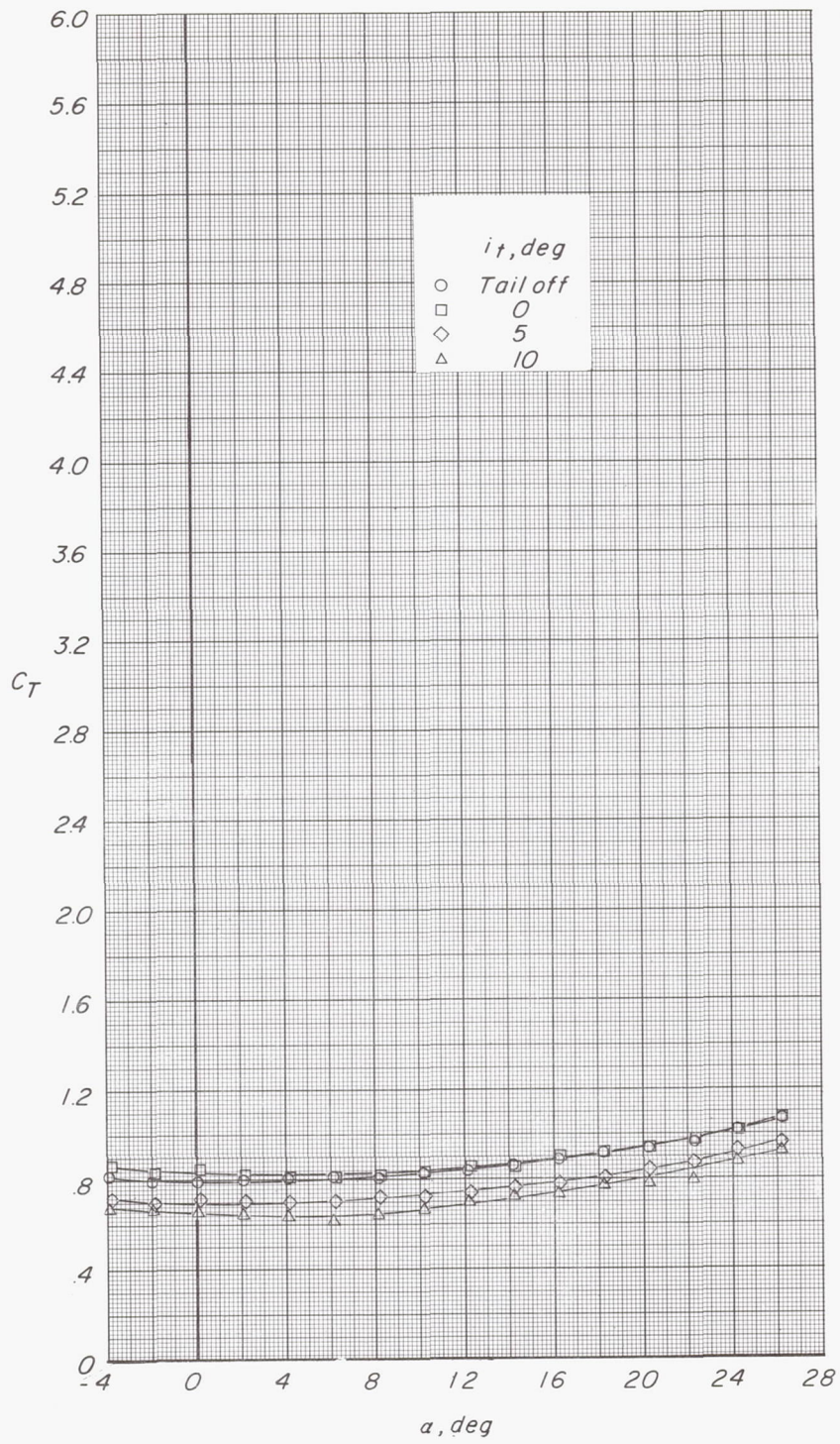

(c) Variation of C_T with α.

Figure 20.- Concluded.

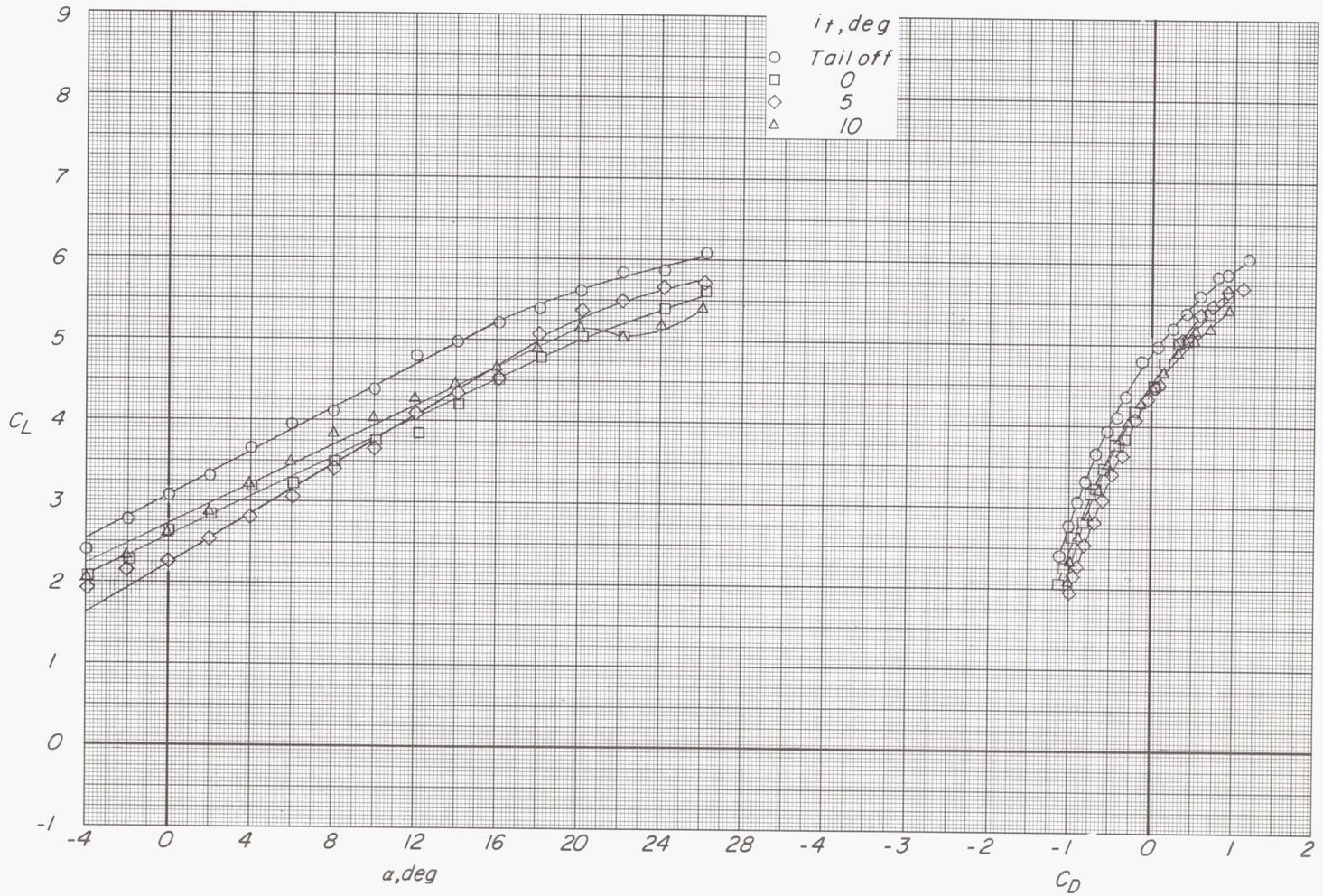

(a) Variation of C_L with α and C_D.

Figure 21.- Effect of tail incidence on longitudinal aerodynamic characteristics. $\delta_f = 45^o$; $C_\mu = 0$; $C_T = 2.10$; $\delta_e = 0^o$.

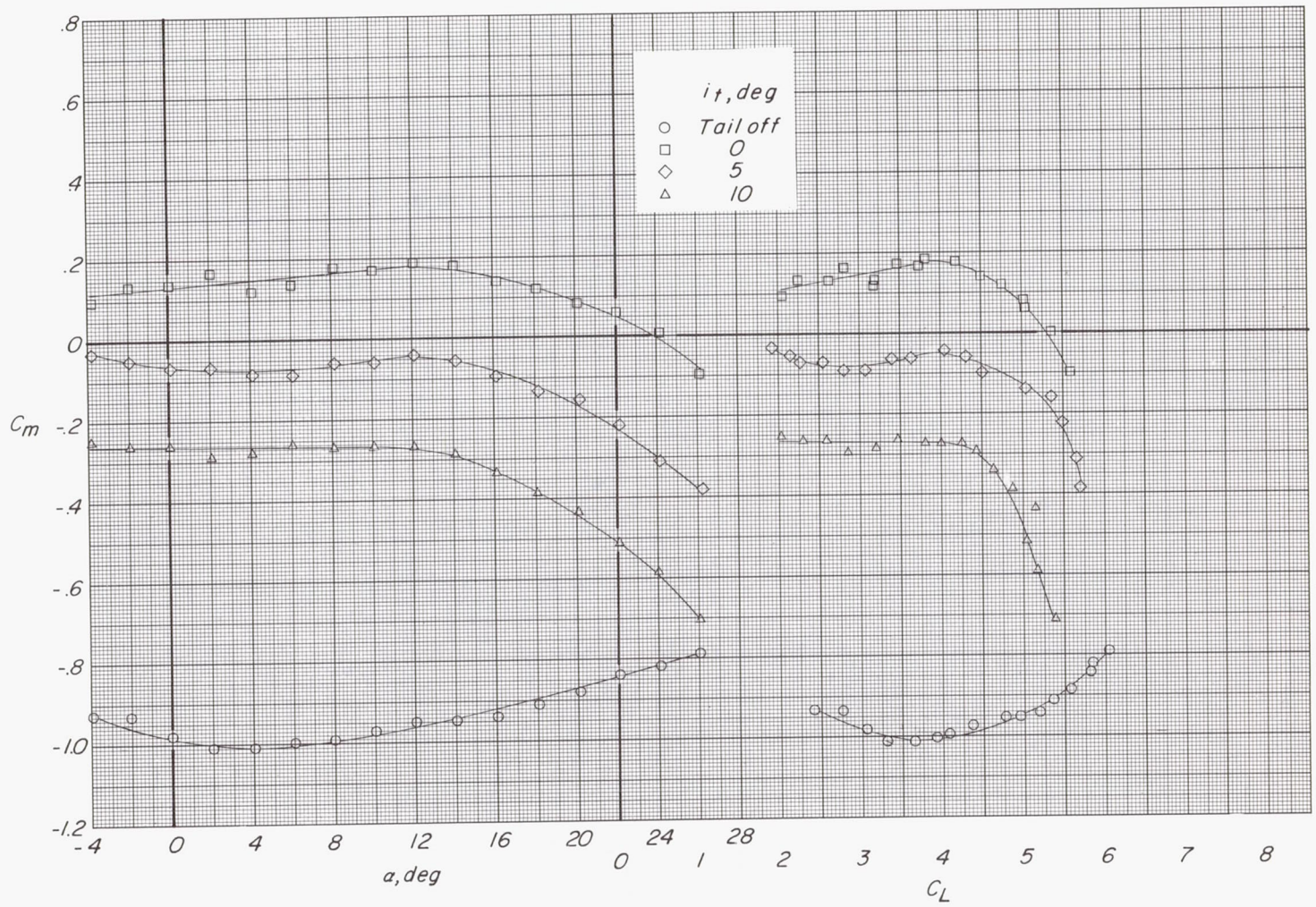

(b) Variation of C_m with α and C_L.

Figure 21.- Continued.

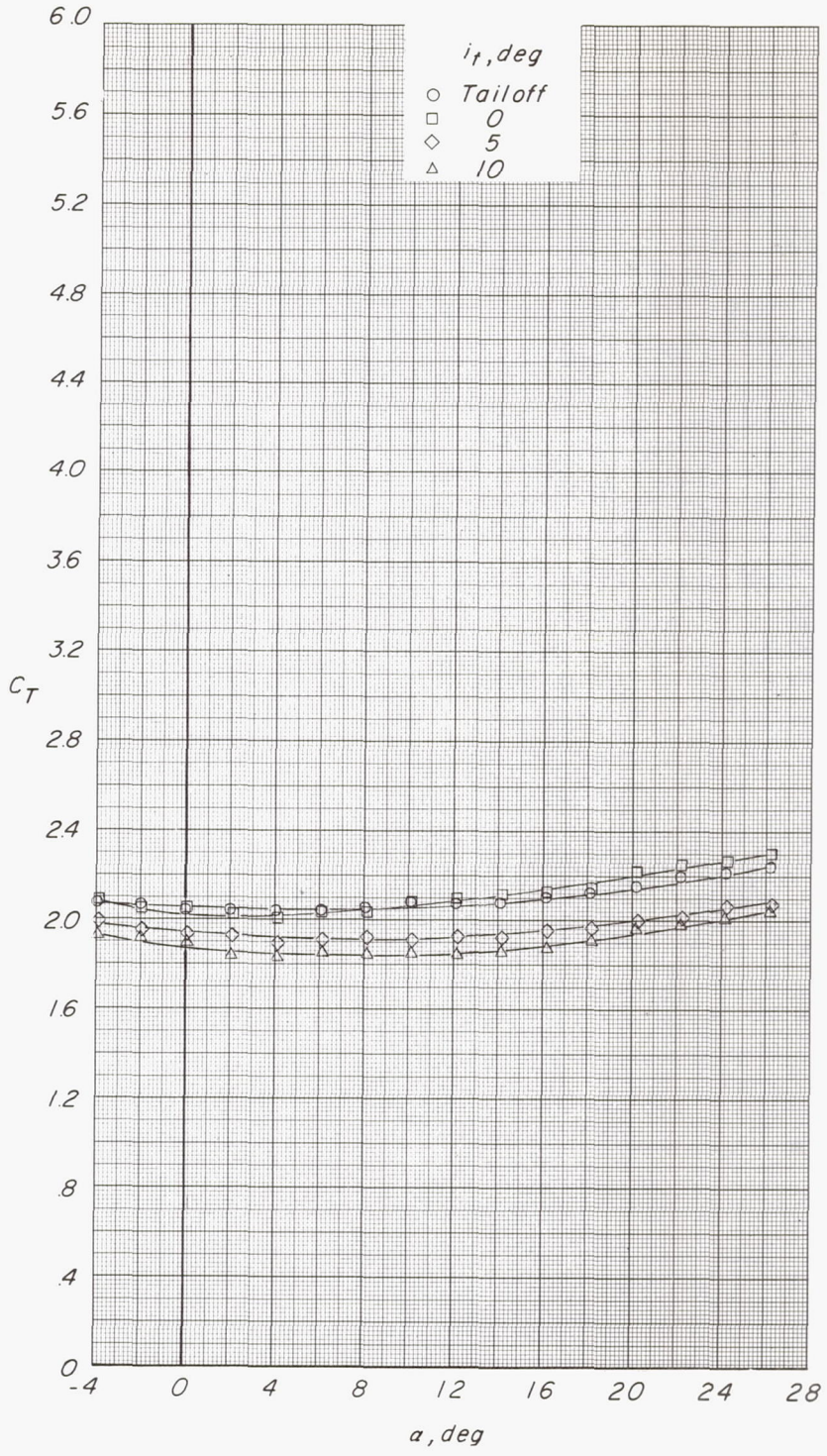

(c) Variation of C_T with α.

Figure 21.- Concluded.

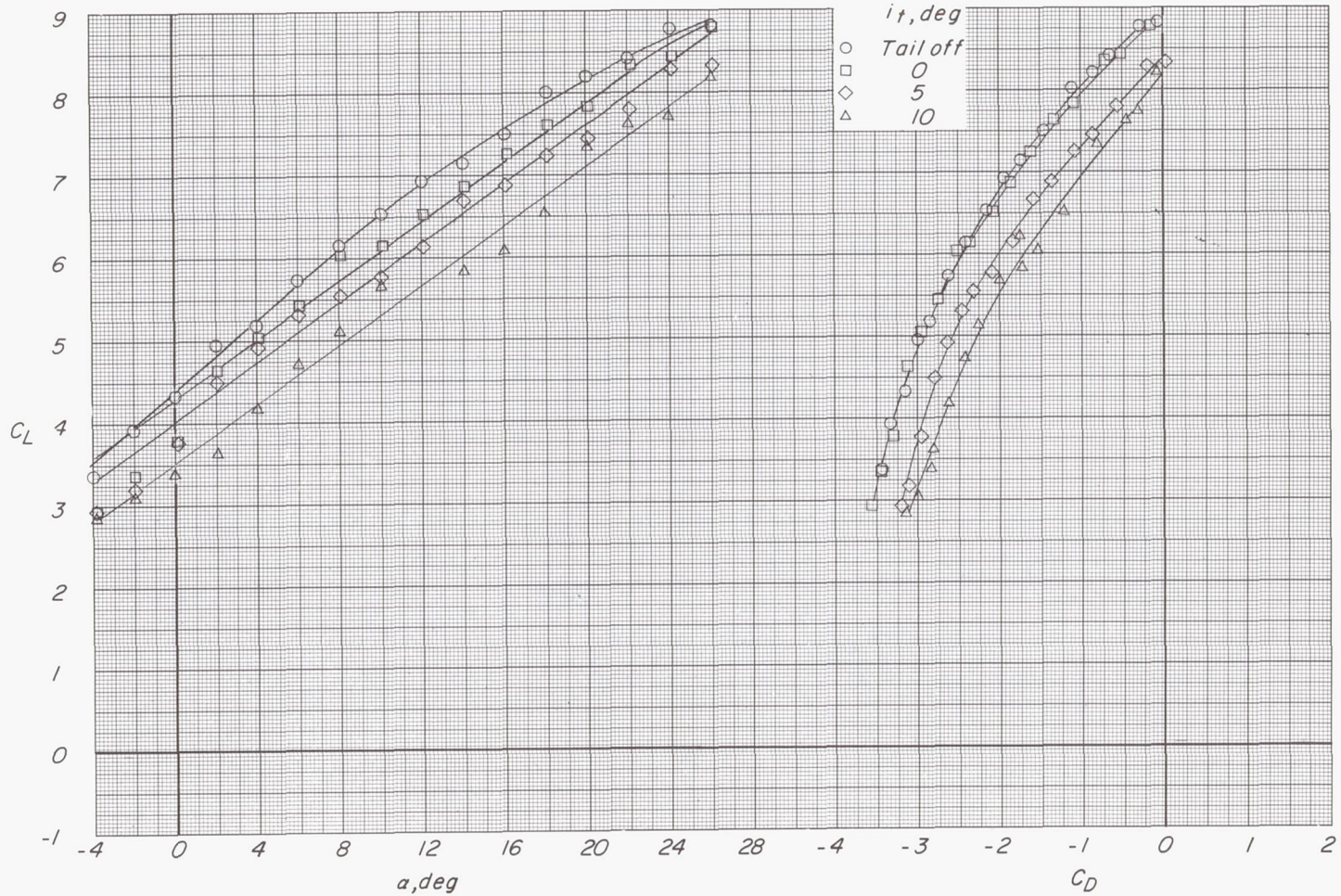

(a) Variation of C_L with α and C_D.

Figure 22.- Effect of tail incidence on longitudinal aerodynamic characteristics. $\delta_f = 45^0$; $C_\mu = 0$; $C_T = 5.10$; $\delta_e = 0^0$.

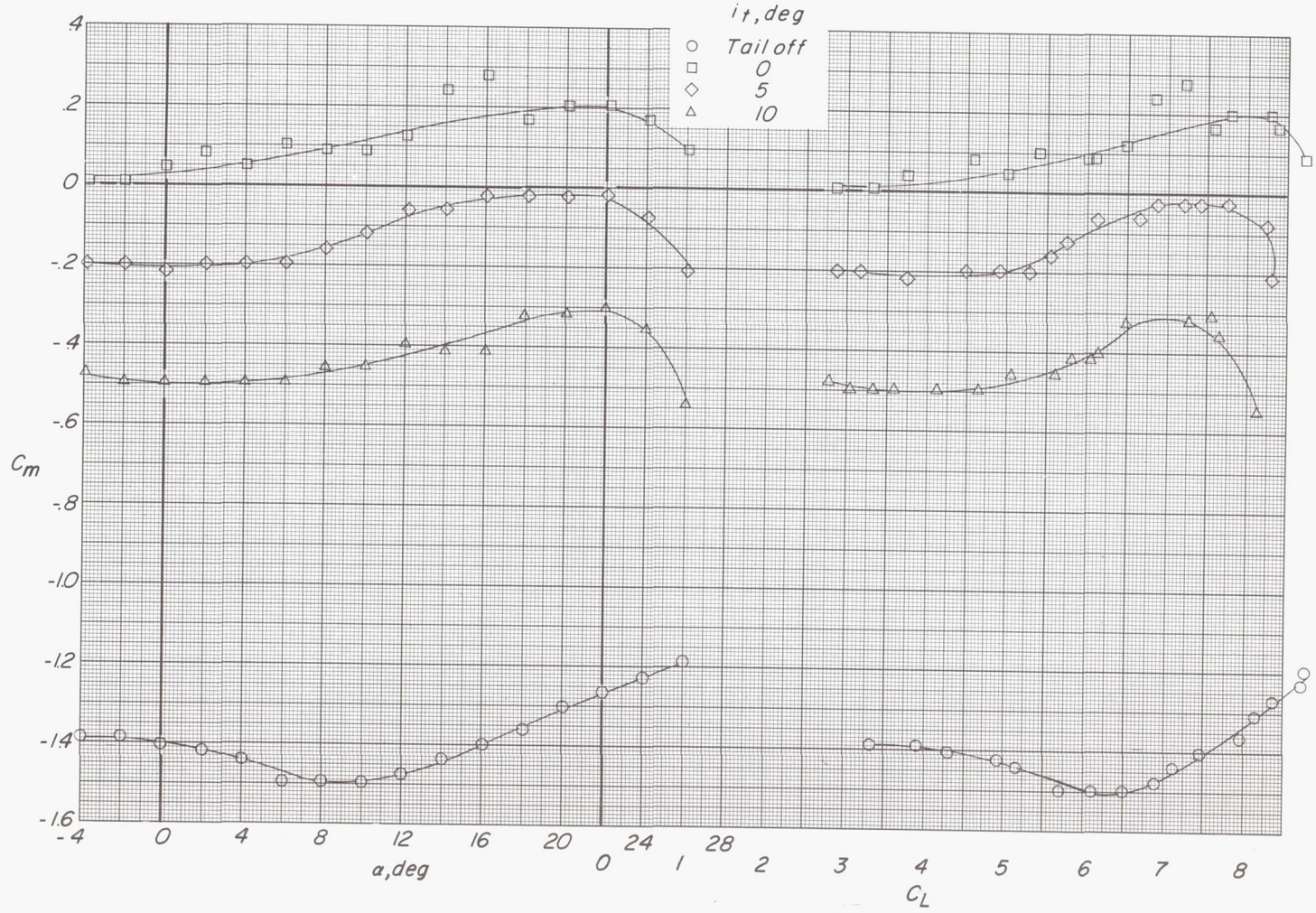

(b) Variation of C_m with α and C_L.

Figure 22.- Continued.

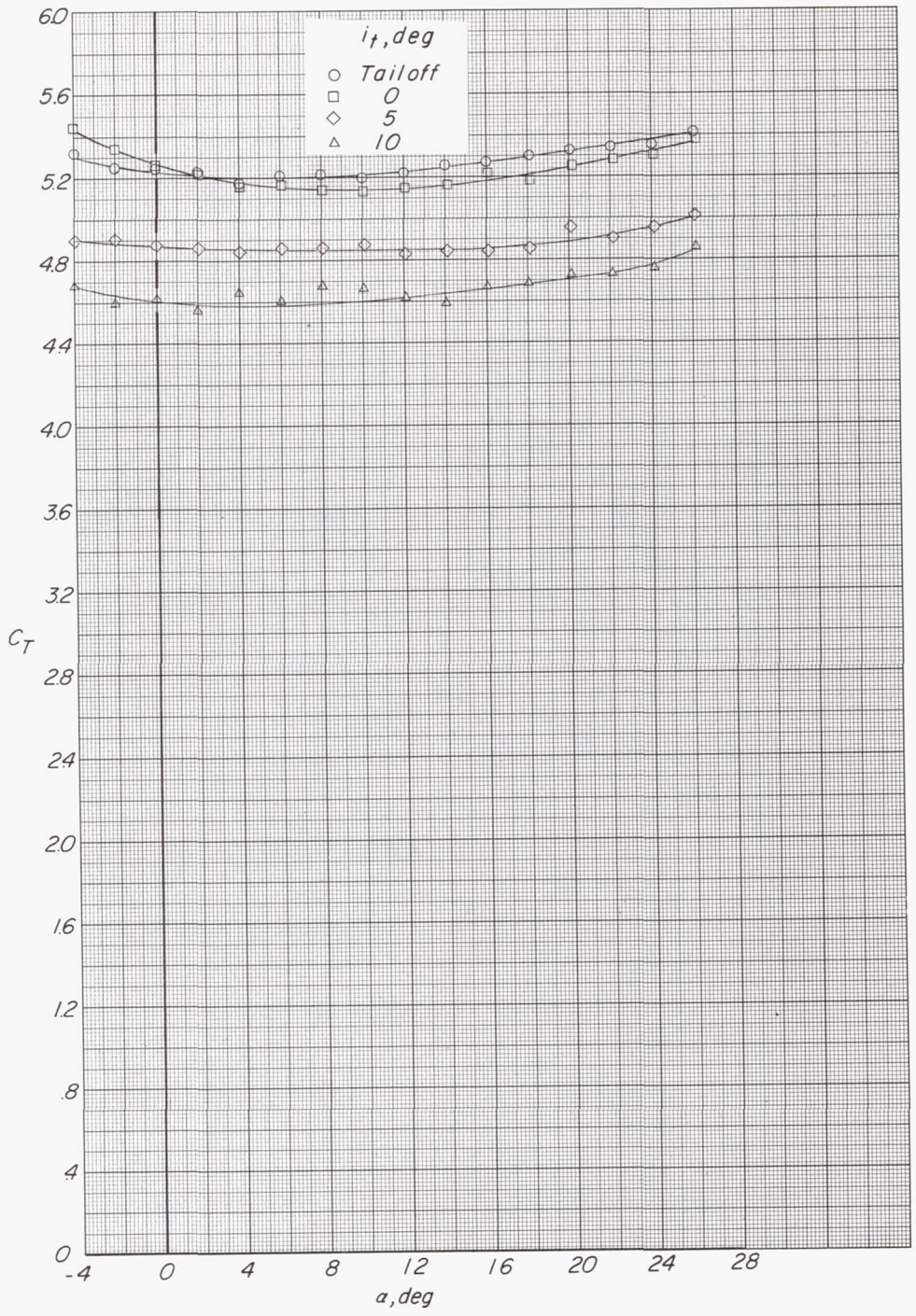

(c) Variation of C_T with α.

Figure 22.- Concluded.

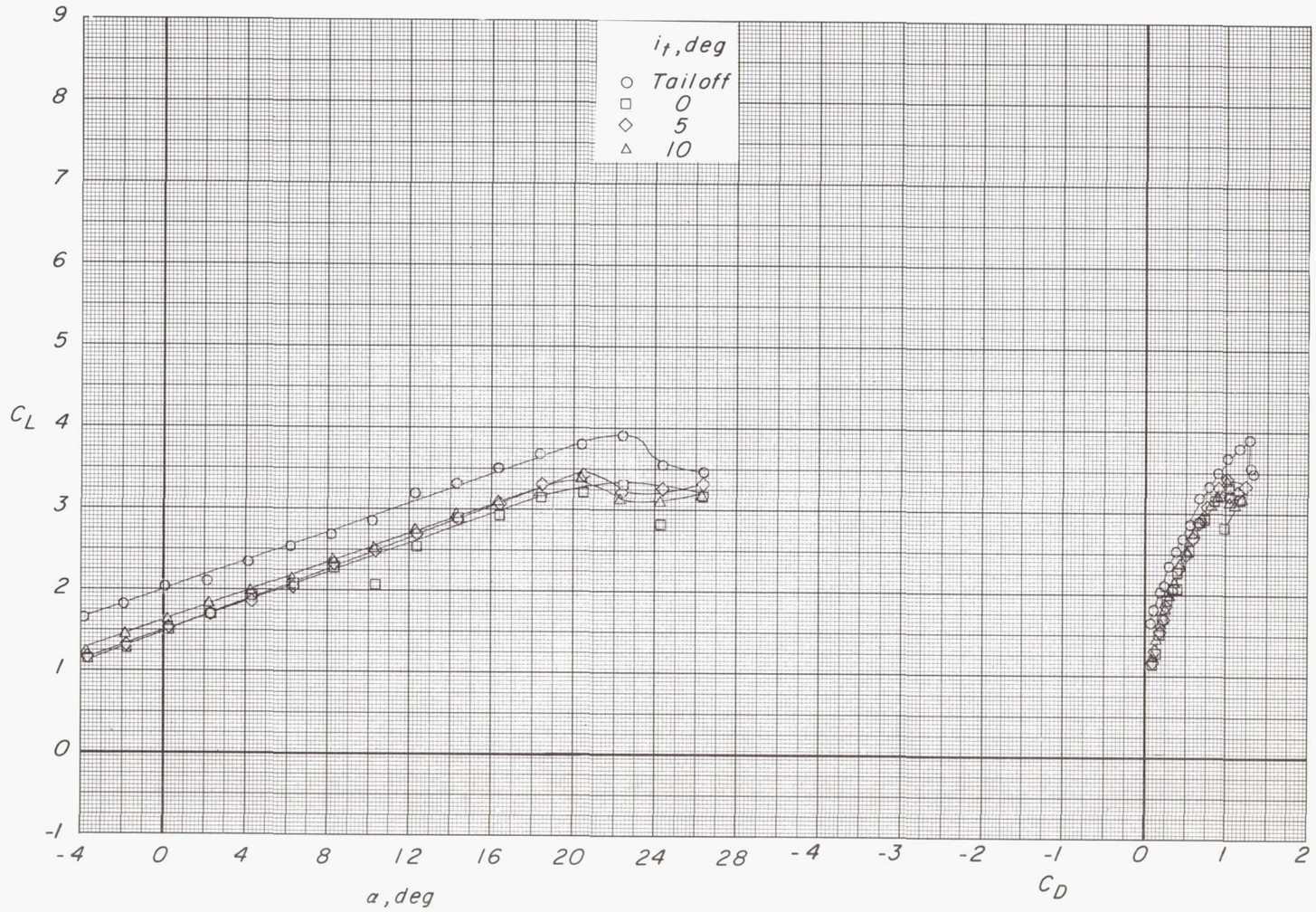

(a) Variation of C_L with α and C_D.

Figure 23.- Effect of tail incidence on longitudinal aerodynamic characteristics. $\delta_f = 45^0$; $C_\mu = 0.05$; $C_T = 0.43$; $\delta_e = 0^0$.

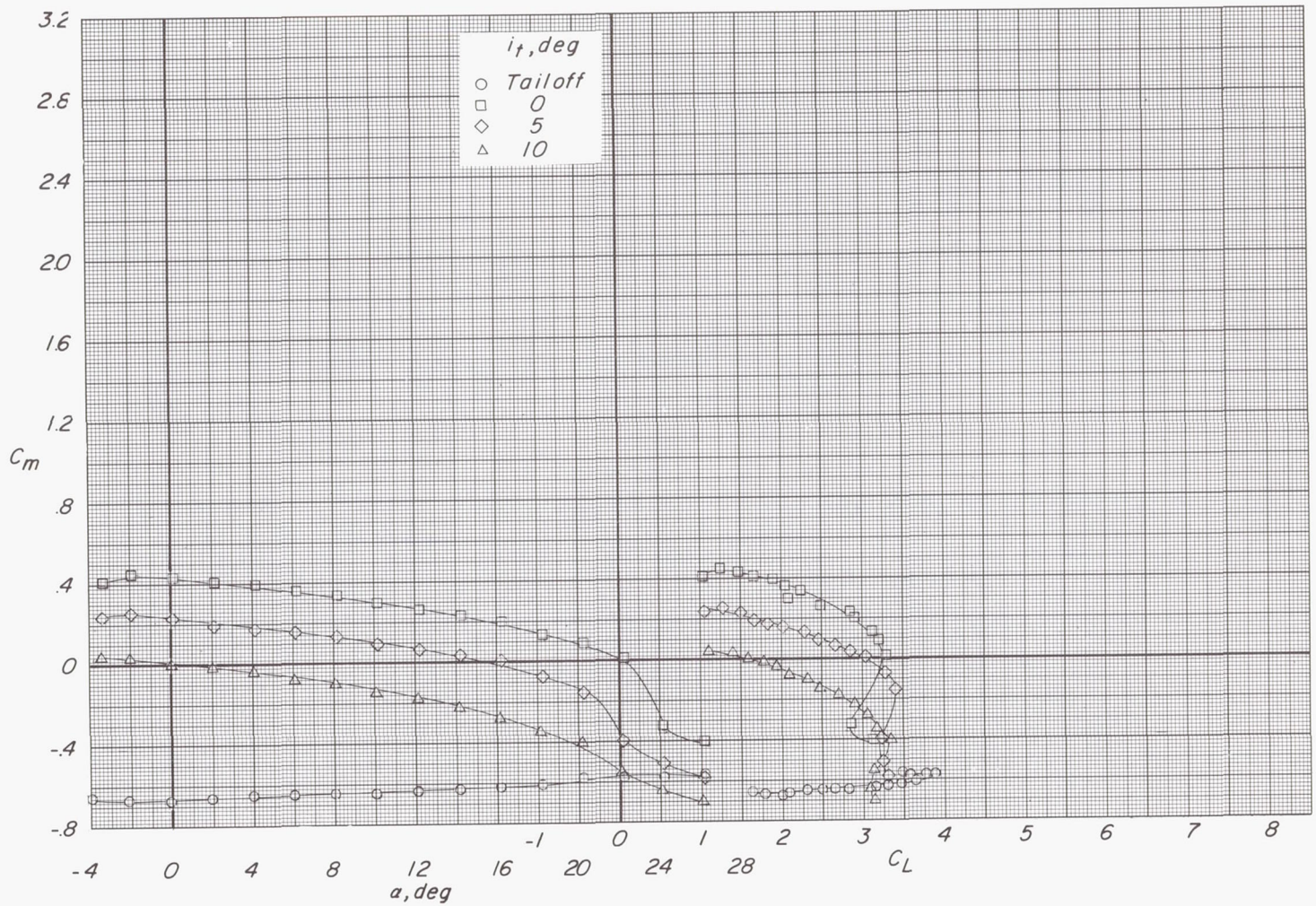

(b) Variation of C_m with α and C_L.

Figure 23.- Continued.

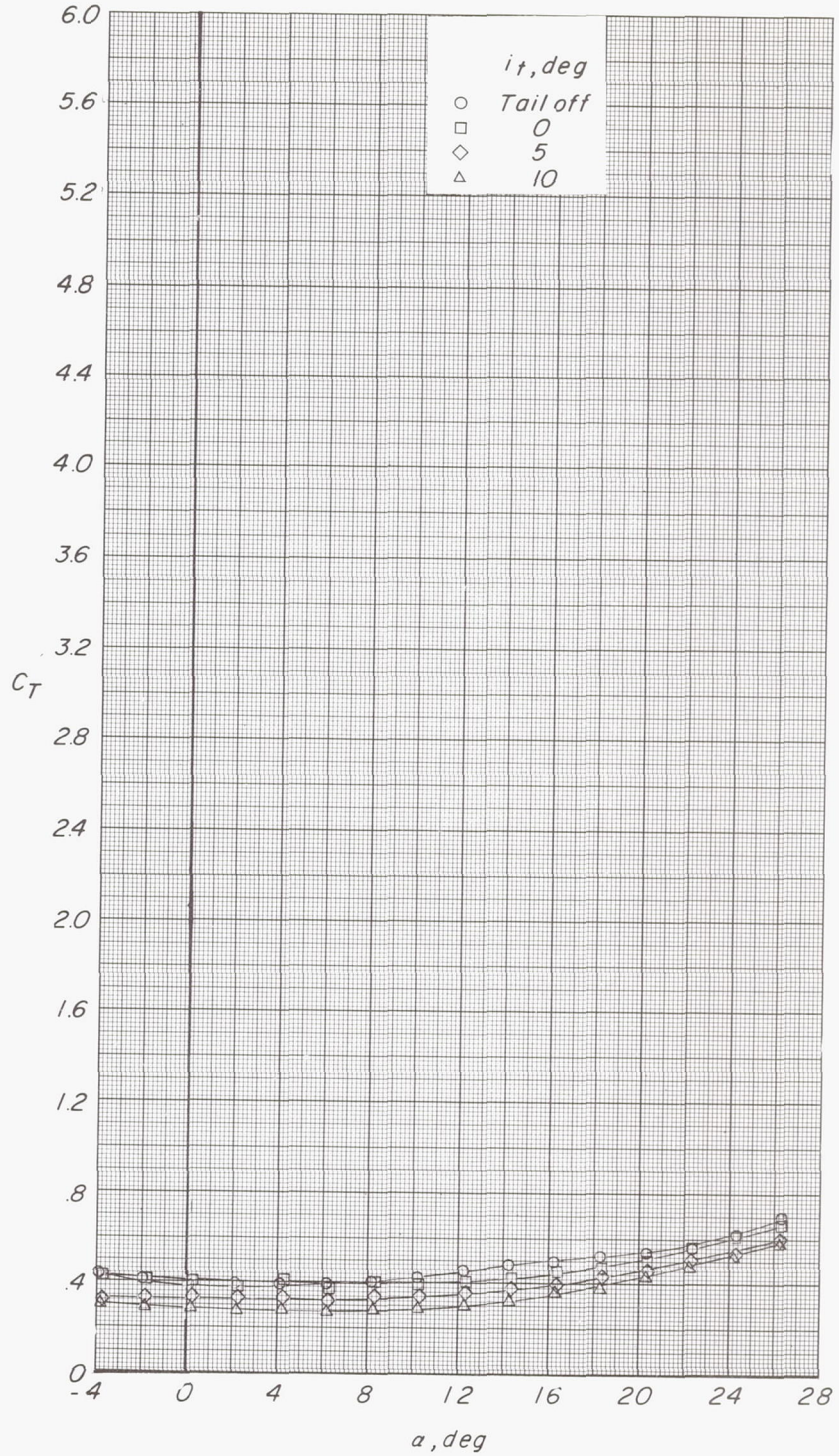

(c) Variation of C_T with α.

Figure 23.- Concluded.

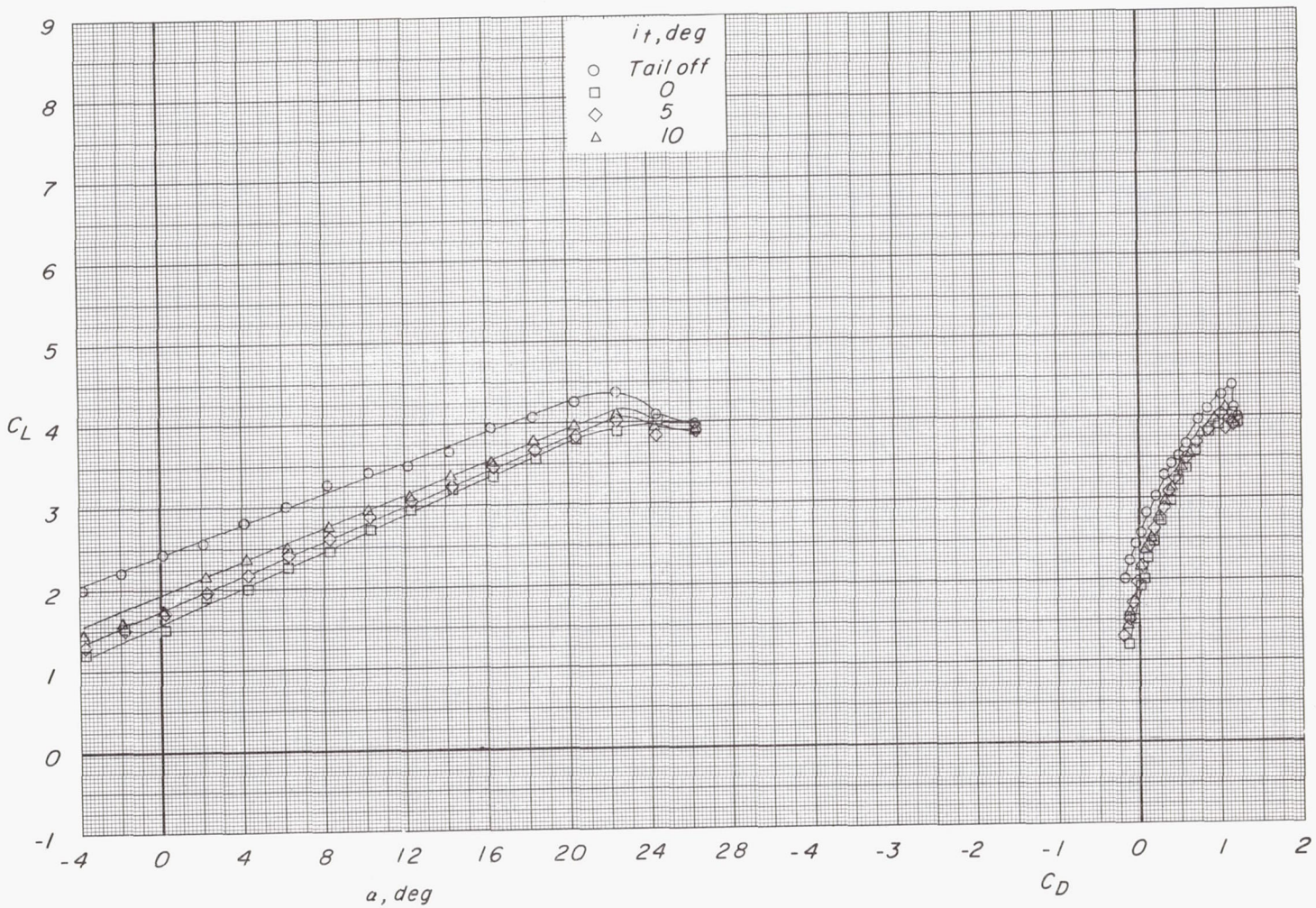

(a) Variation of C_L with α and C_D.

Figure 24.- Effect of tail incidence on longitudinal aerodynamic characteristics. $\delta_f = 45^0$; $C_\mu = 0.10$; $C_T = 0.83$; $\delta_e = 0^0$.

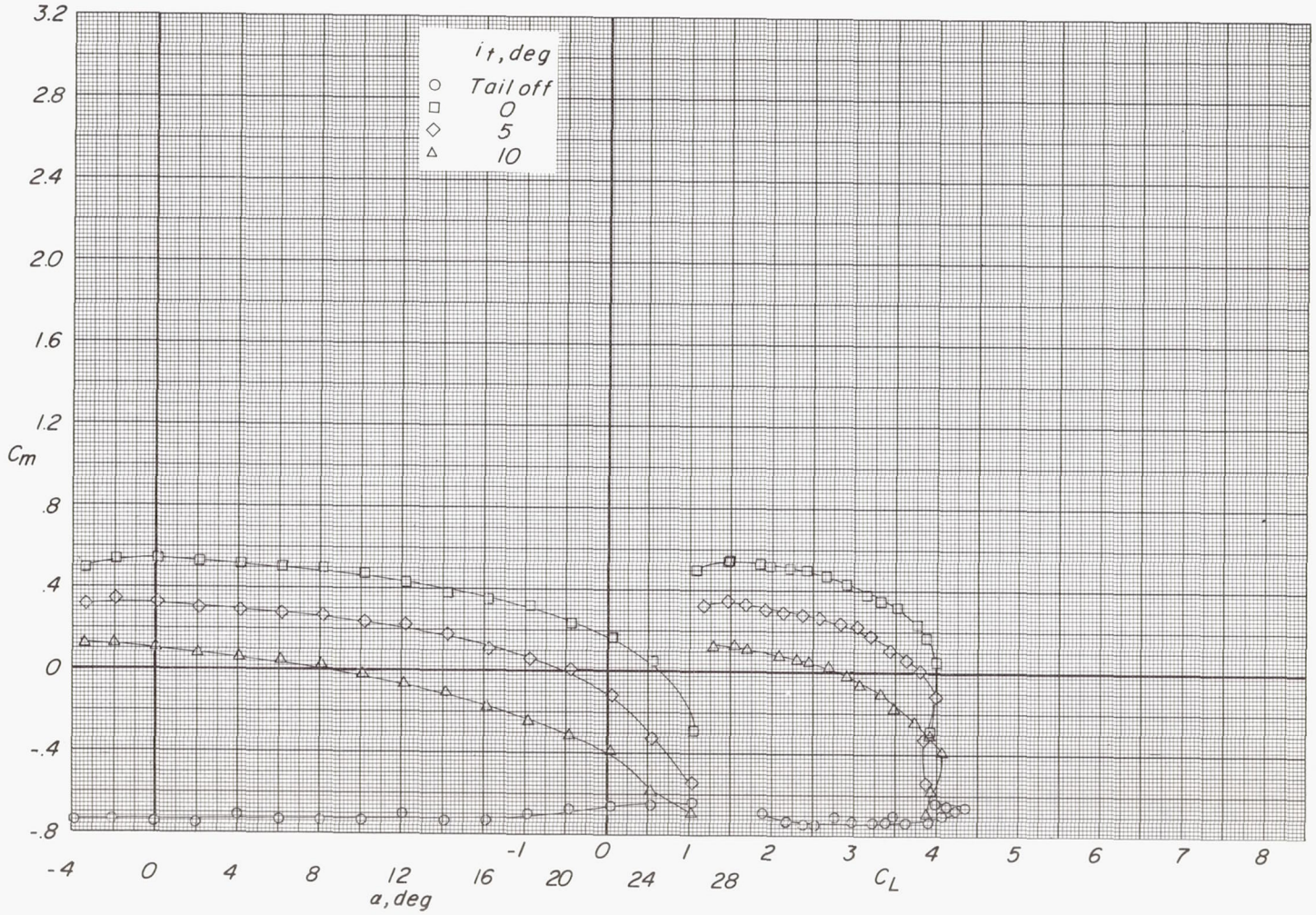

(b) Variation of C_m with α and C_L.

Figure 24.- Continued.

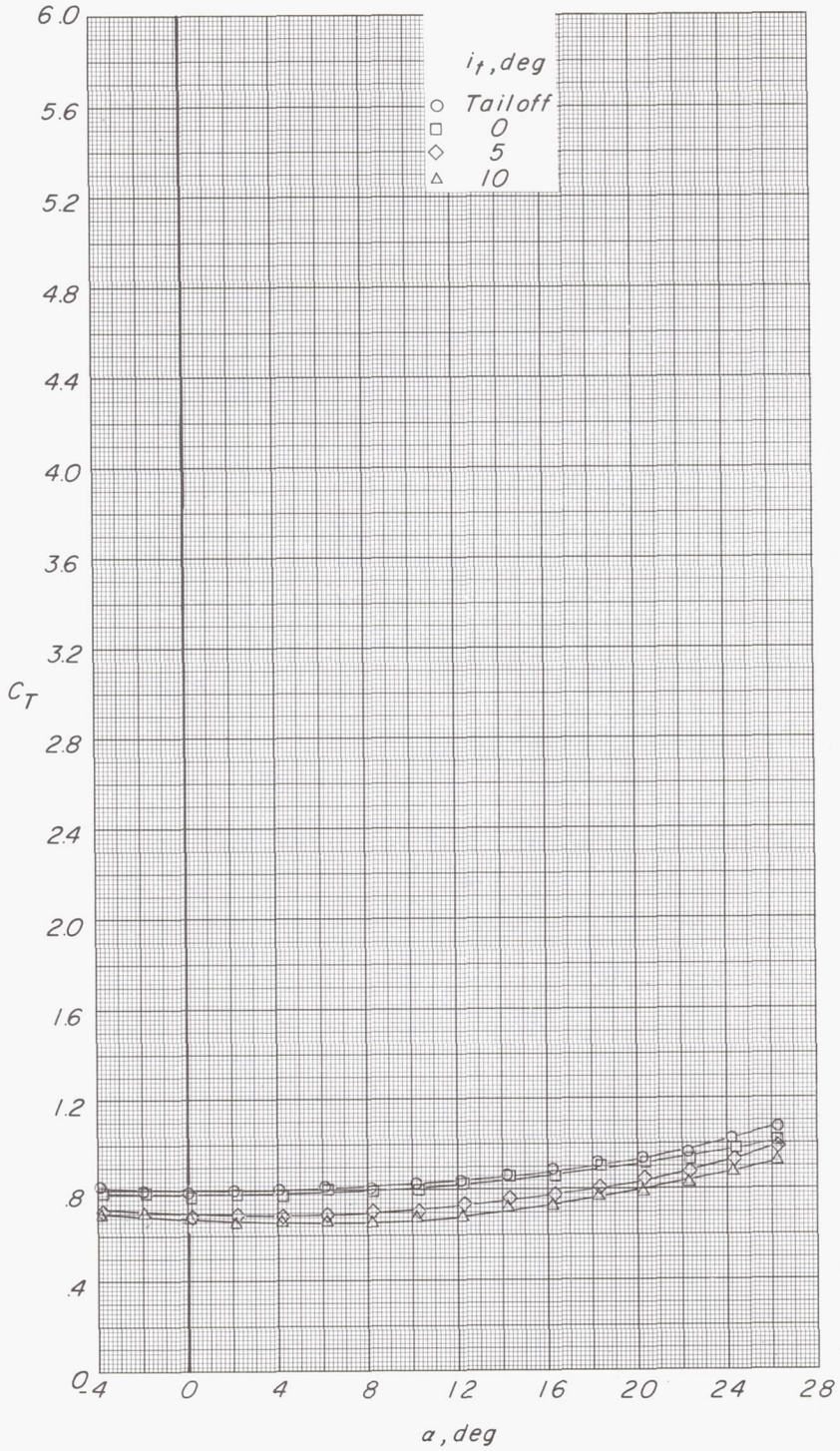

(c) Variation of C_T with α.

Figure 24.- Concluded.

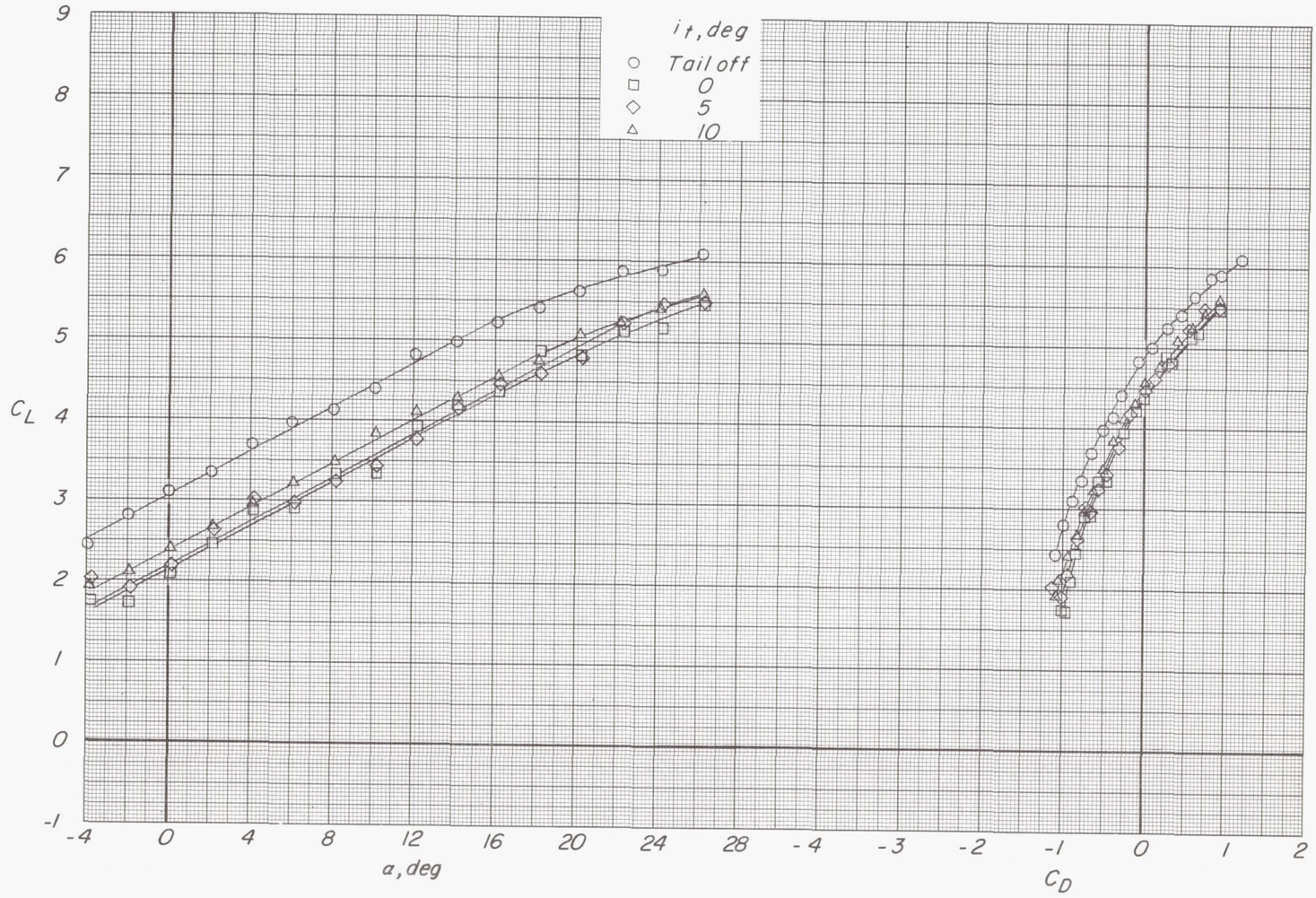

(a) Variation of C_L with α and C_D.

Figure 25.- Effect of tail incidence on longitudinal aerodynamic characteristics. $\delta_f = 45^o$; $C_\mu = 0.21$; $C_T = 2.10$; $\delta_e = 0^o$.

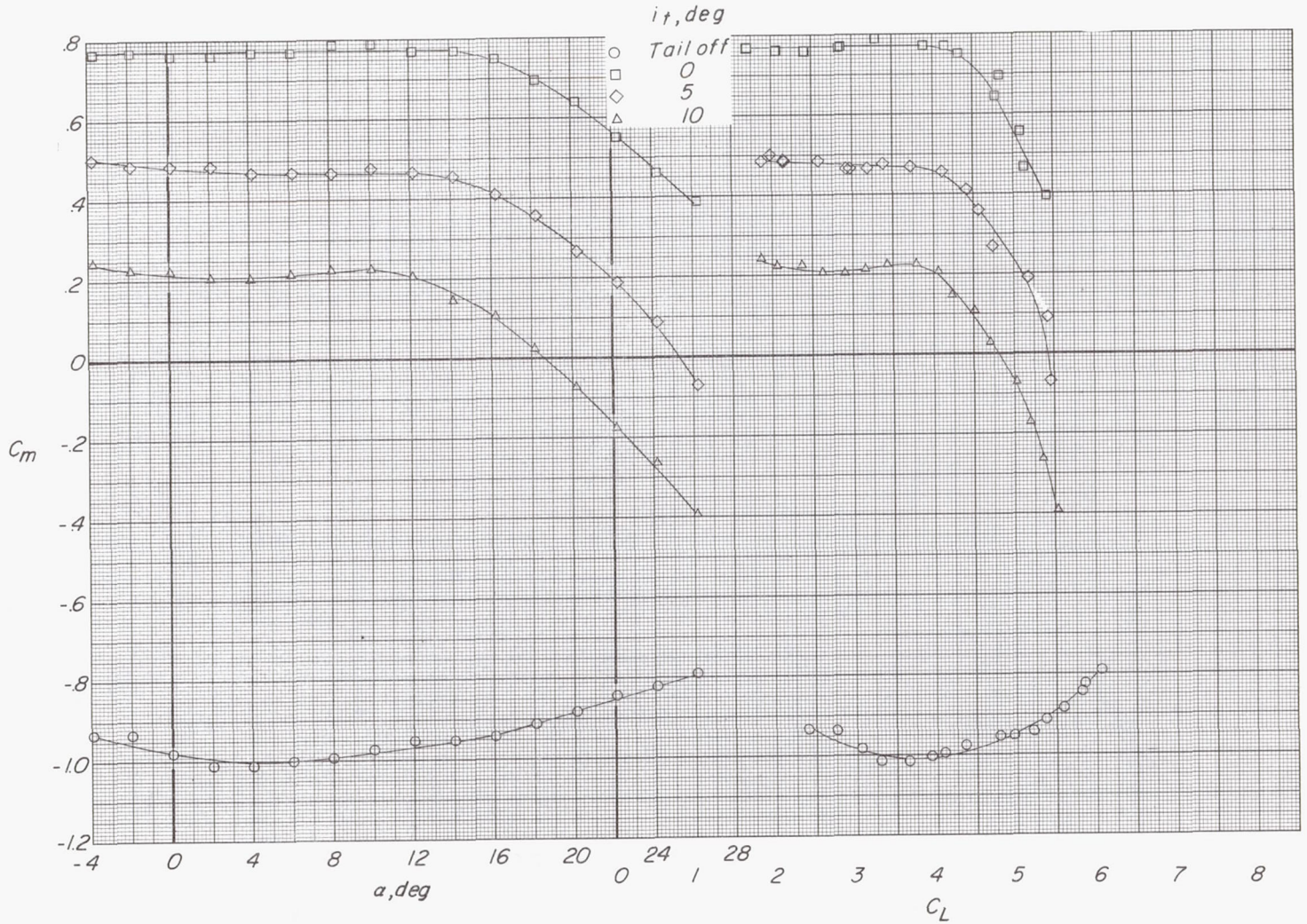

(b) Variation of C_m with α and C_L.

Figure 25.- Continued.

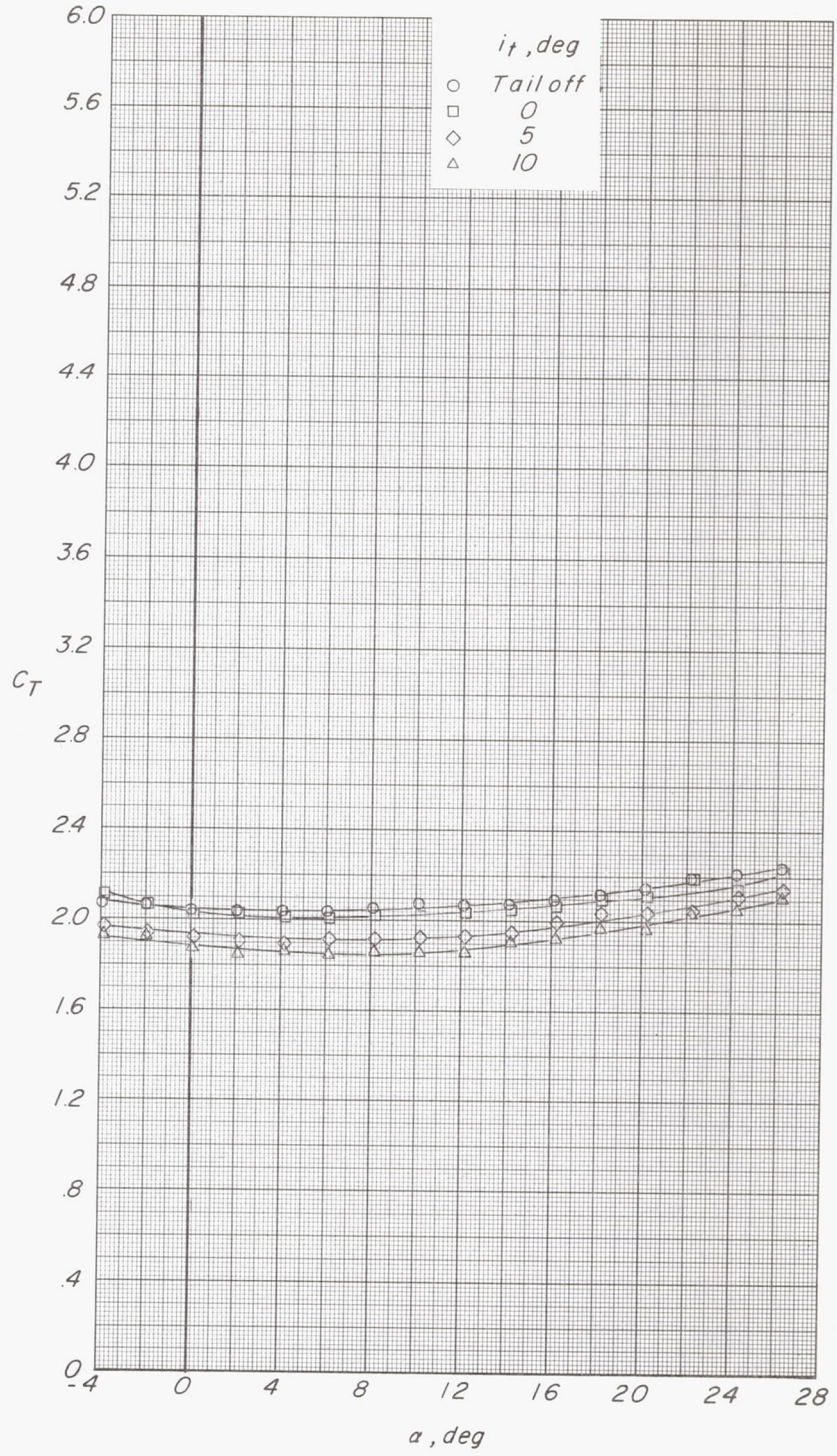

(c) Variation of C_T with α.

Figure 25.- Concluded.

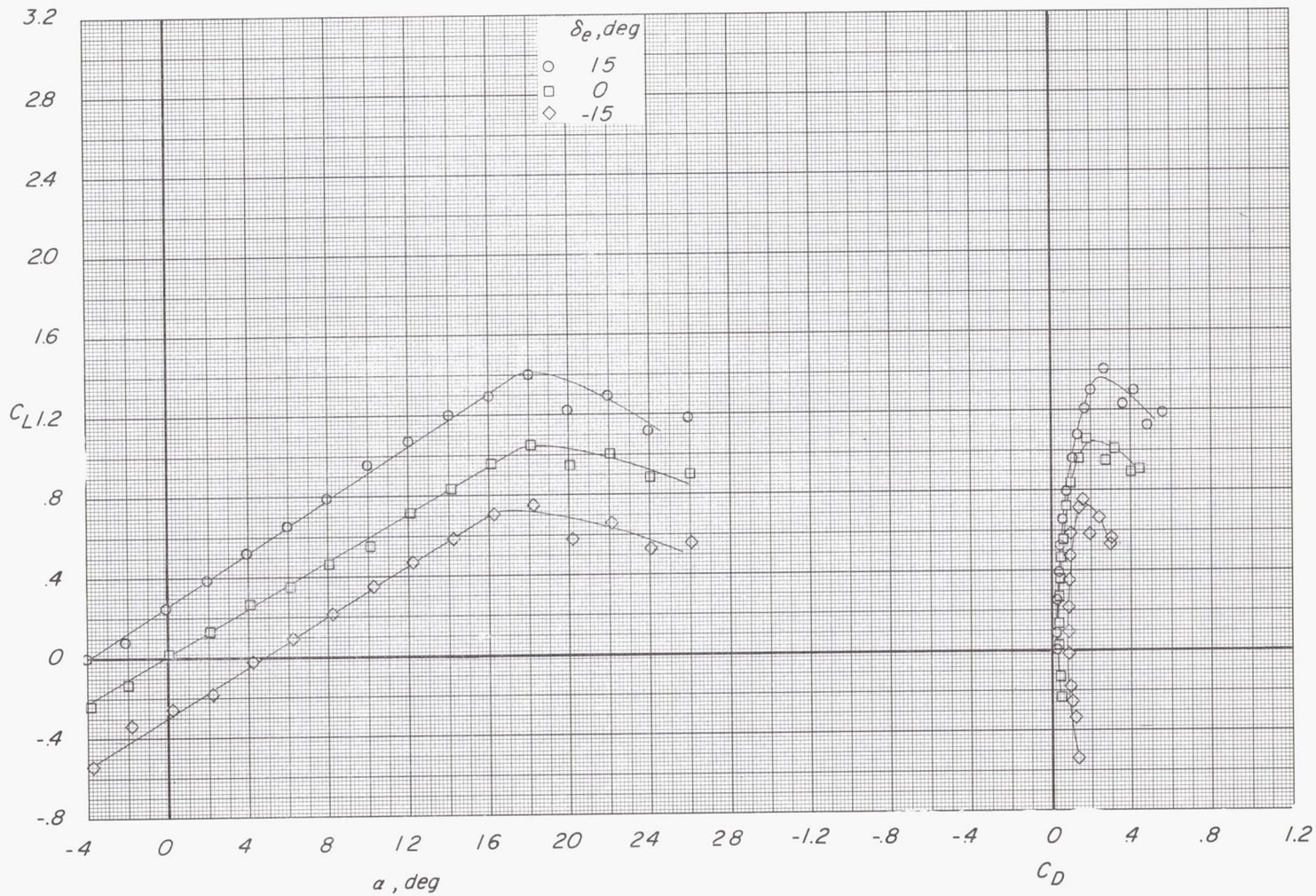

(a) Variation of C_L with α and C_D.

Figure 26.- Effect of elevator deflection on longitudinal aerodynamic characteristics. $\delta_f = 0^o$; $C_\mu = 0$; $C_T = 0$; $i_t = 0^o$.

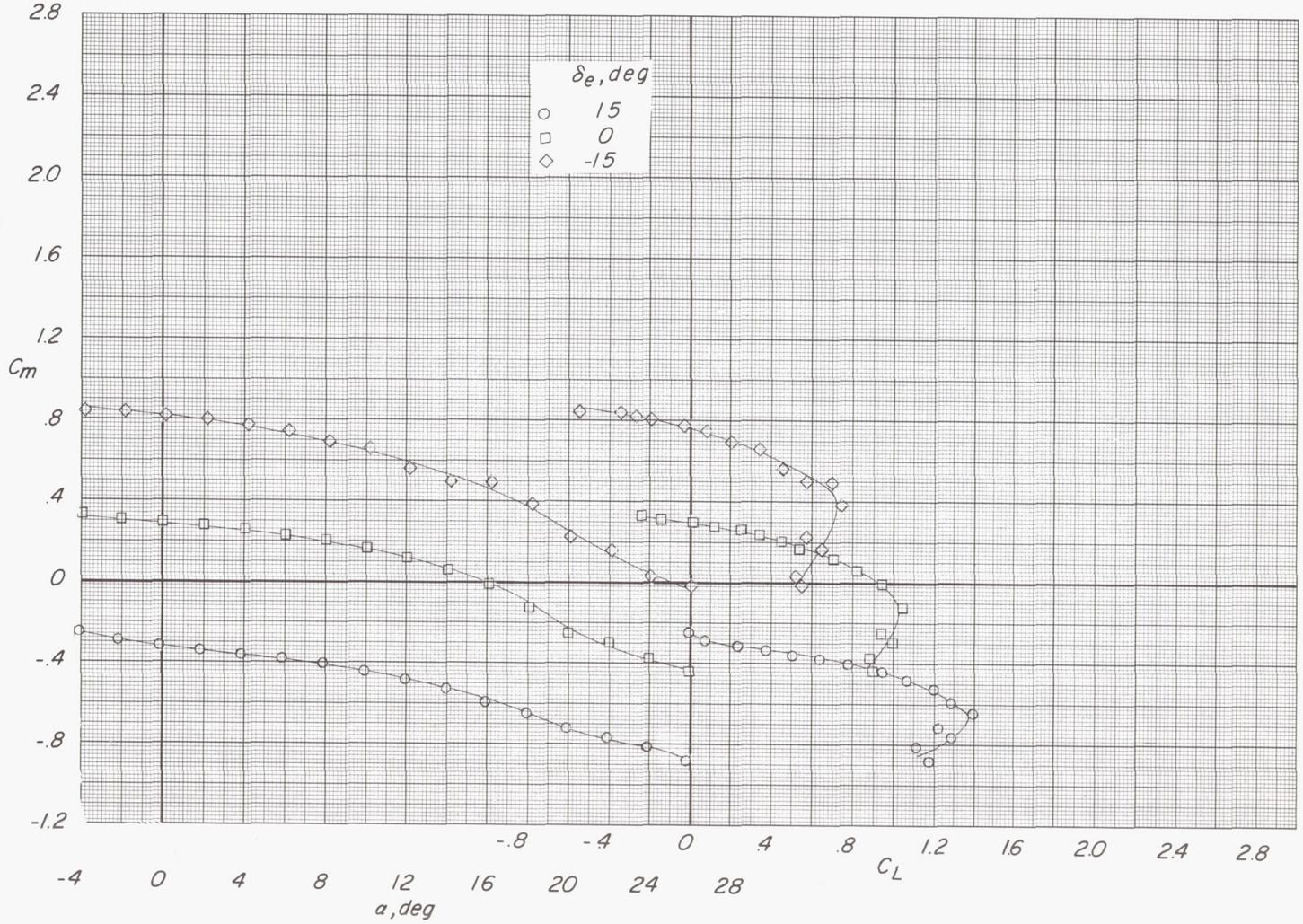

(b) Variation of C_m with α and C_L.

Figure 26.- Concluded.

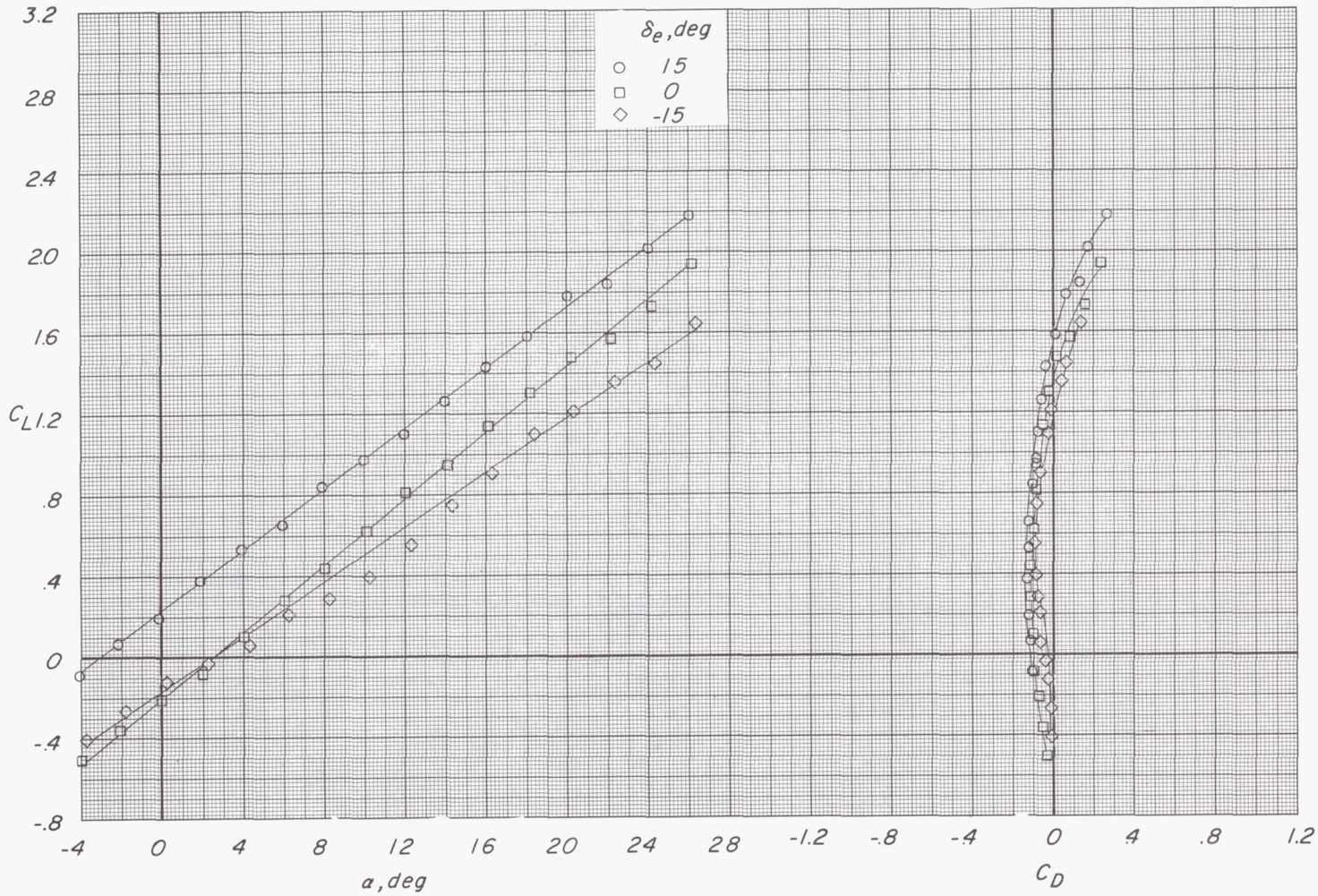

(a) Variation of C_L with α and C_D.

Figure 27.- Effect of elevator deflection on longitudinal aerodynamic characteristics. $\delta_f = 0^0$; $C_\mu = 0.02$; $C_T = 0.14$; $i_t = 0^0$.

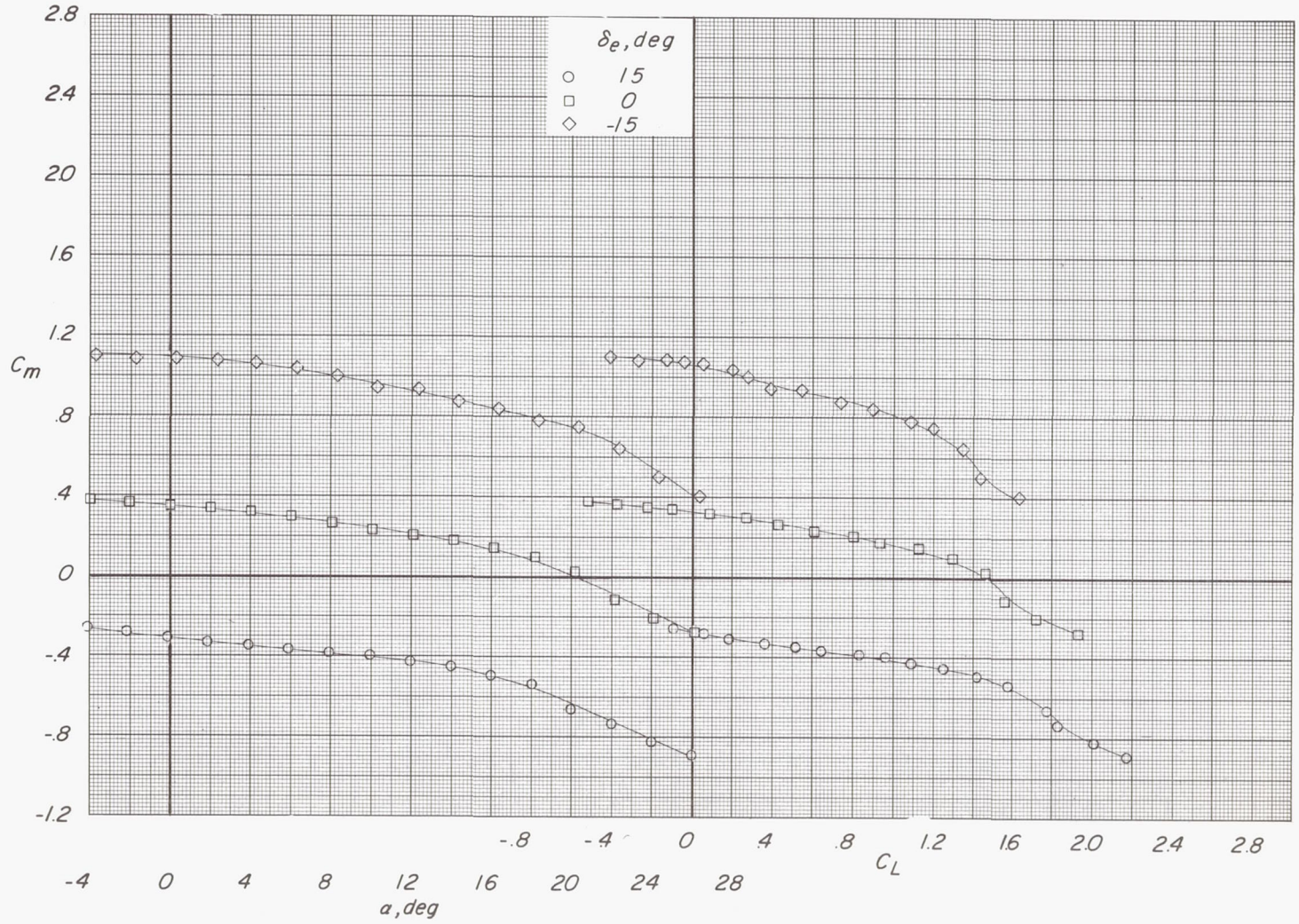

(b) Variation of C_m with α and C_L.

Figure 27.- Continued.

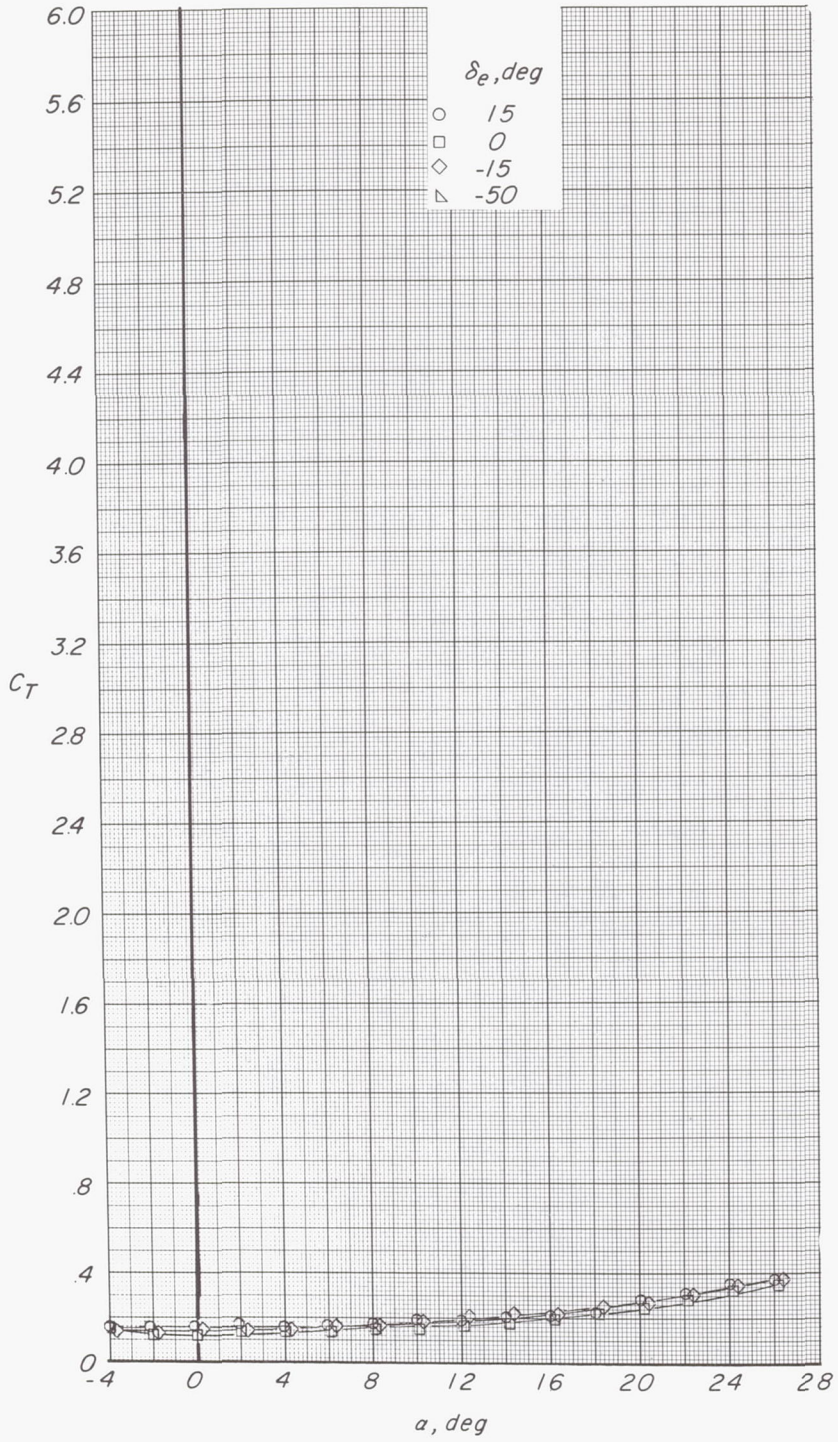

(c) Variation of C_T with α.

Figure 27.- Concluded.

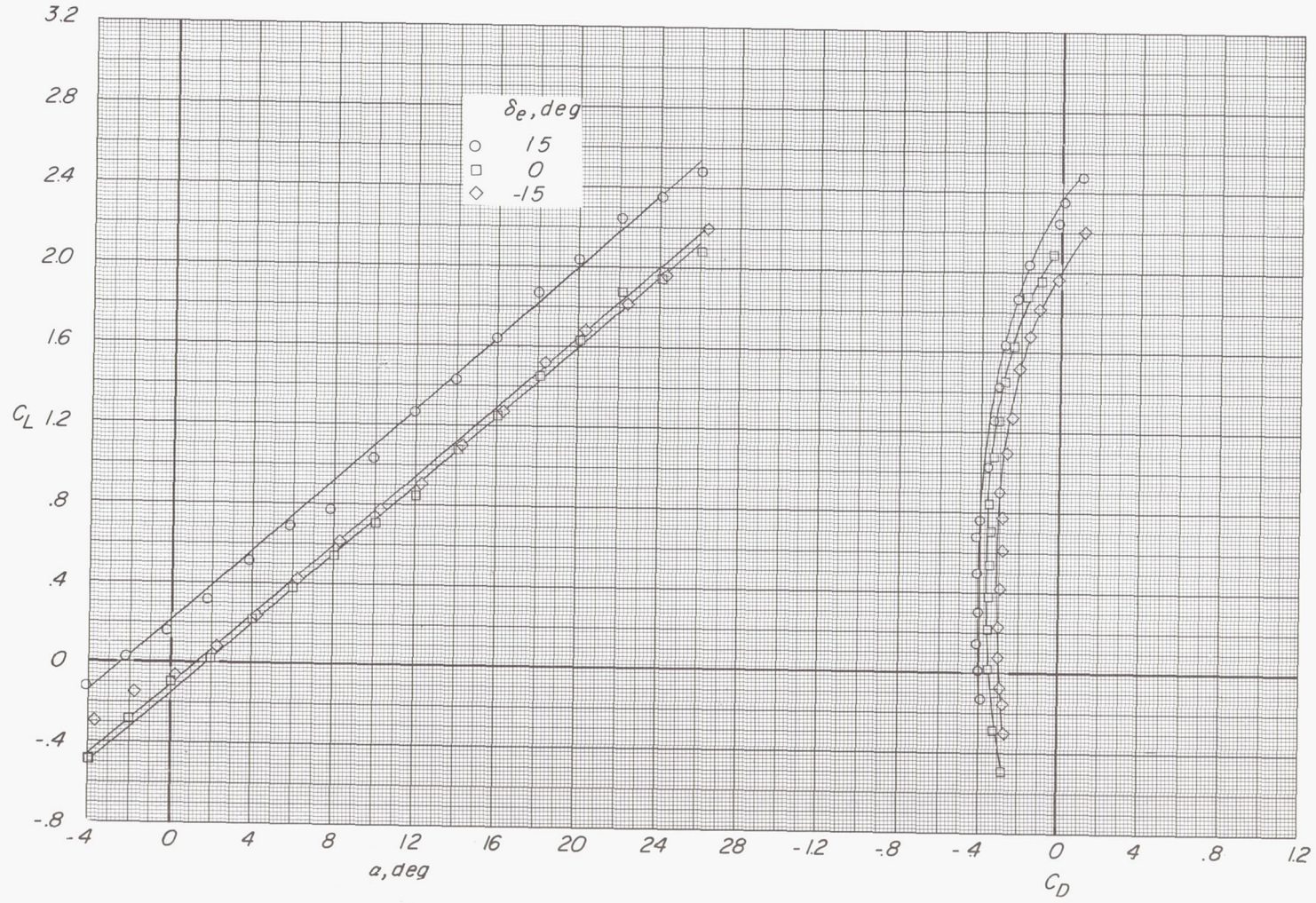

(a) Variation of C_L with α and C_D.

Figure 28.- Effect of elevator deflection on longitudinal aerodynamic characteristics. $\delta_f = 0^o$; $C_\mu = 0.05$; $C_T = 0.43$; $i_t = 0^o$.

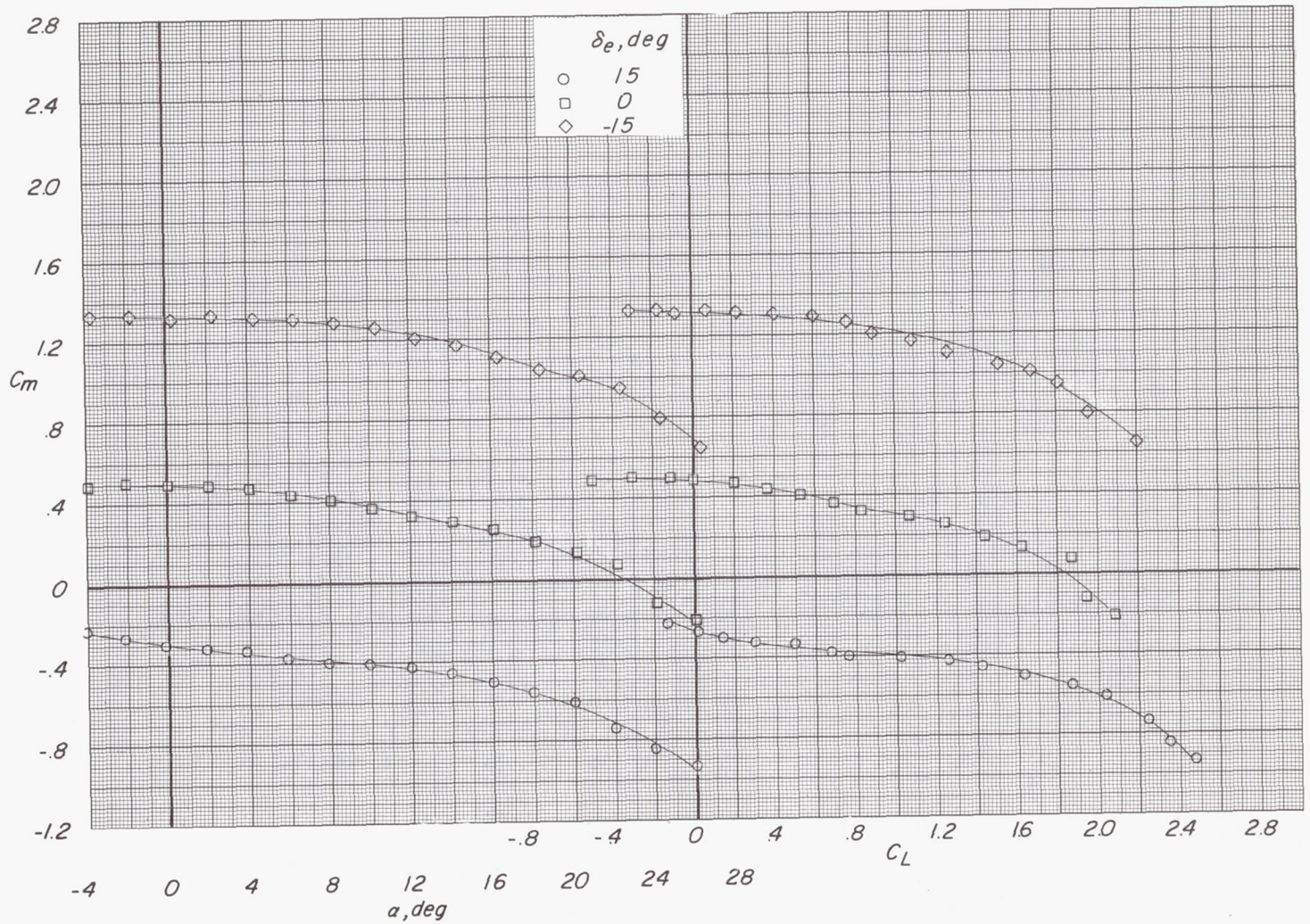

(b) Variation of C_m with α and C_L.

Figure 28.- Continued.

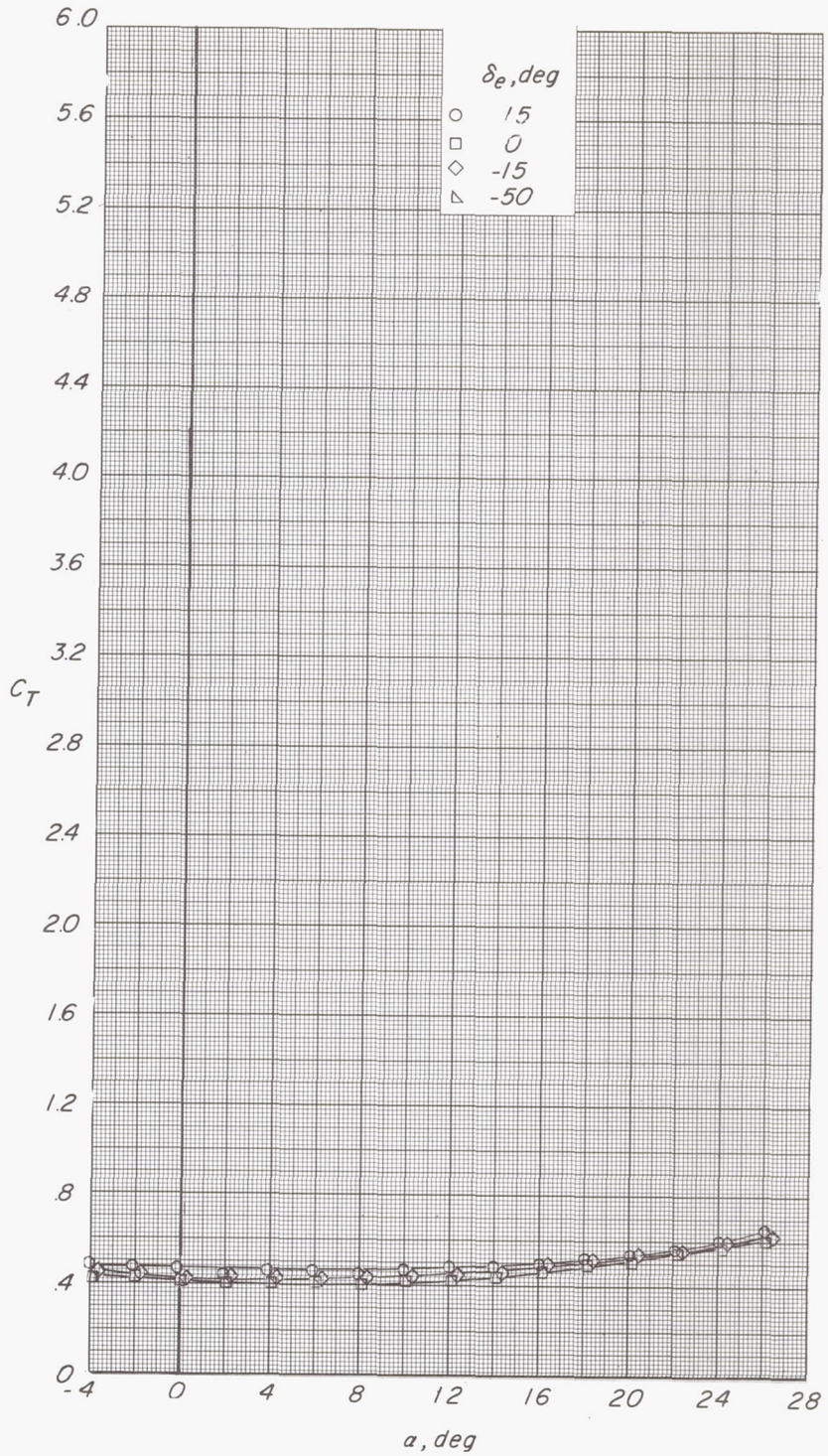

(c) Variation of C_T with α.

Figure 28.- Concluded.

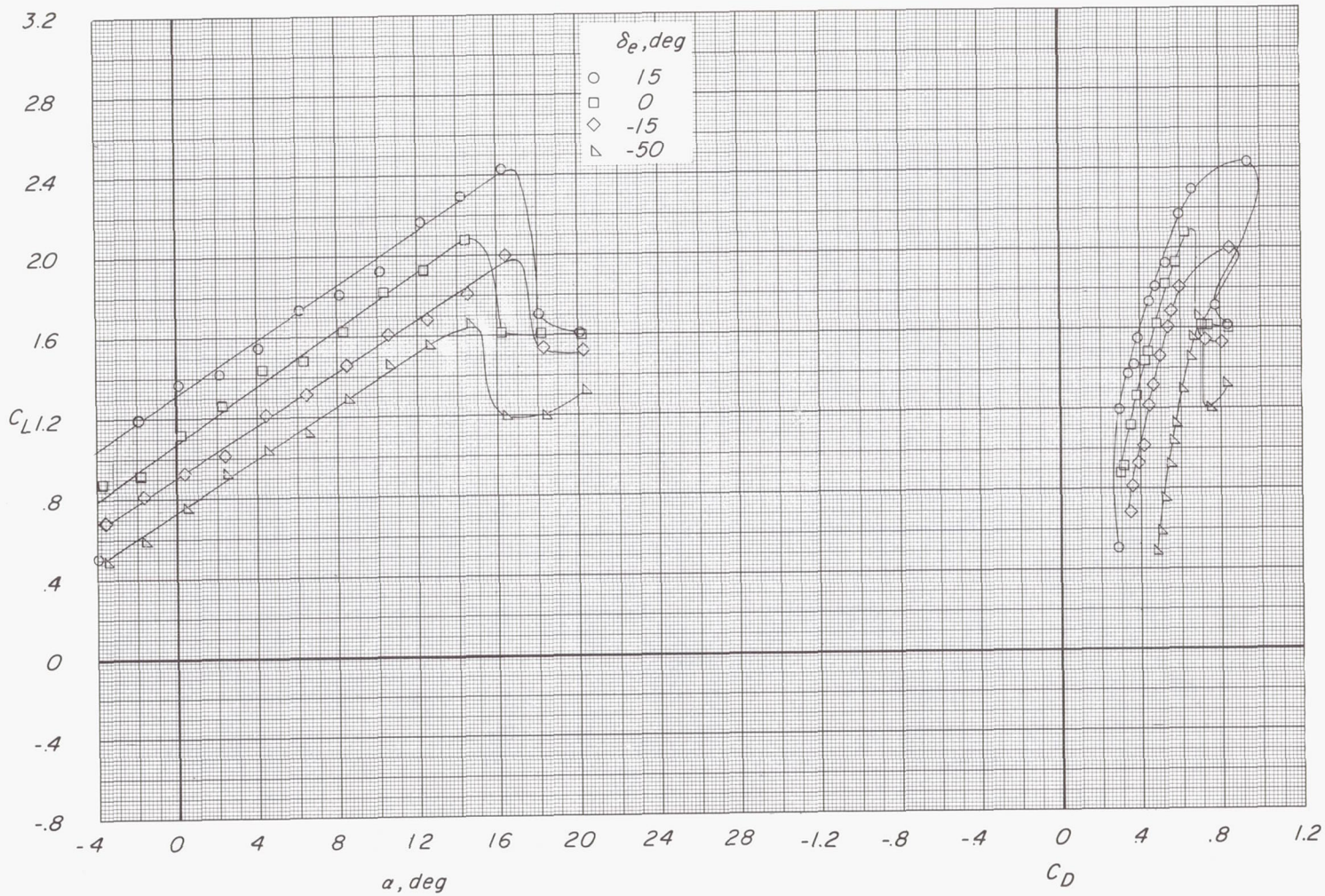

(a) Variation of C_L with α and C_D.

Figure 29.- Effect of elevator deflection on longitudinal aerodynamic characteristics. $\delta_f = 45^0$; $C_\mu = 0$; $C_T = 0$; $i_t = 0^0$.

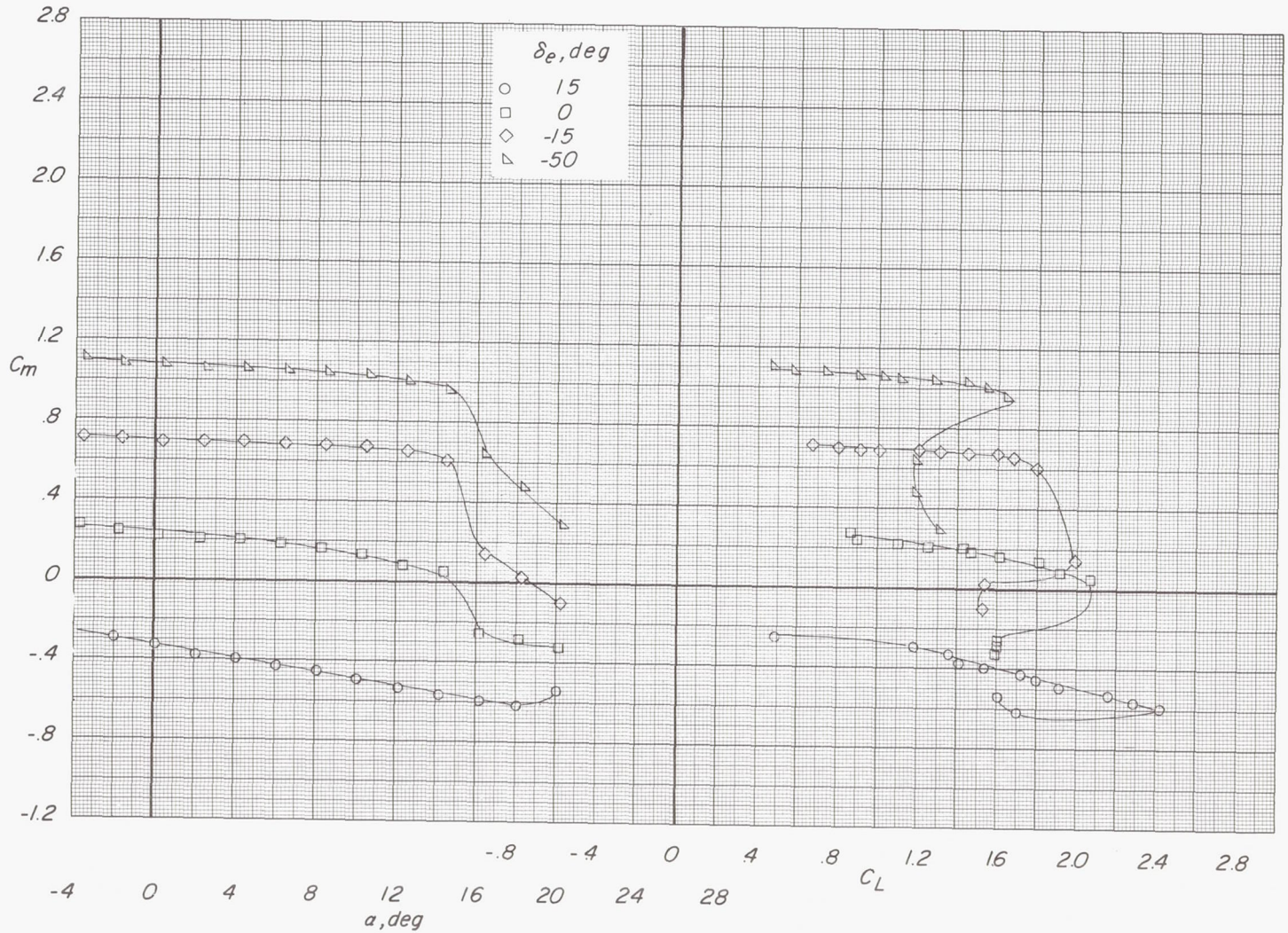

(b) Variation of C_m with α and C_L.

Figure 29.- Concluded.

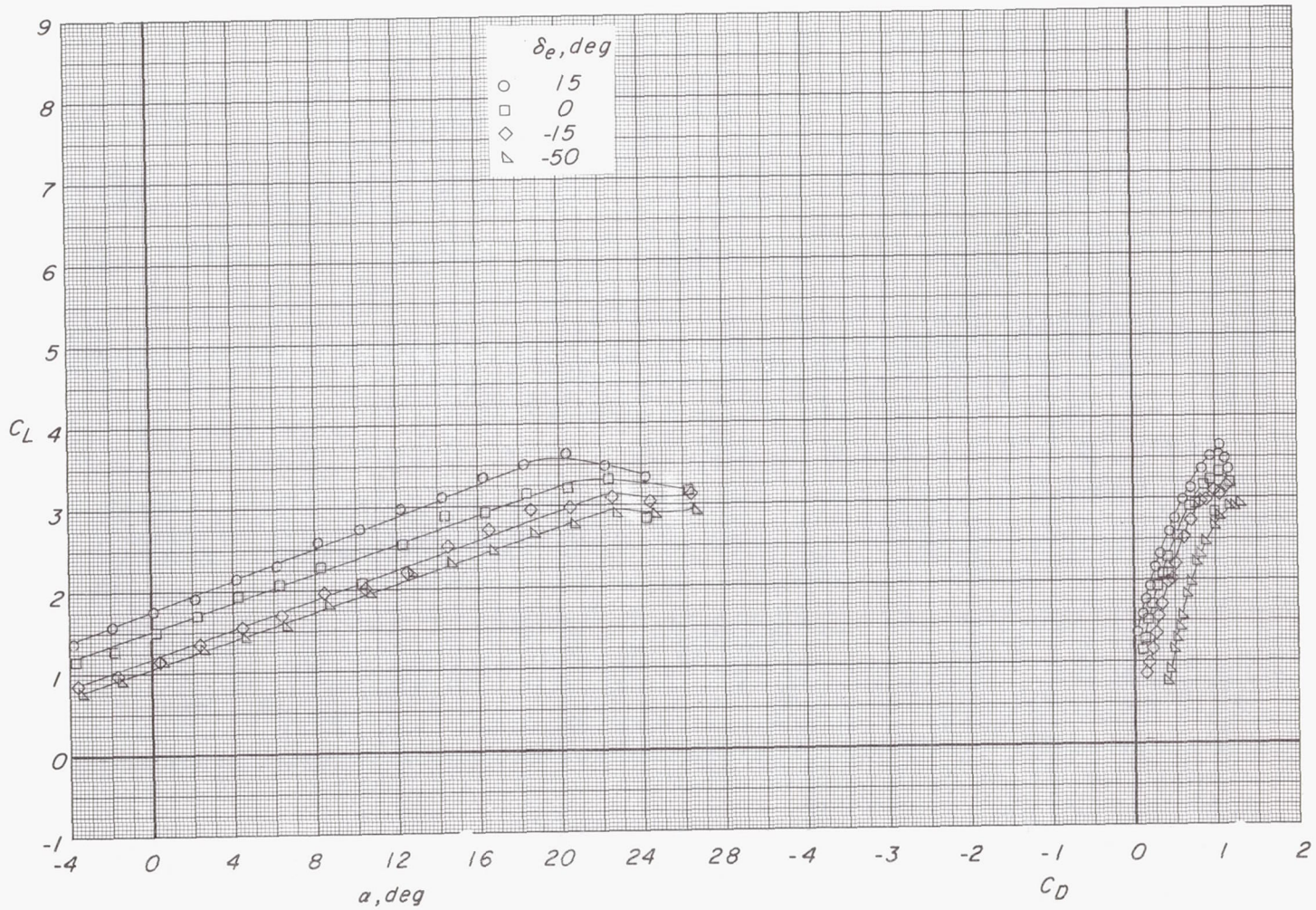

(a) Variation of C_L with α and C_D.

Figure 30.- Effect of elevator deflection on longitudinal aerodynamic characteristics. $\delta_f = 45^o$; $C_\mu = 0.05$; $C_T = 0.43$; $i_t = 0^o$.

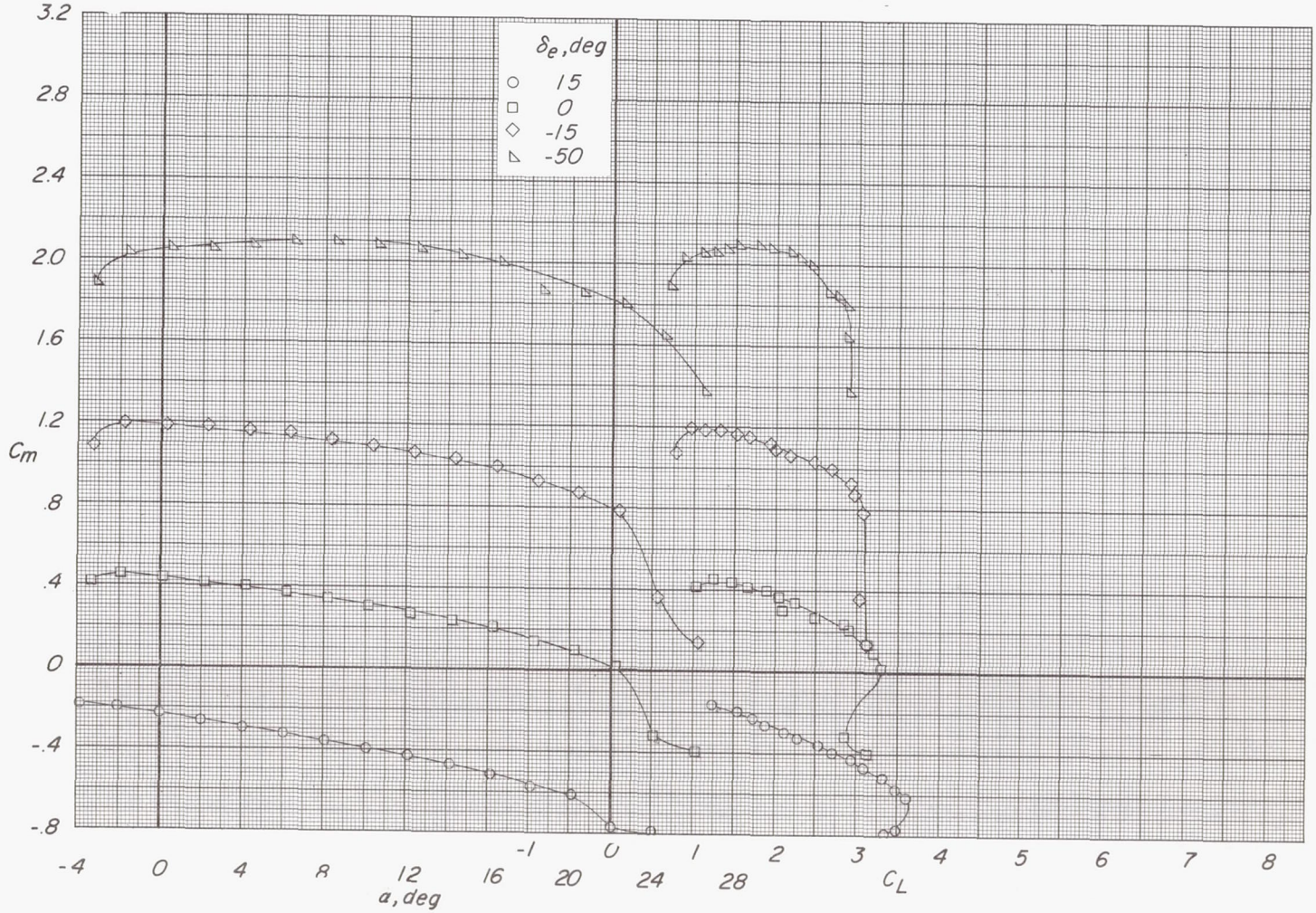

(b) Variation of C_m with α and C_L.

Figure 30.- Continued.

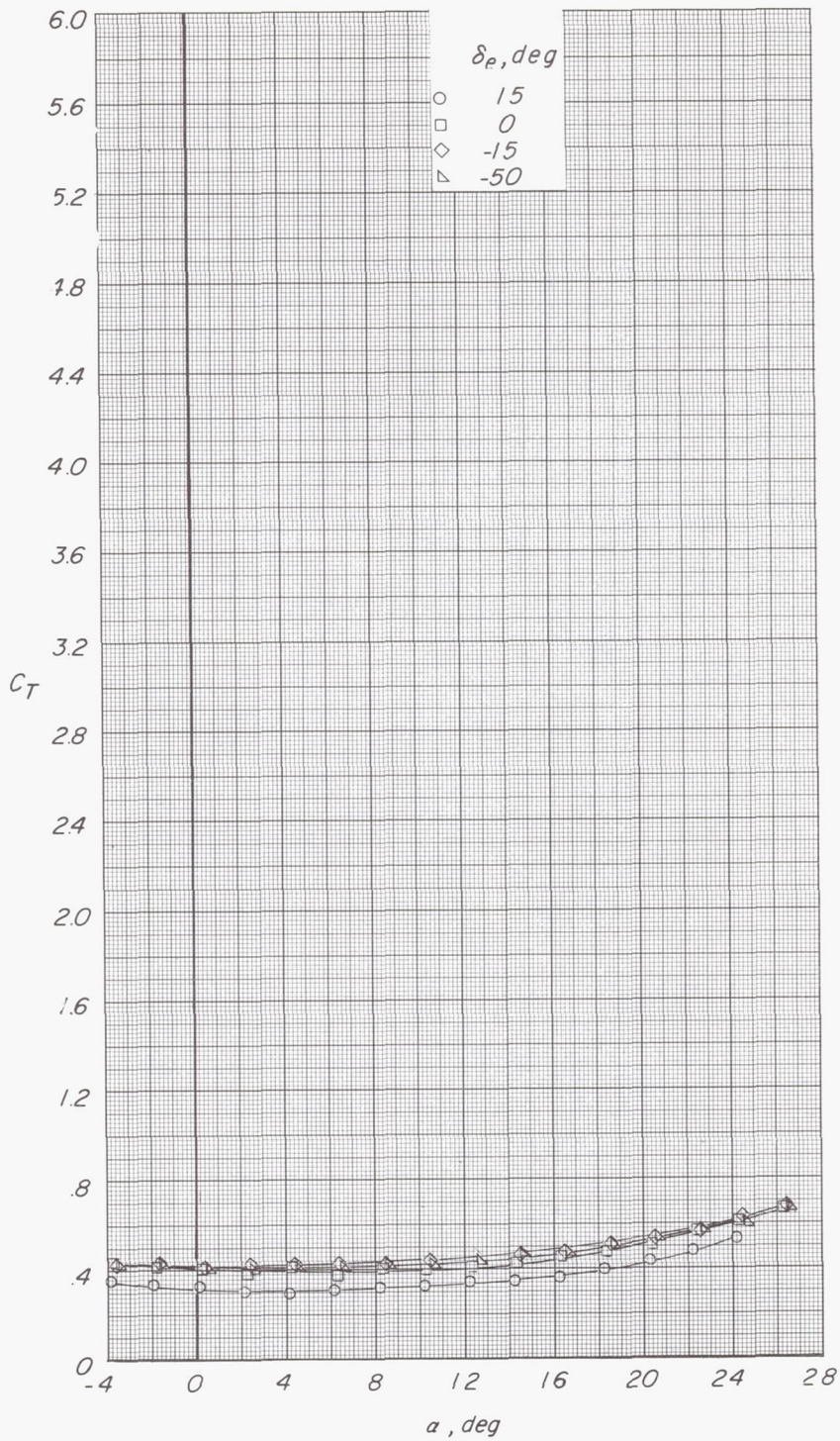

(c) Variation of C_T with α.

Figure 30.- Concluded.

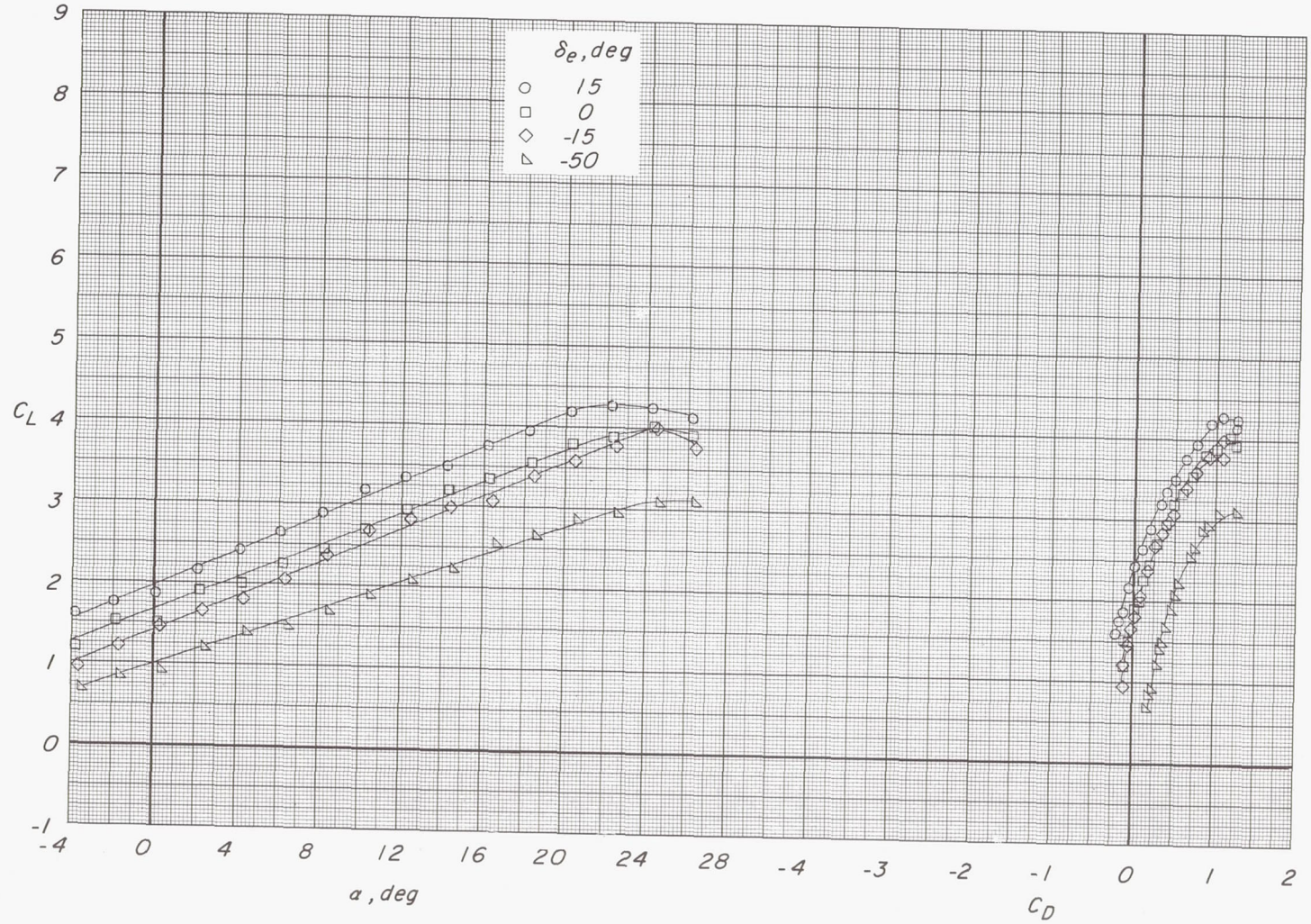

(a) Variation of C_L with α and C_D.

Figure 31.- Effect of elevator deflection on longitudinal aerodynamic characteristics. $\delta_f = 45^0$; $C_\mu = 0.10$; $C_T = 0.83$; $i_t = 0^0$.

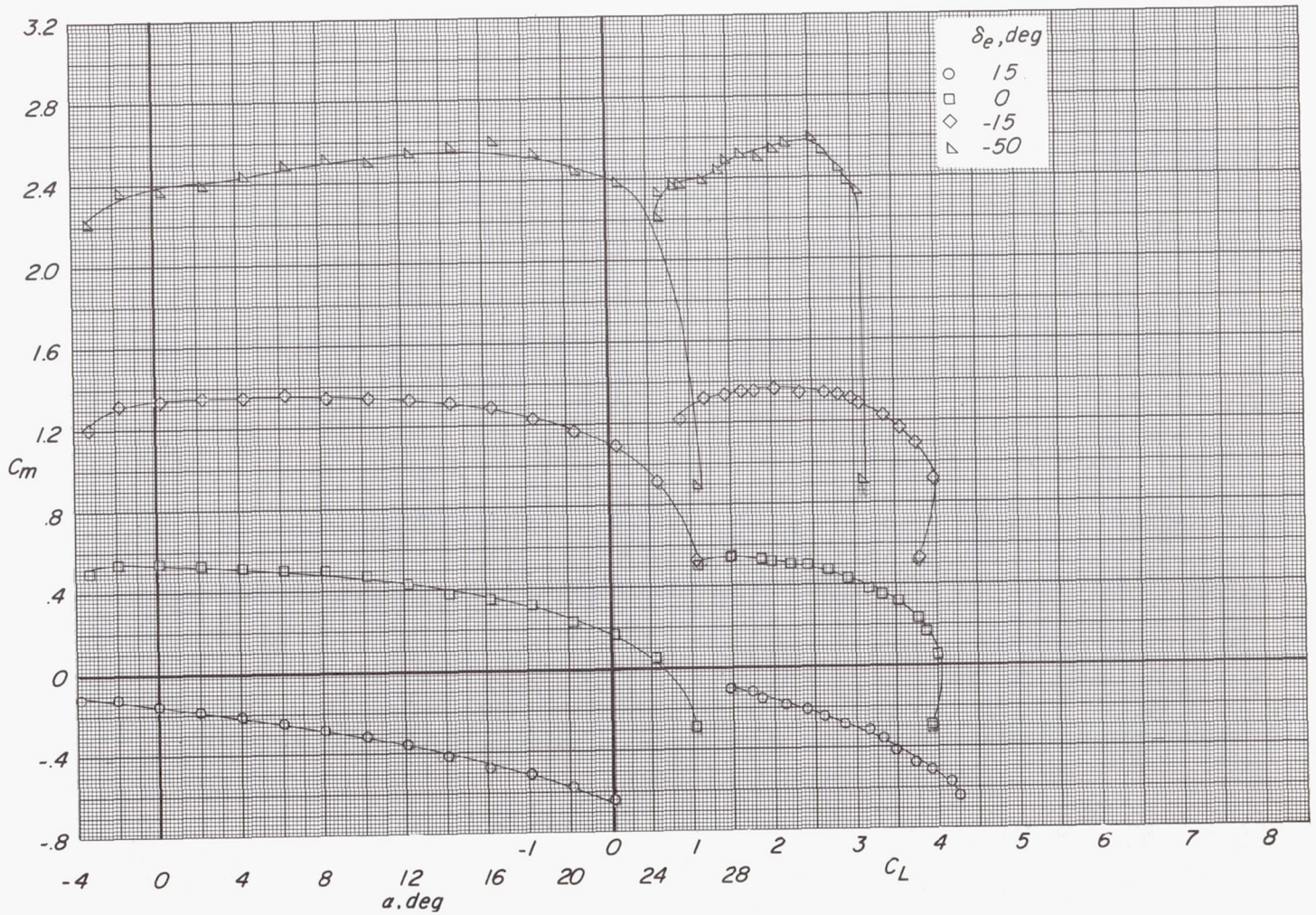

(b) Variation of C_m with α and C_L.

Figure 31.- Continued.

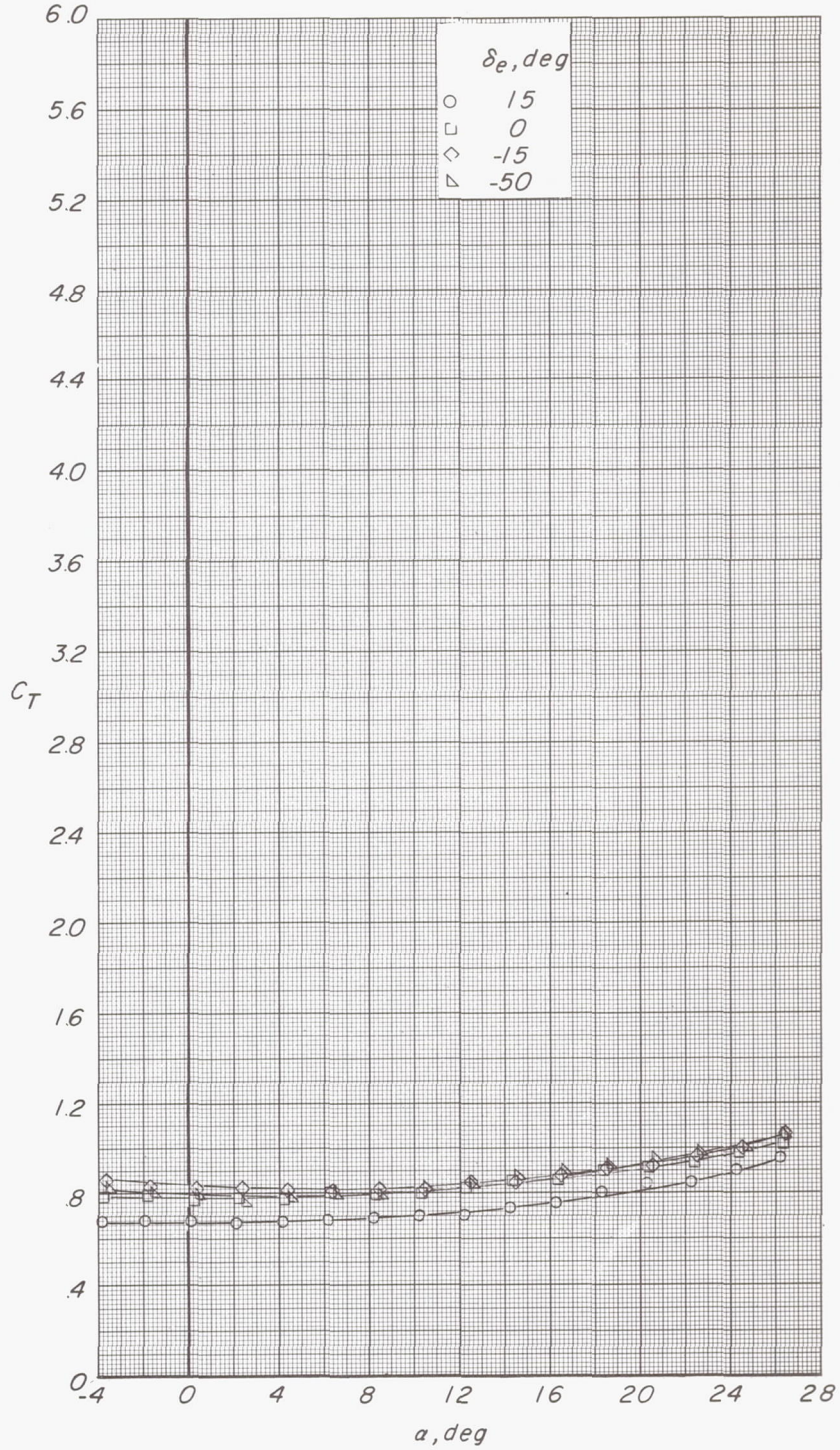

(c) Variation of C_T with α.

Figure 31.- Concluded.

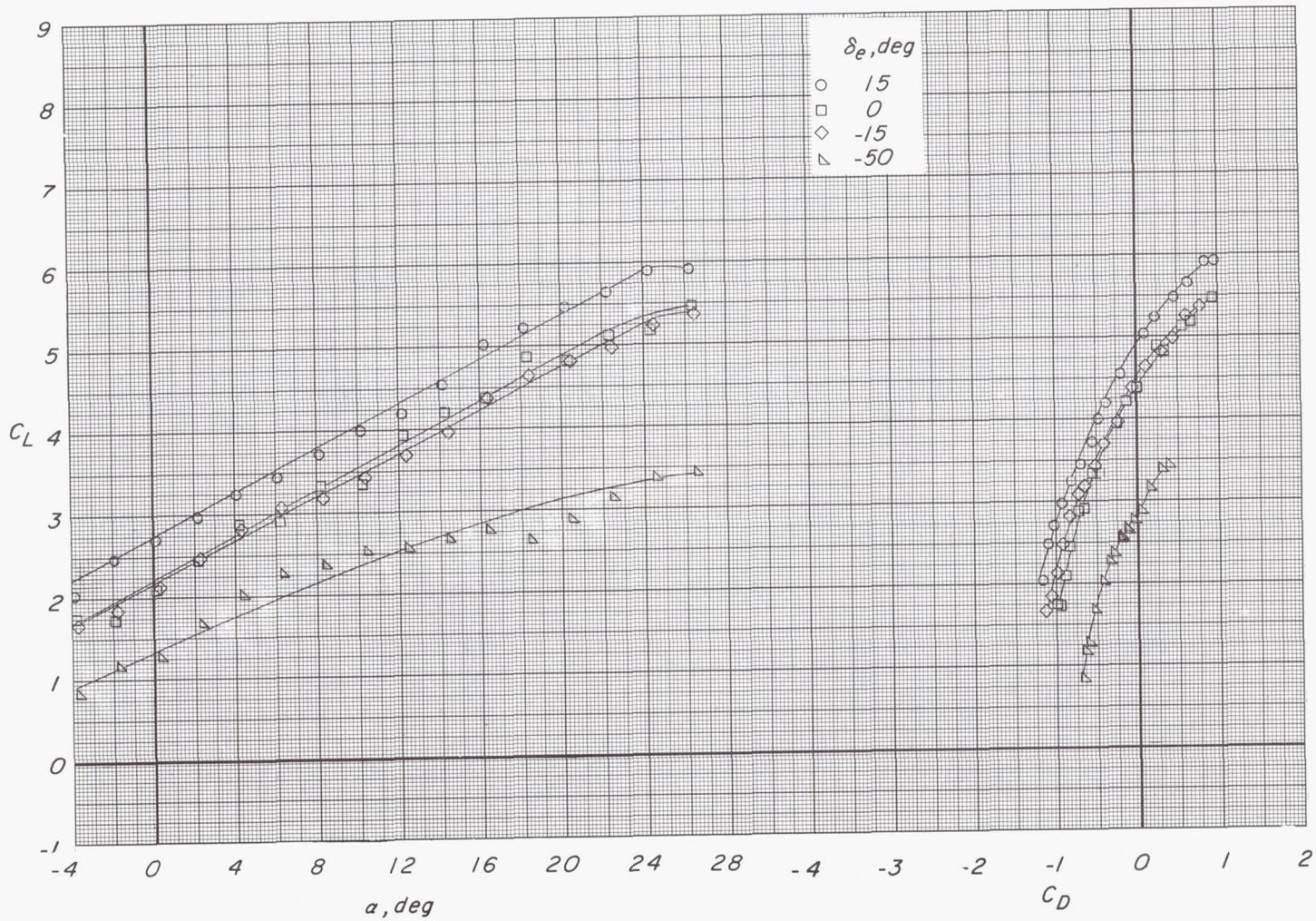

(a) Variation of C_L with α and C_D.

Figure 32.- Effect of elevator deflection on longitudinal aerodynamic characteristics. $\delta_f = 45^o$; $C_\mu = 0.21$; $C_T = 2.10$; $i_t = 0^o$.

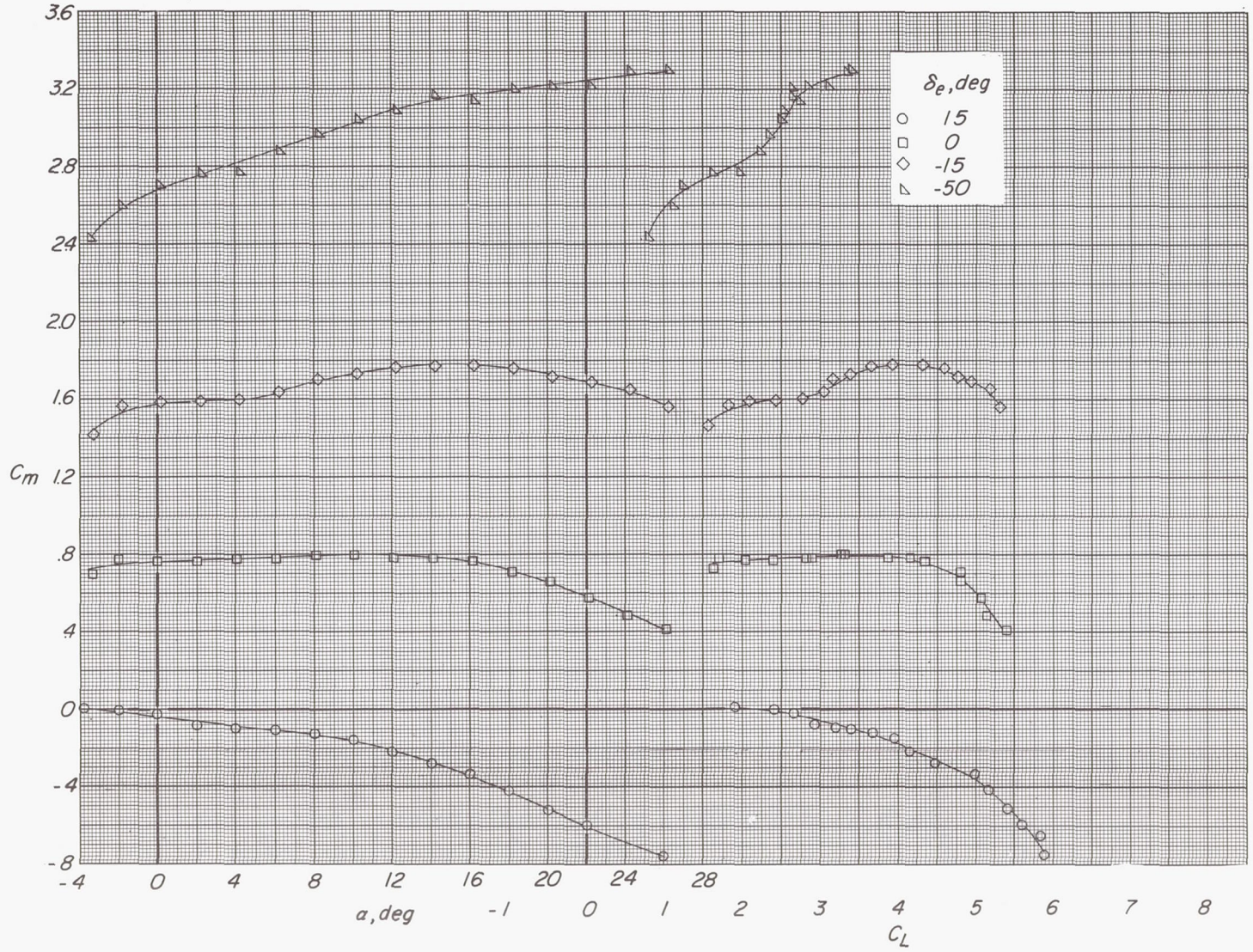

(b) Variation of C_m with α and C_L.

Figure 32.- Continued.

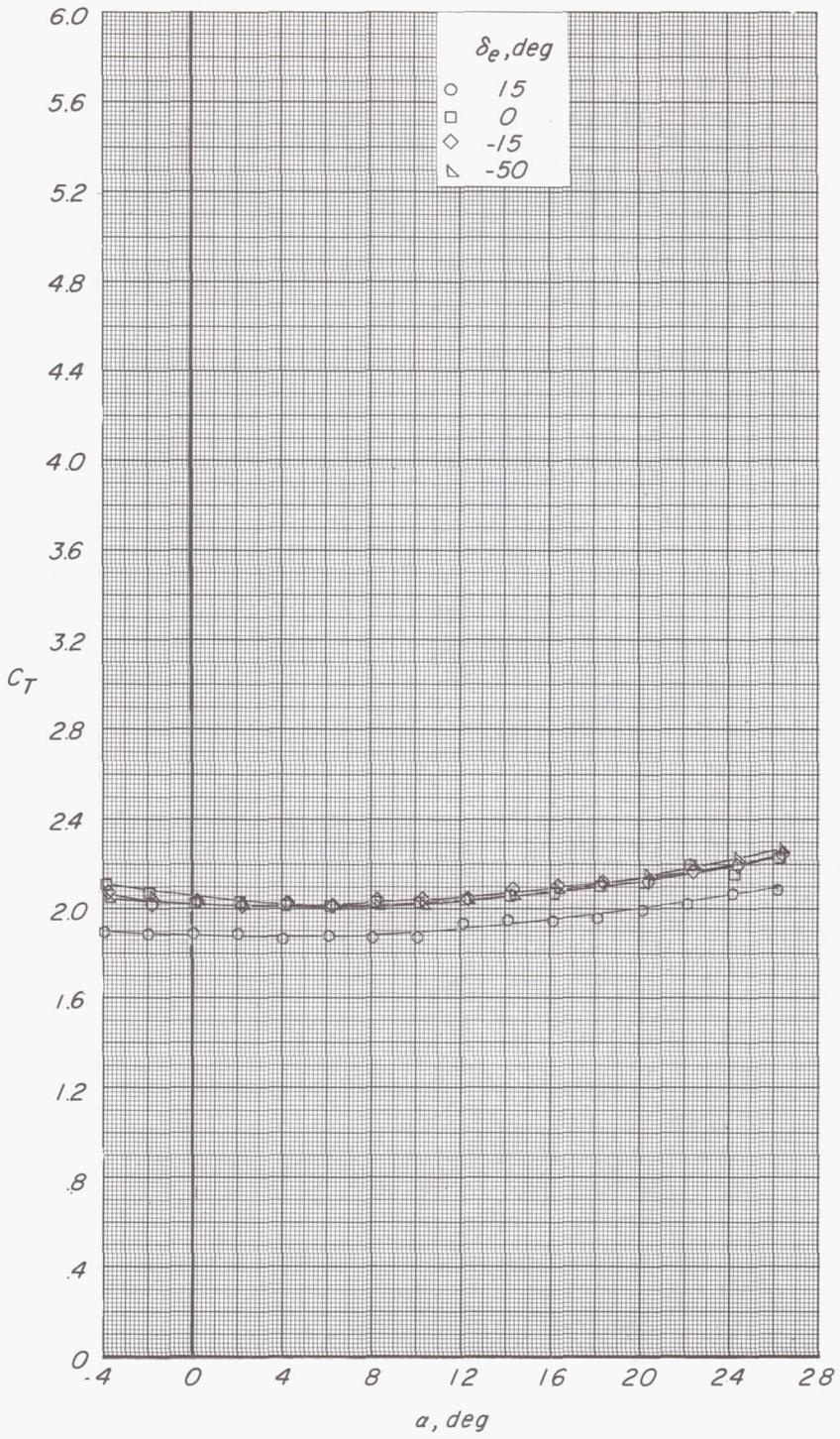

(c) Variation of C_T with α.

Figure 32.- Concluded.

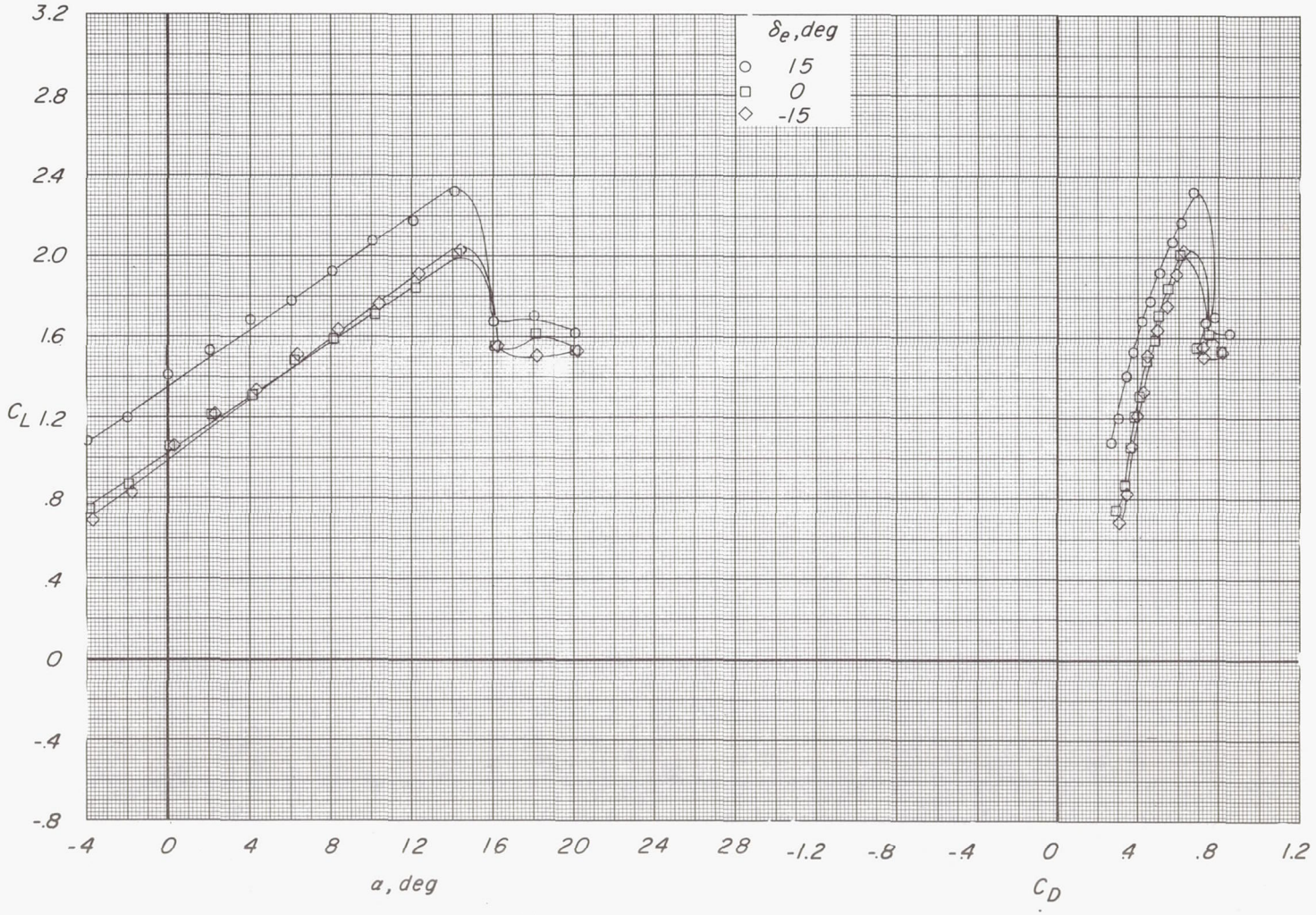

(a) Variation of C_L with α and C_D.

Figure 33.- Effect of elevator deflection on longitudinal aerodynamic characteristics. $\delta_f = 45^o$; $C_\mu = 0$; $C_T = 0$; $i_t = 10^o$.

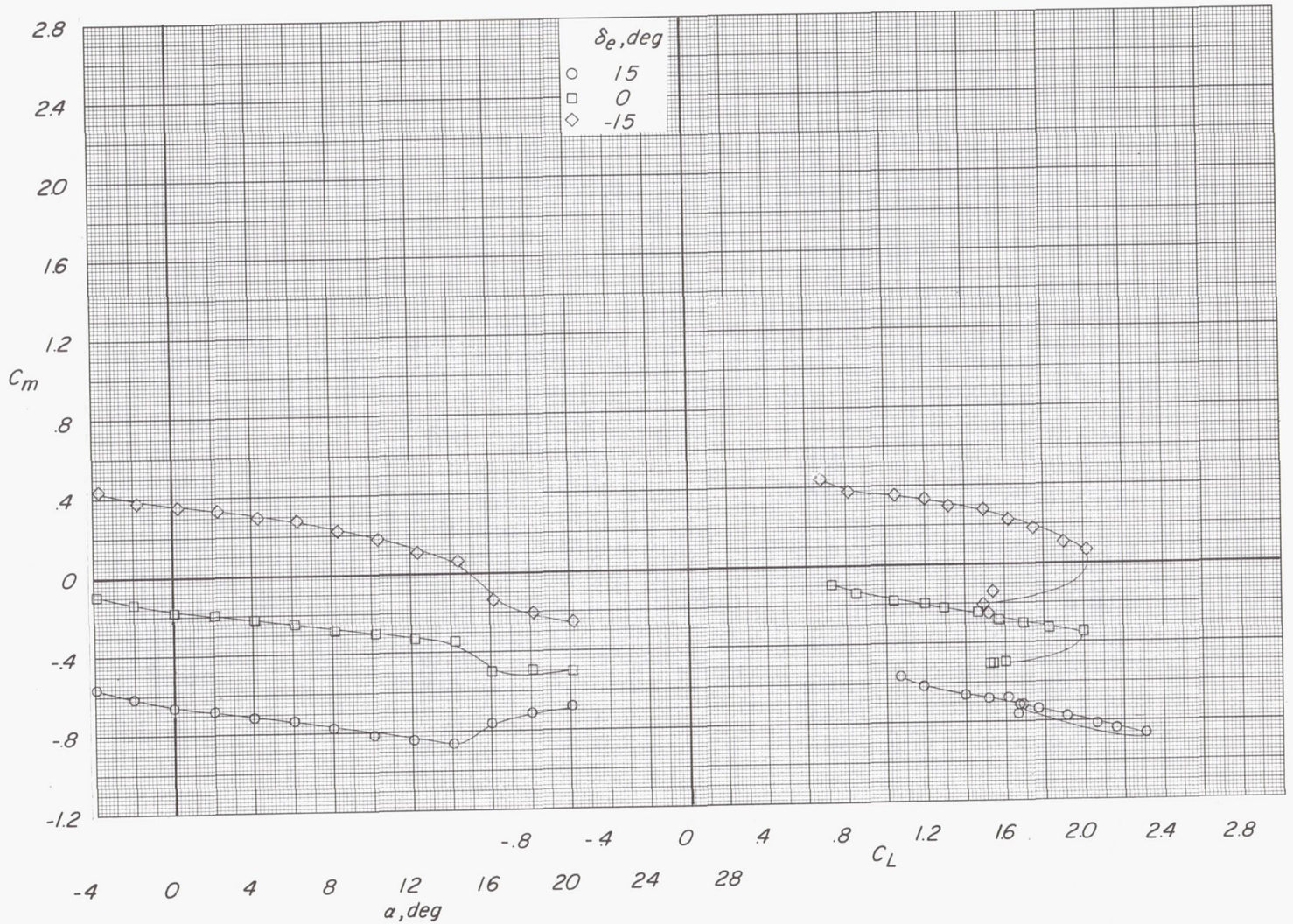

(b) Variation of C_m with α and C_L.

Figure 33.- Concluded.

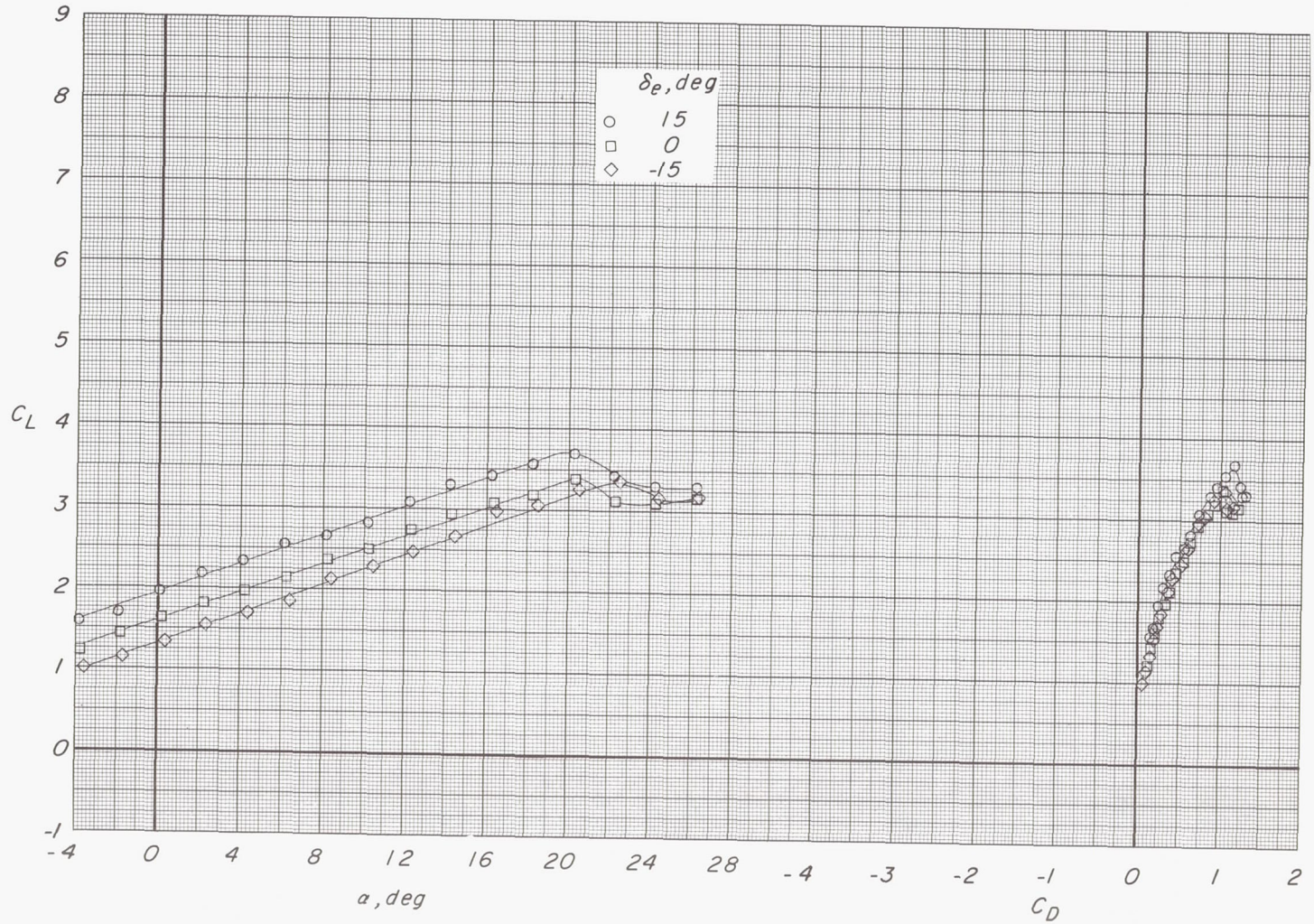

(a) Variation of C_L with α and C_D.

Figure 34.- Effect of elevator deflection on longitudinal aerodynamic characteristics. $\delta_f = 45^0$; $C_\mu = 0.05$; $C_T = 0.43$; $i_t = 10^0$.

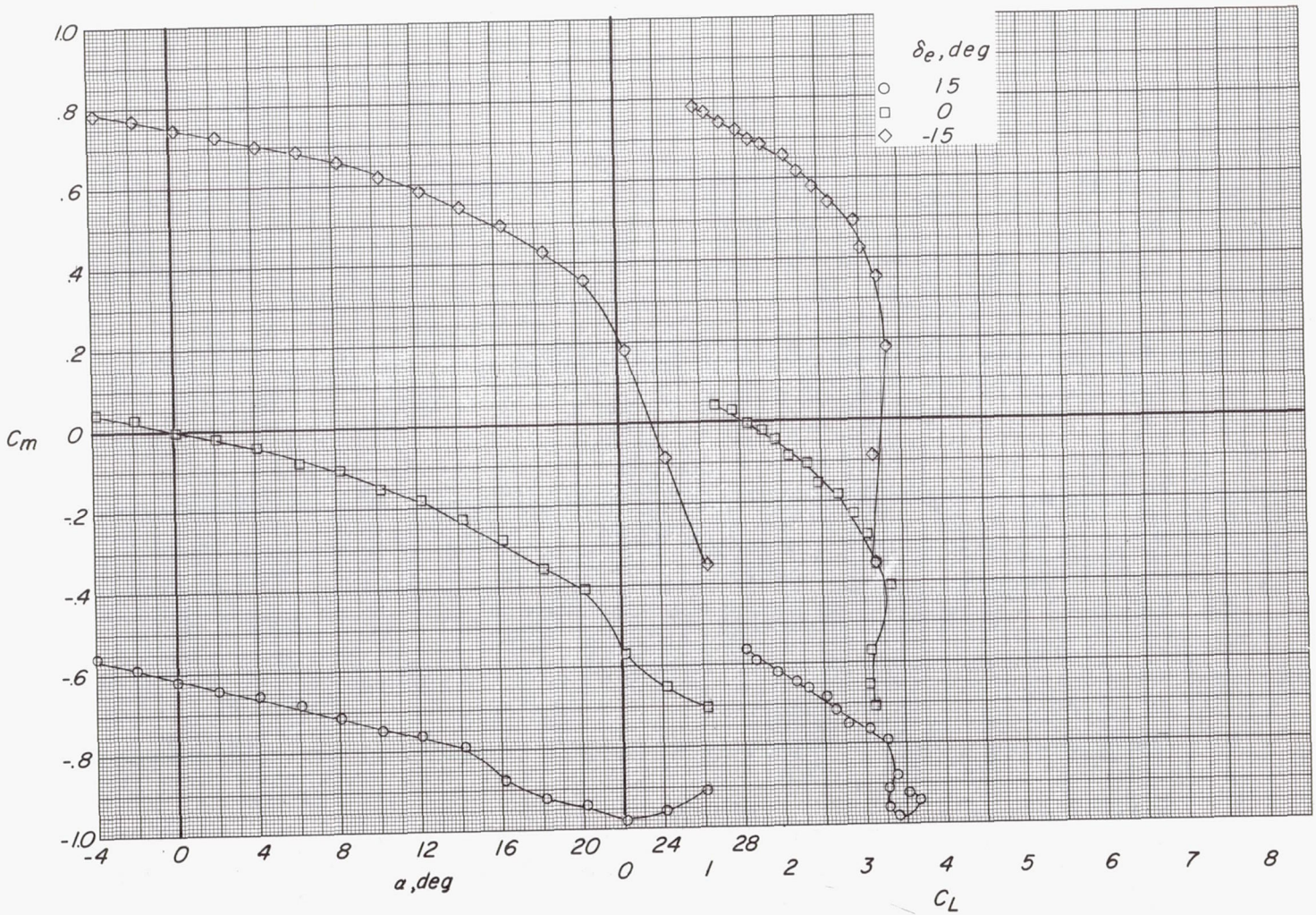

(b) Variation of C_m with α and C_L.

Figure 34.- Continued.

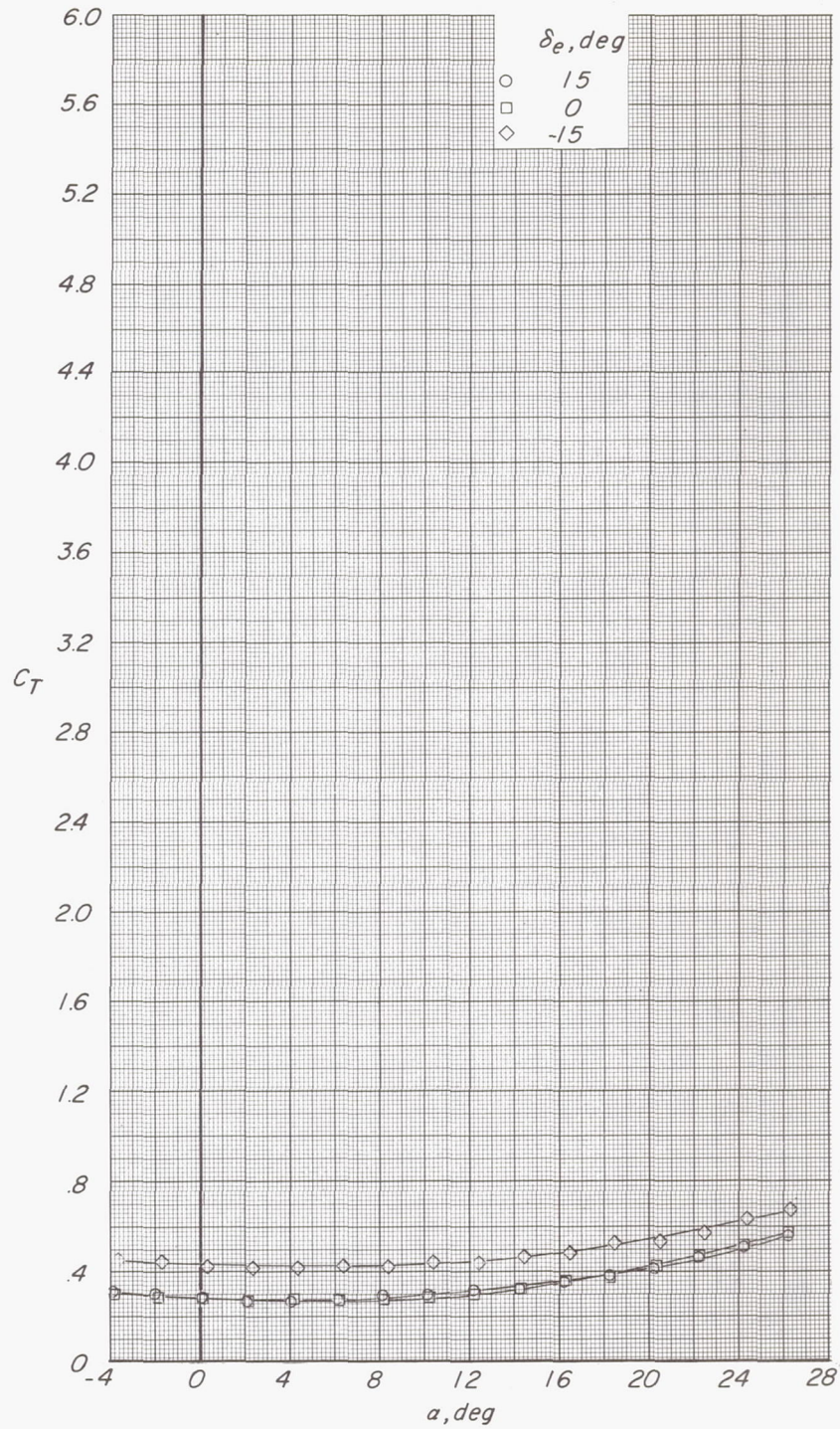

(c) Variation of C_T with α.

Figure 34.- Concluded.

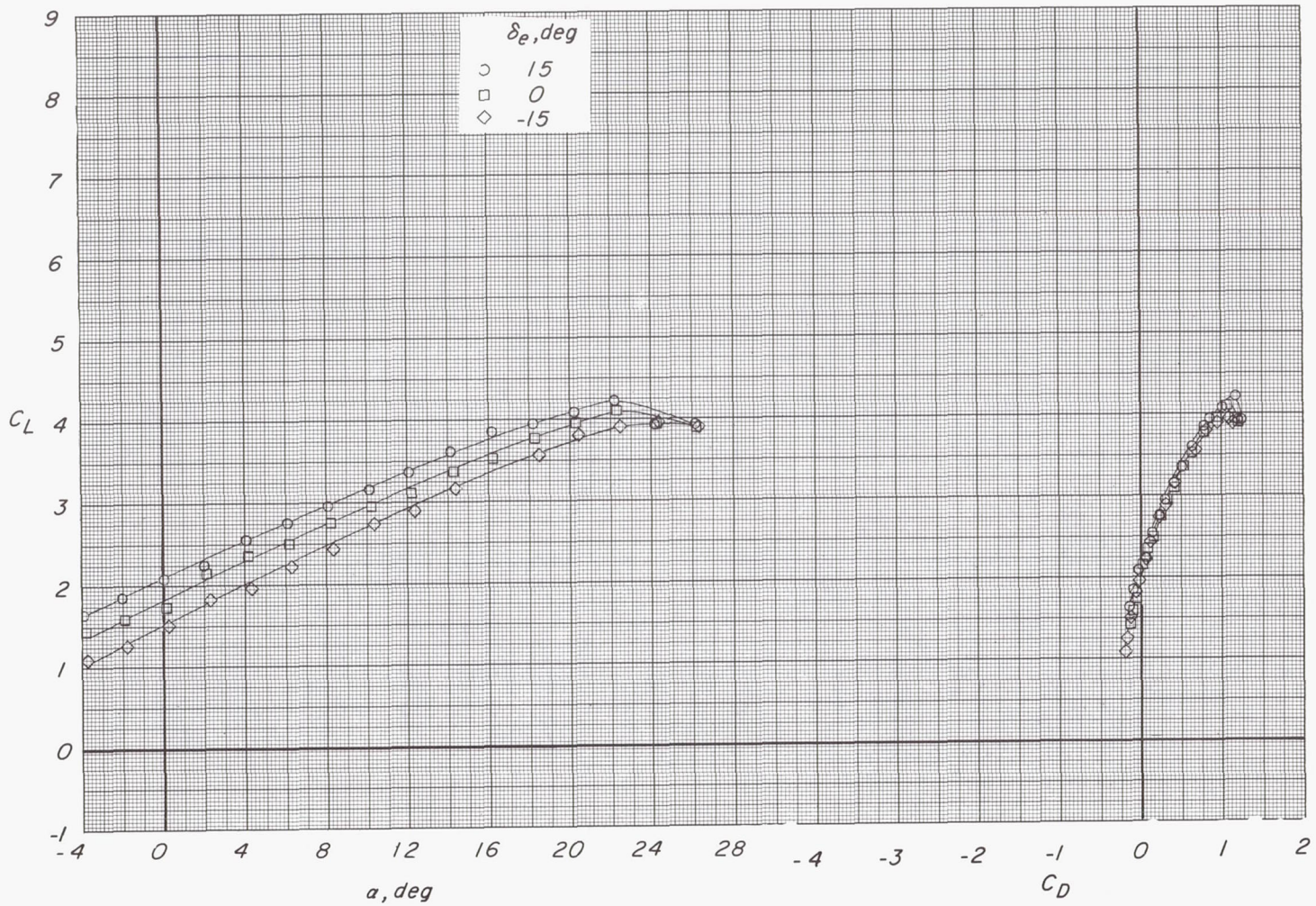

(a) Variation of C_L with α and C_D.

Figure 35.- Effect of elevator deflection on longitudinal aerodynamic characteristics. $\delta_f = 45^0$; $C_\mu = 0.10$; $C_T = 0.83$; $i_t = 10^0$.

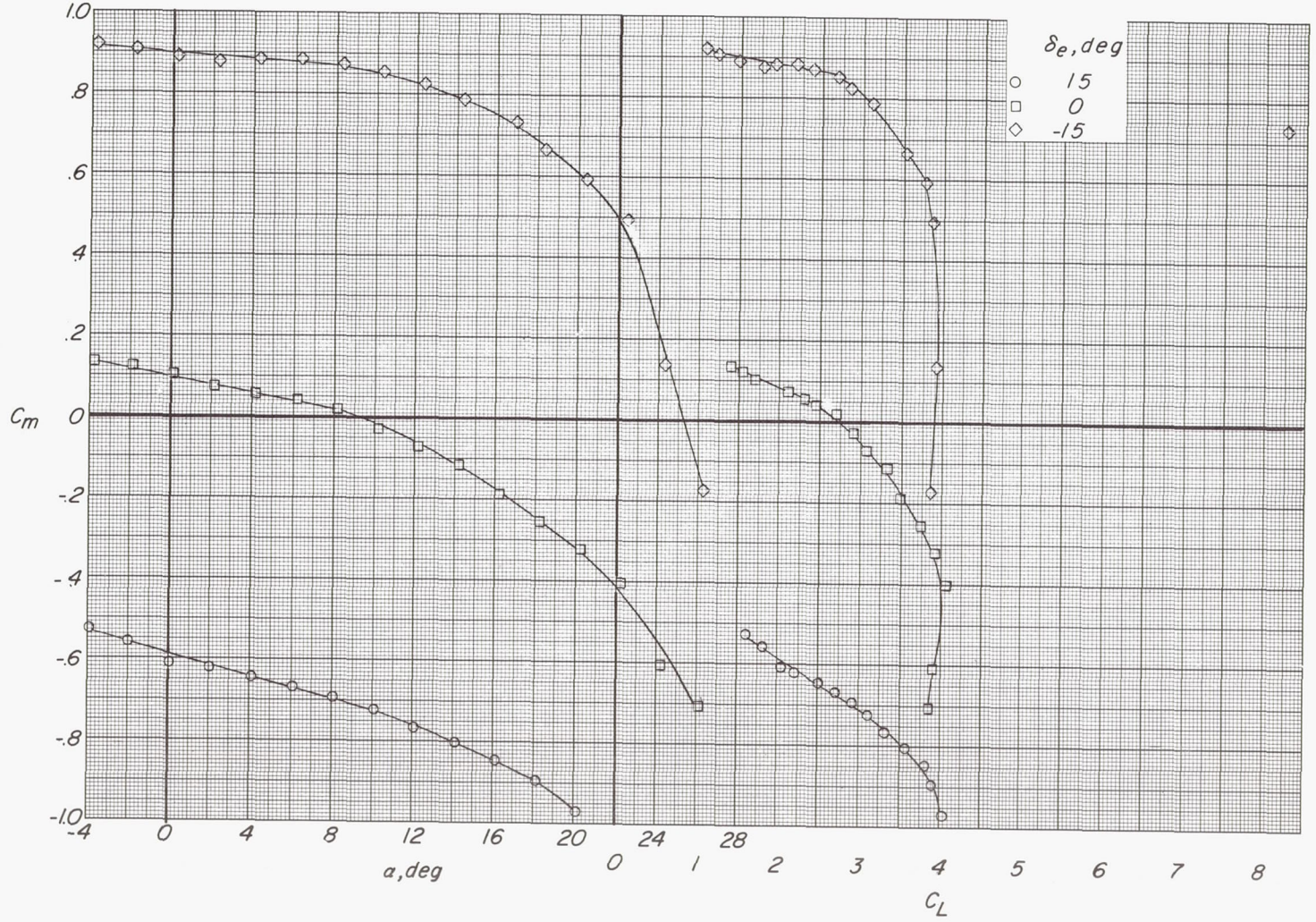

(b) Variation of C_m with α and C_L.

Figure 35.- Continued.

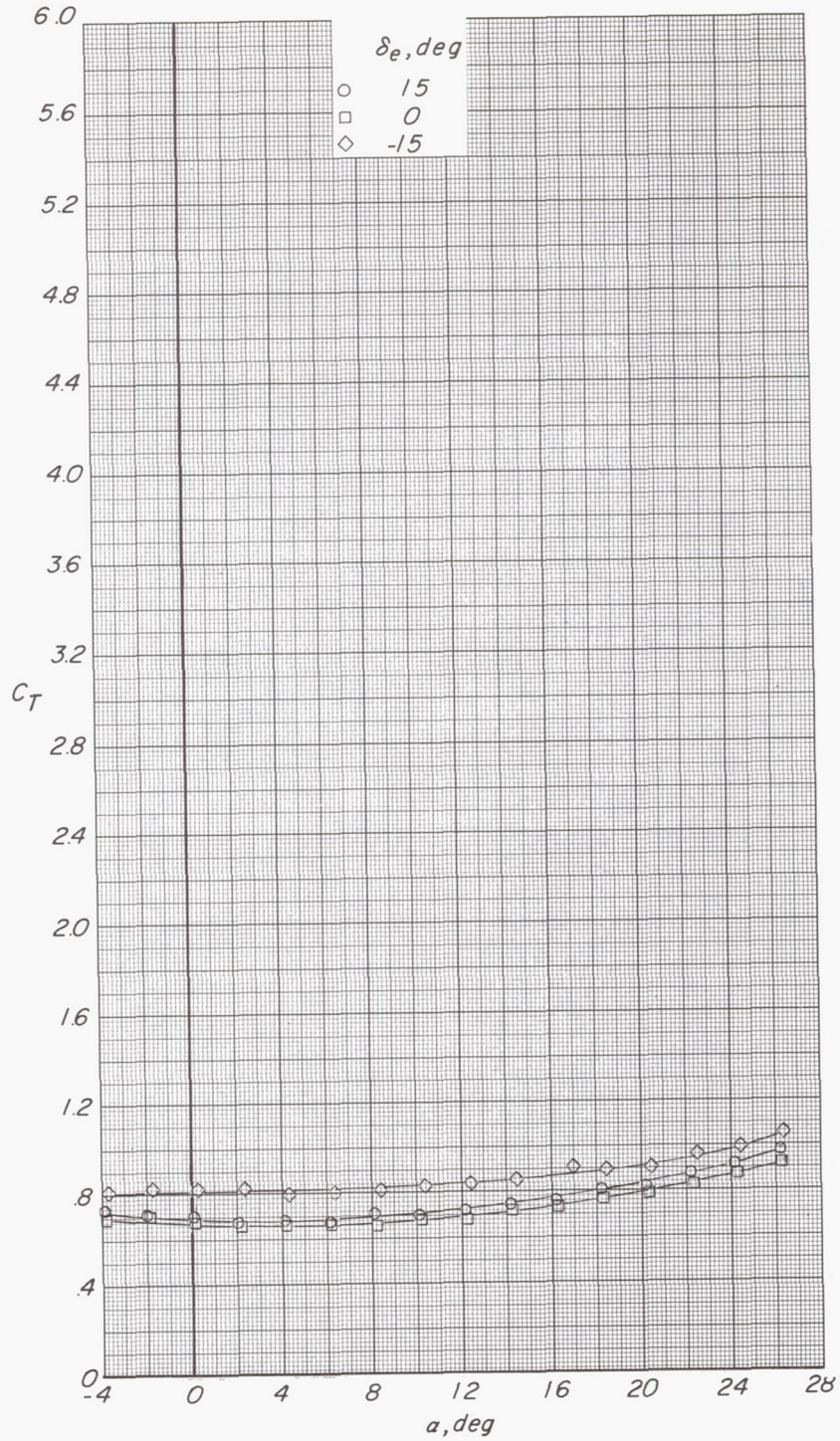

(c) Variation of C_T with α.

Figure 35.- Concluded.

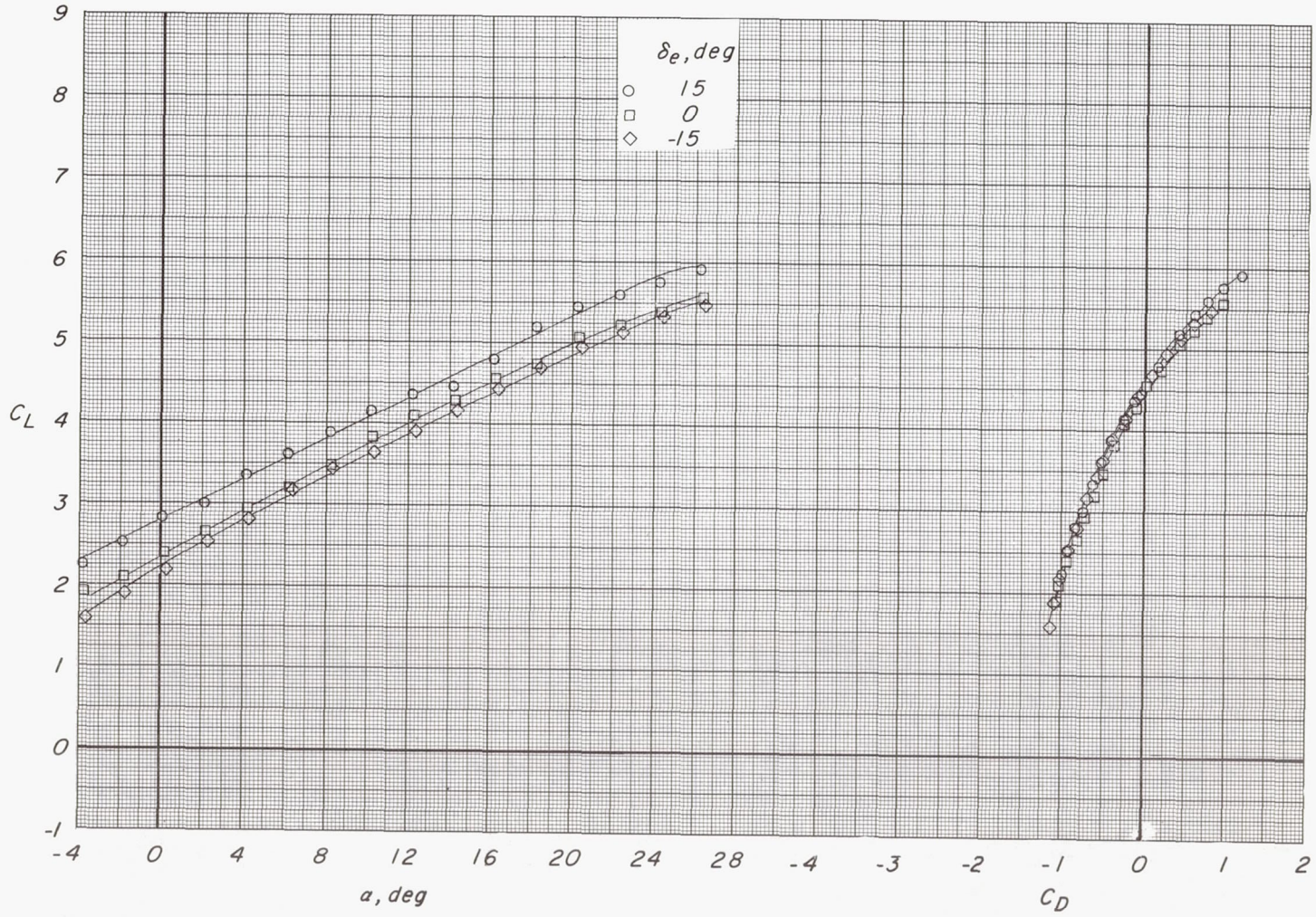

(a) Variation of C_L with α and C_D.

Figure 36.- Effect of elevator deflection on longitudinal aerodynamic characteristics. $\delta_f = 45^0$; $C_\mu = 0.21$; $C_T = 2.10$; $i_t = 10^0$.

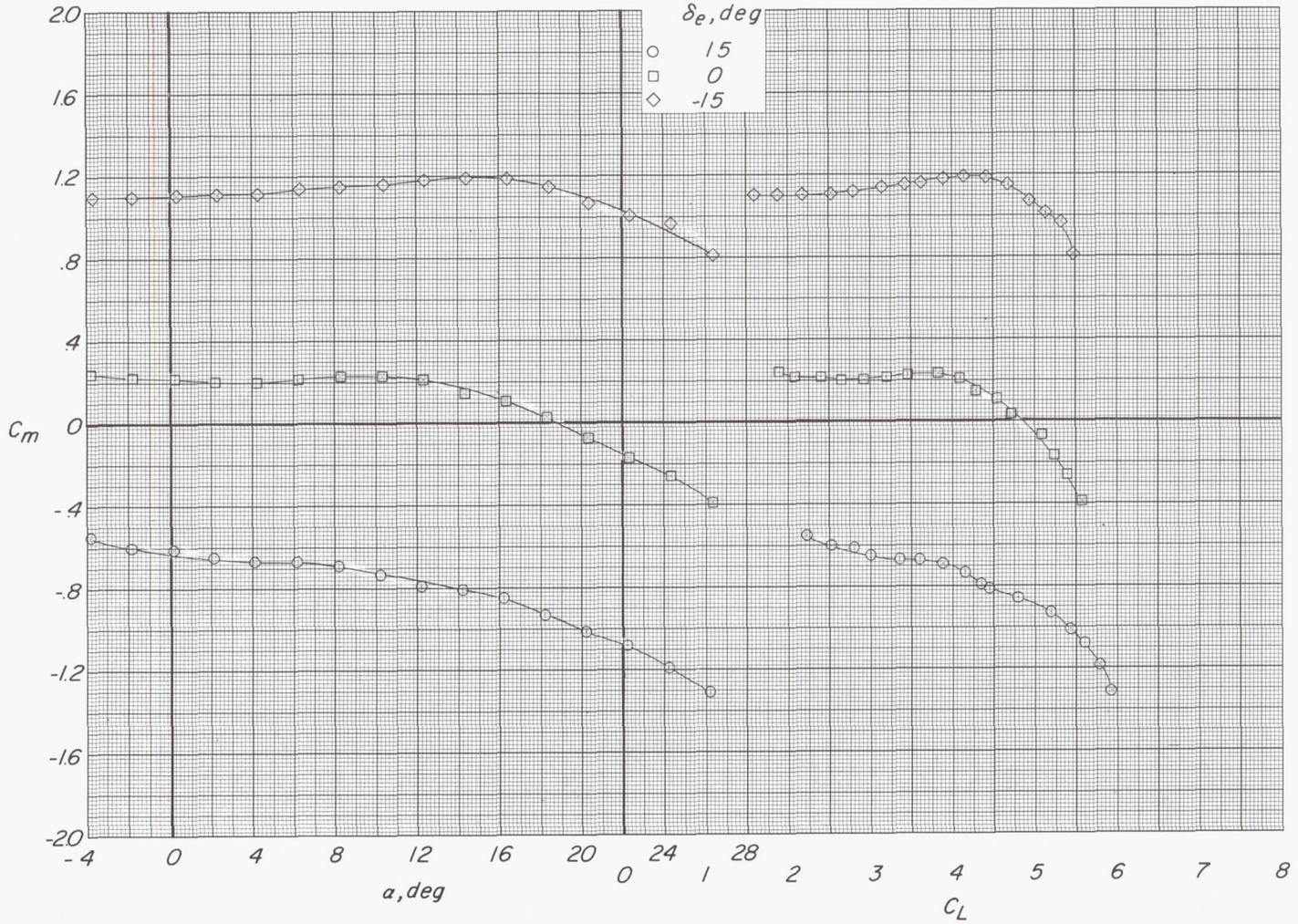

(b) Variation of C_m with α and C_L.

Figure 36.- Continued.

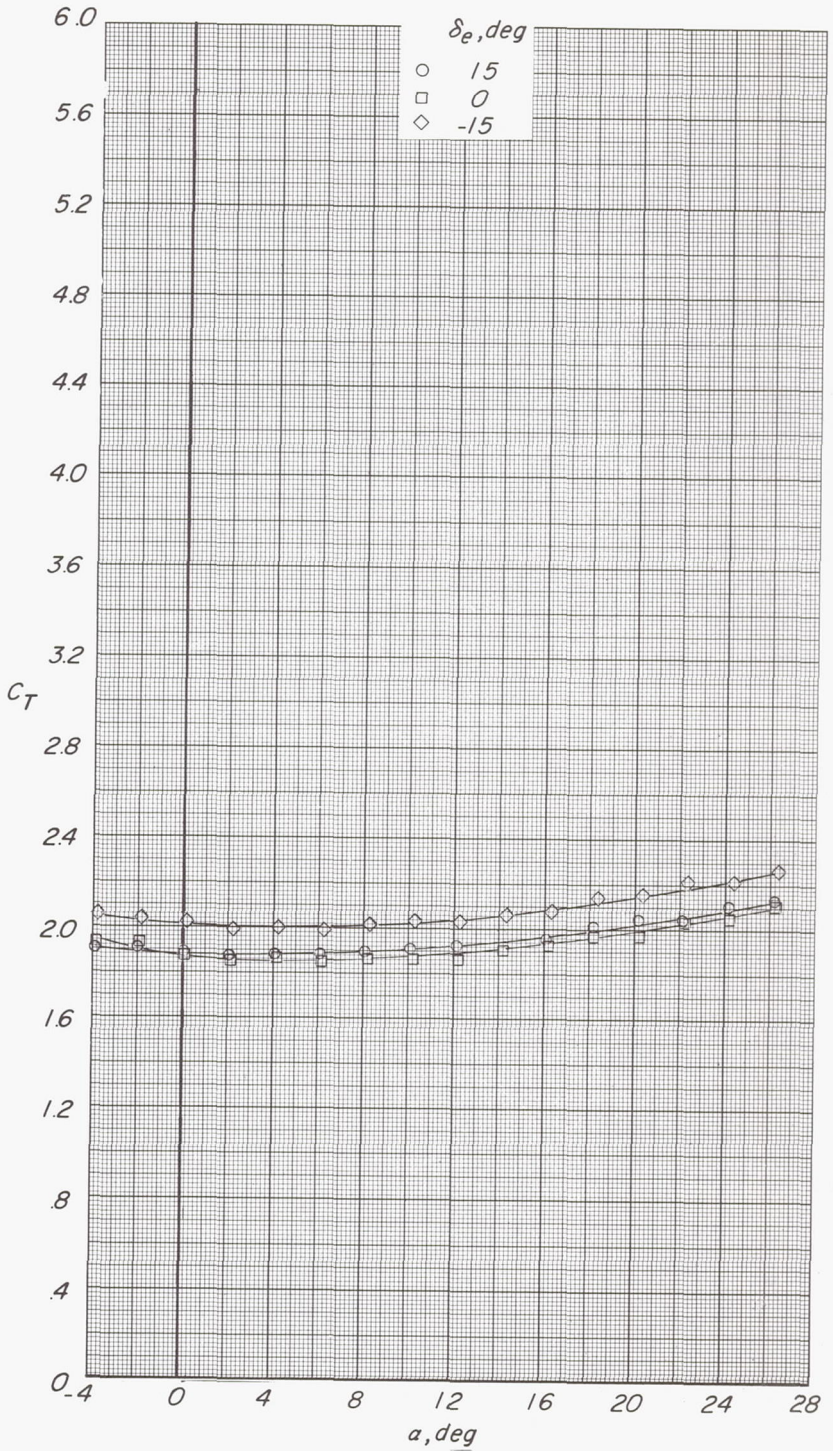

(c) Variation of C_T with α.

Figure 36.- Concluded.

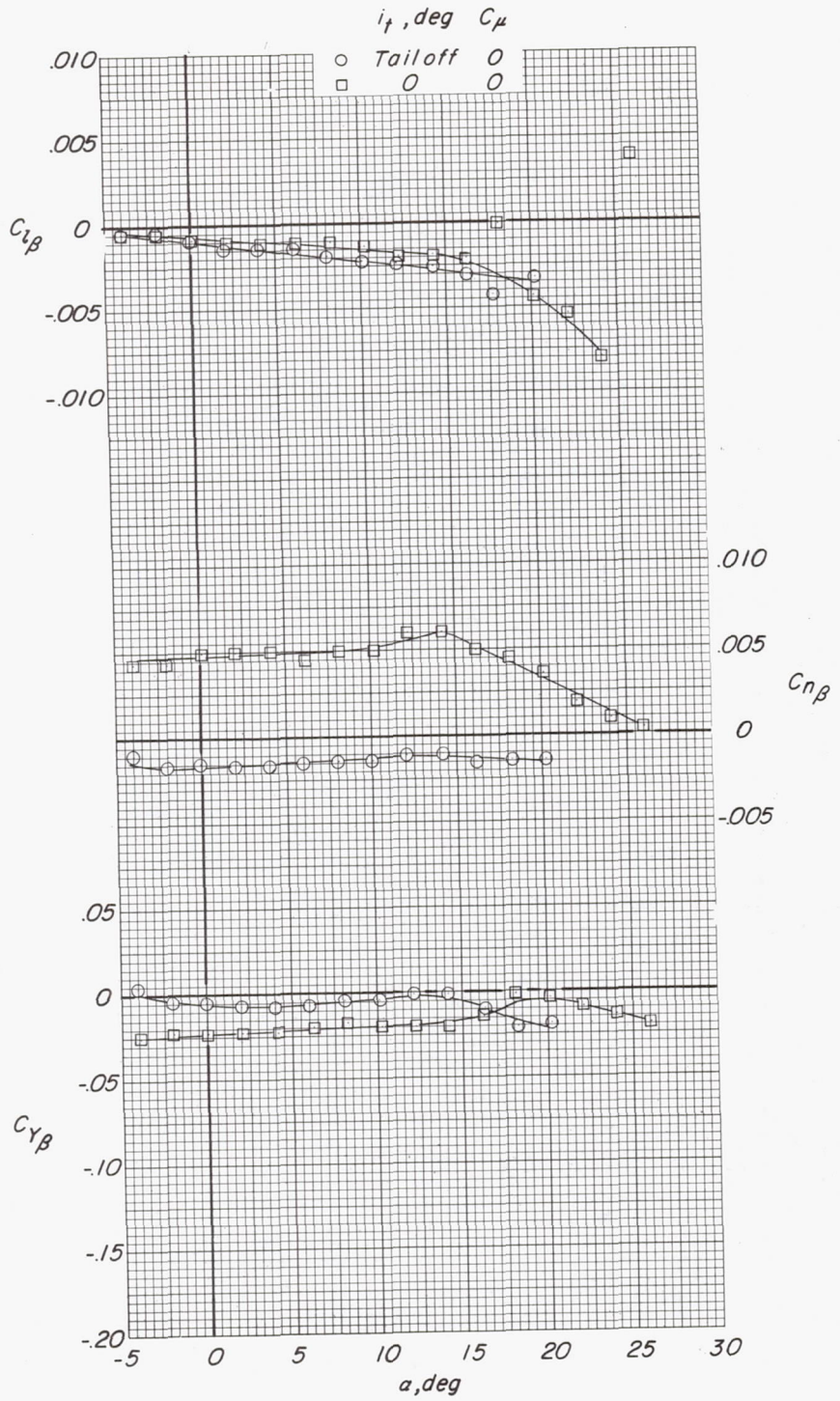

(a) $C_T = 0$.

Figure 37.- Effect of tail and tail momentum coefficient on lateral-directional stability derivatives. $\delta_f = 0^0$.

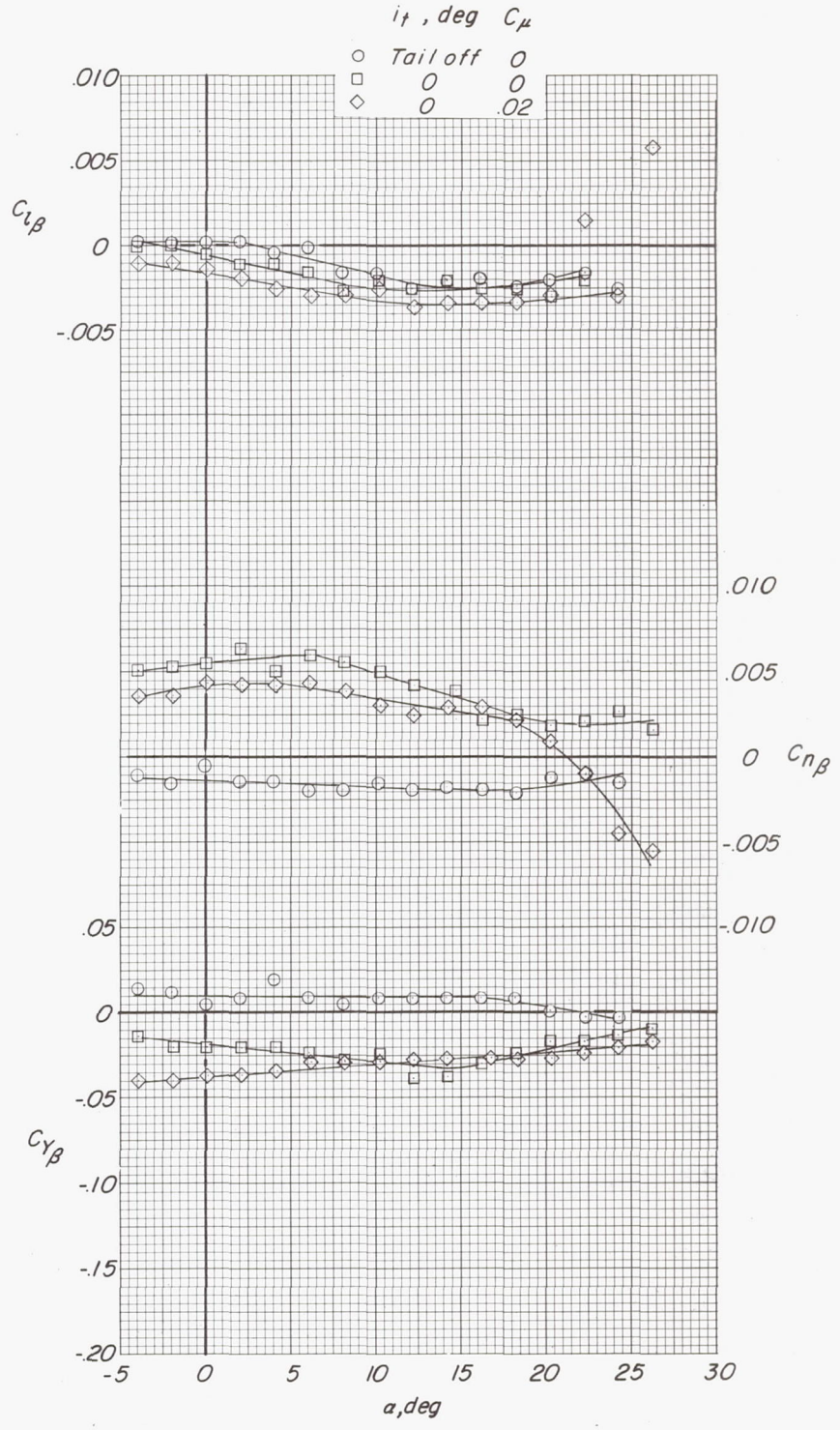

(b) $C_T = 0.14$.

Figure 37.- Continued.

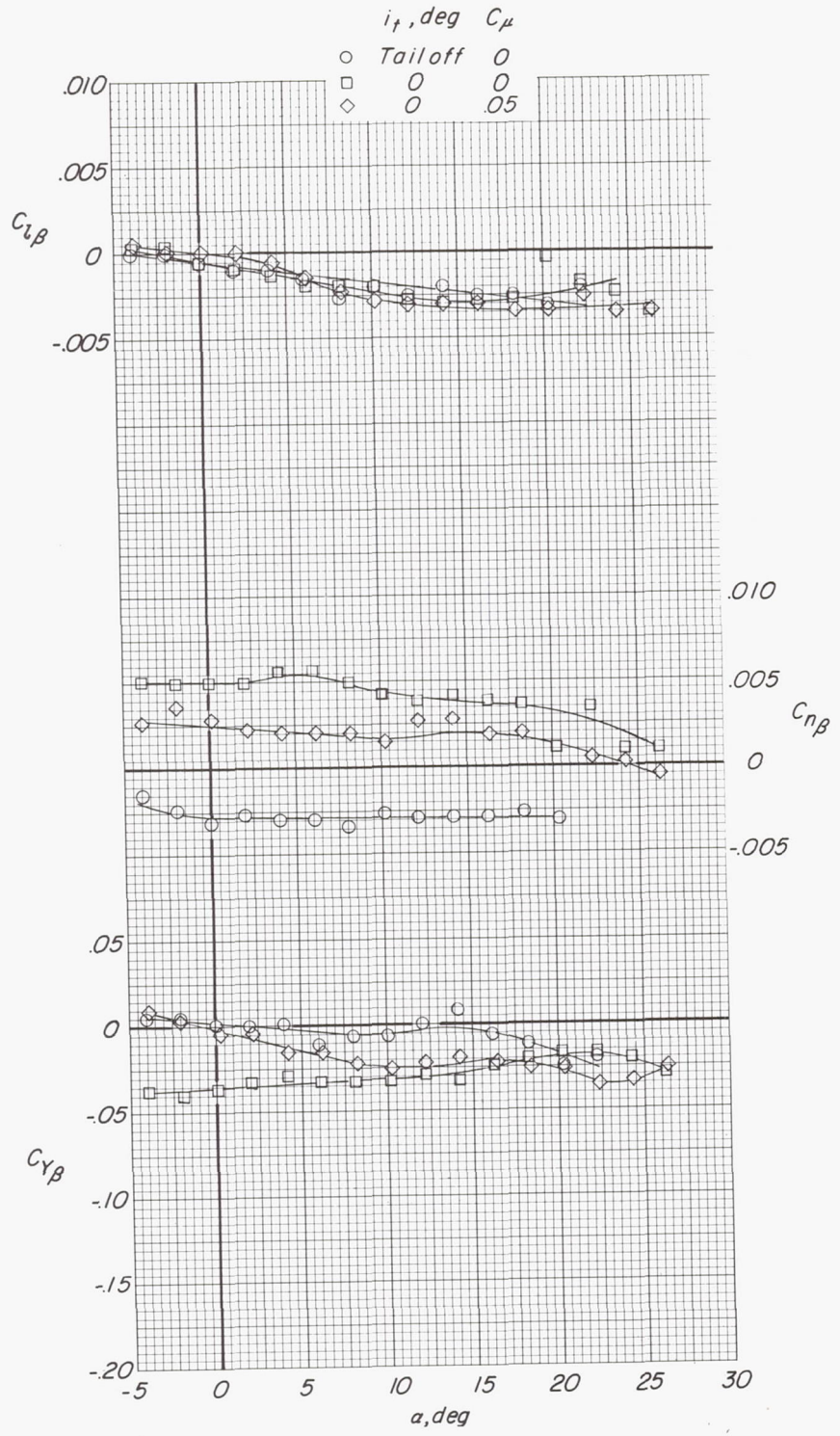

(c) C_T = 0.43.

Figure 37.- Concluded.

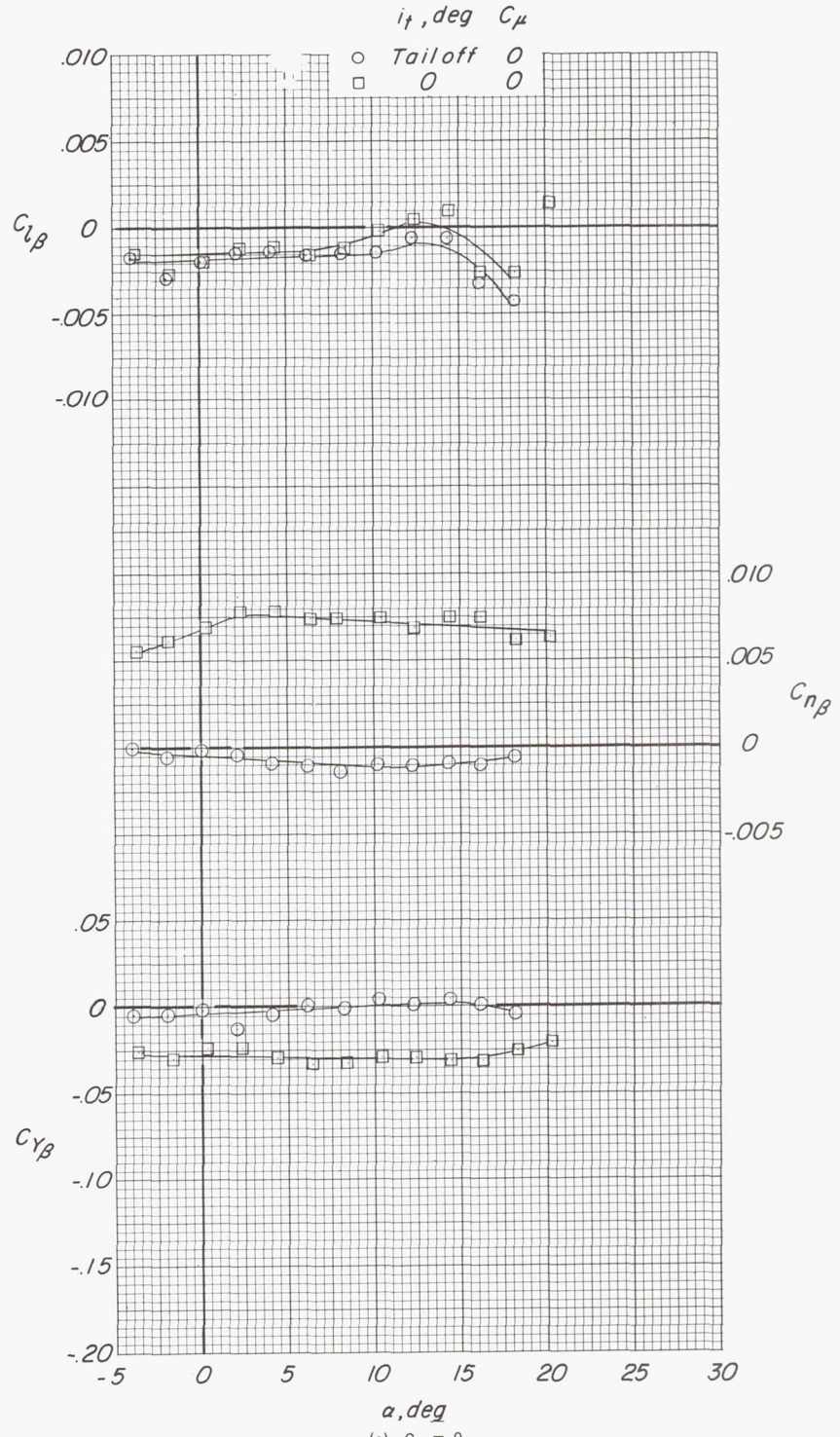

(a) $C_T = 0$.

Figure 38.- Effect of tail and tail momentum coefficient on lateral-directional stability derivatives. $\delta_f = 45^0$.

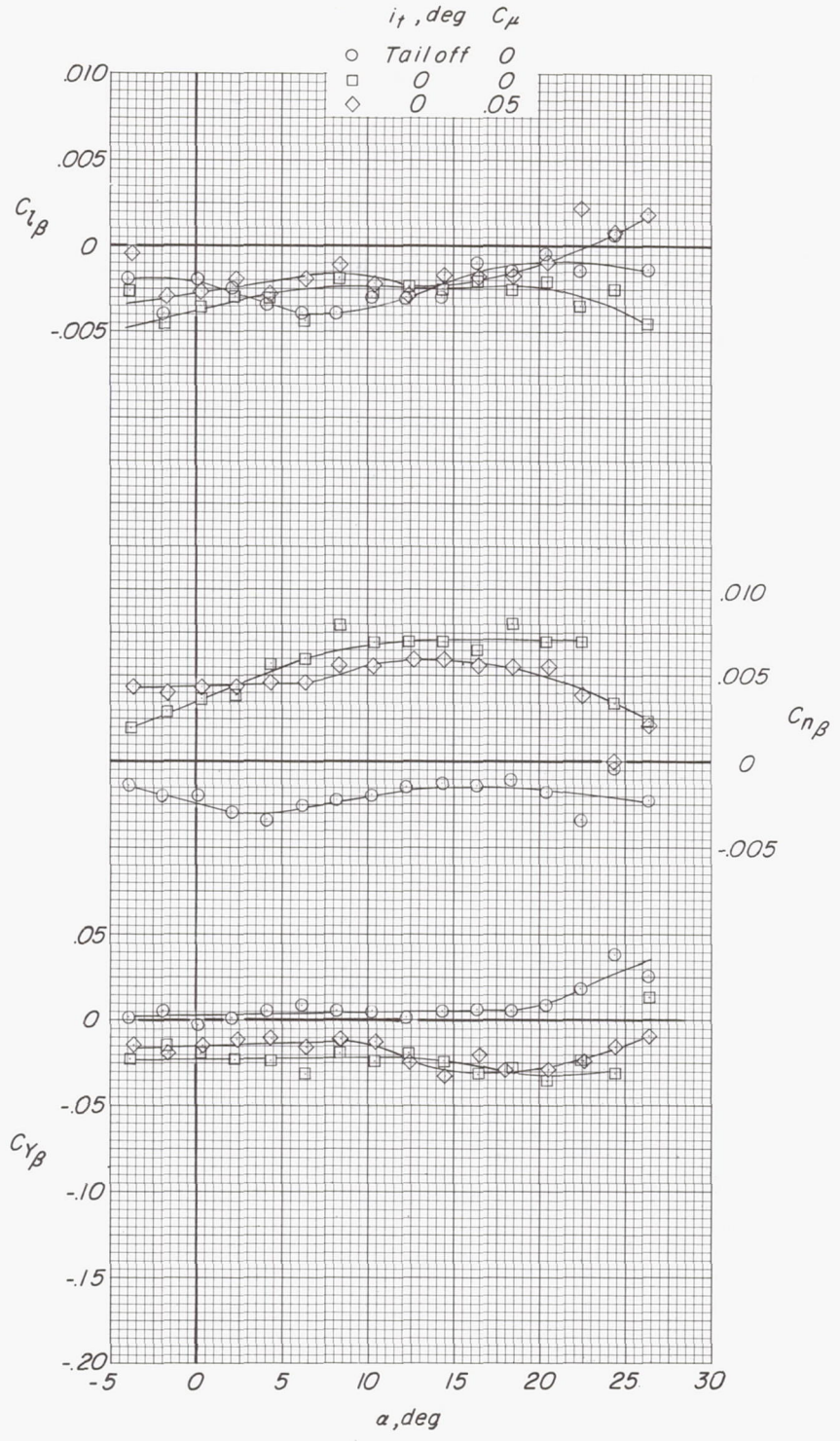

(b) $C_T = 0.43$.

Figure 38.- Continued.

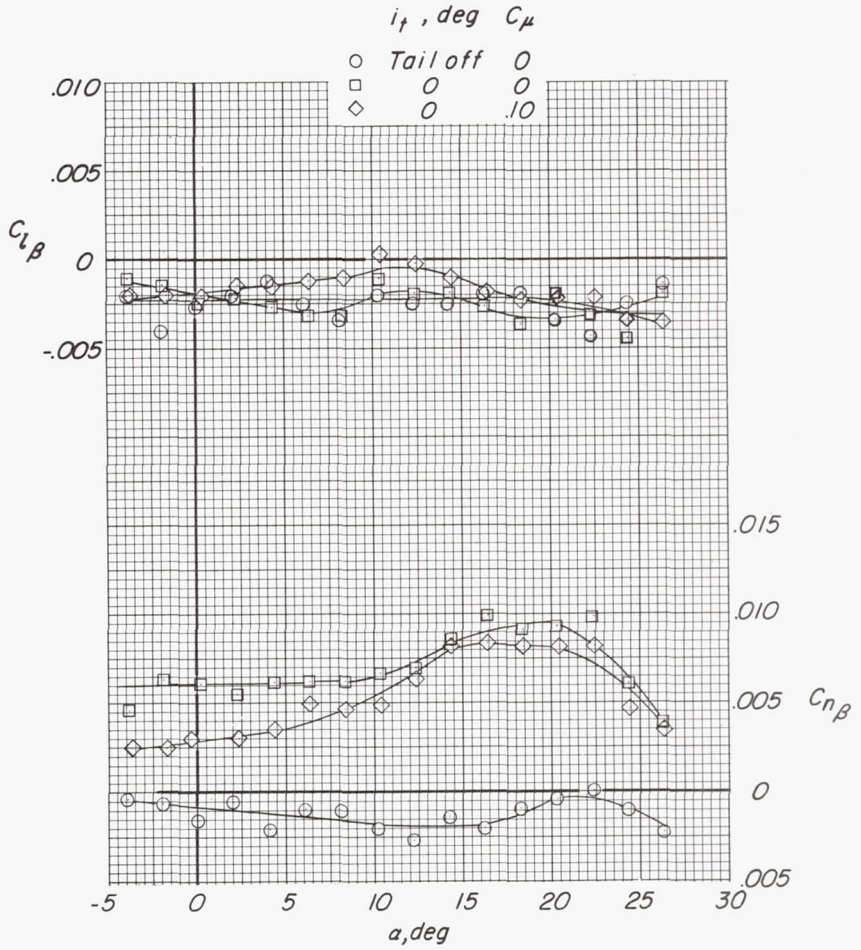

(c) C_T = 0.83.

Figure 38.- Continued.

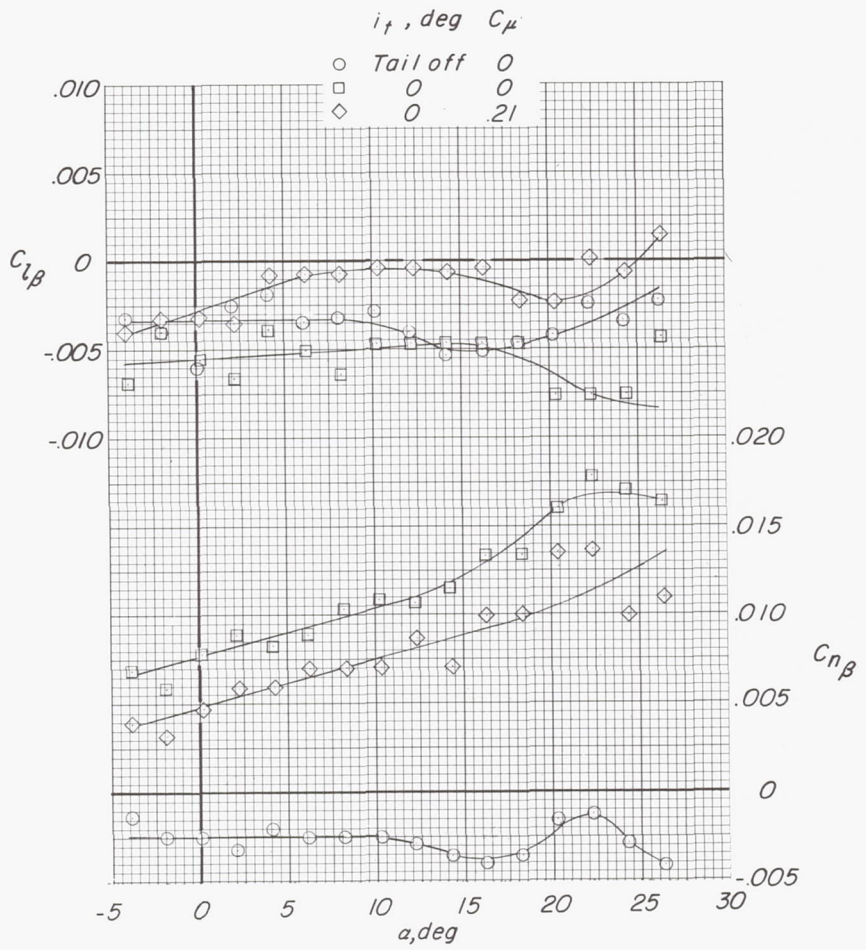

(d) C_T = 2.10.

Figure 38.- Concluded.

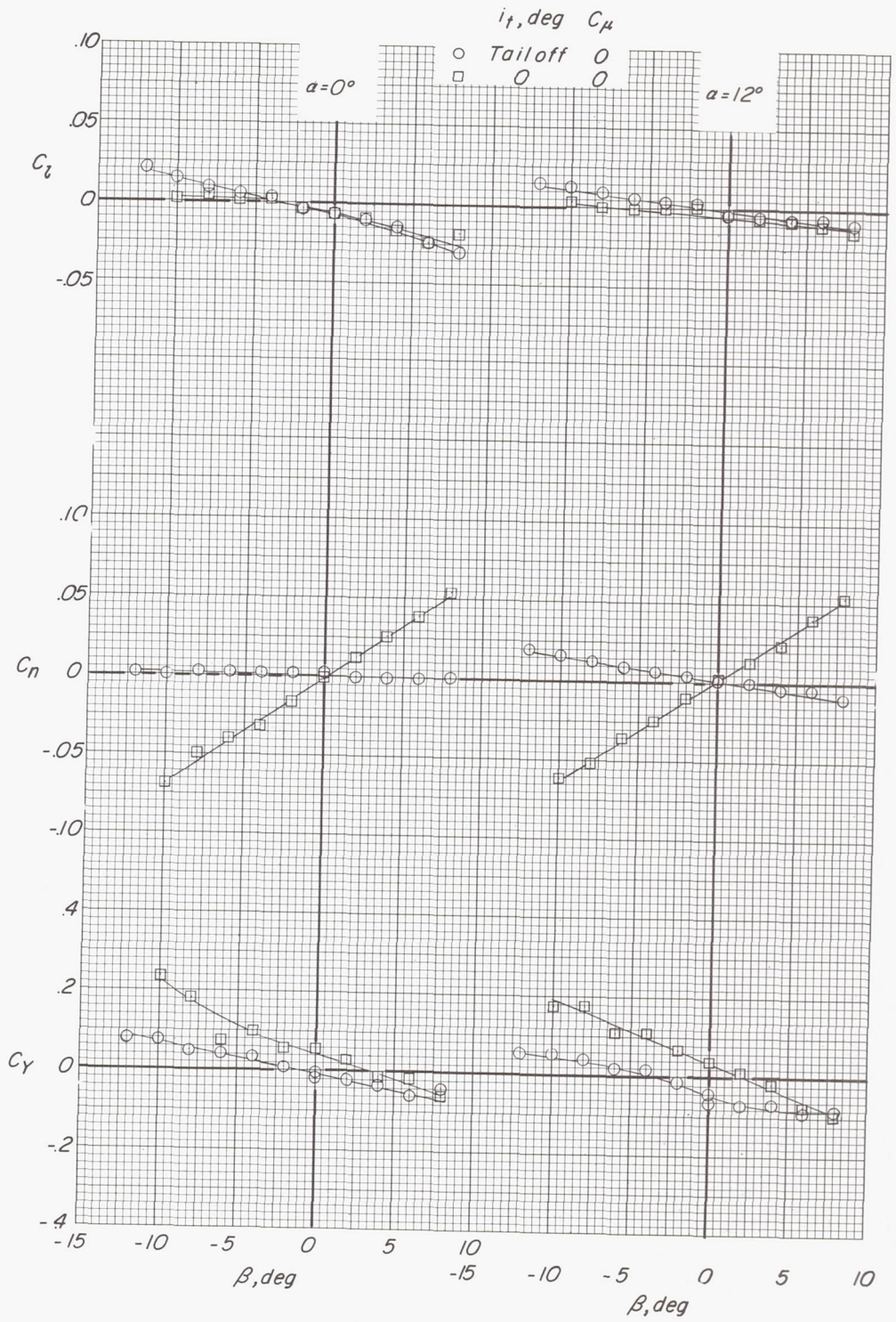

(a) Variation of C_l, C_n, and C_Y with β.

Figure 39.- Effect of tail on lateral-directional aerodynamic characteristics. $\delta_f = 45^0$; $C_T = 0$.

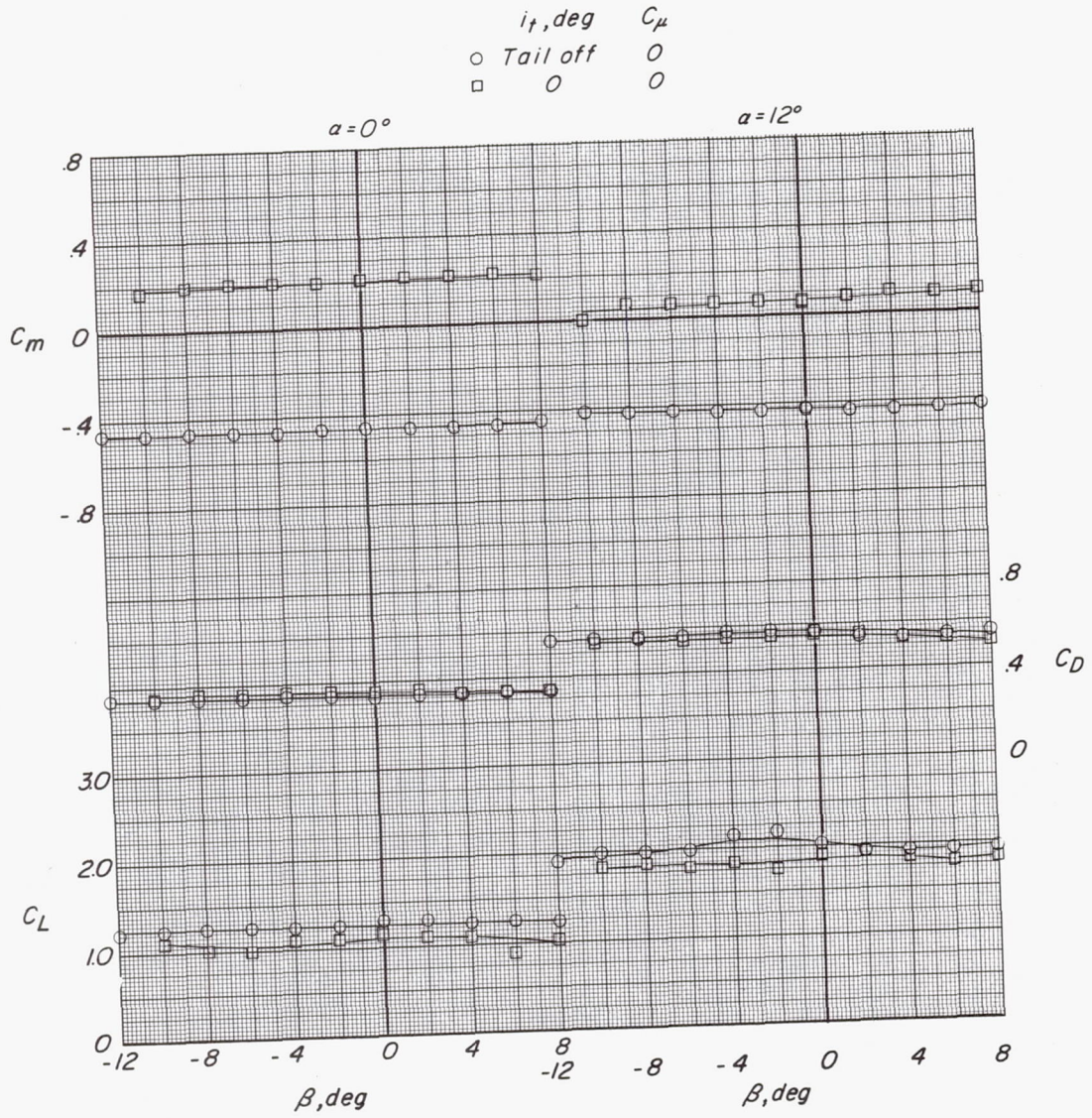

(b) Variation of C_L, C_m, and C_D with β.

Figure 39.- Concluded.

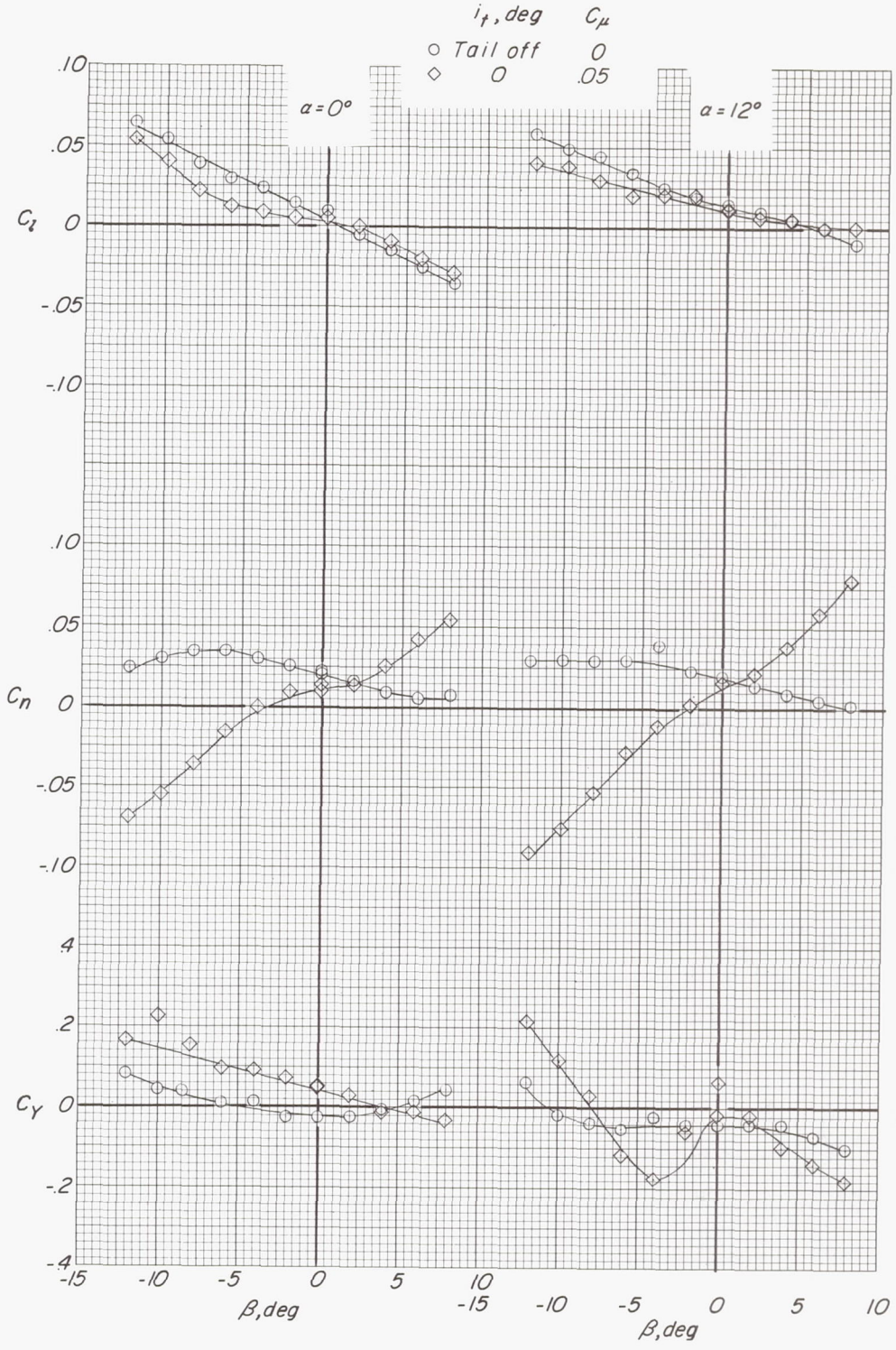

(a) Variation of C_l, C_n, and C_Y with β.

Figure 40.- Effect of tail boundary-layer control on lateral-directional aerodynamic characteristics. $\delta_f = 45^o$; $C_T = 0.43$.

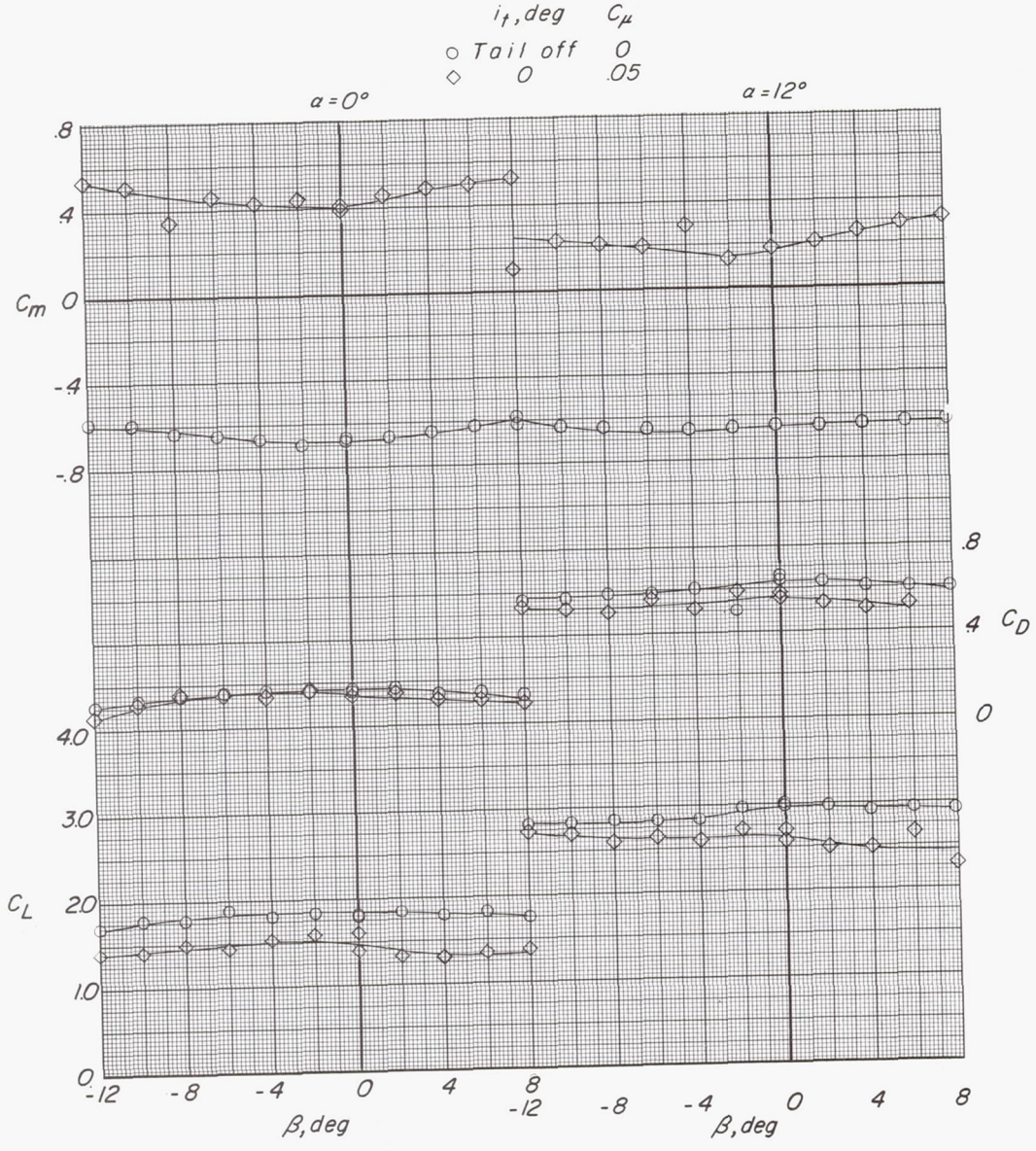

(b) Variation of C_L, C_m, and C_D with β.

Figure 40.- Continued.

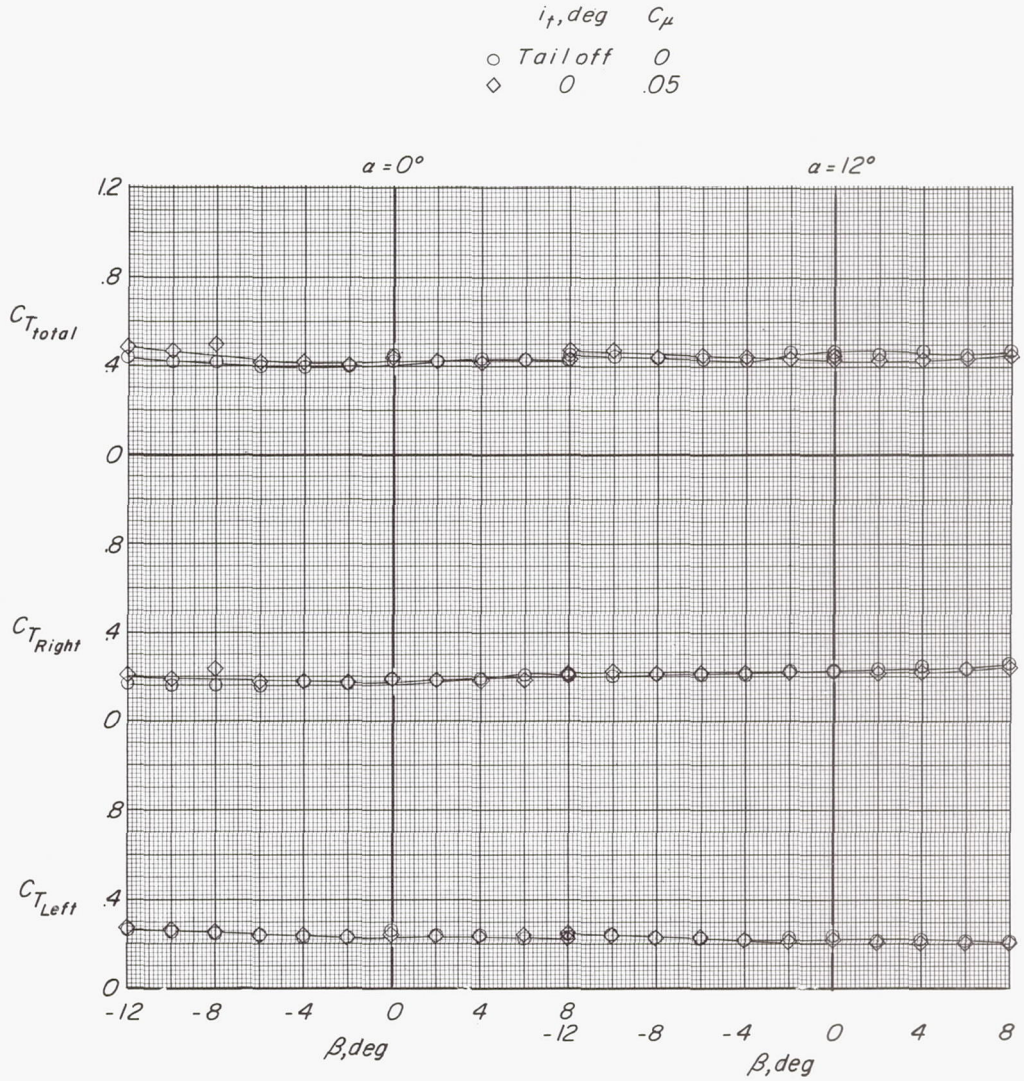

(c) Variation of C_T with β.

Figure 40.- Concluded.

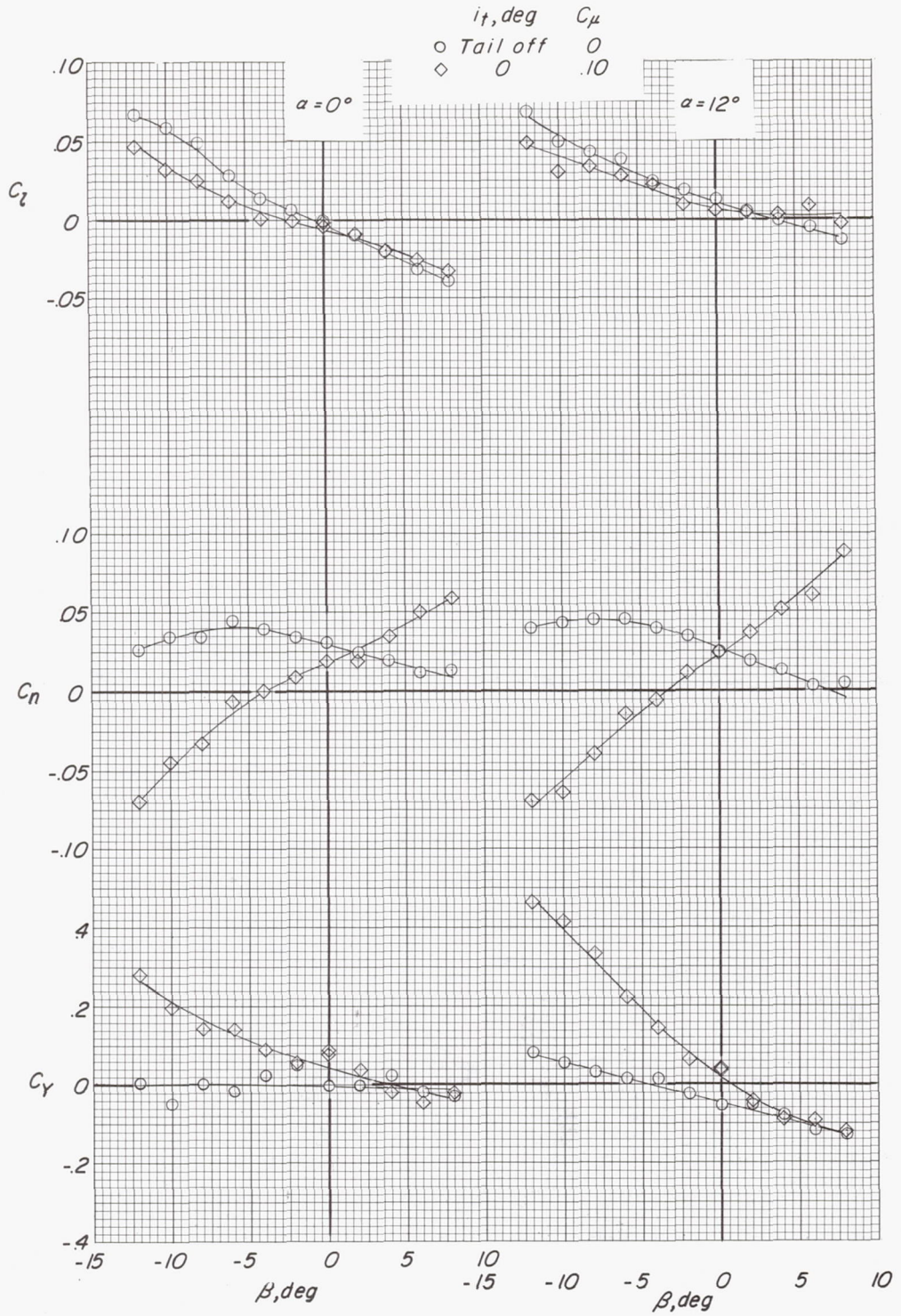

(a) Variation of C_l, C_n, and C_Y with β.

Figure 41.- Effect of tail boundary-layer control on lateral-directional aerodynamic characteristics. $\delta_f = 45^0$; $C_T = 0.83$.

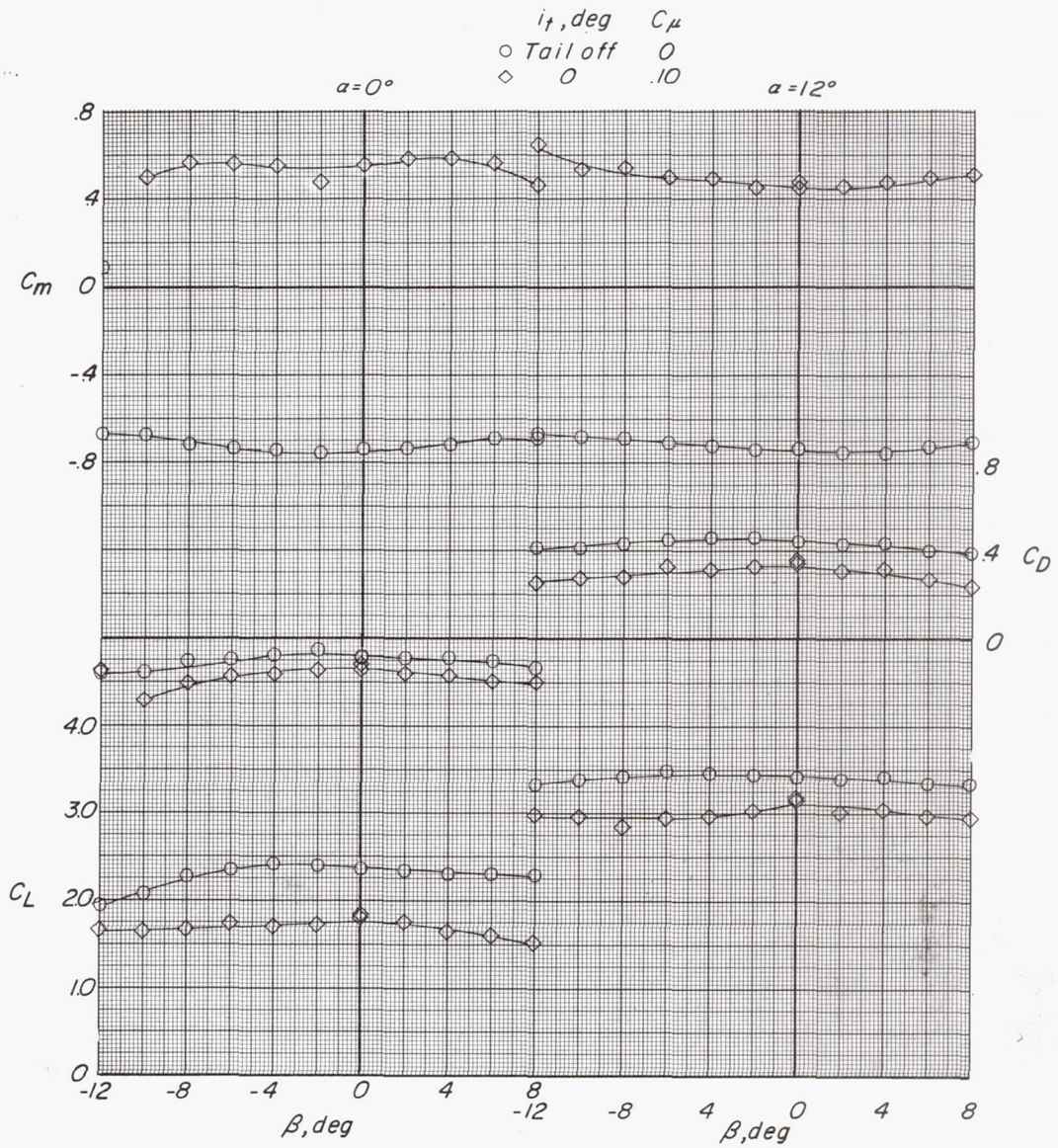

(b) Variation of C_L, C_m, and C_D with β.

Figure 41.- Continued.

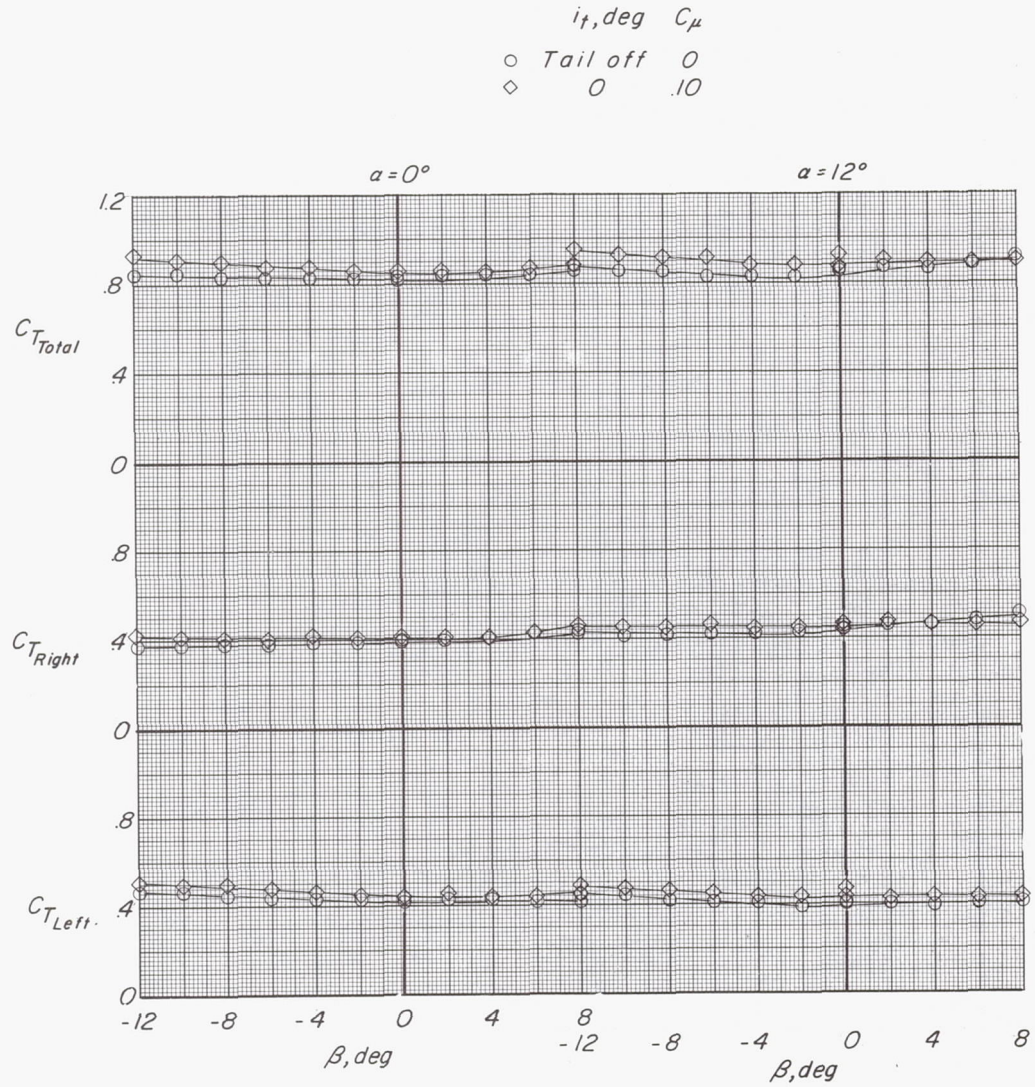

(c) Variation of C_T with β

Figure 41.- Concluded.

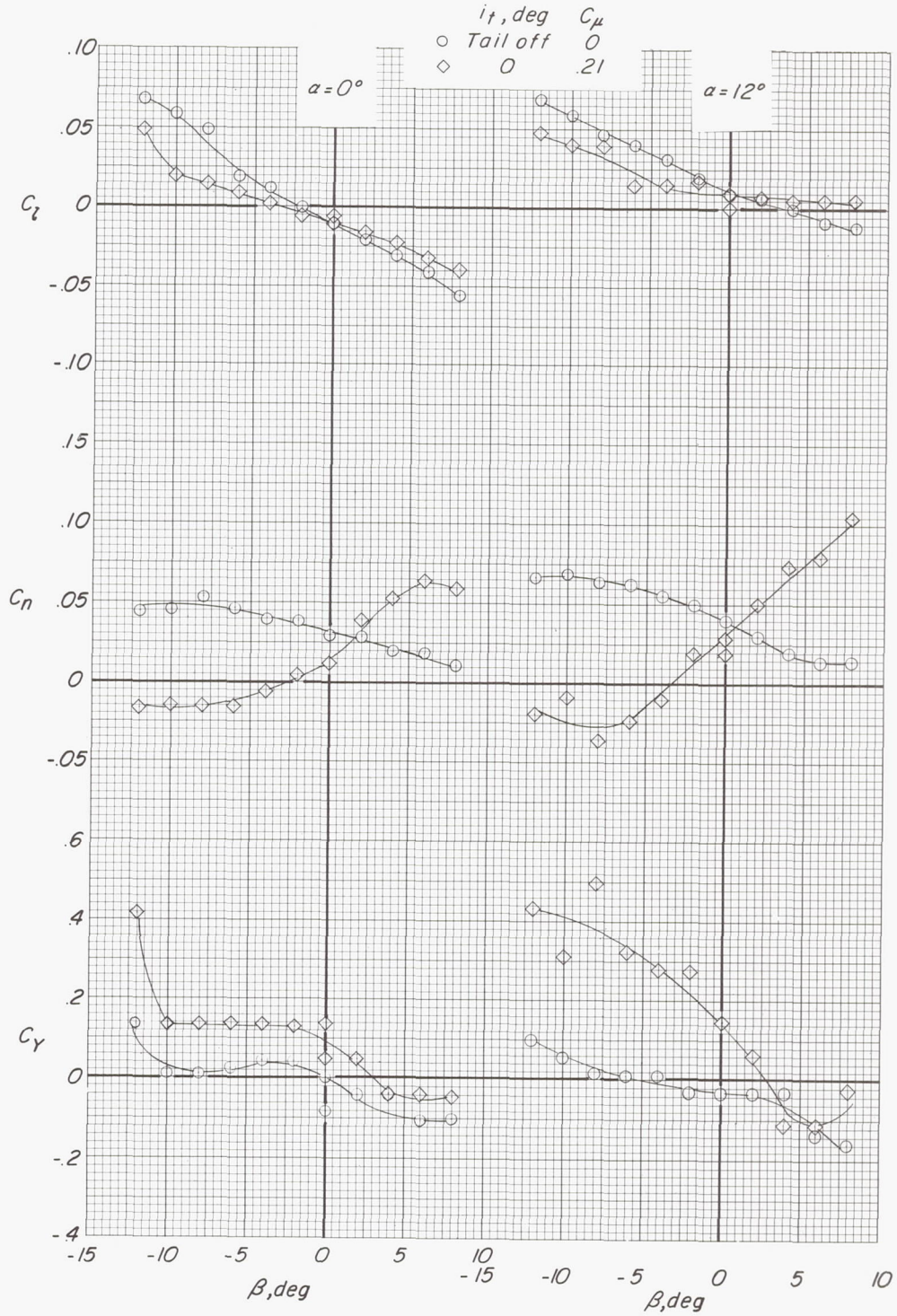

(a) Variation of C_l, C_n, and C_Y with β.

Figure 42.- Effect of tail boundary-layer control on lateral-directional aerodynamic characteristics. $\delta_f = 45^o$; $C_T = 2.10$.

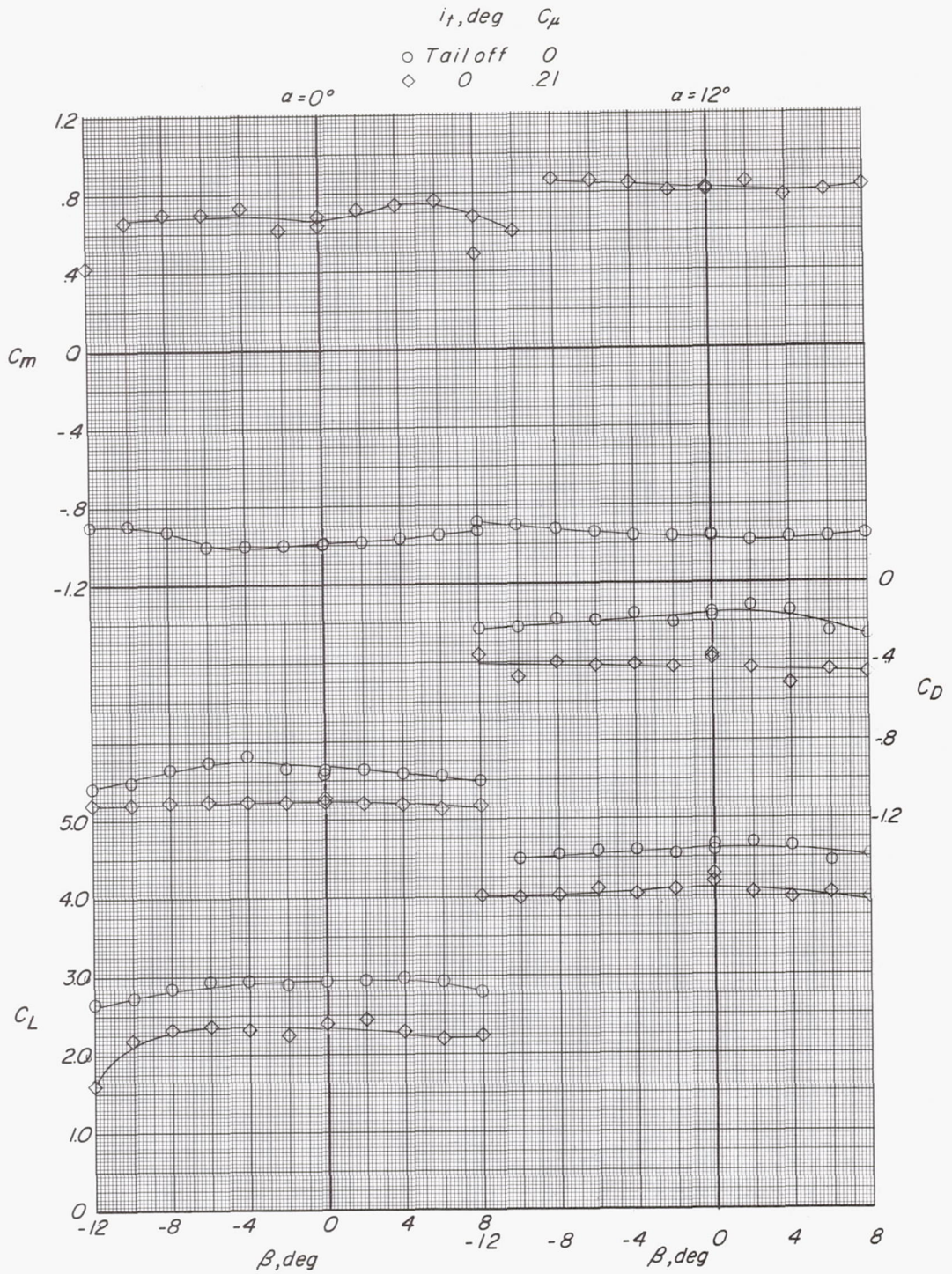

(b) Variation of C_L, C_m, and C_D with β.

Figure 42.- Continued.

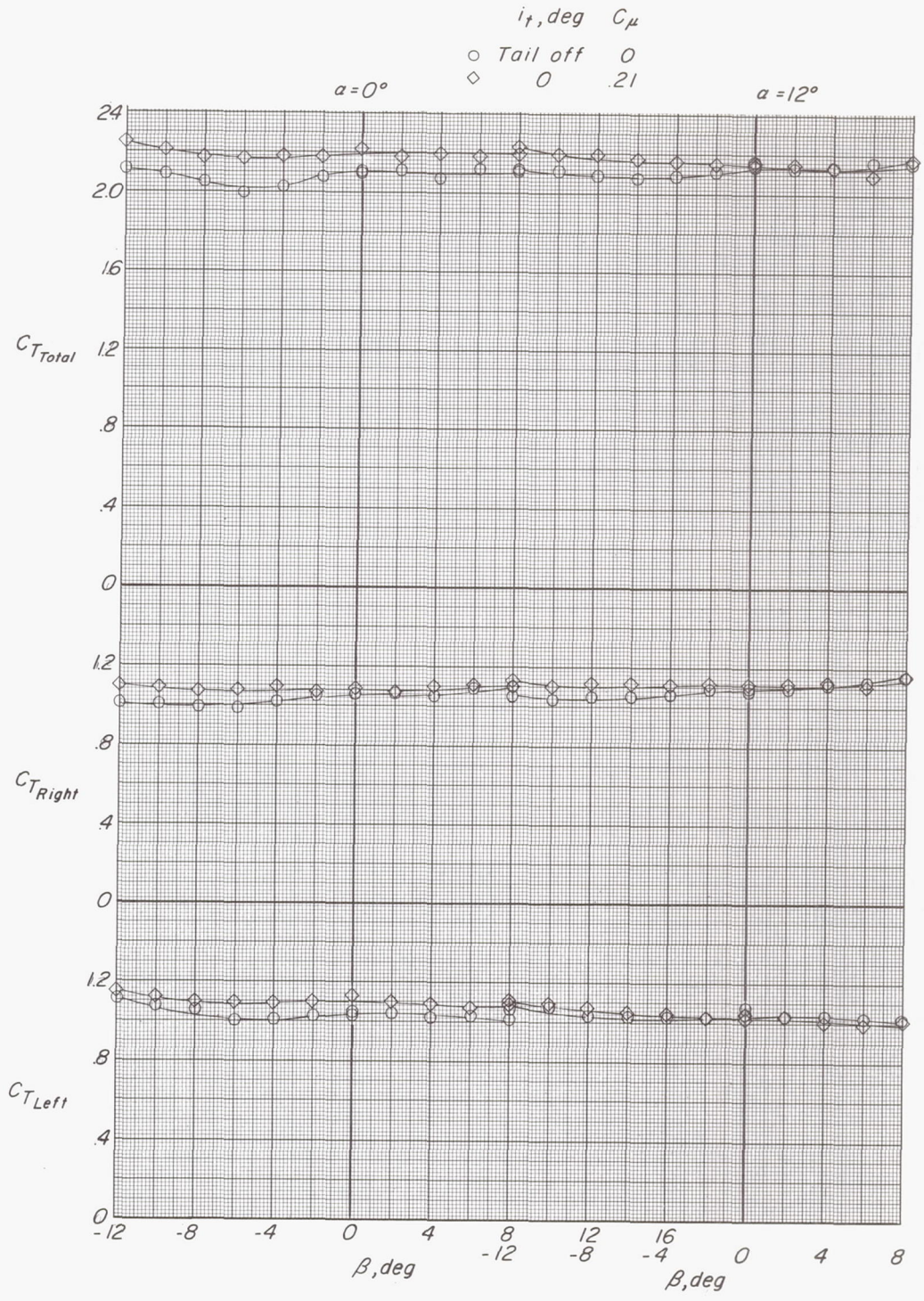

(c) Variation of C_T with β.

Figure 42.- Concluded.

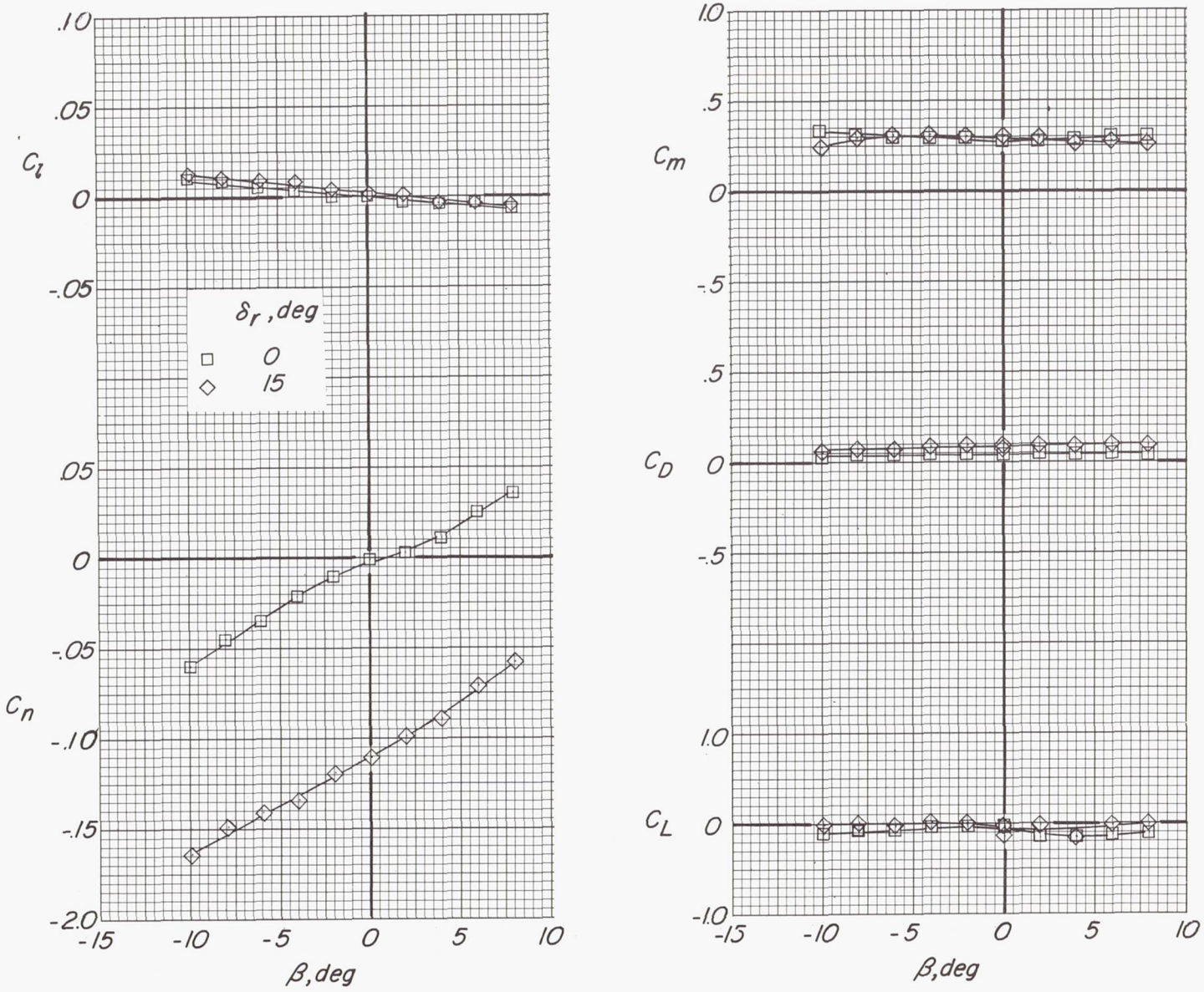

Figure 43.- Effect of rudder deflection on aerodynamic characteristics. $\delta_f = 0^0$; $C_\mu = 0$; $C_T = 0$; $\alpha = 0^0$; $i_t = 0^0$.

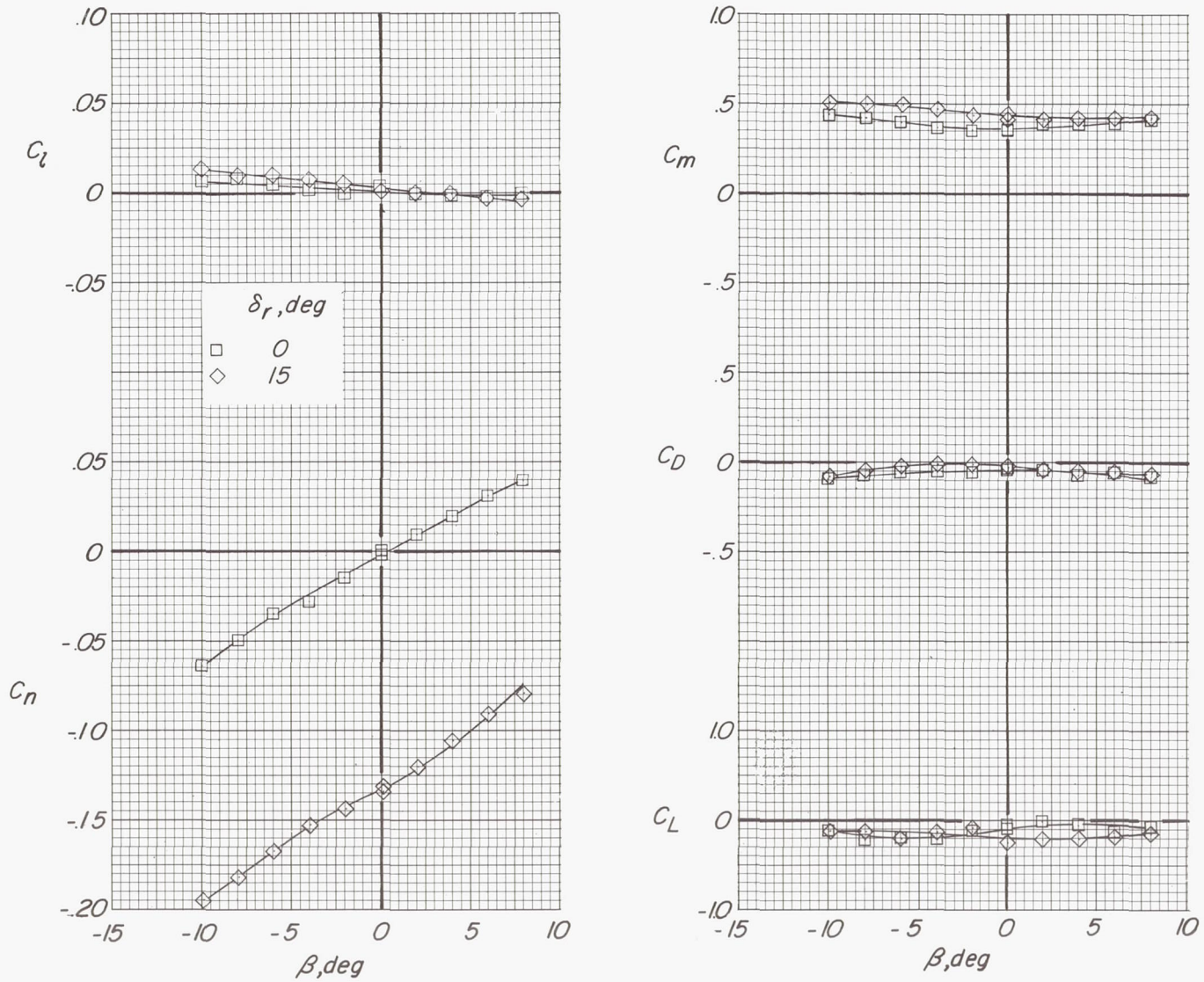

(a) Variation of aerodynamic characteristics with β.

Figure 44.- Effect of rudder deflection on aerodynamic characteristics. $\delta_f = 0^0$; $C_\mu = 0.02$; $C_T = 0.14$; $\alpha = 0^0$; $i_t = 0^0$.

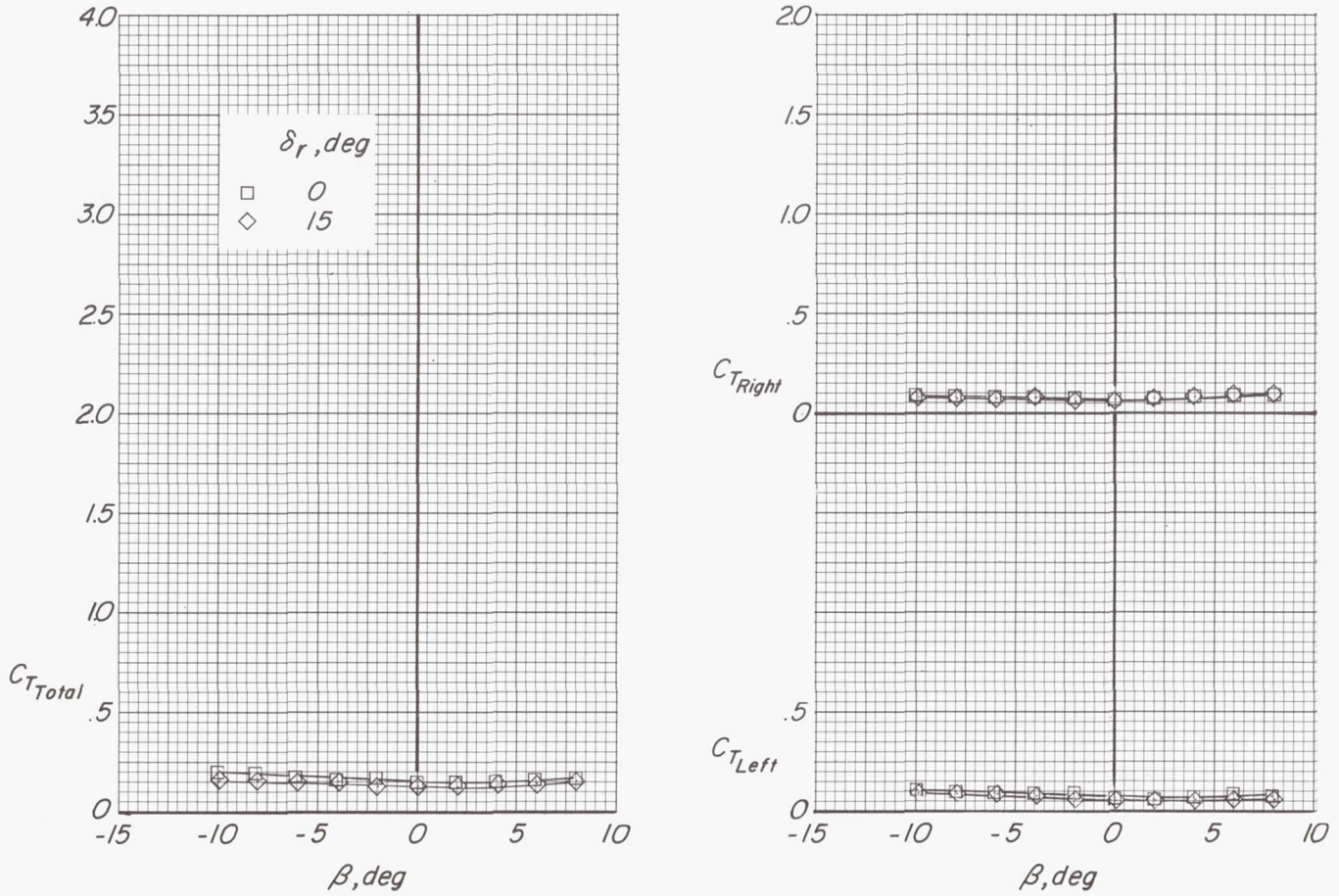

(b) Variation of C_T with β.

Figure 44.- Concluded.

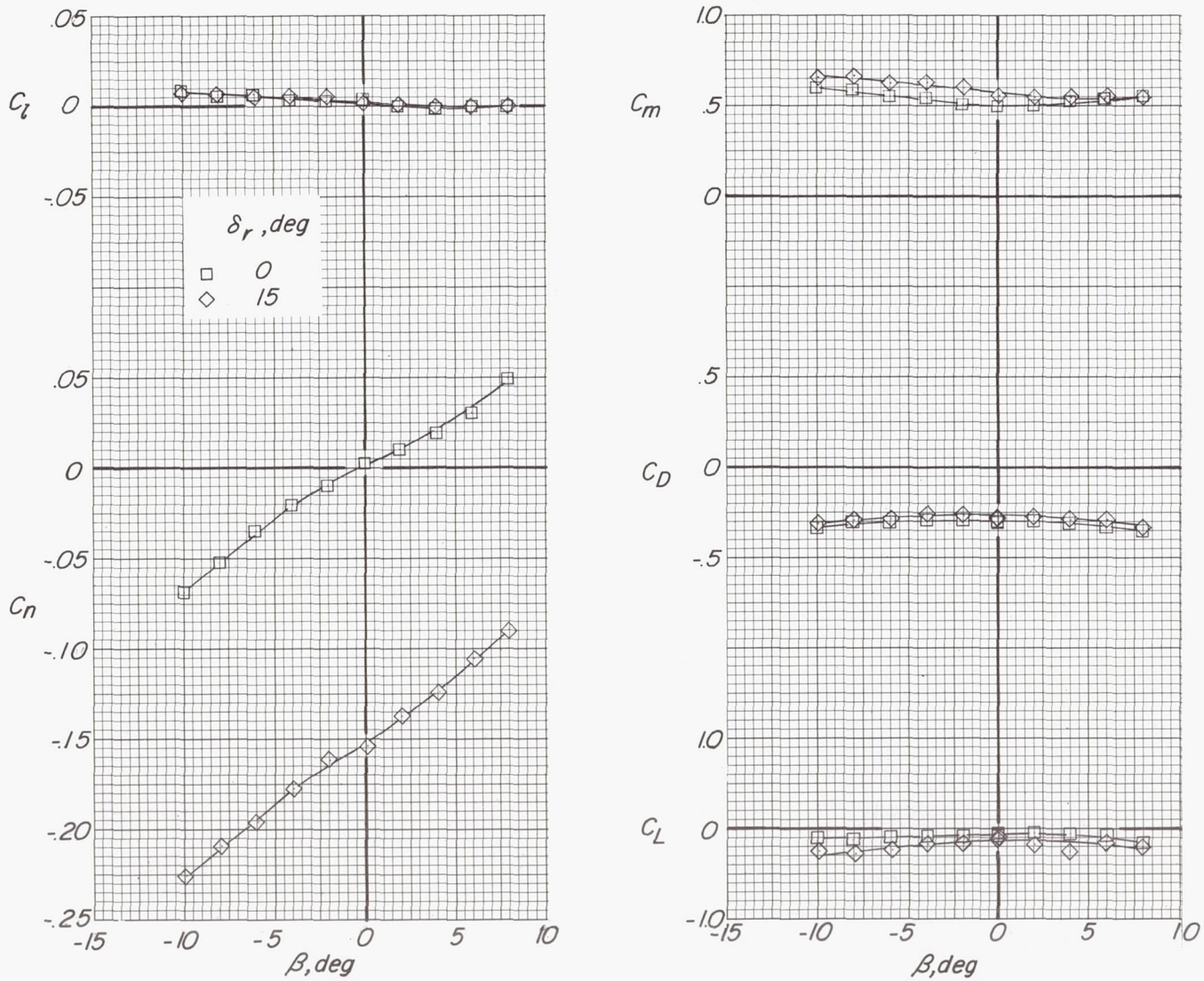

(a) Variation of aerodynamic characteristics with β.

Figure 45.- Effect of rudder deflection on aerodynamic characteristics. $\delta_f = 0^0$; $C_\mu = 0.05$; $C_T = 0.43$; $\alpha = 0^0$; $i_t = 0^0$.

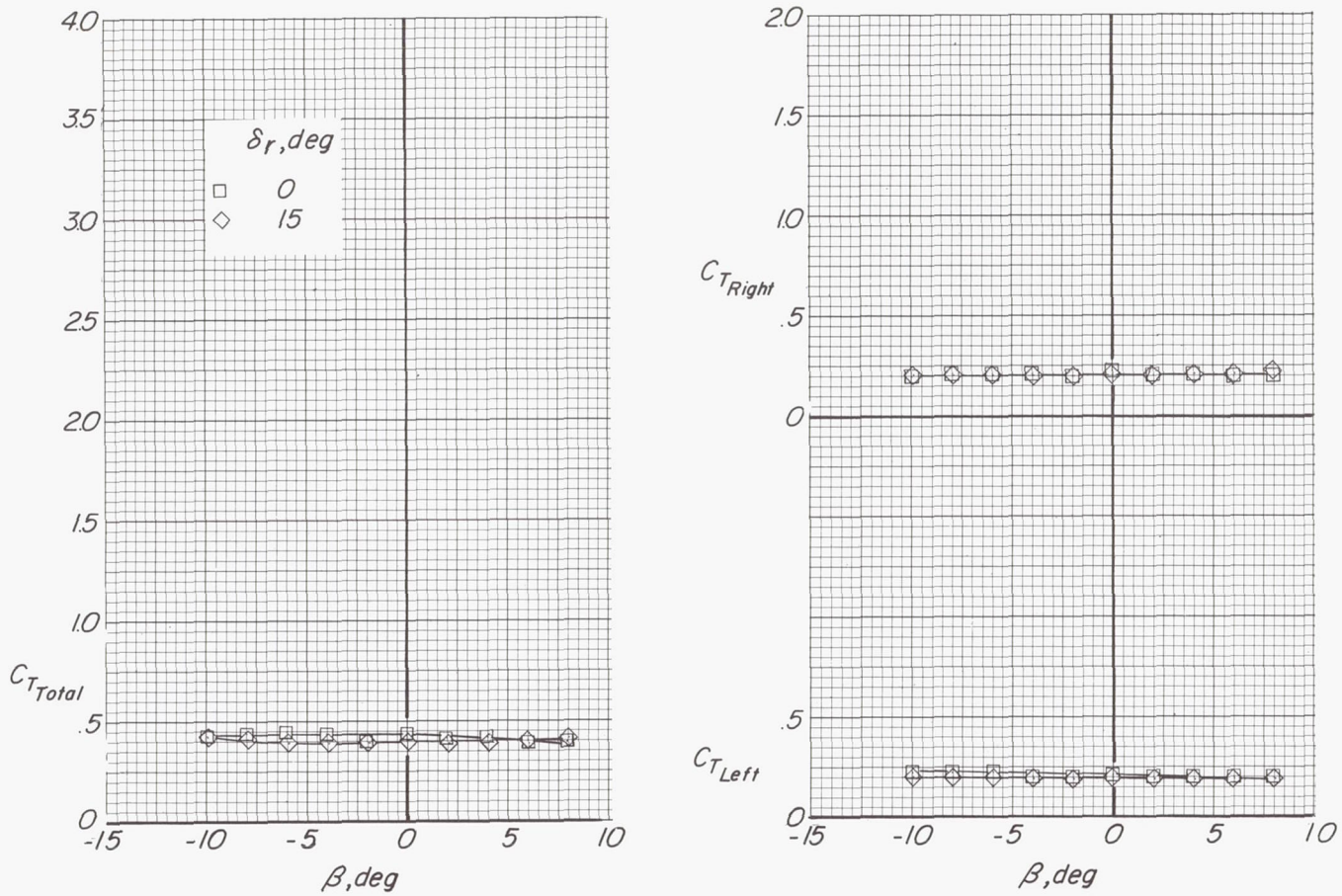

(b) Variation of C_T with β.

Figure 45.- Concluded.

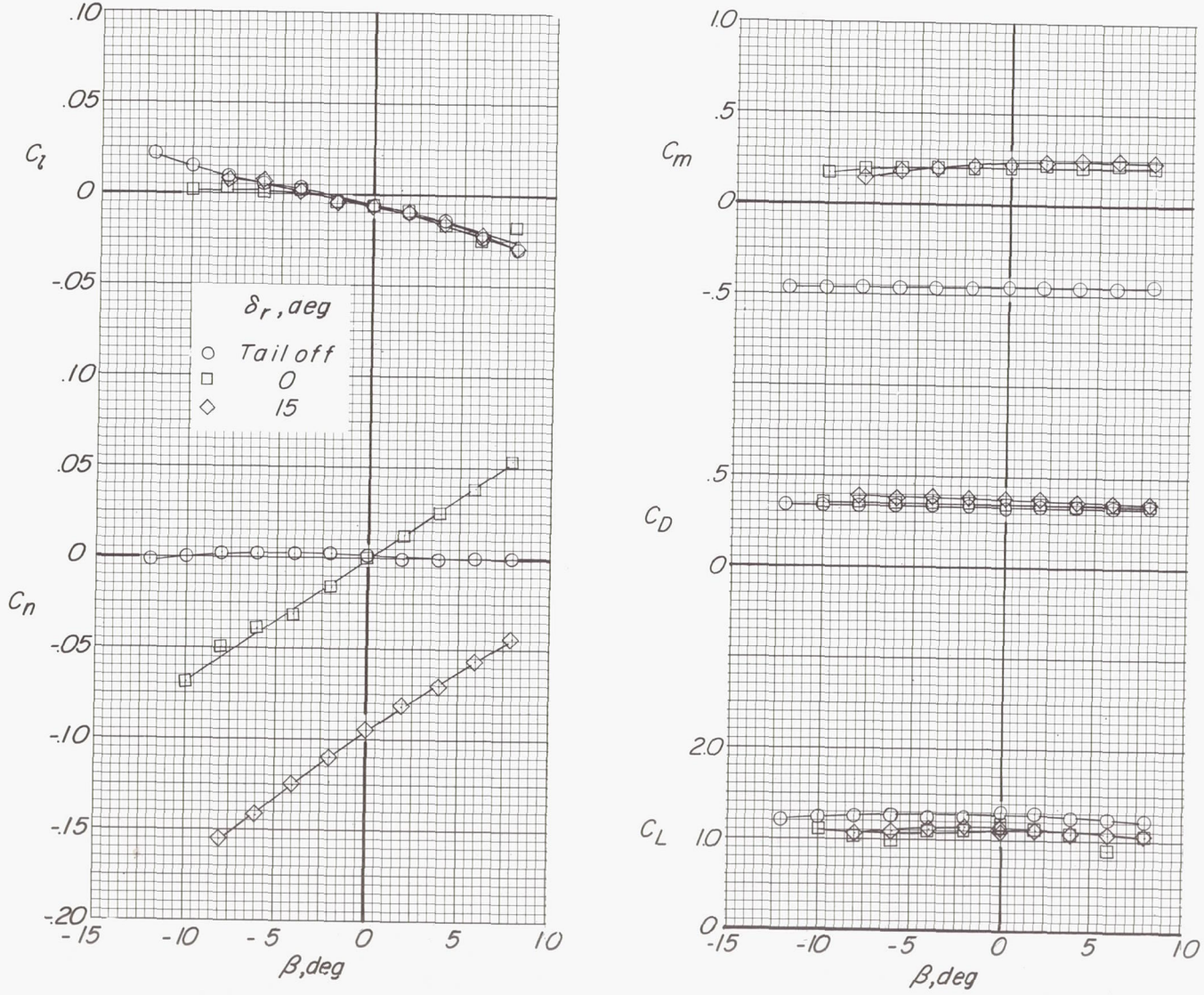

Figure 46.- Effect of rudder deflection on aerodynamic characteristics. $\delta_f = 45^0$; $C_\mu = 0$; $C_T = 0$; $\alpha = 0^0$; $i_t = 0^0$.

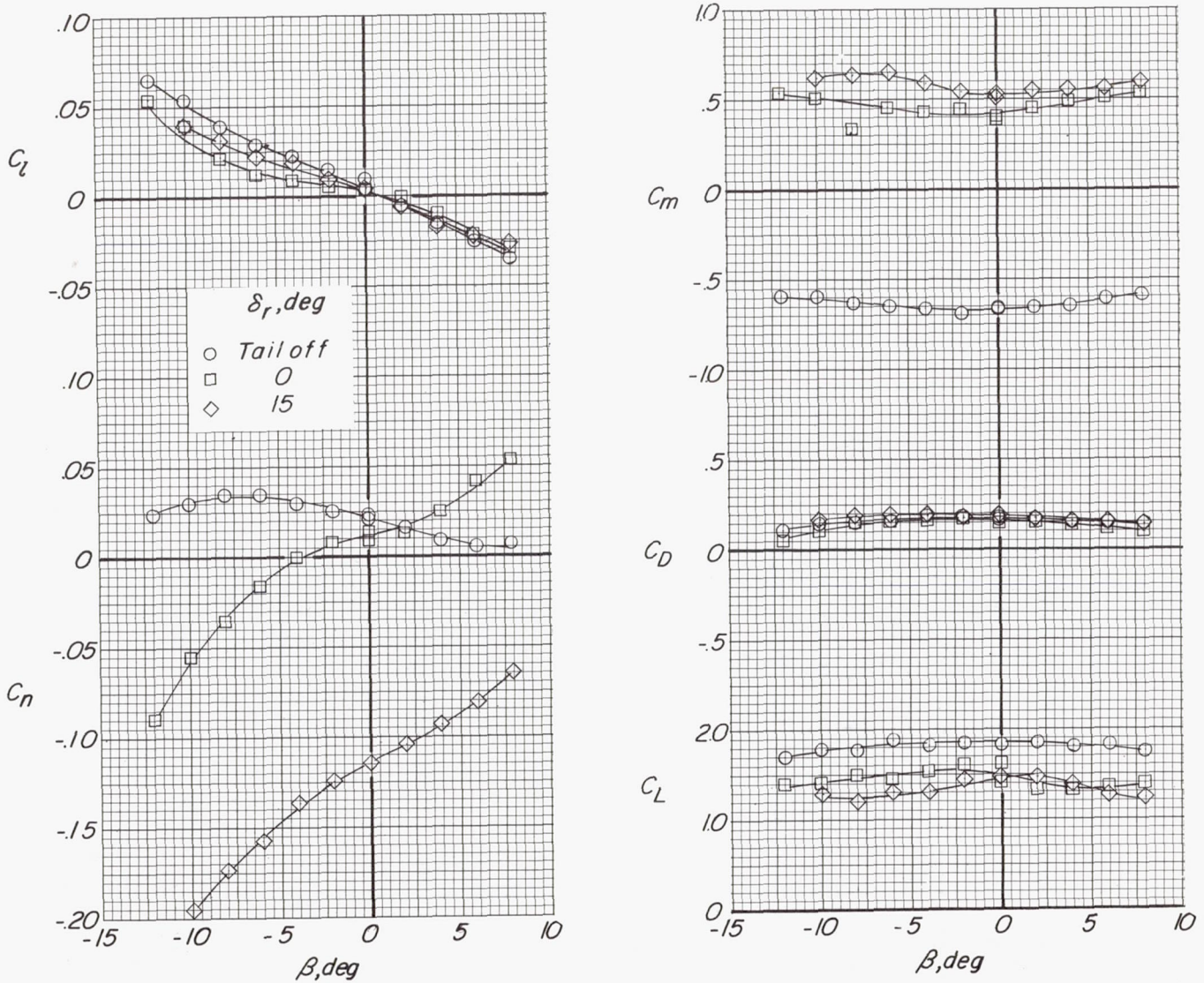

(a) Variation of aerodynamic characteristics with β.

Figure 47.- Effect of rudder deflection on aerodynamic characteristics. $\delta_f = 45^0$; $C_\mu = 0.05$; $C_T = 0.43$; $\alpha = 0^0$; $i_t = 0^0$.

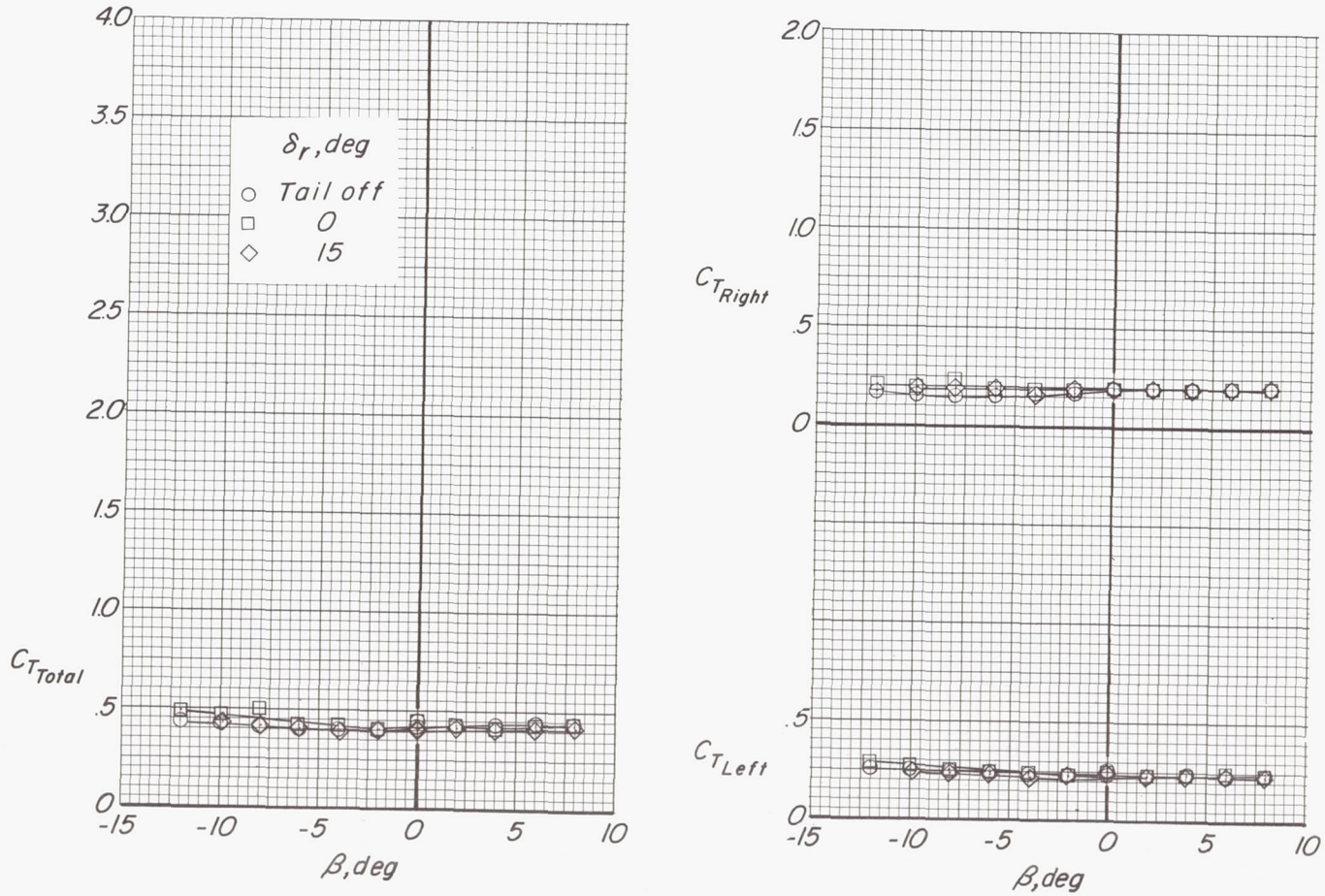

(b) Variation of C_T with β.

Figure 47.- Concluded.

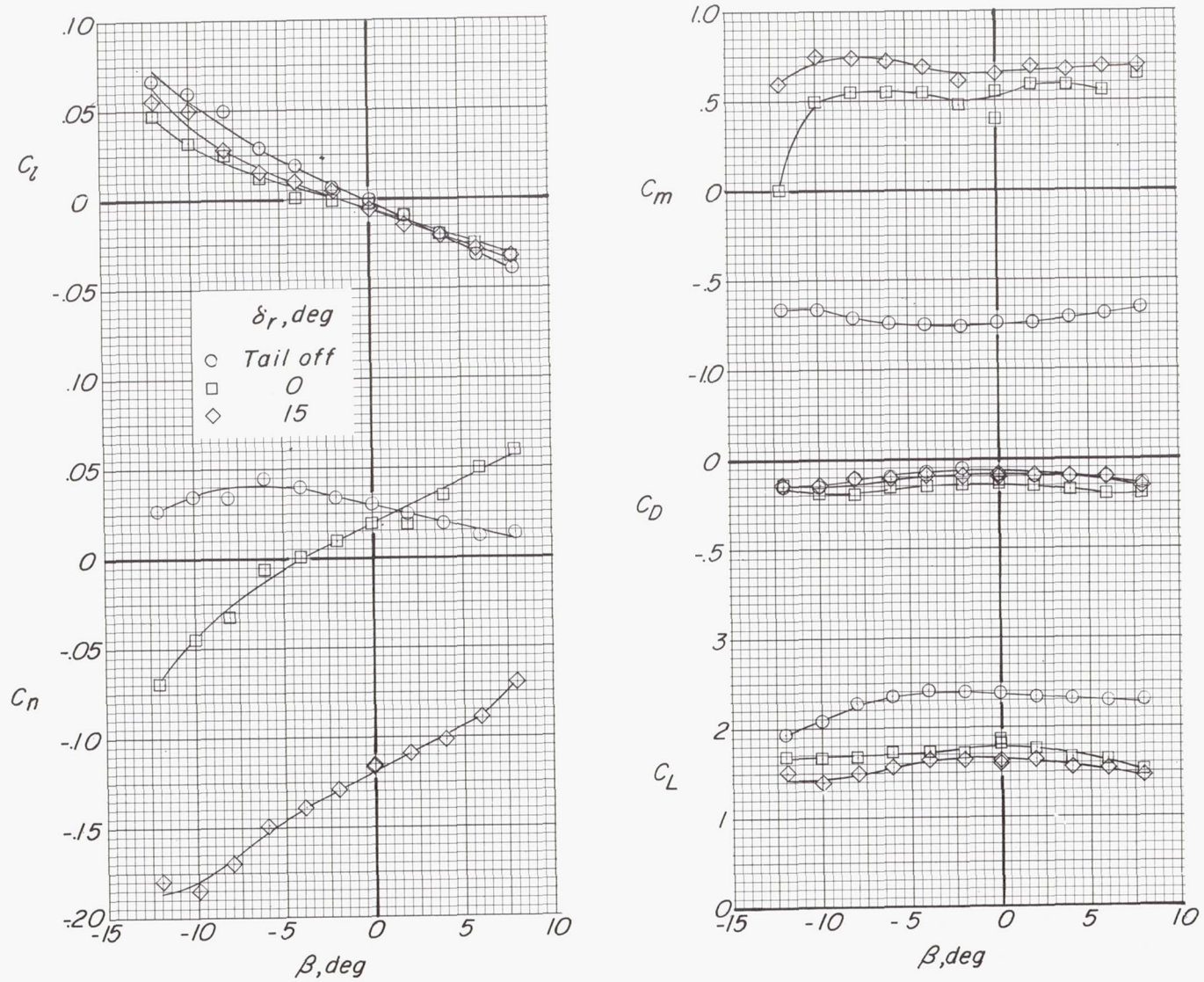

(a) Variation of aerodynamic characteristics with β.

Figure 48.- Effect of rudder deflection on aerodynamic characteristics. $\delta_f = 45^0$; $C_\mu = 0.10$; $C_T = 0.83$; $\alpha = 0^0$; $i_t = 0^0$.

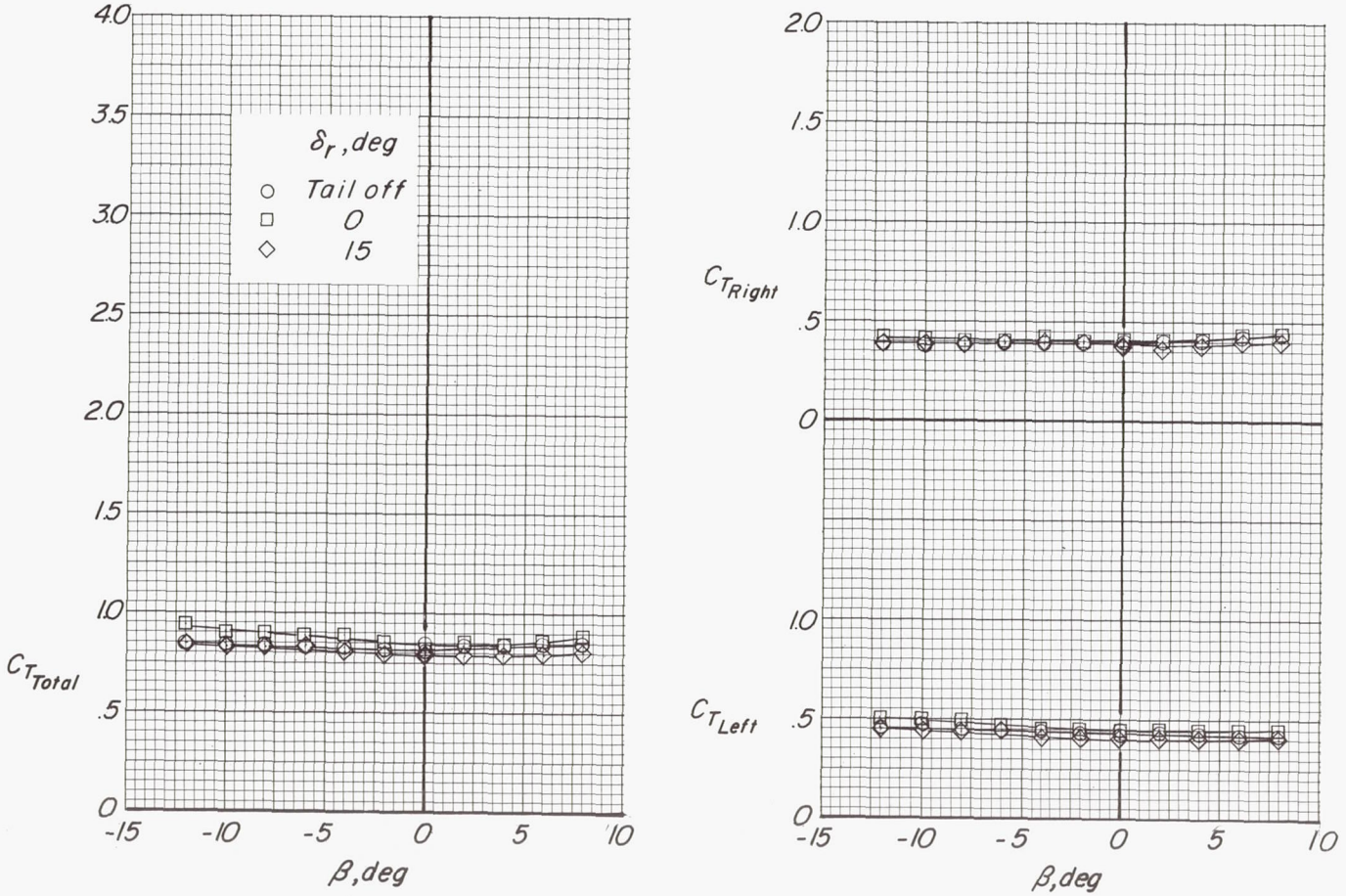

(b) Variation of C_T with β.

Figure 48.- Concluded.

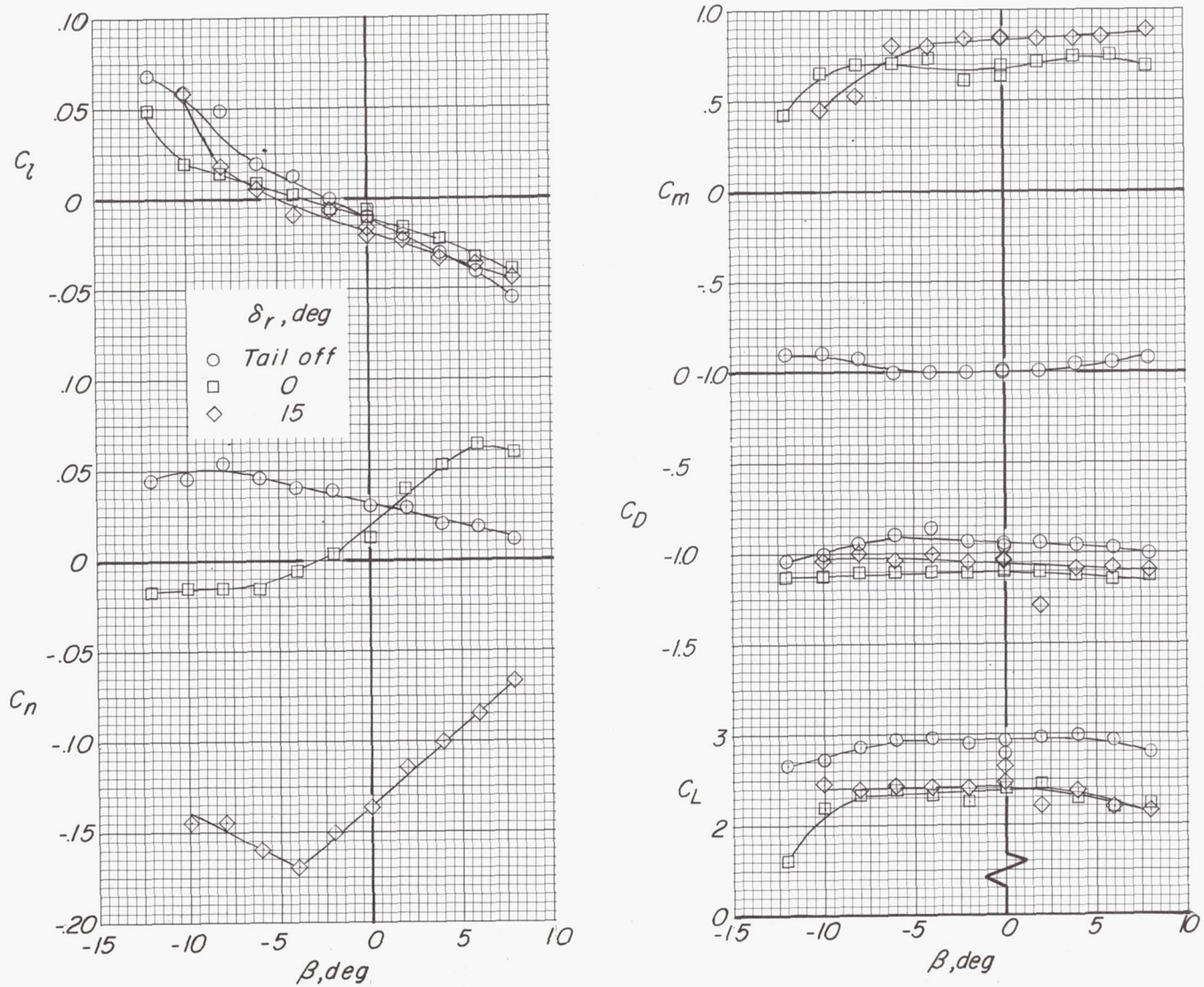

(a) Variation of aerodynamic characteristics with β.

Figure 49.- Effect of rudder deflection on aerodynamic characteristics. $\delta_f = 45^o$; $C_\mu = 0.21$; $C_T = 2.10$; $\alpha = 0^o$; $i_t = 0^o$.

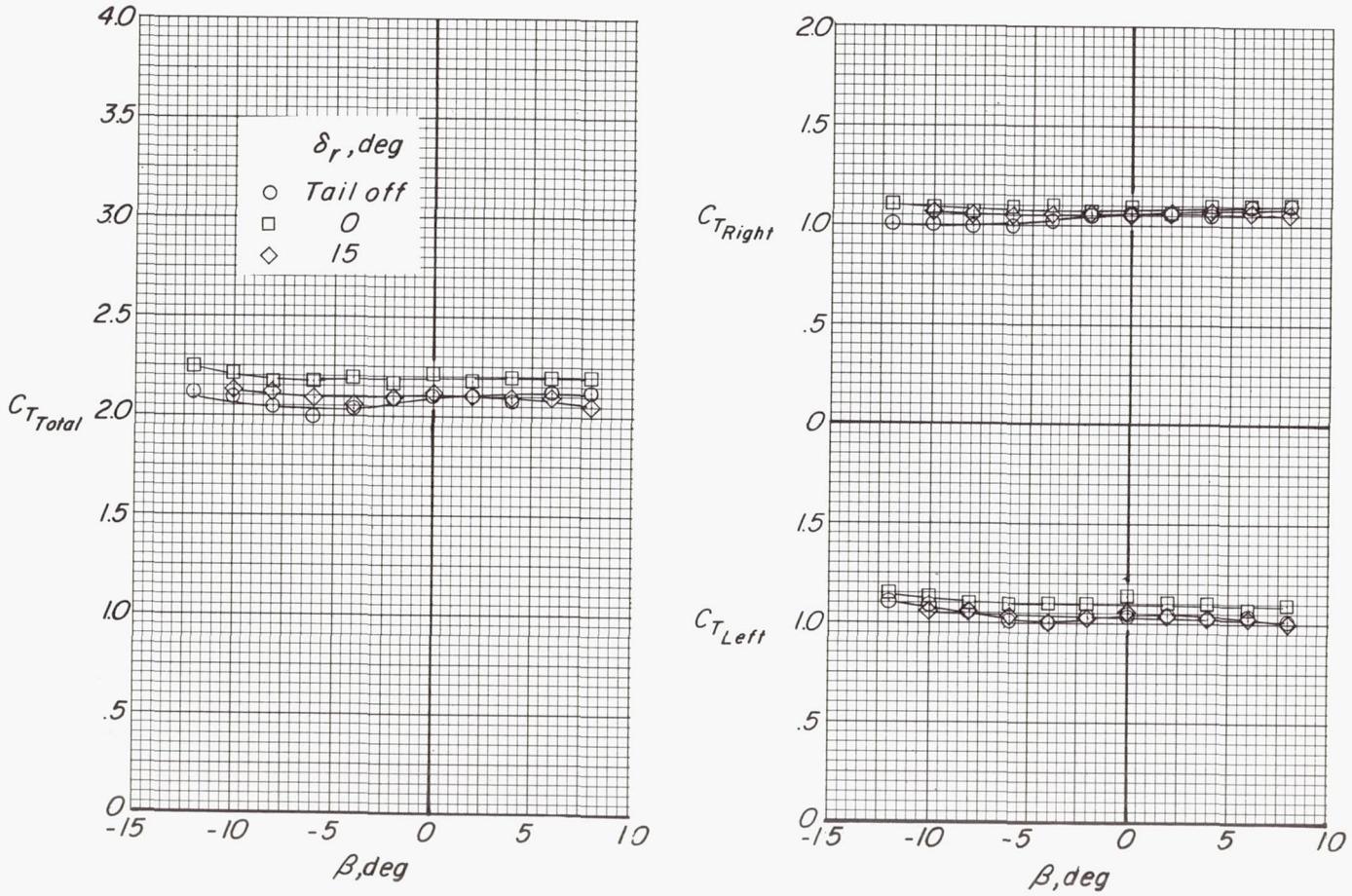

(b) Variation of C_T with β.

Figure 49.- Concluded.

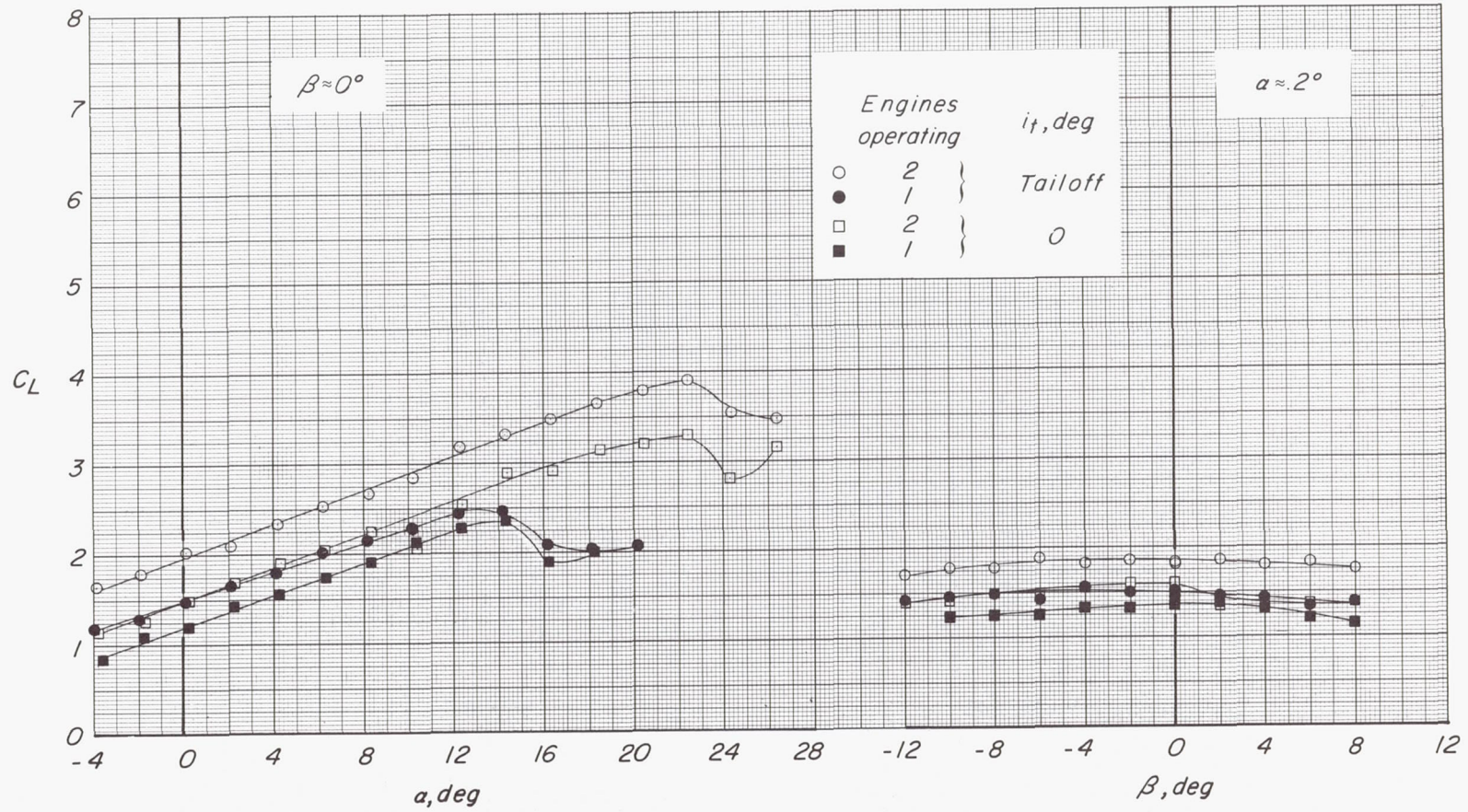

(a) Variation of C_L with α and β.

Figure 50.- Longitudinal and lateral-directional aerodynamic characteristics showing effect of loss of power from right engine. $\delta_f = 45^0$; $C_T = 0.43$; $i_t = 0^0$; $\delta_e = 0^0$.

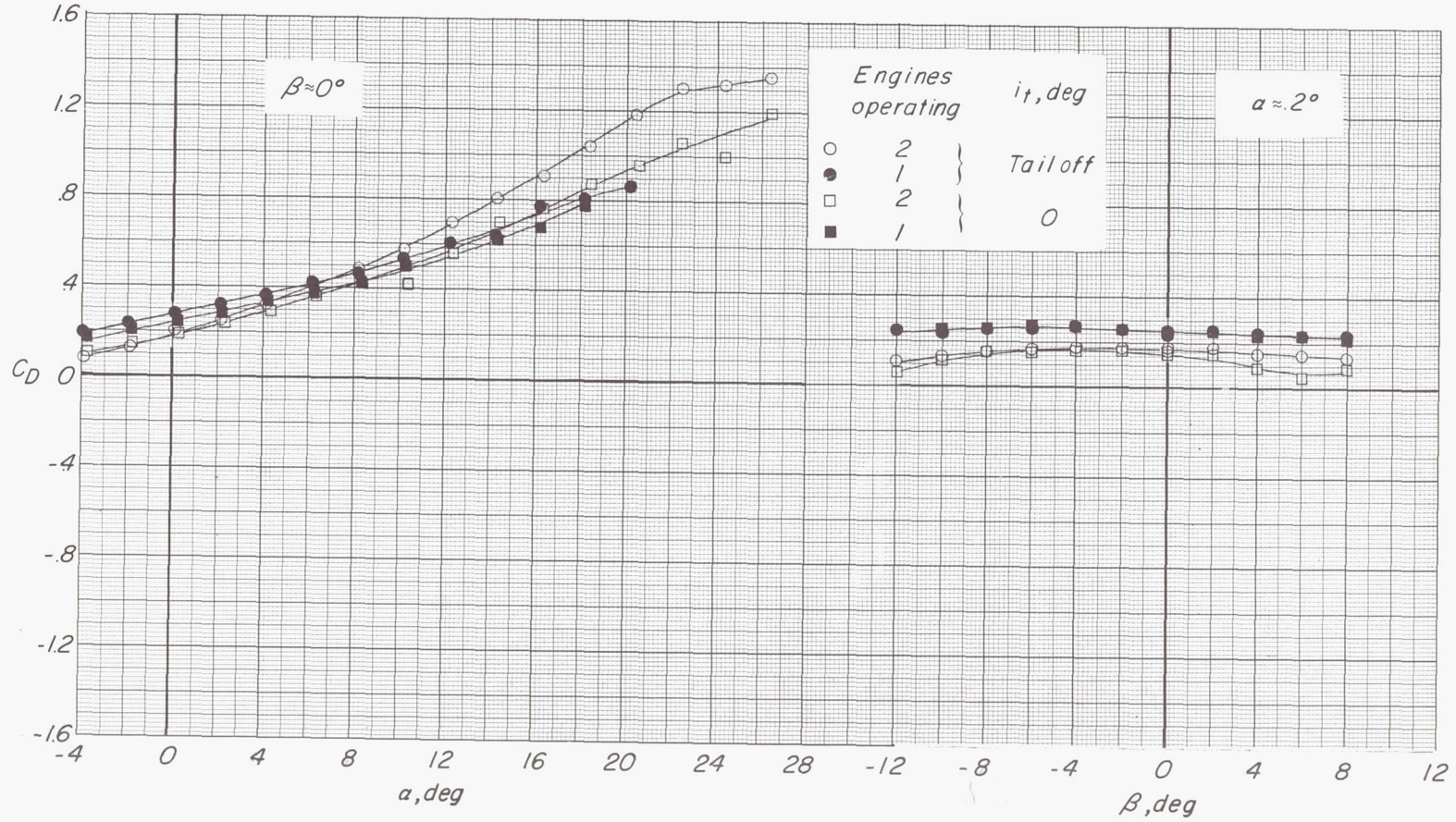

(b) Variation of C_D with α and β.

Figure 50.- Continued.

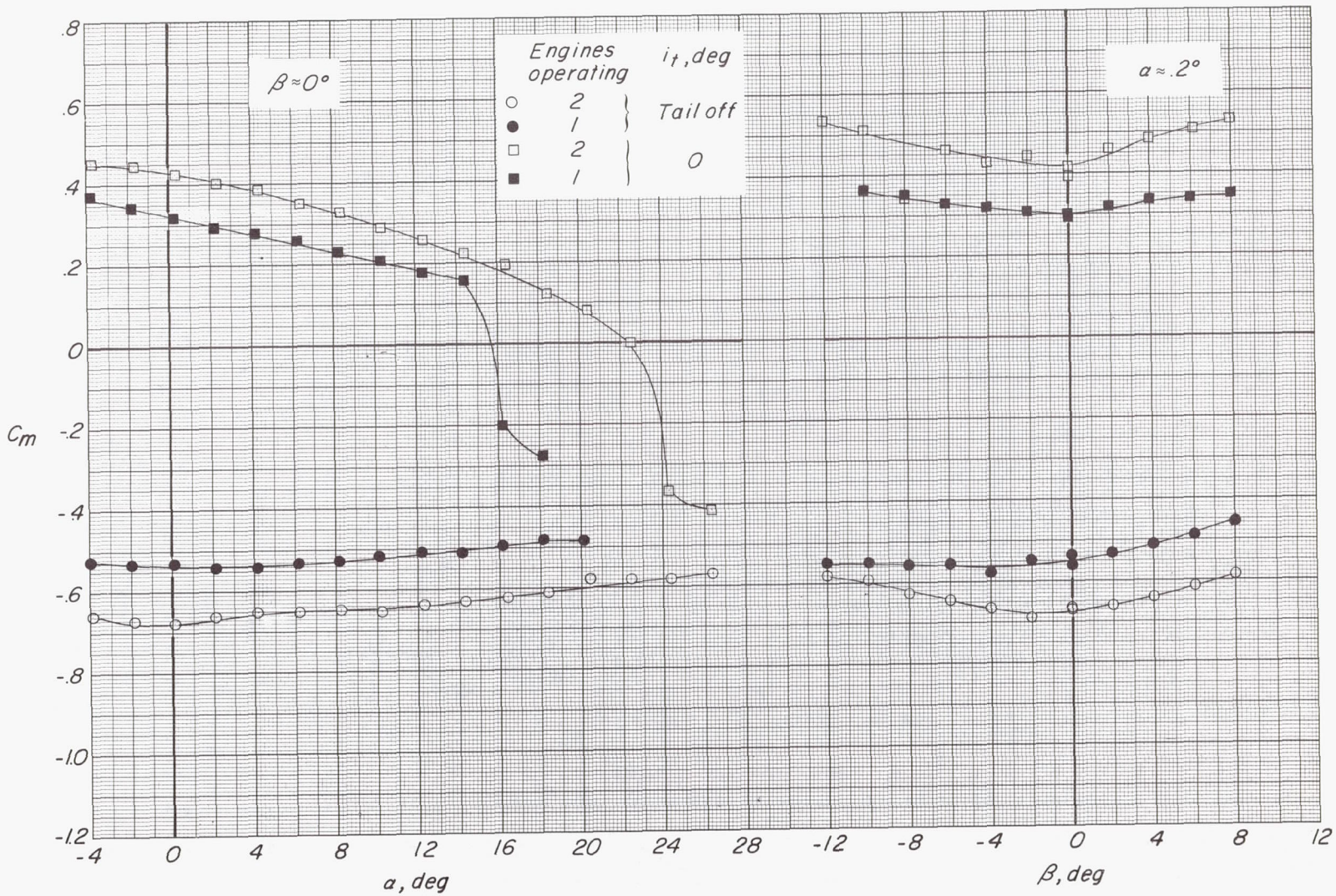

(c) Variation of C_m with α and β.

Figure 50.- Continued.

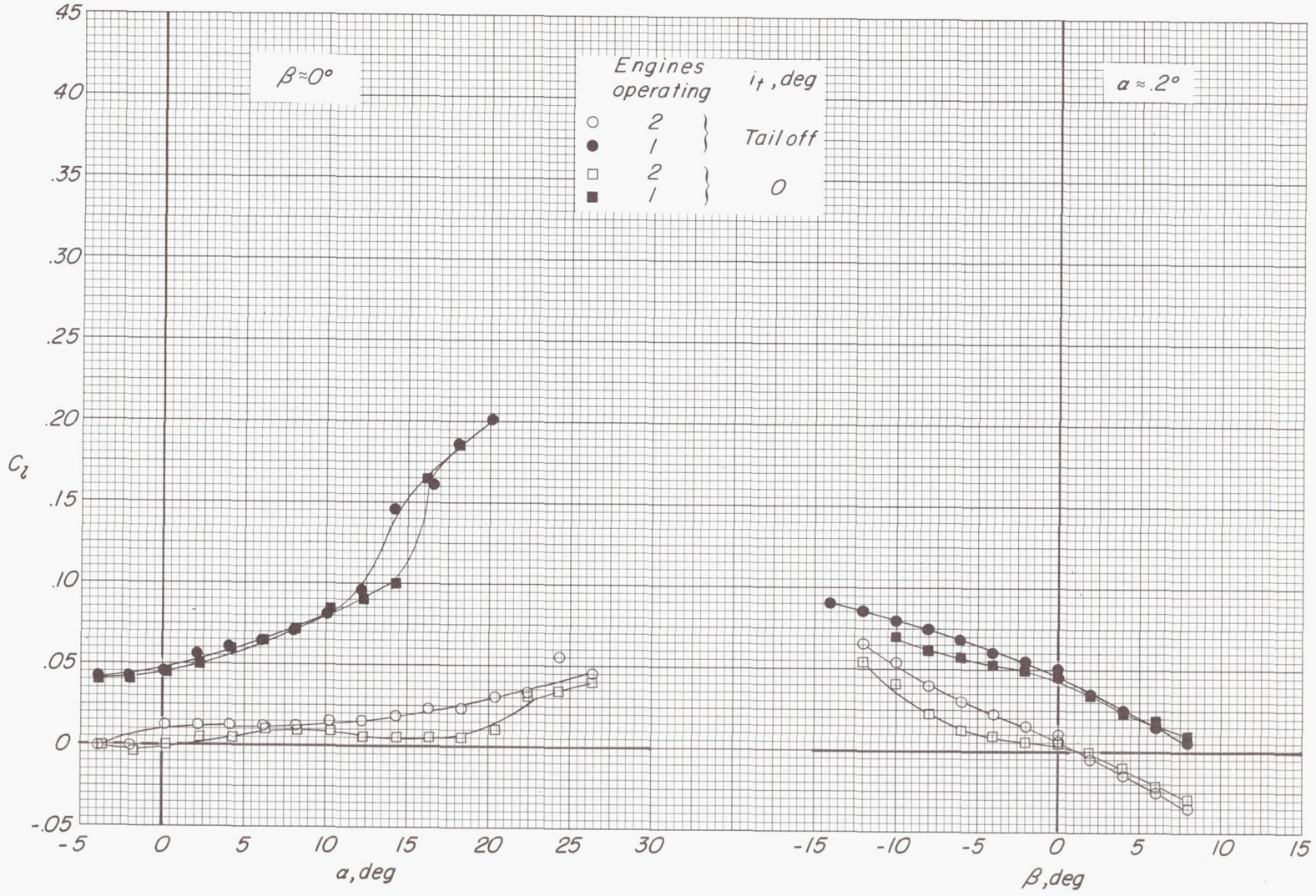

(d) Variation of C_l with α and β.

Figure 50.- Continued.

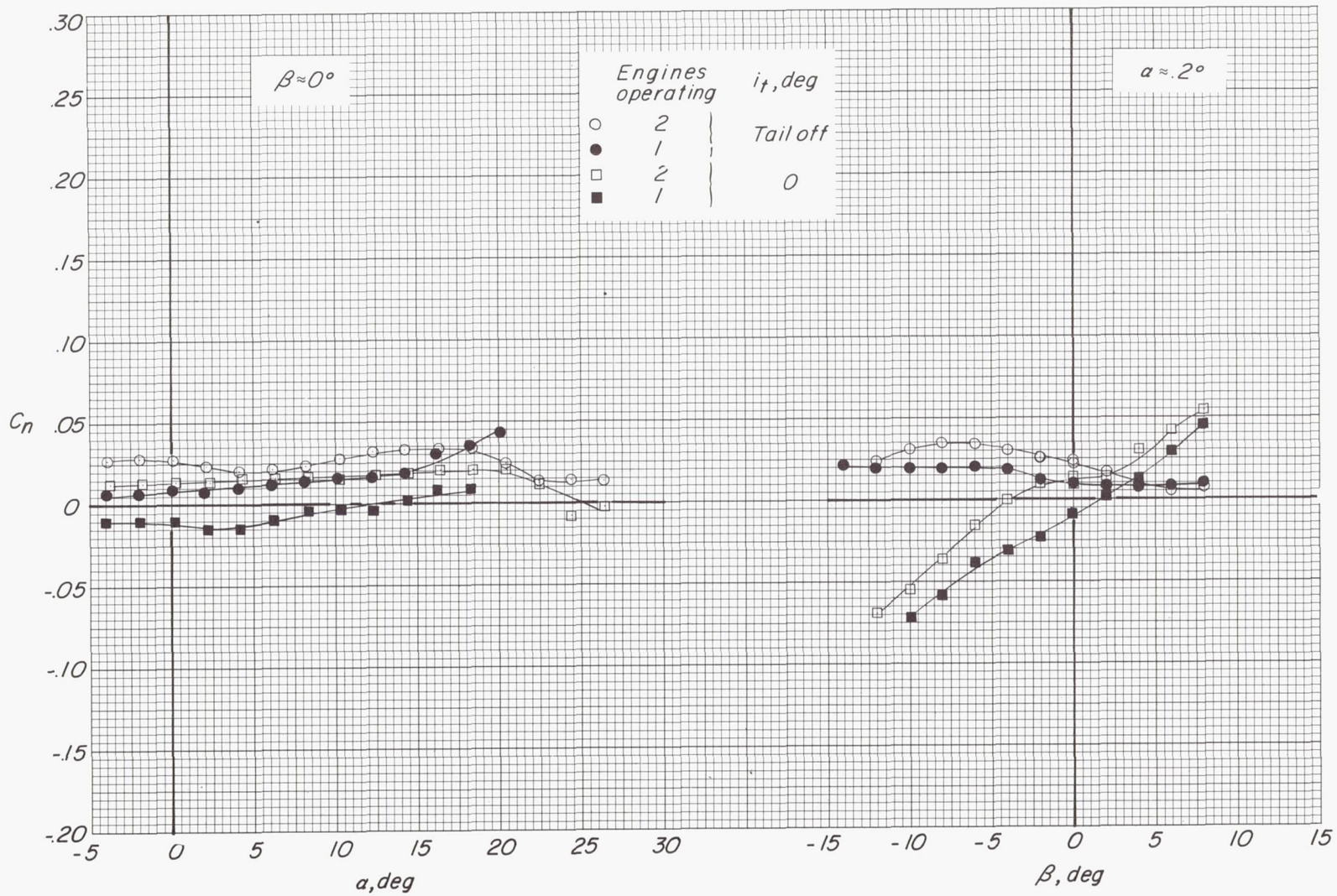

(e) Variation of C_n with α and β.

Figure 50.- Continued.

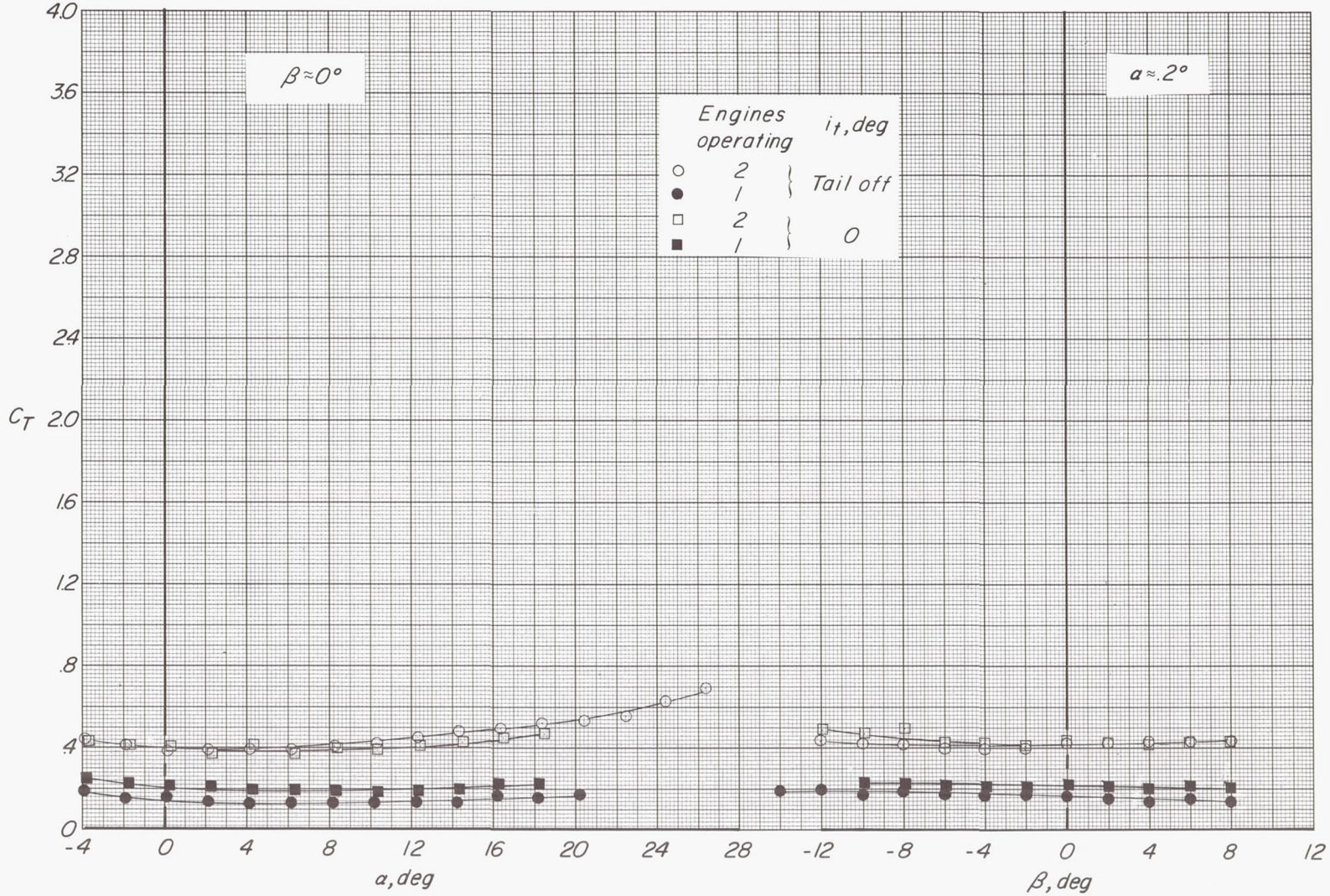

(f) Variation of C_T with α and β.

Figure 50.- Concluded.

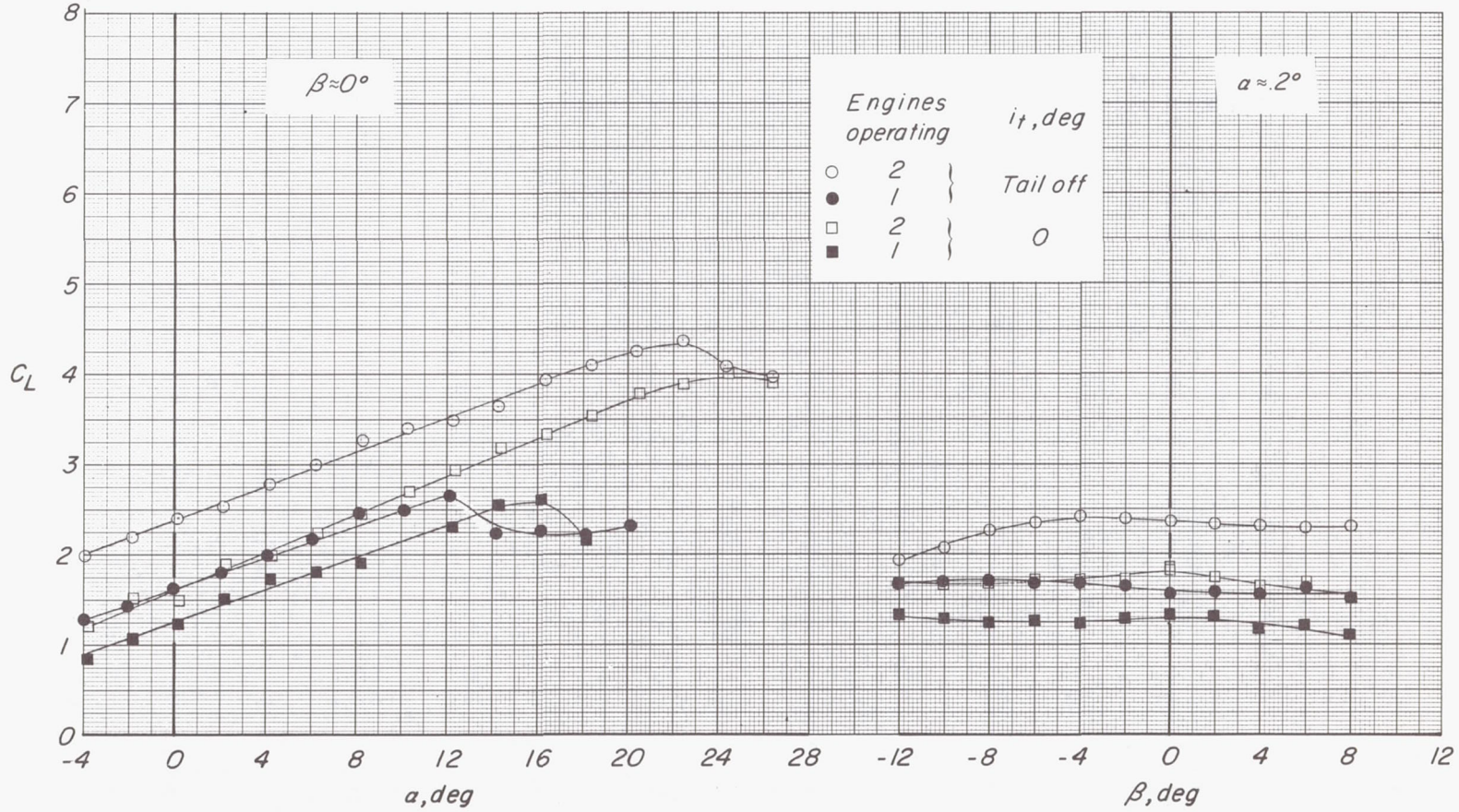

(a) Variation of C_L with α and β.

Figure 51.- Longitudinal and lateral-directional aerodynamic characteristics showing effect of loss of power from right engine. $\delta_f = 45^0$; $C_T = 0.83$; $i_t = 0^0$; $\delta_e = 0^0$.

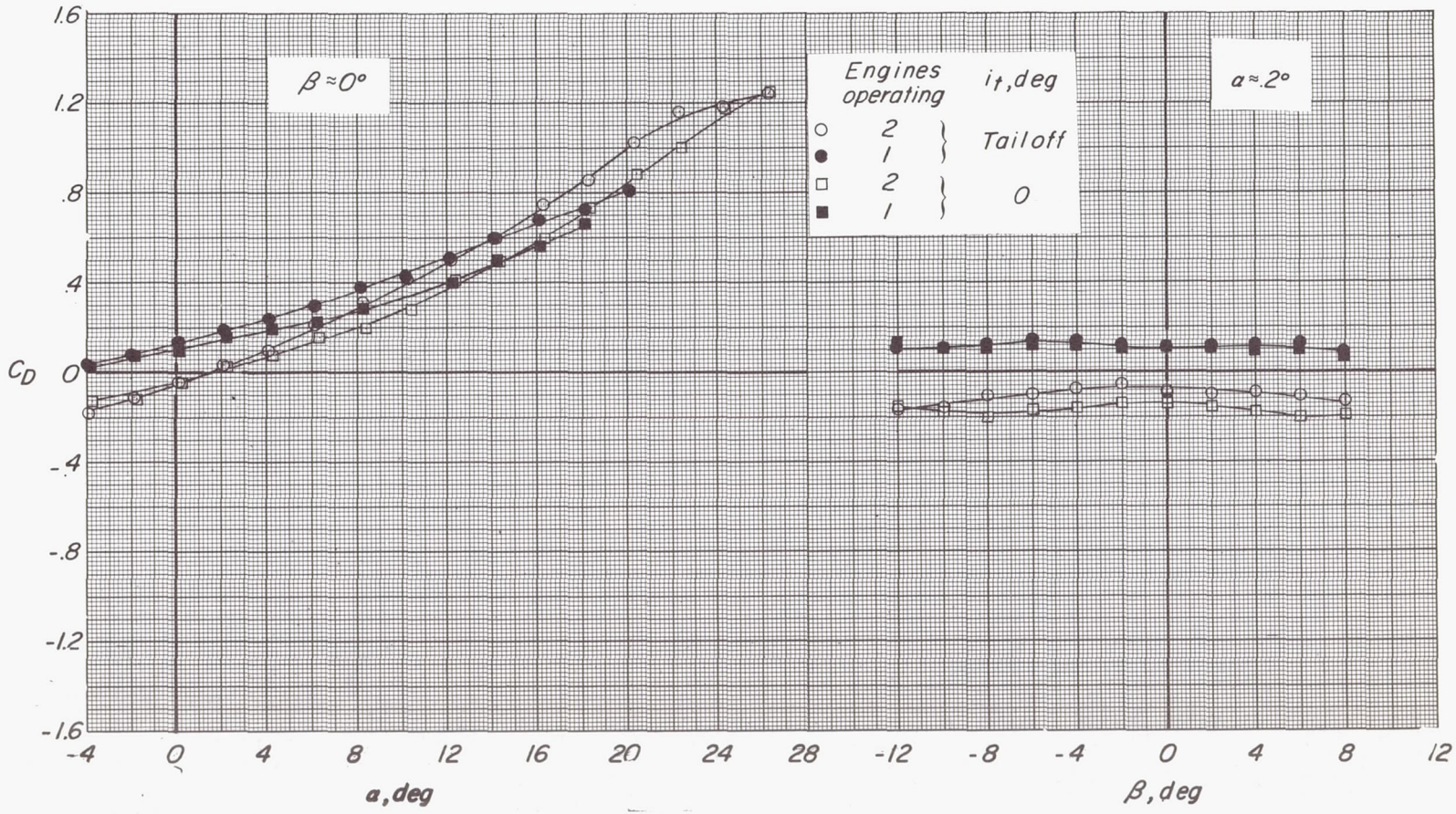

(b) Variation of C_D with α and β.

Figure 51.- Continued.

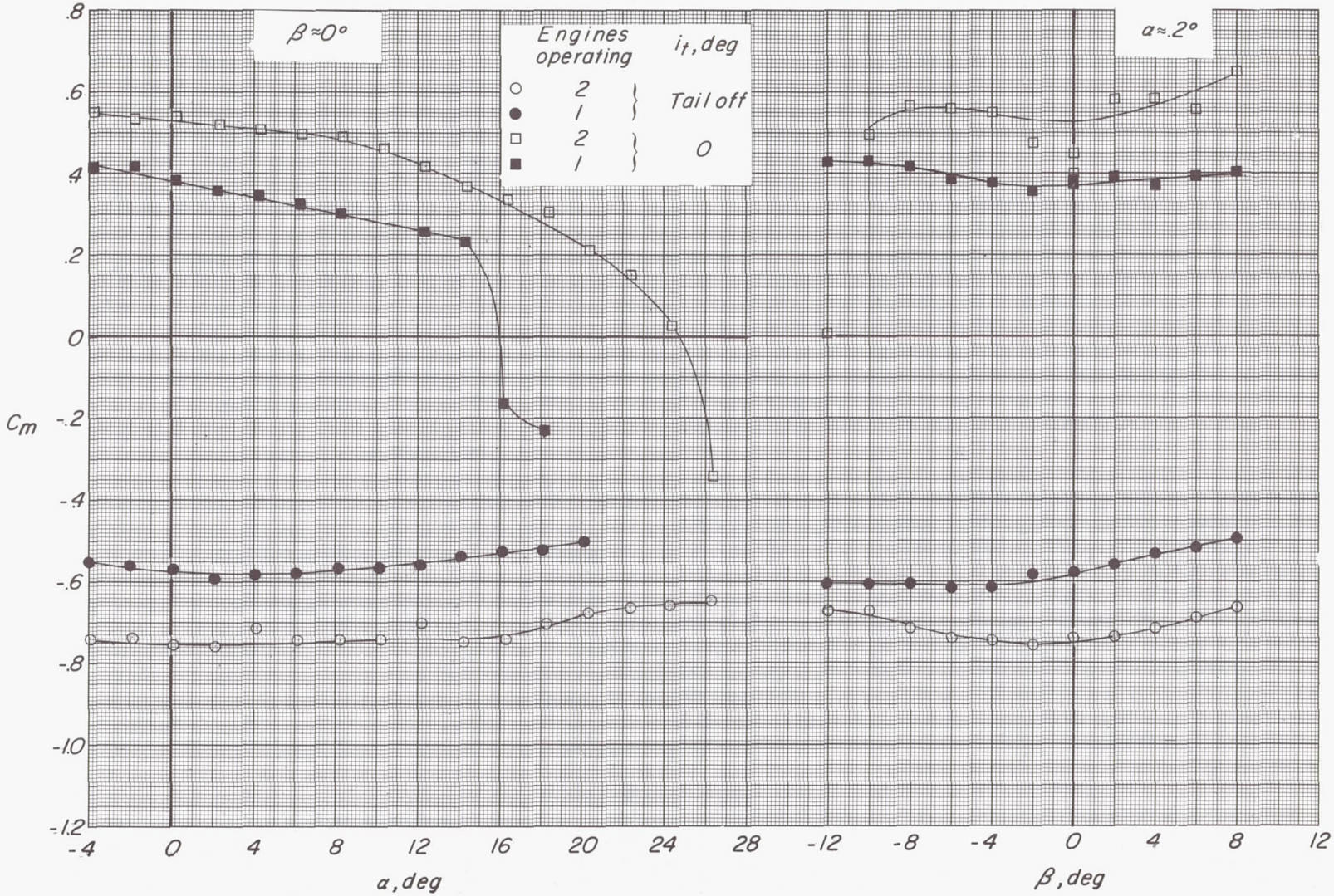

(c) Variation of C_m with α and β.

Figure 51.- Continued.

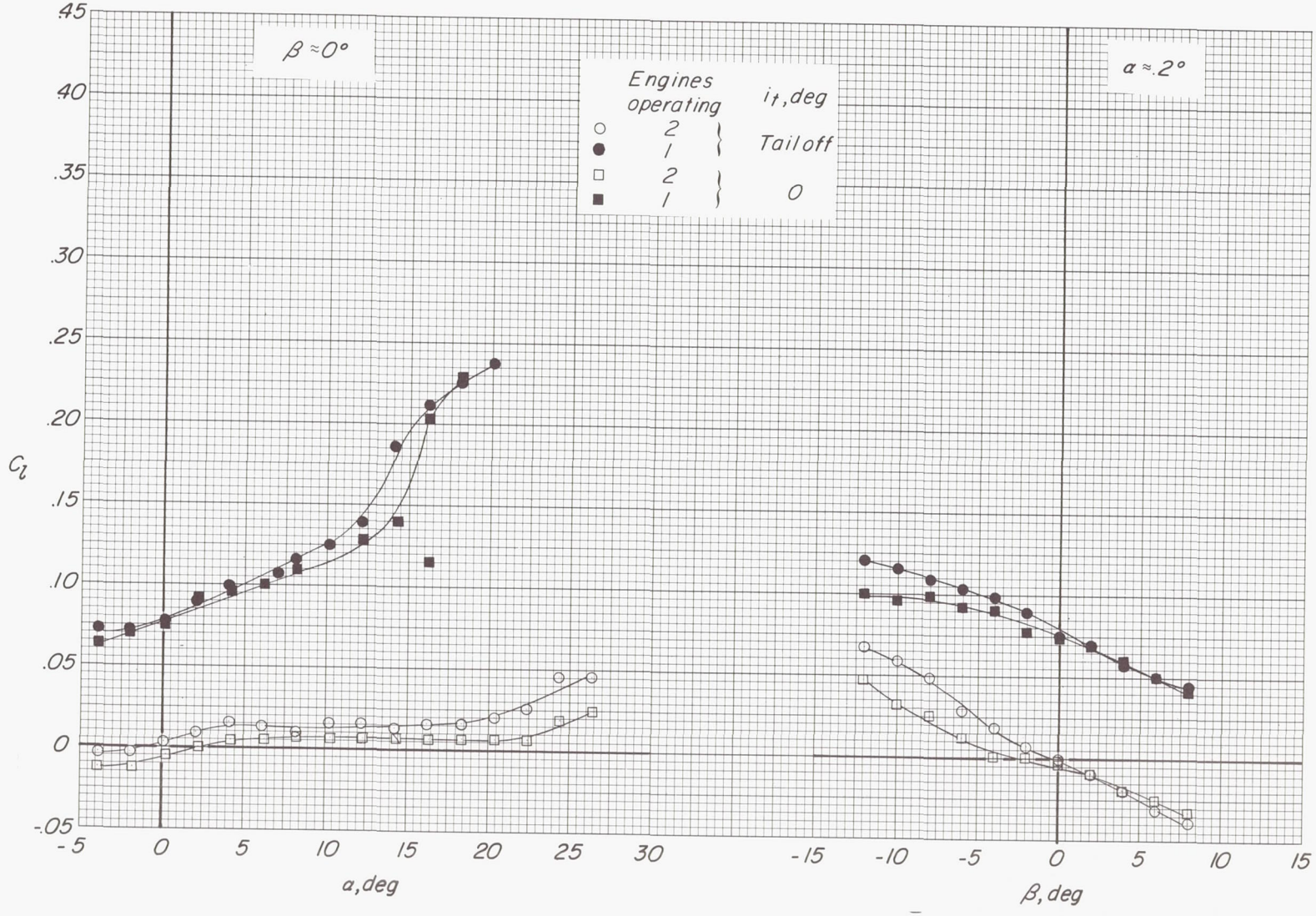

(d) Variation of C_l with α and β.

Figure 51.- Continued.

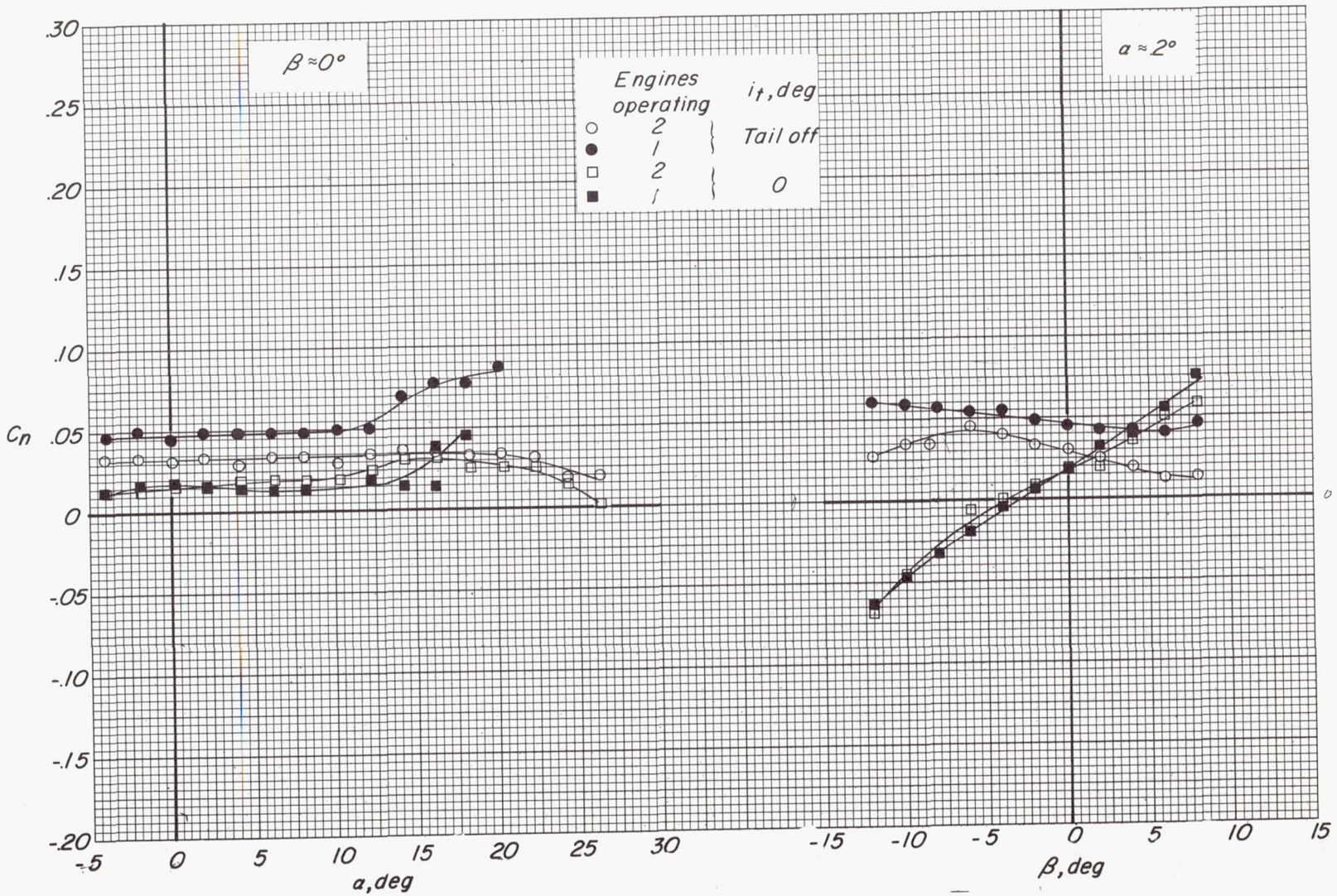

(e) Variation of C_n with α and β.

Figure 51.- Continued.

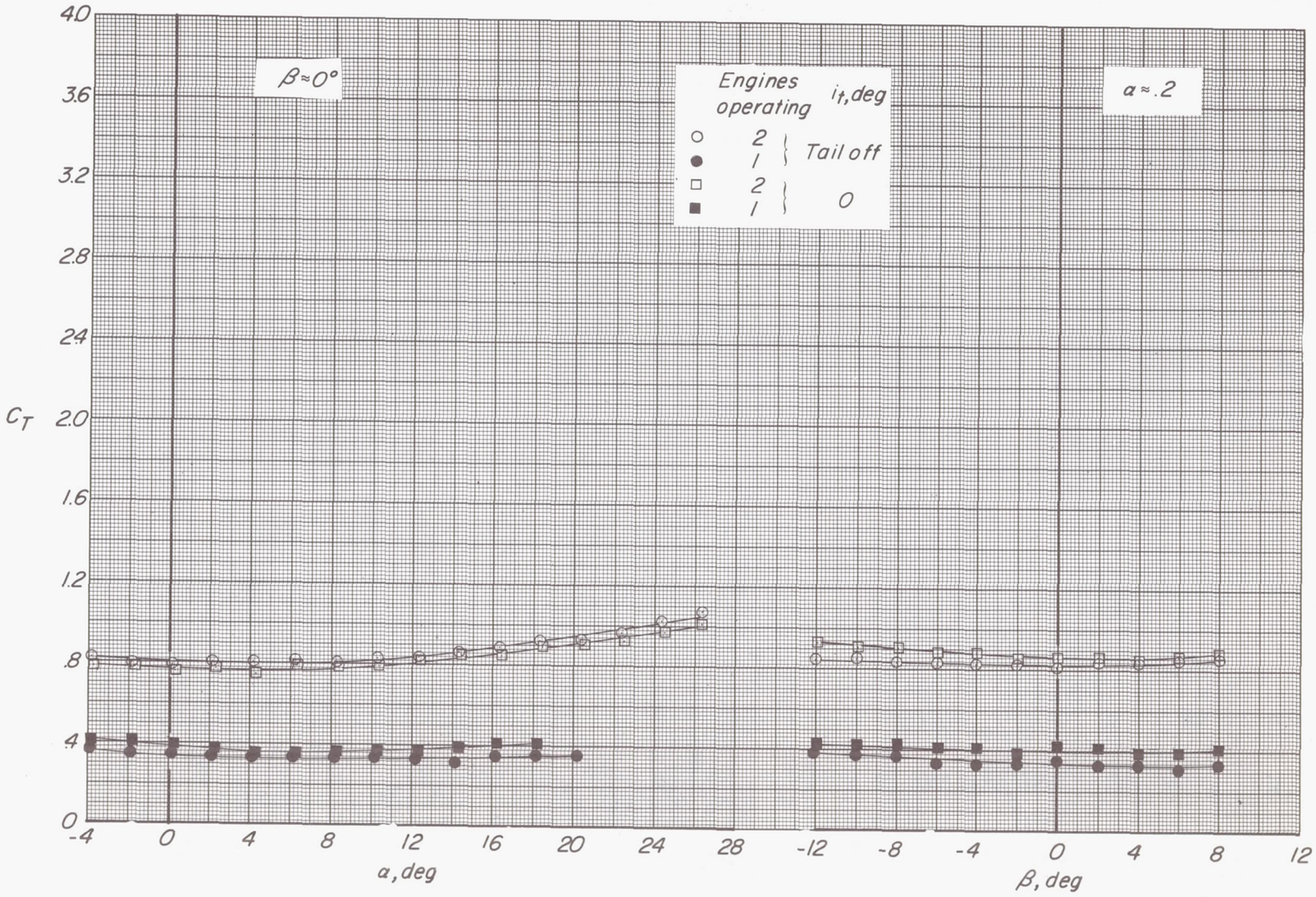

(f) Variation of C_T with α and β.

Figure 51.- Concluded.

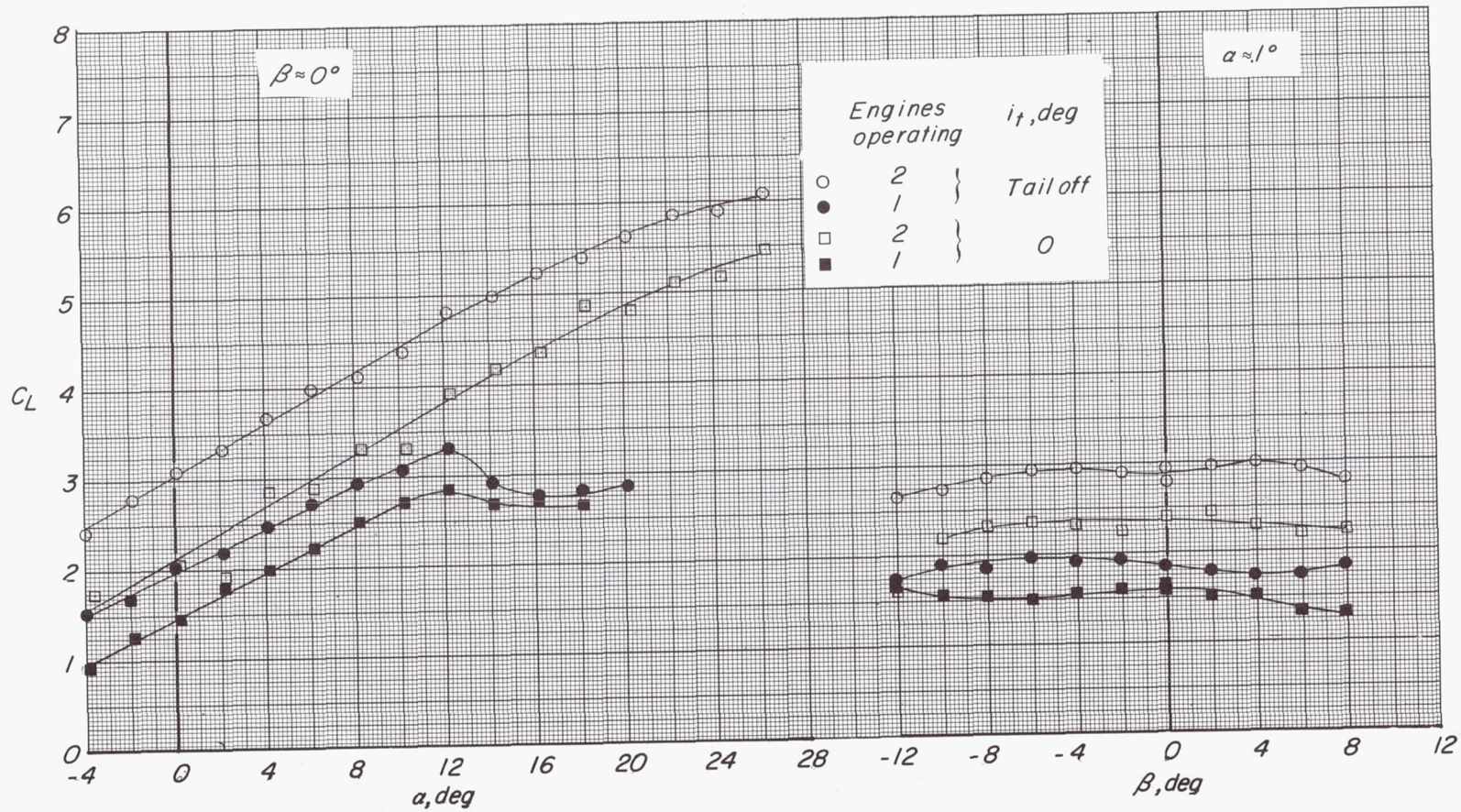

(a) Variation of C_L with α and β.

Figure 52.- Longitudinal and lateral-directional aerodynamic characteristics showing effect of loss of power from right engine. $\delta_f = 45^0$; $C_T = 2.10$; $i_t = 0^0$; $\delta_e = 0^0$.

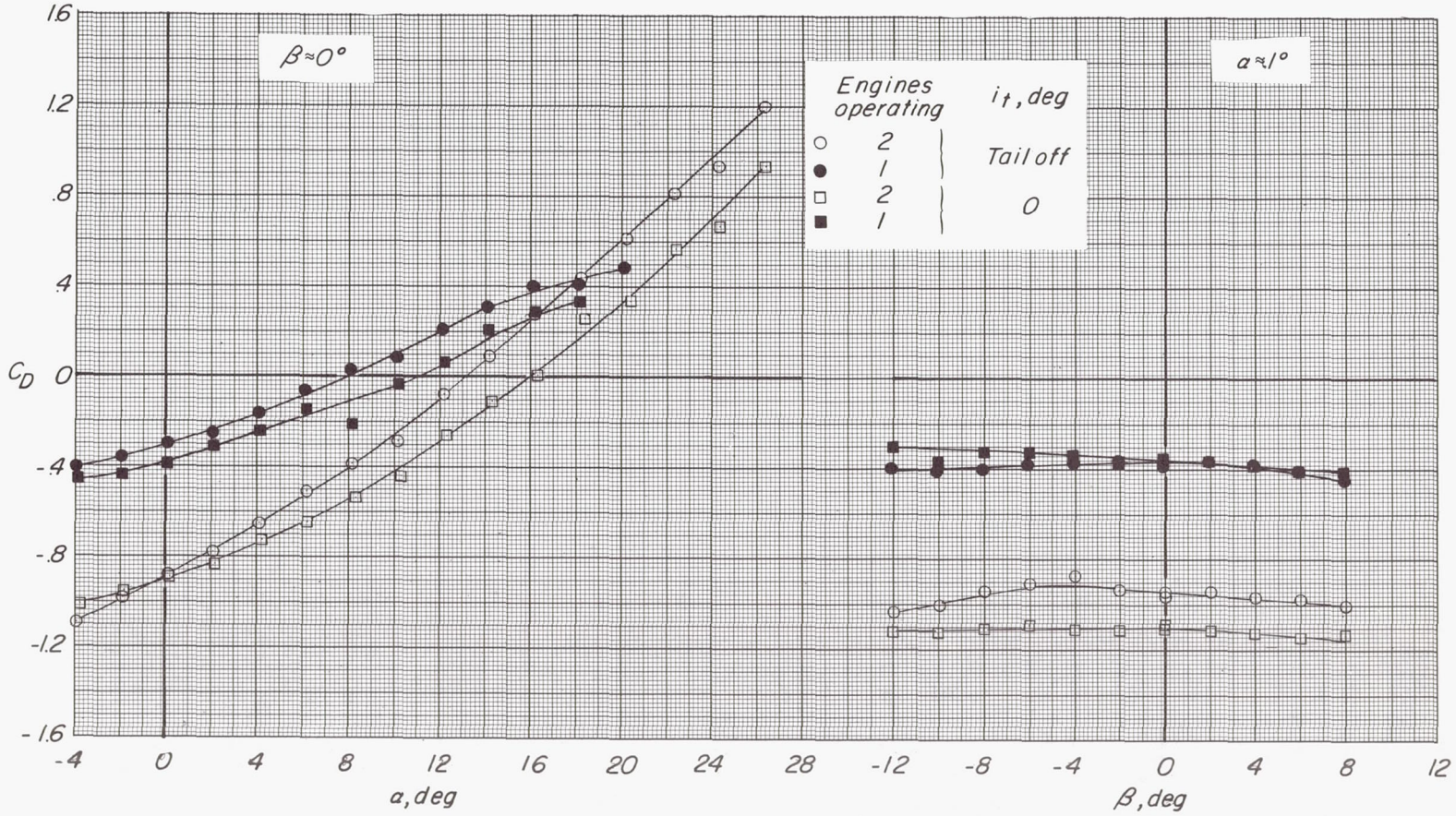

(b) Variation of C_D with α and β.

Figure 52.- Continued.

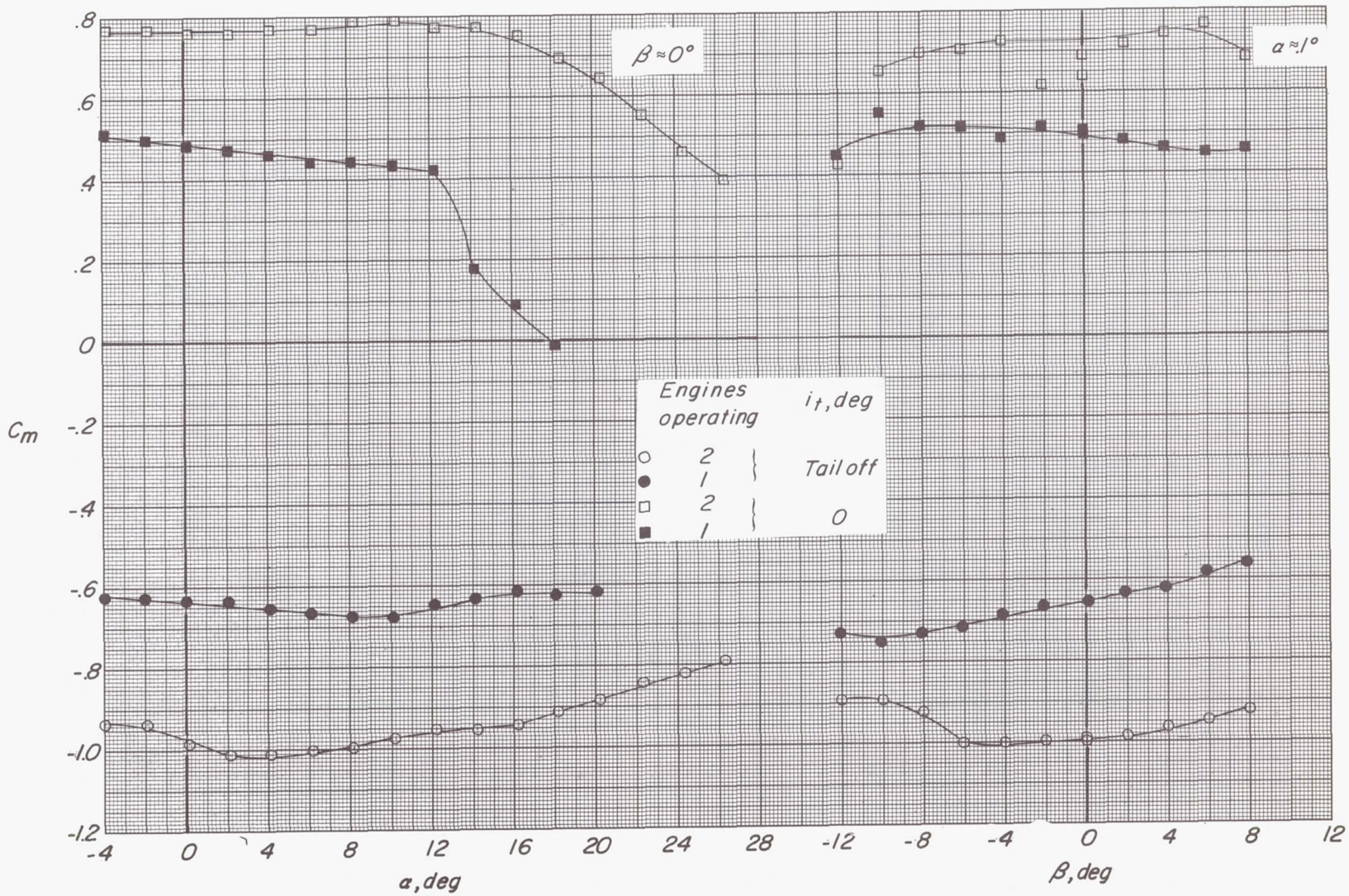

(c) Variation of C_m with α and β.

Figure 52.- Continued.

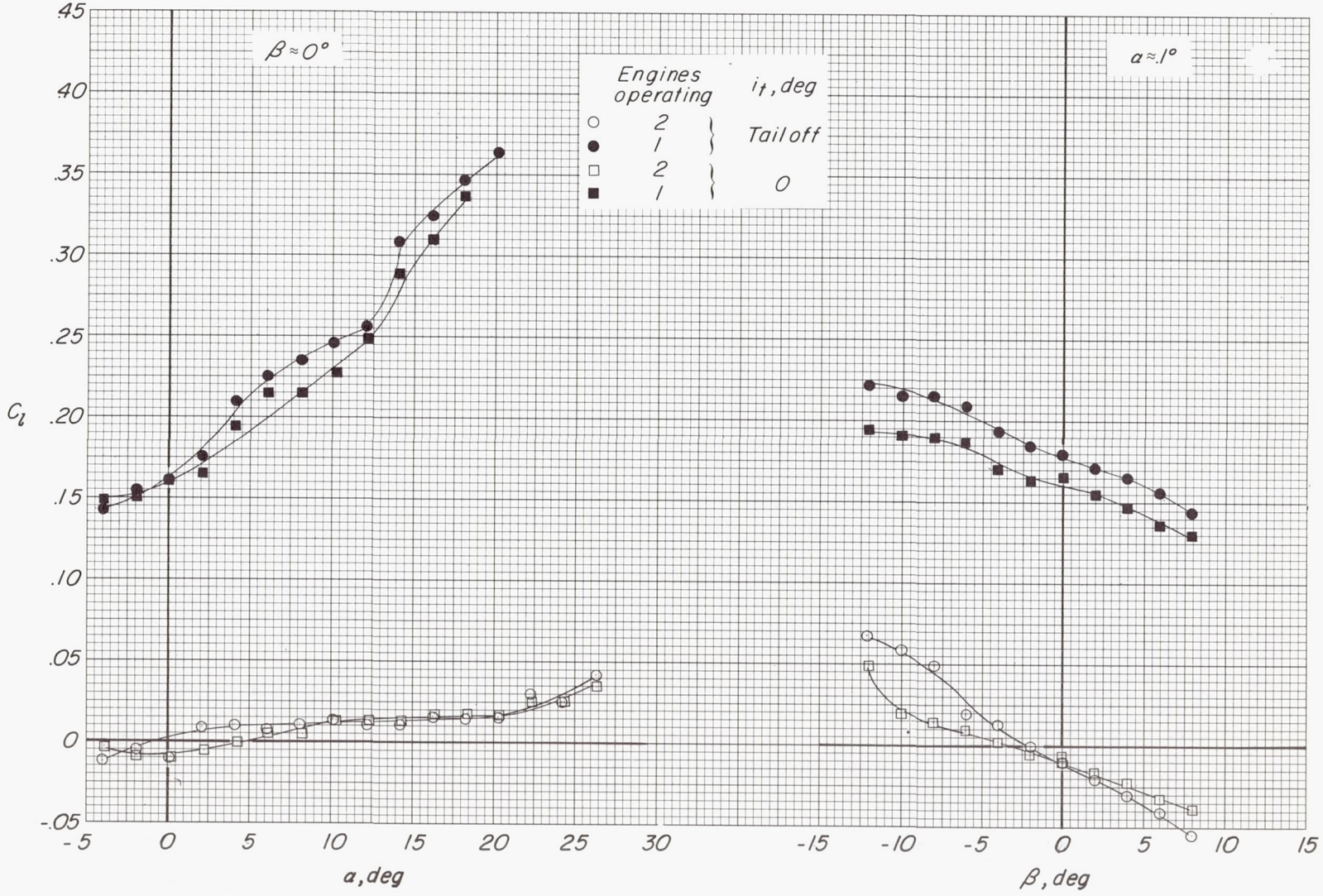

(d) Variation of C_l with α and β.

Figure 52.- Continued.

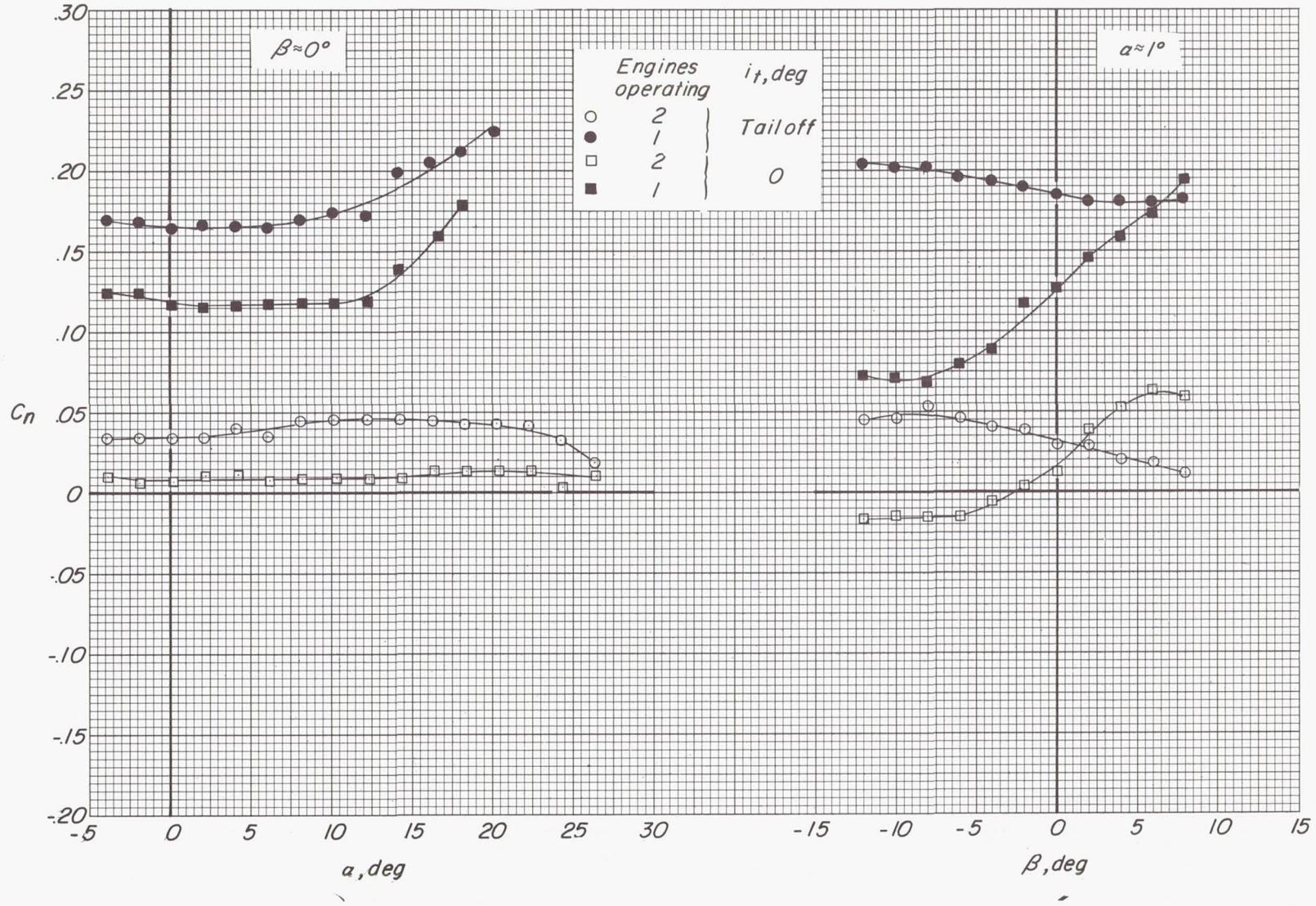

(e) Variation of C_n with α and β.

Figure 52.- Continued.

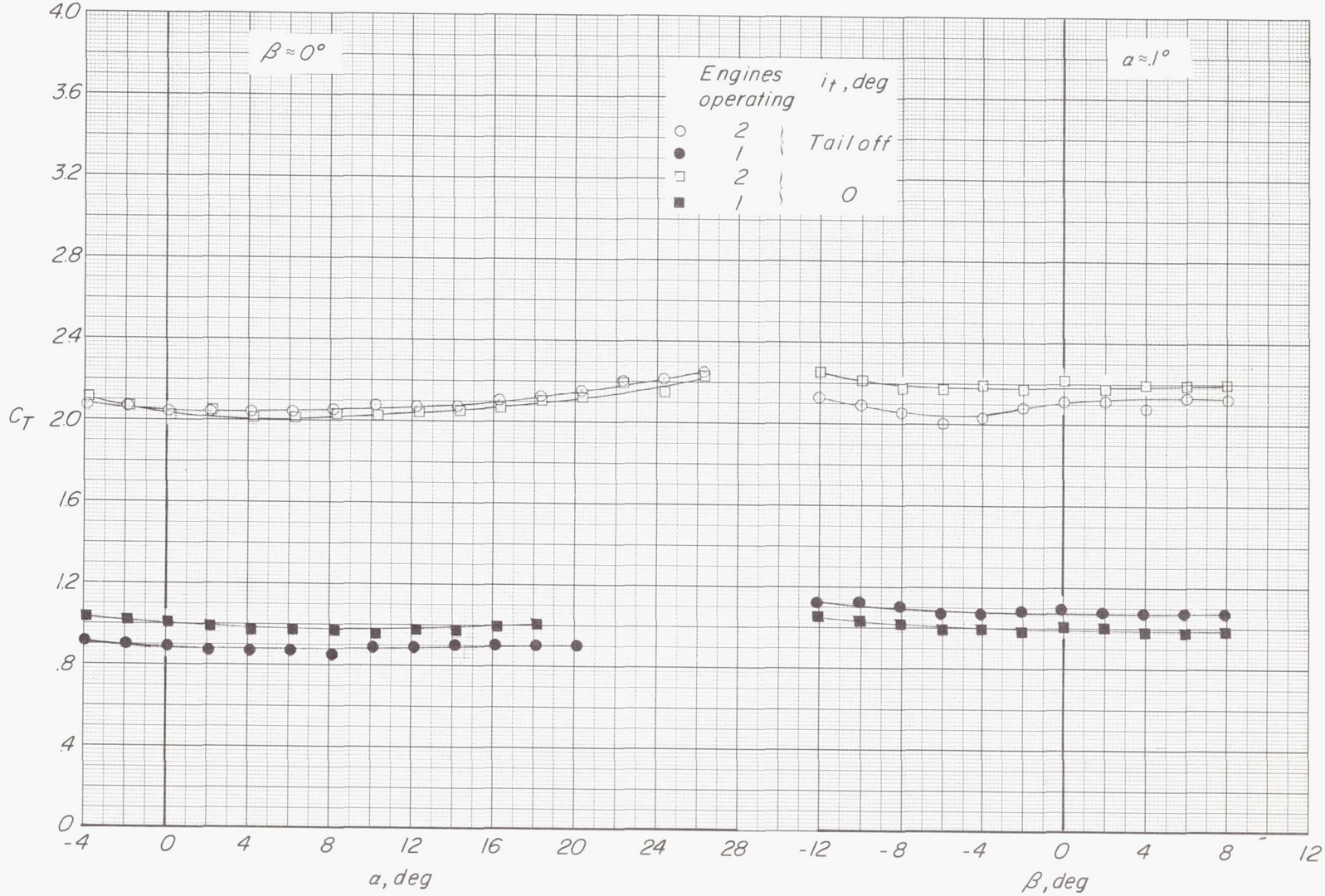

(f) Variation of C_T with α and β.

Figure 52.- Concluded.

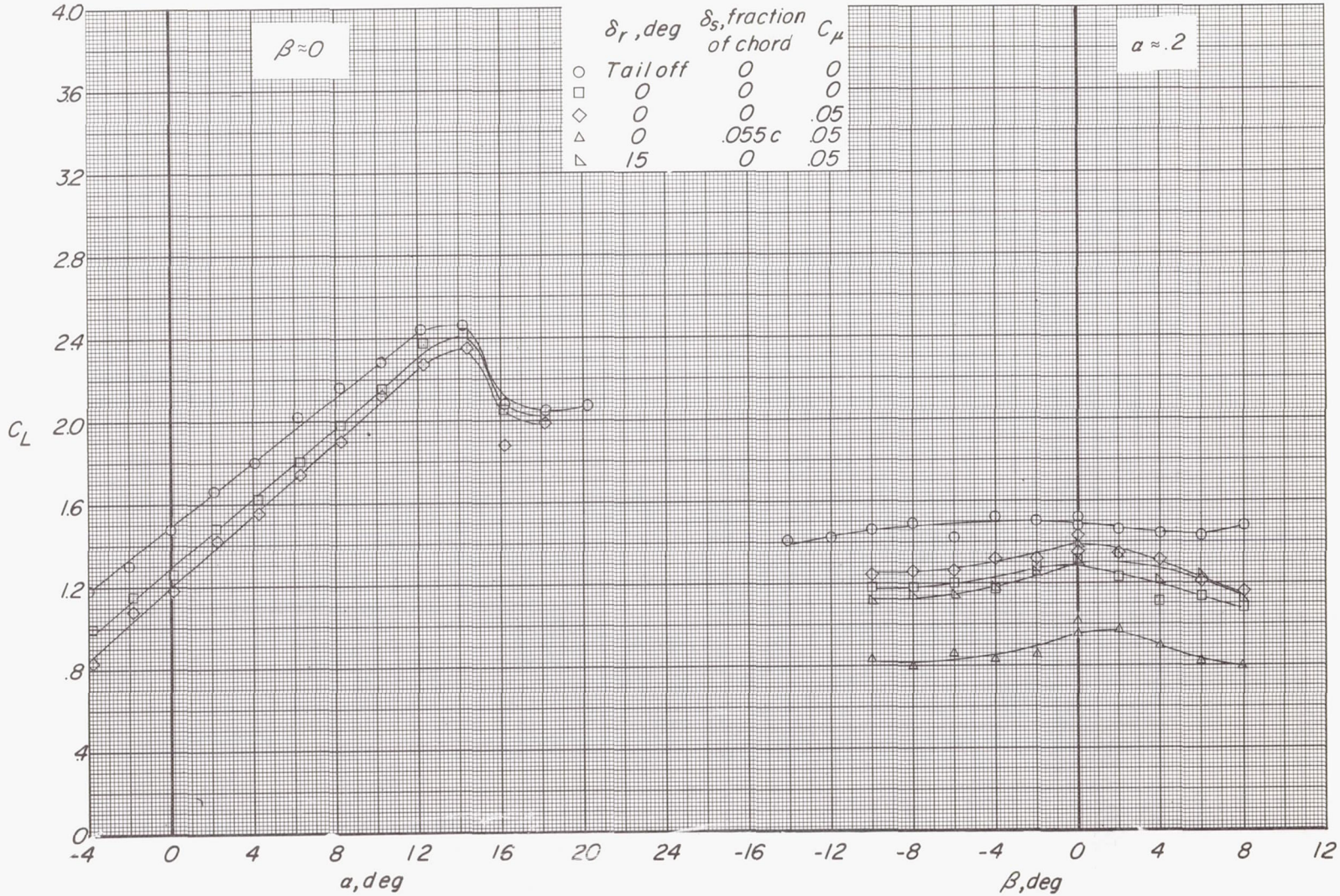

(a) Variation of C_L with α and β.

Figure 53.- Longitudinal and lateral-directional aerodynamic characteristics showing effect of control devices with right engine out. $\delta_f = 45^0$; $C_T \approx 0.43/2$; $i_t = 0^0$.

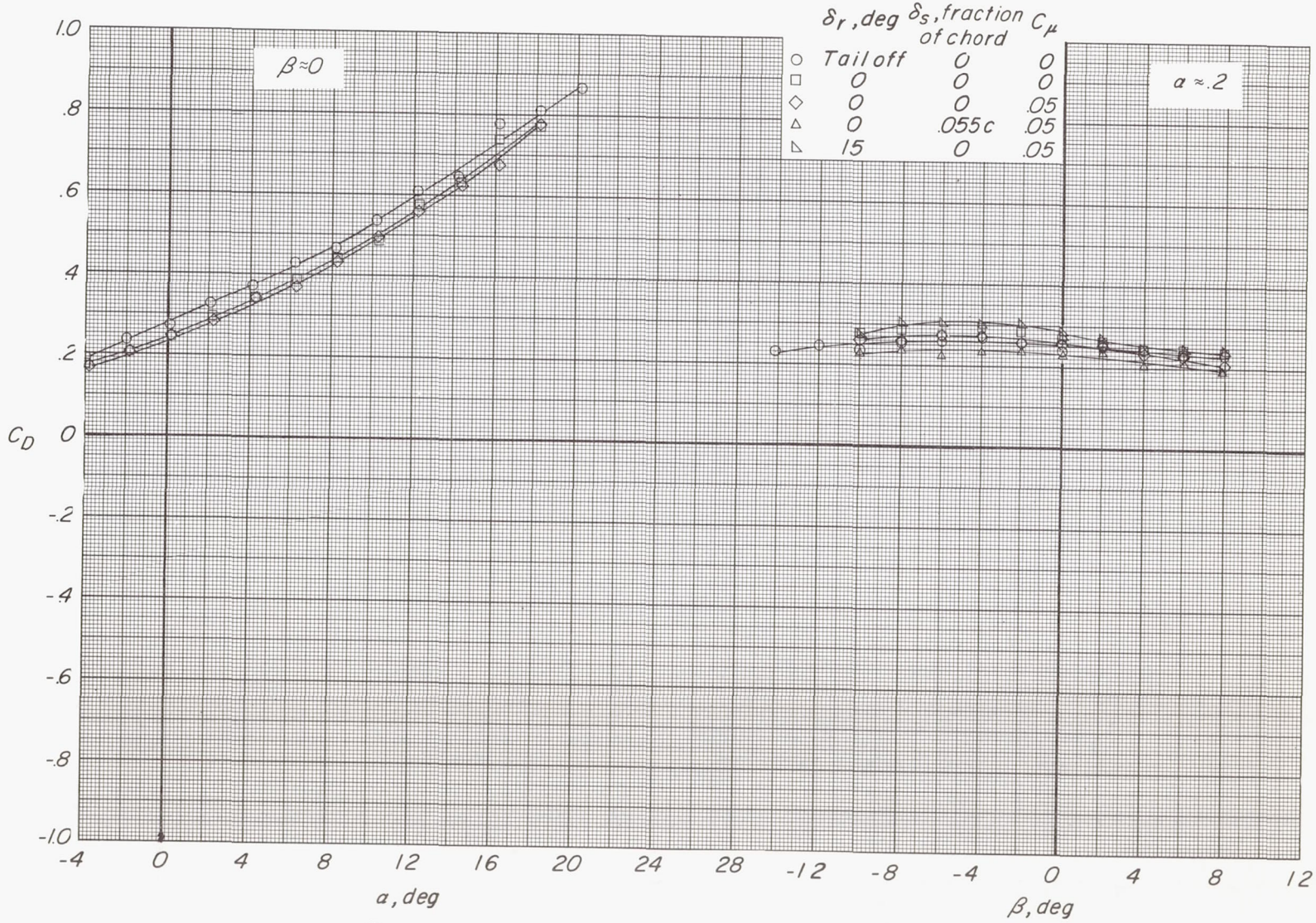

(b) Variation of C_D with α and β.

Figure 53.- Continued.

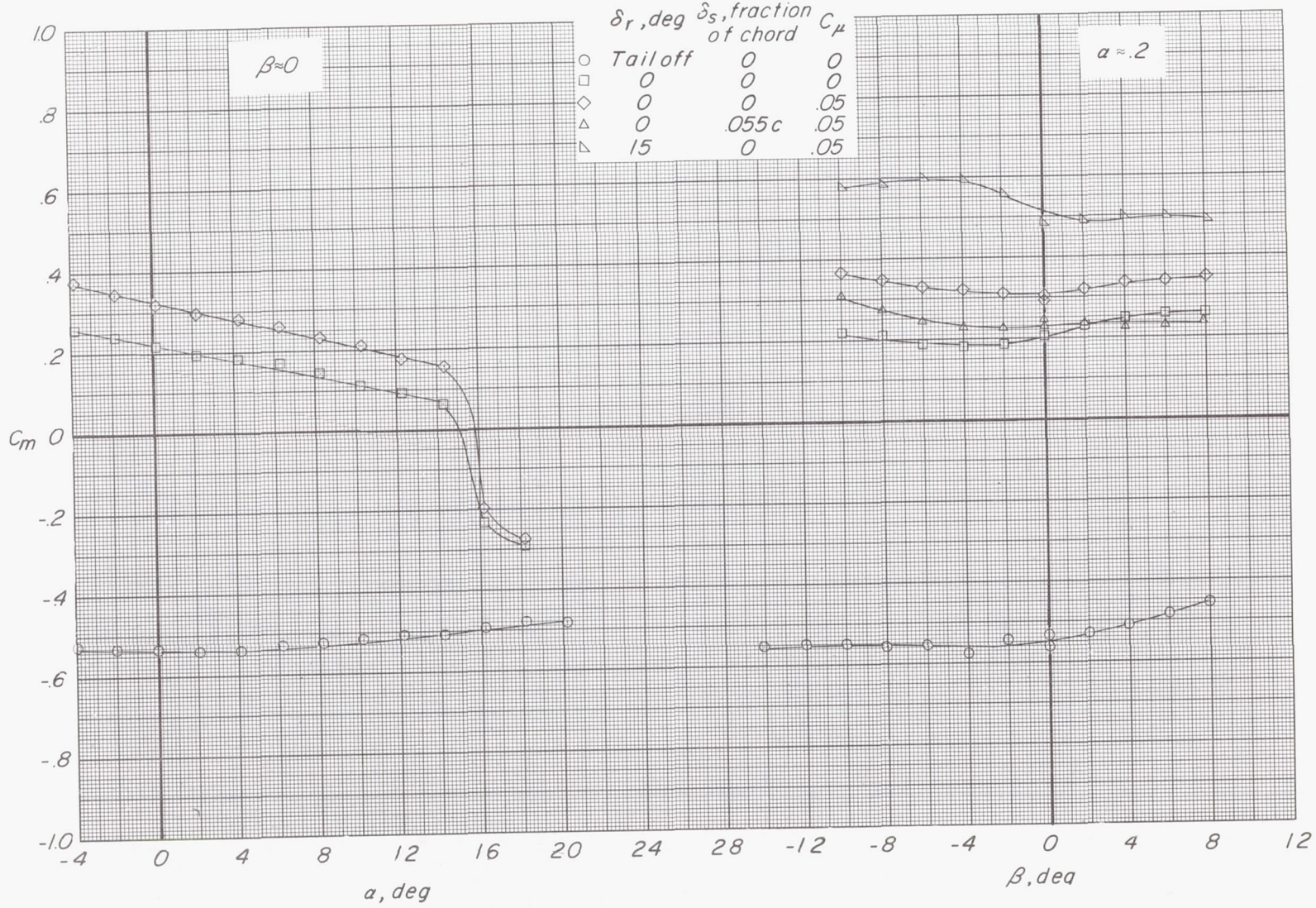

(c) Variation of C_m with α and β.

Figure 53.- Continued.

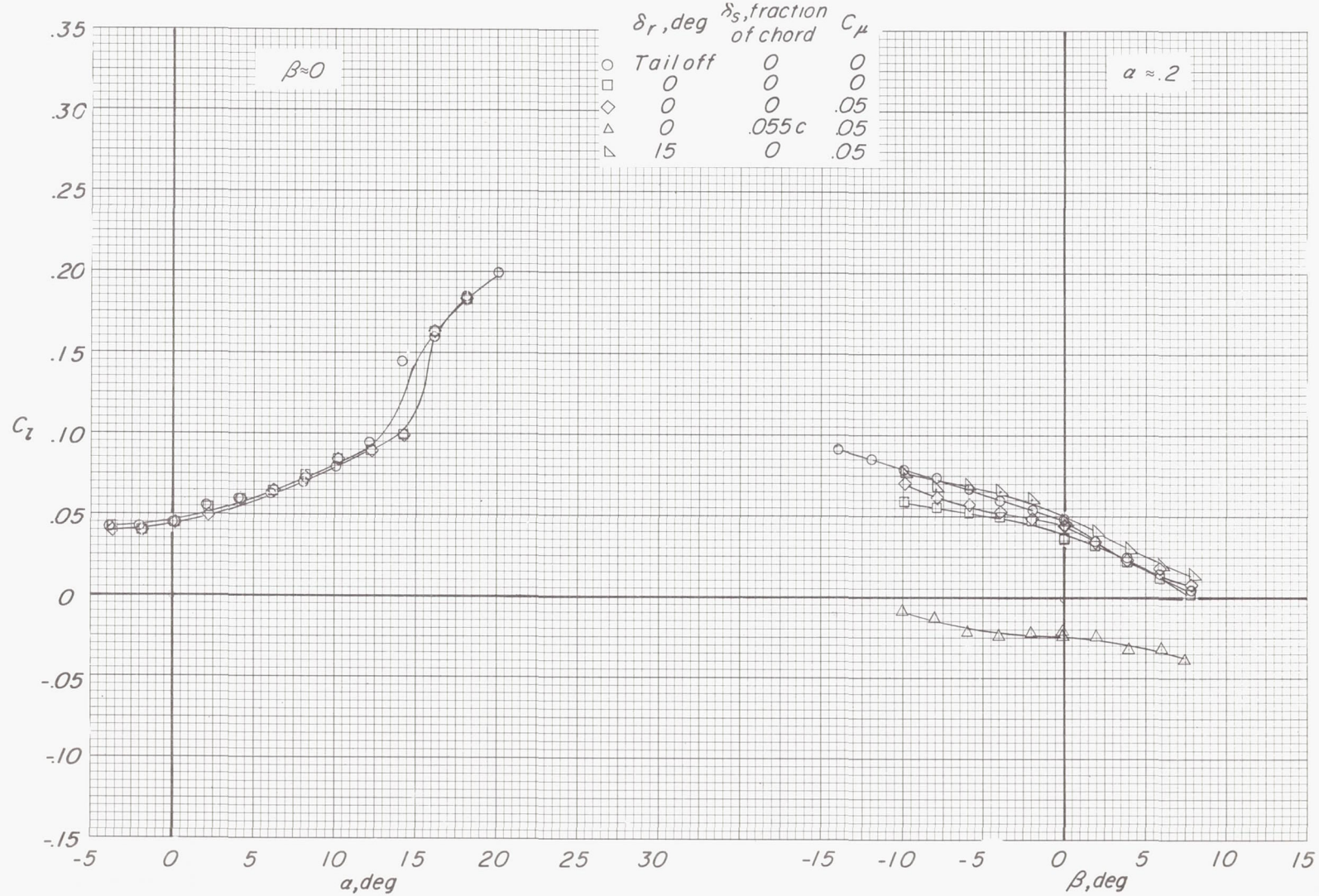

(d) Variation of C_l with α and β.

Figure 53.- Continued.

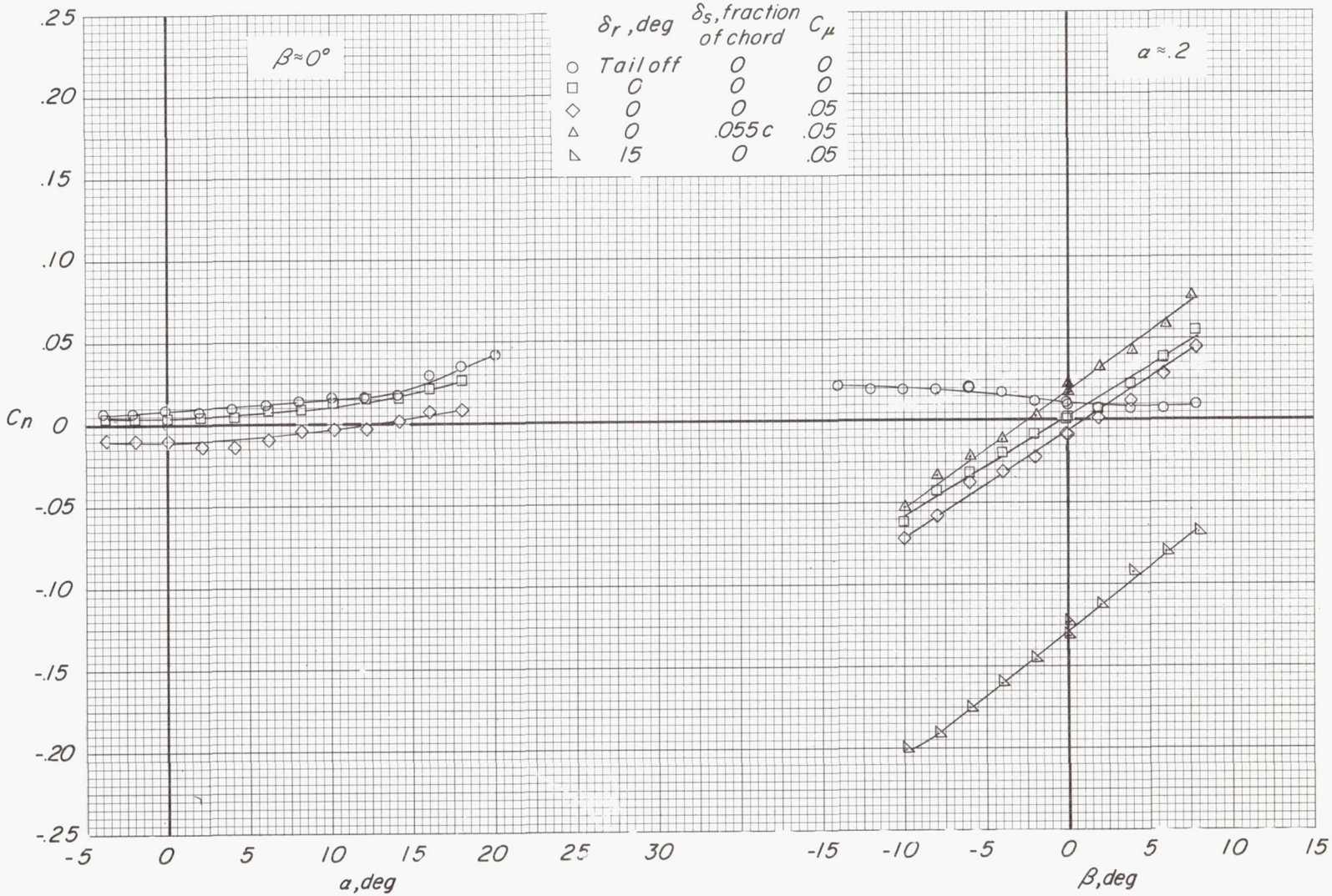

(e) Variation of C_n with α and β.

Figure 53.- Continued.

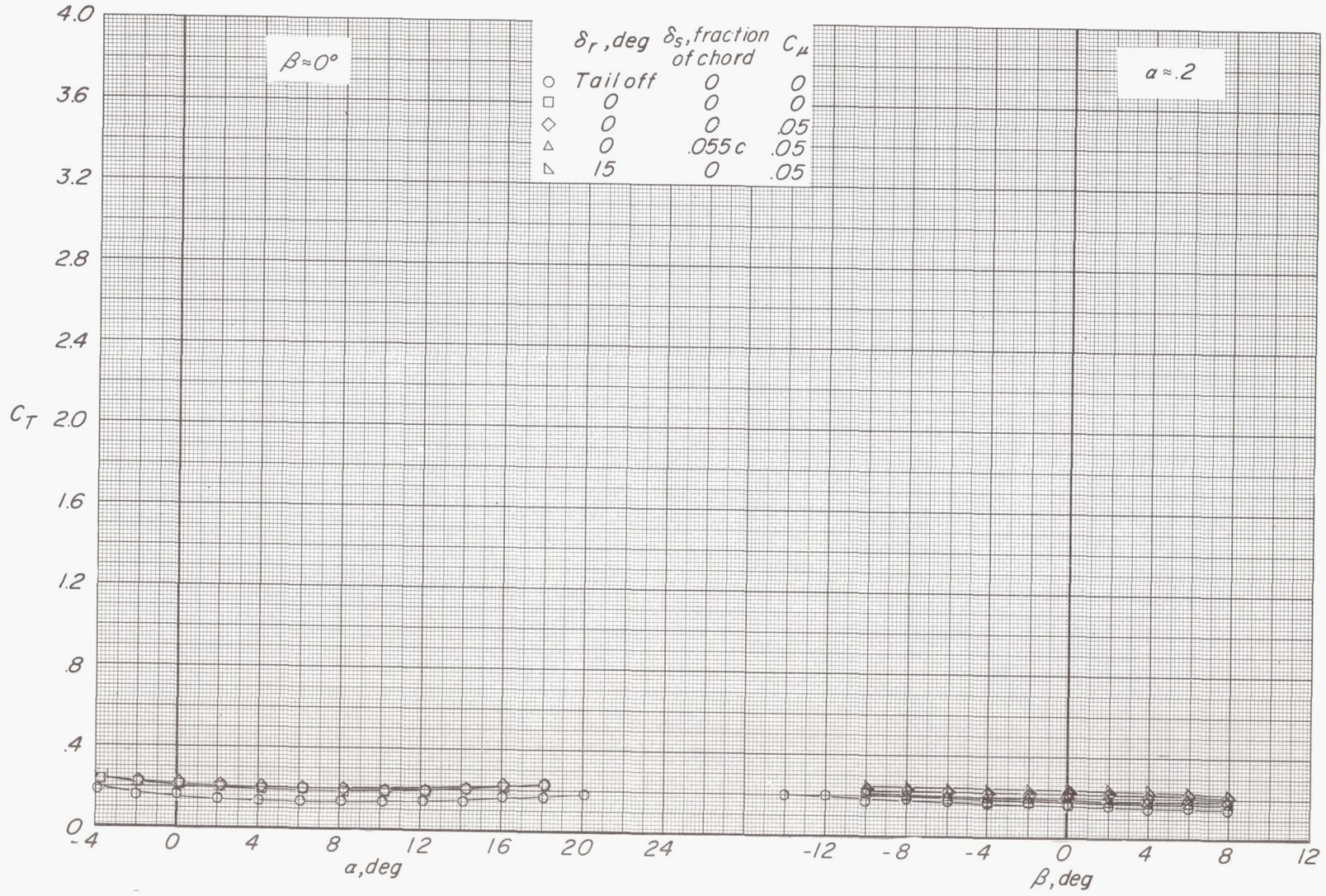

(f) Variation of C_T with α and β.

Figure 53.- Concluded.

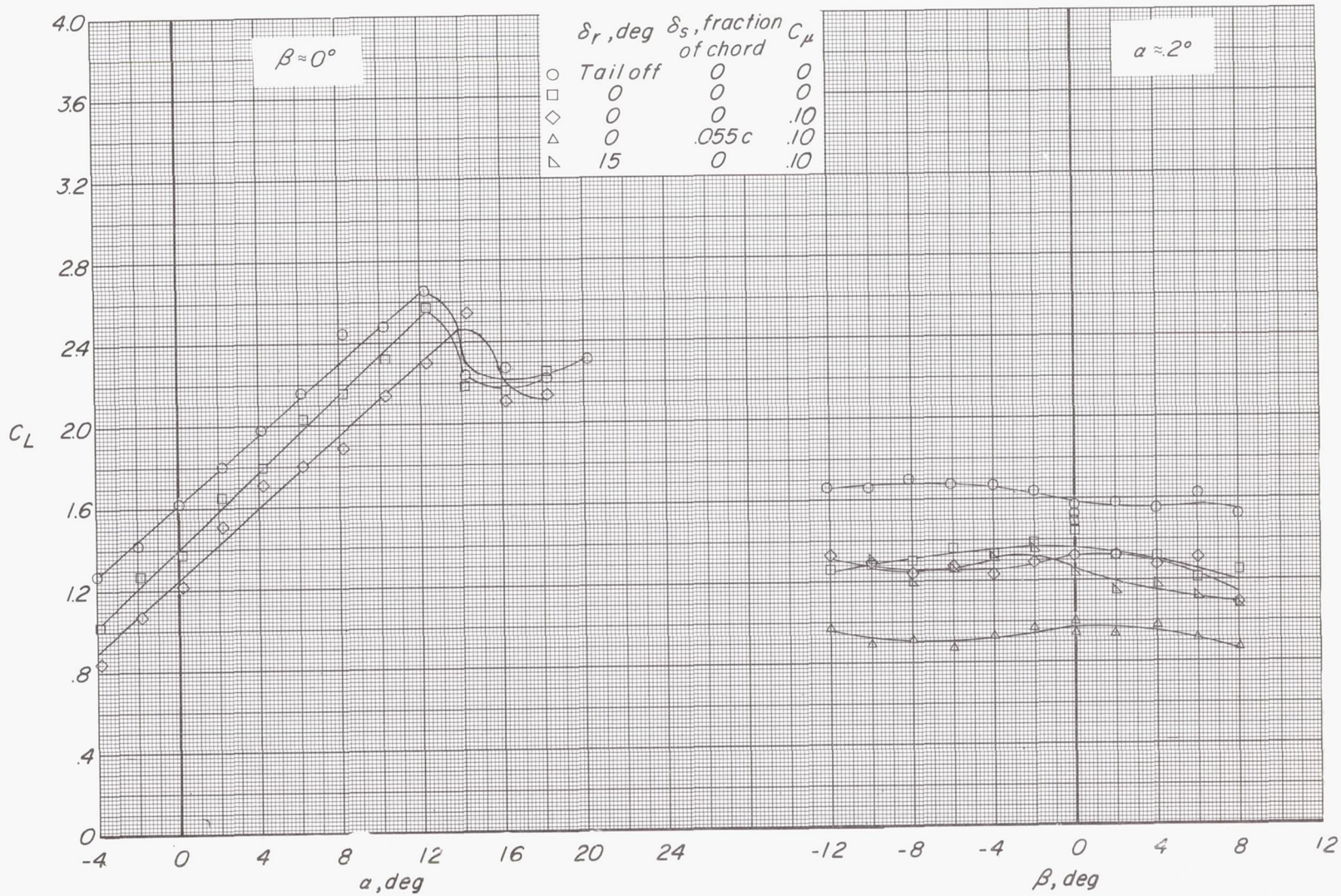

(a) Variation of C_L with α and β.

Figure 54.- Longitudinal and lateral-directional aerodynamic characteristics showing effect of control devices with right engine out. $\delta_f = 45^0$; $C_T \approx 0.83/2$; $i_t = 0^0$.

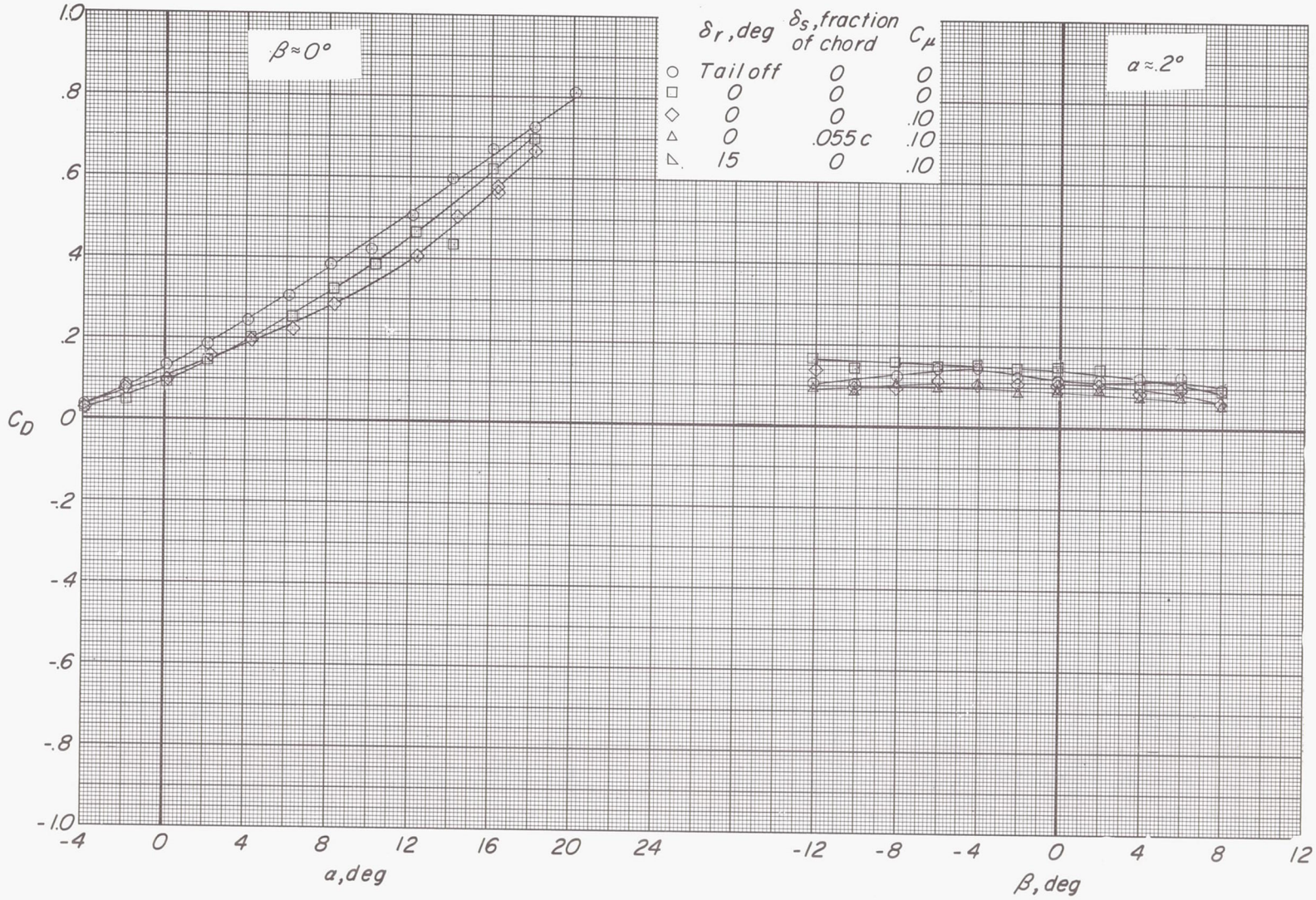

(b) Variation of C_D with α and β.

Figure 54.- Continued.

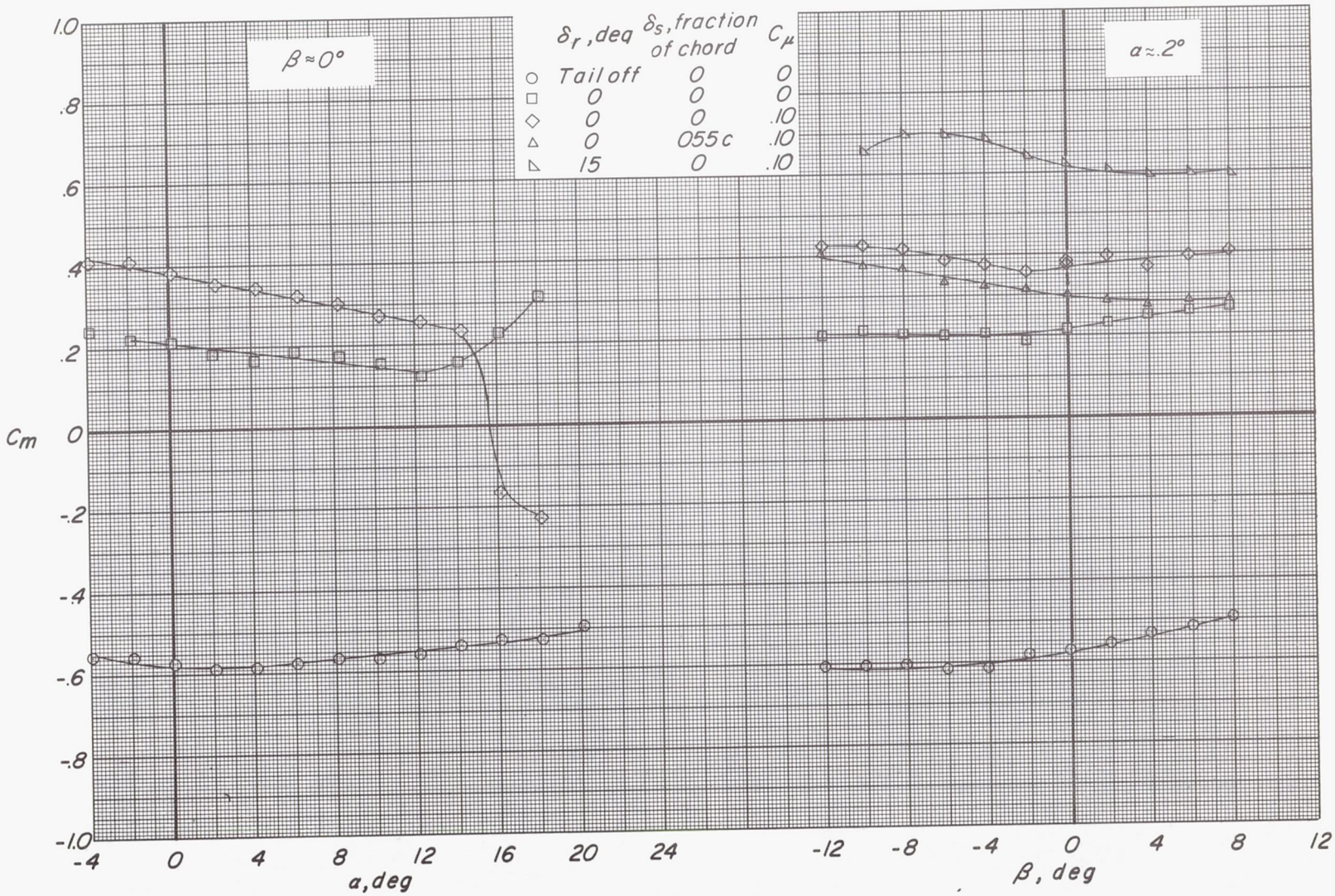

(c) Variation of C_m with α and β.

Figure 54.- Continued.

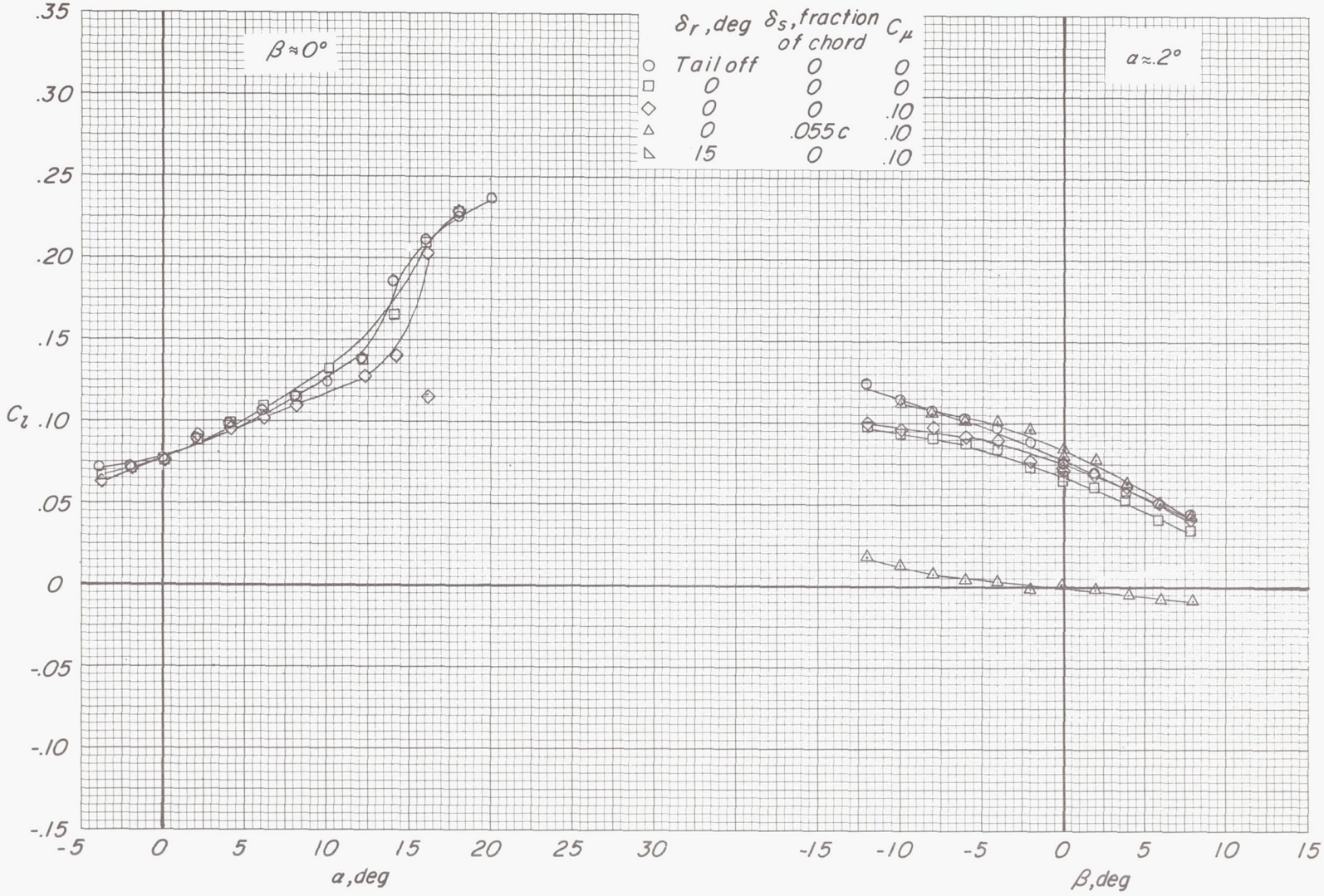

(d) Variation of C_l with α and β.

Figure 54.- Continued.

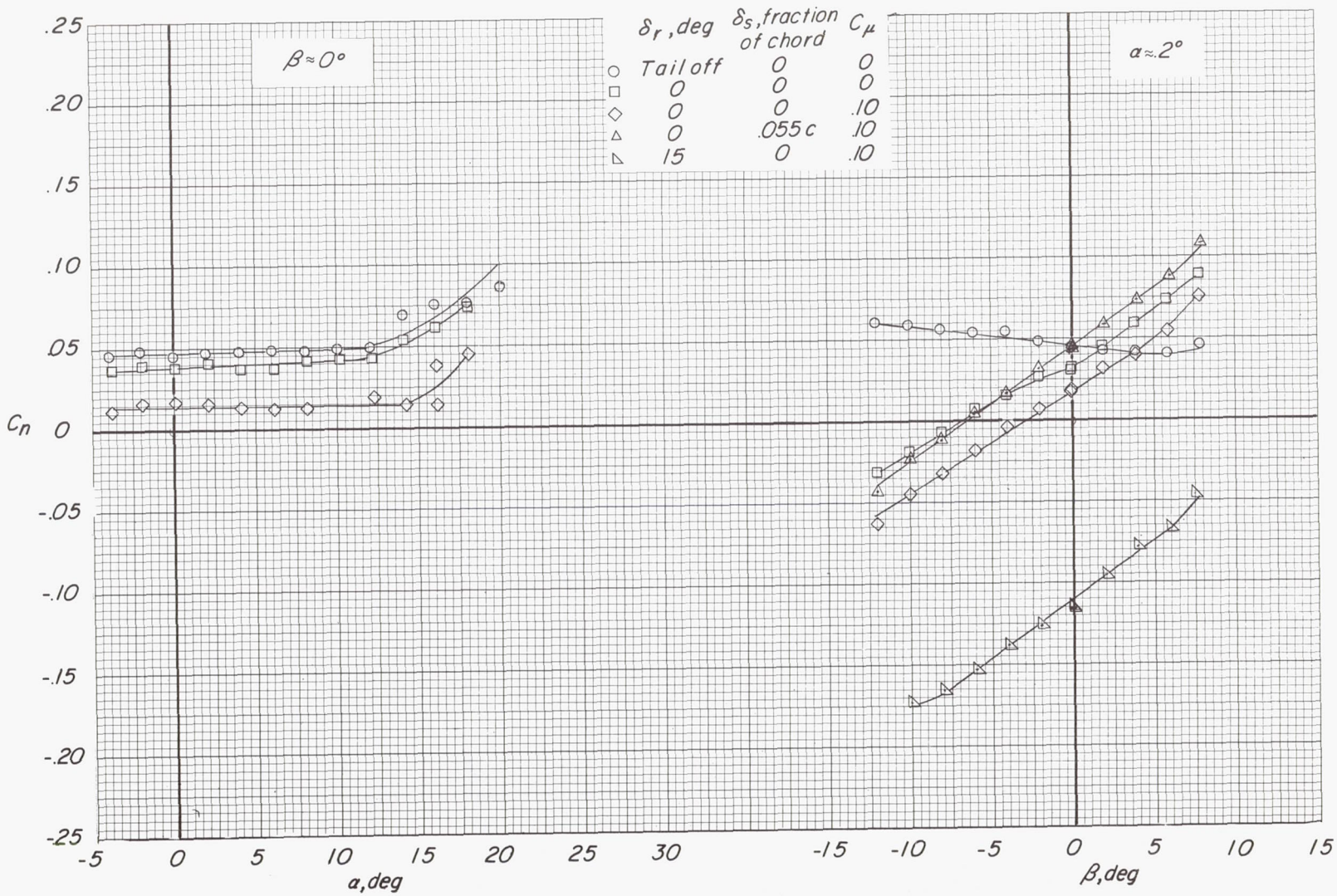

(e) Variation of C_n with α and β.

Figure 54.- Continued.

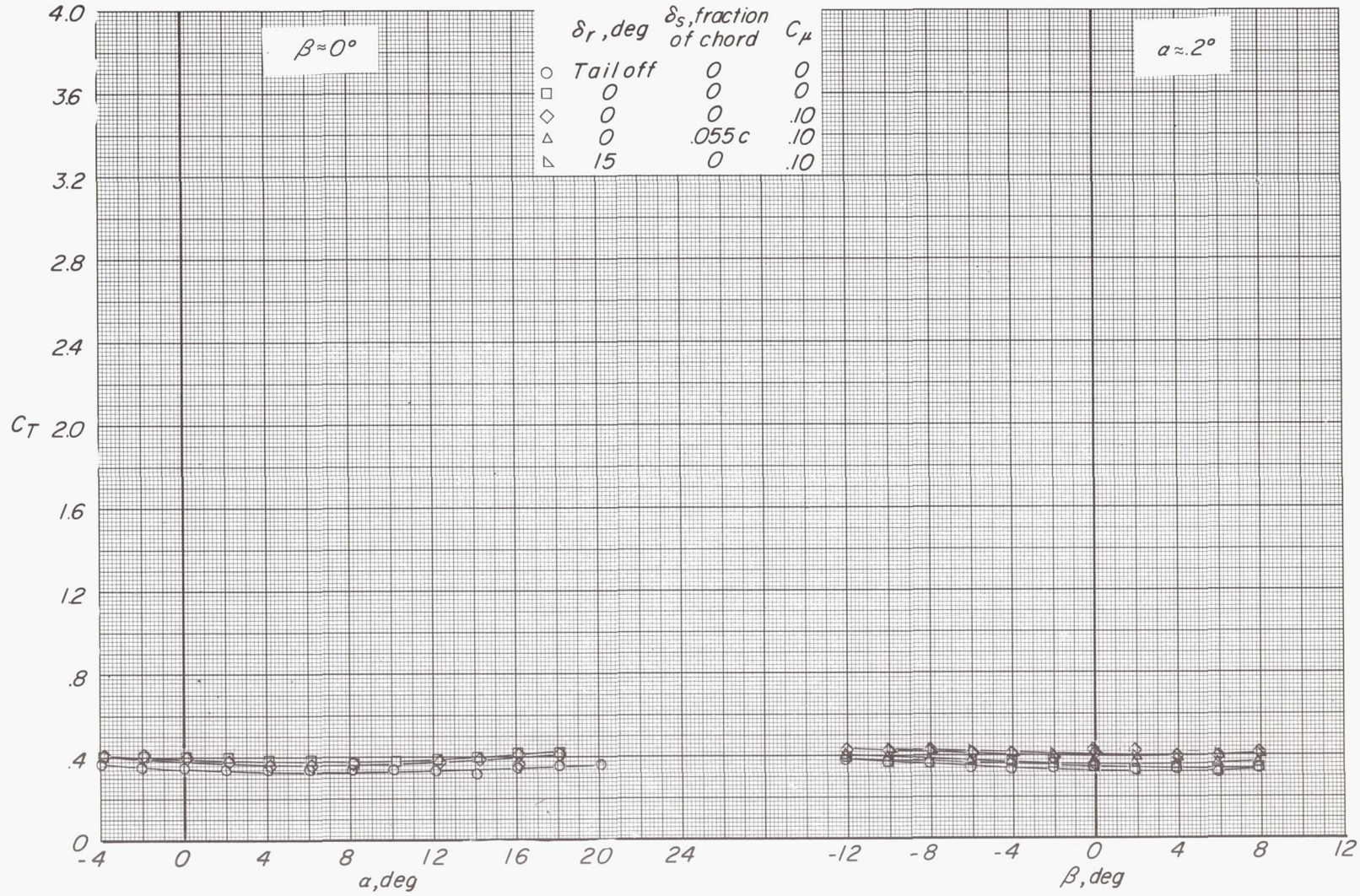

(f) Variation of C_T with α and β.

Figure 54.- Concluded.

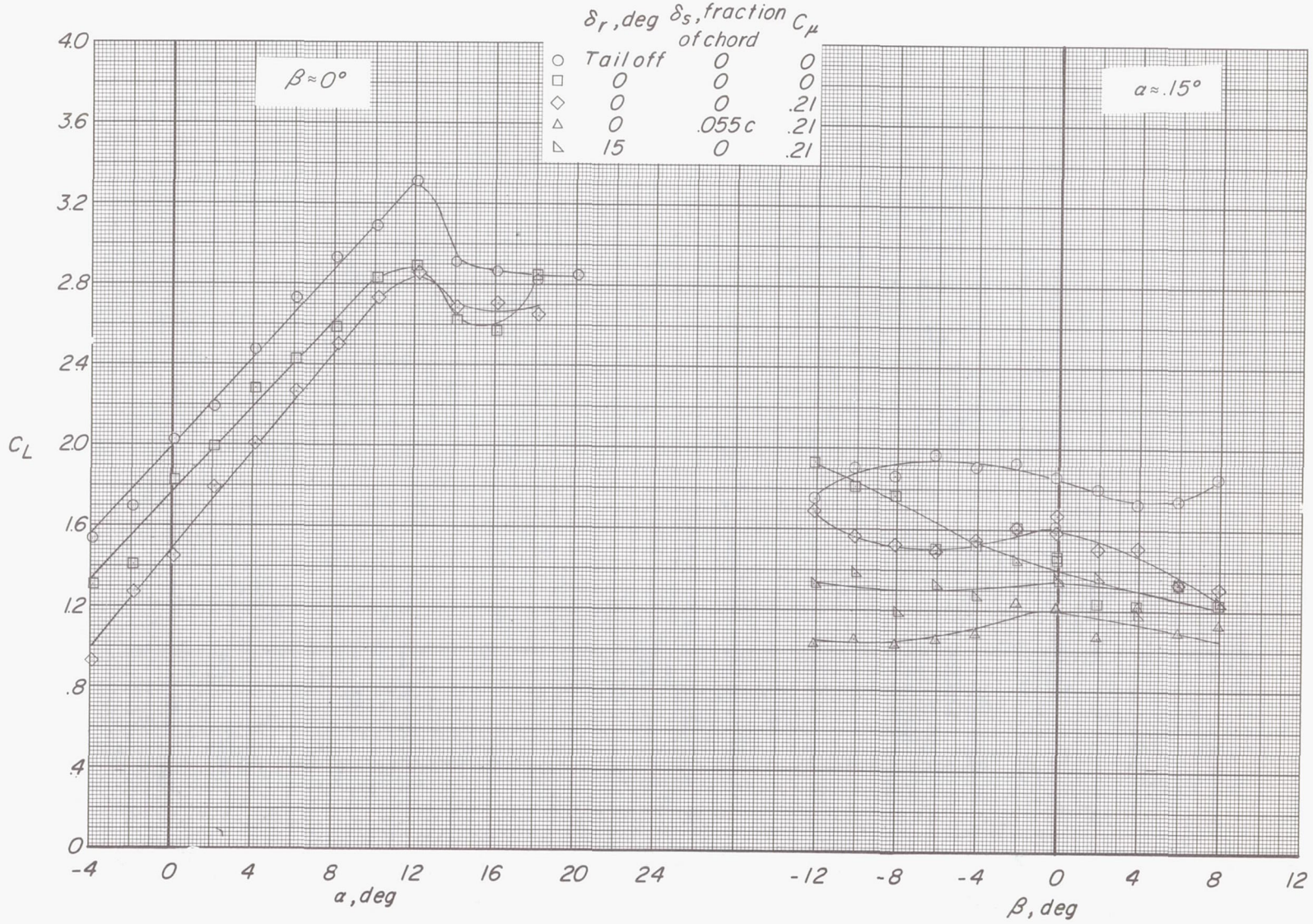

(a) Variation of C_L with α and β.

Figure 55.- Longitudinal and lateral-directional aerodynamic characteristics showing effect of control devices with right engine out. $\delta_f = 45^0$; $C_T \approx 2.10/2$; $i_t = 0^0$.

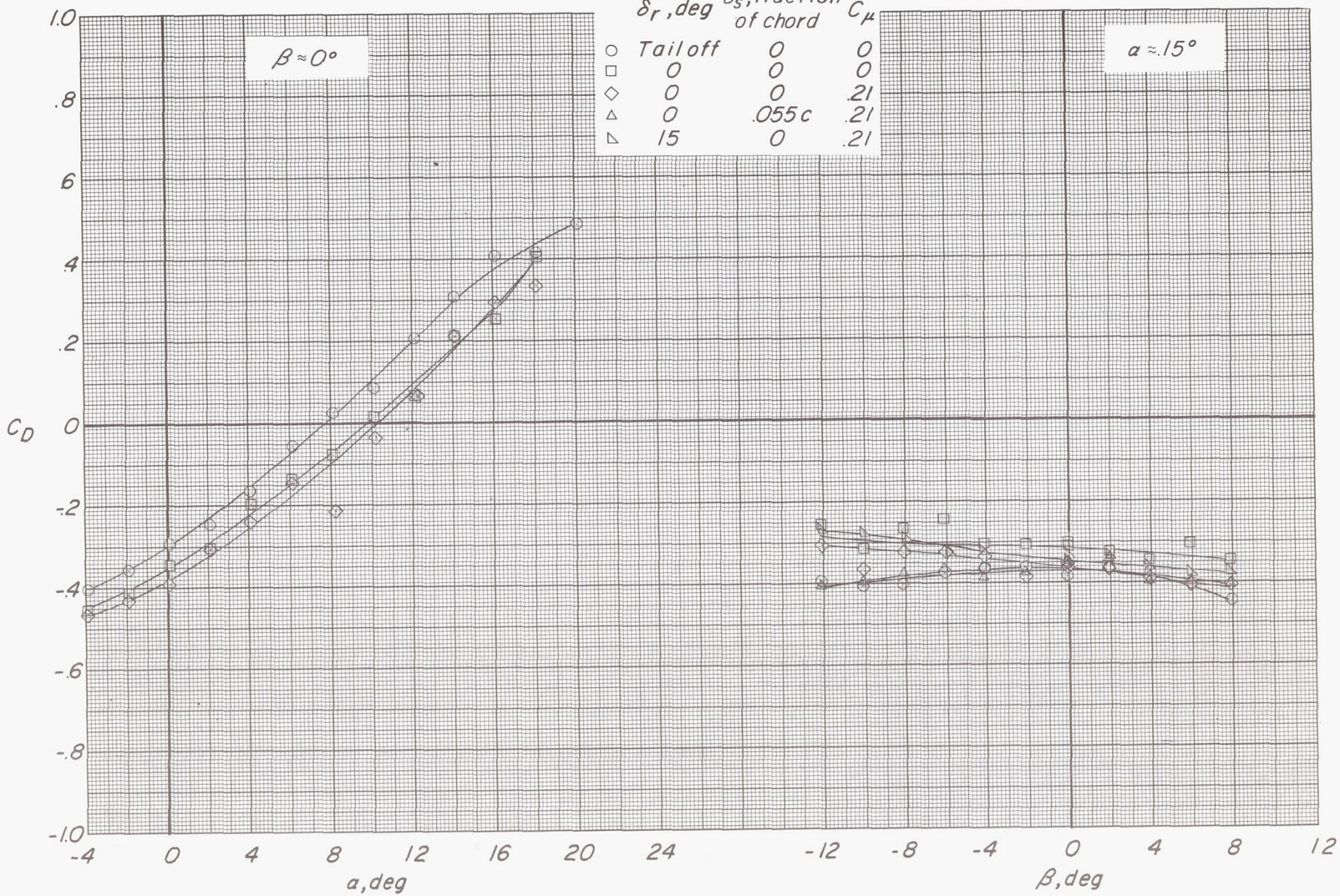

(b) Variation of C_D with α and β.

Figure 55.- Continued.

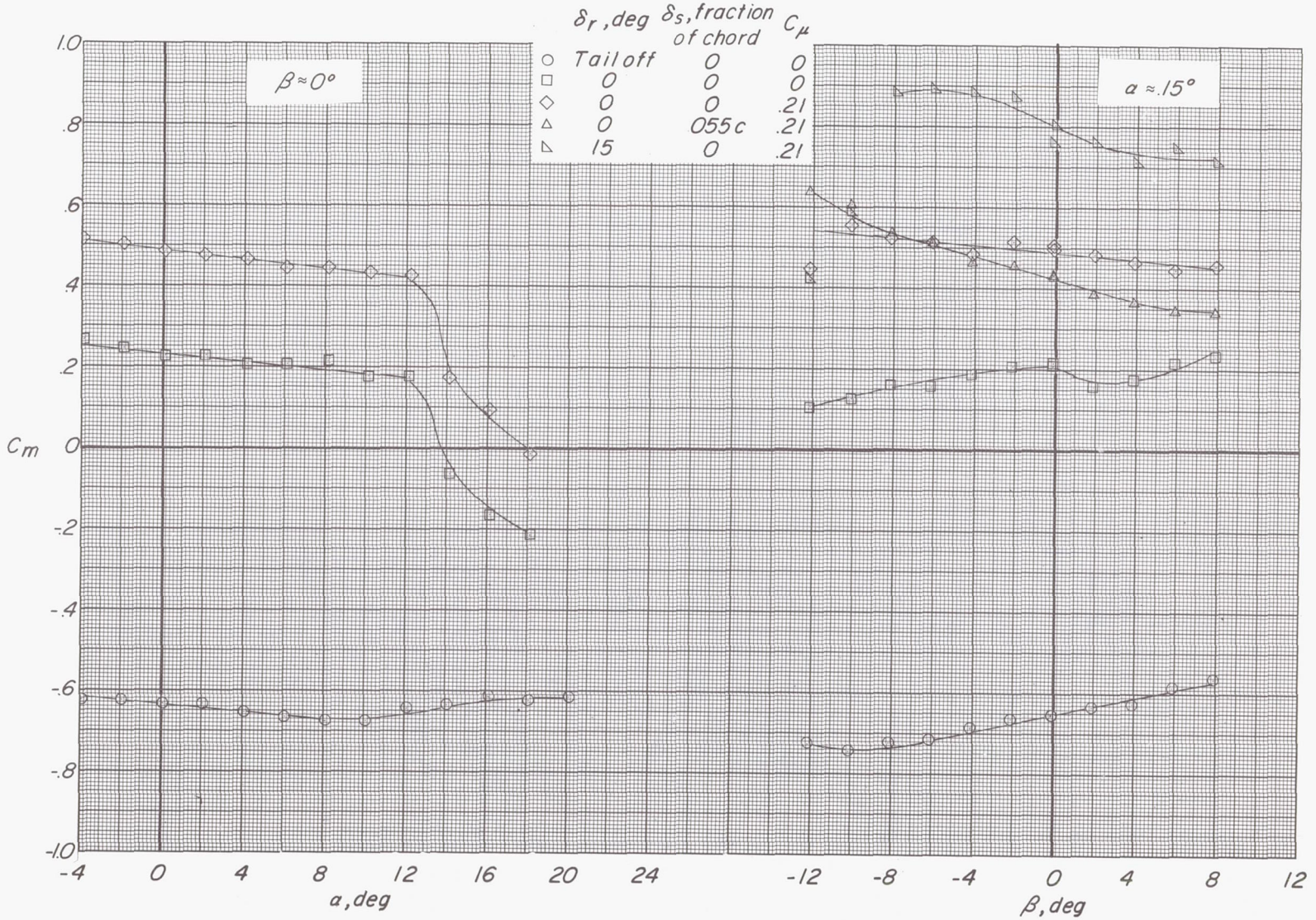

(c) Variation of C_m with α and β.

Figure 55.- Continued.

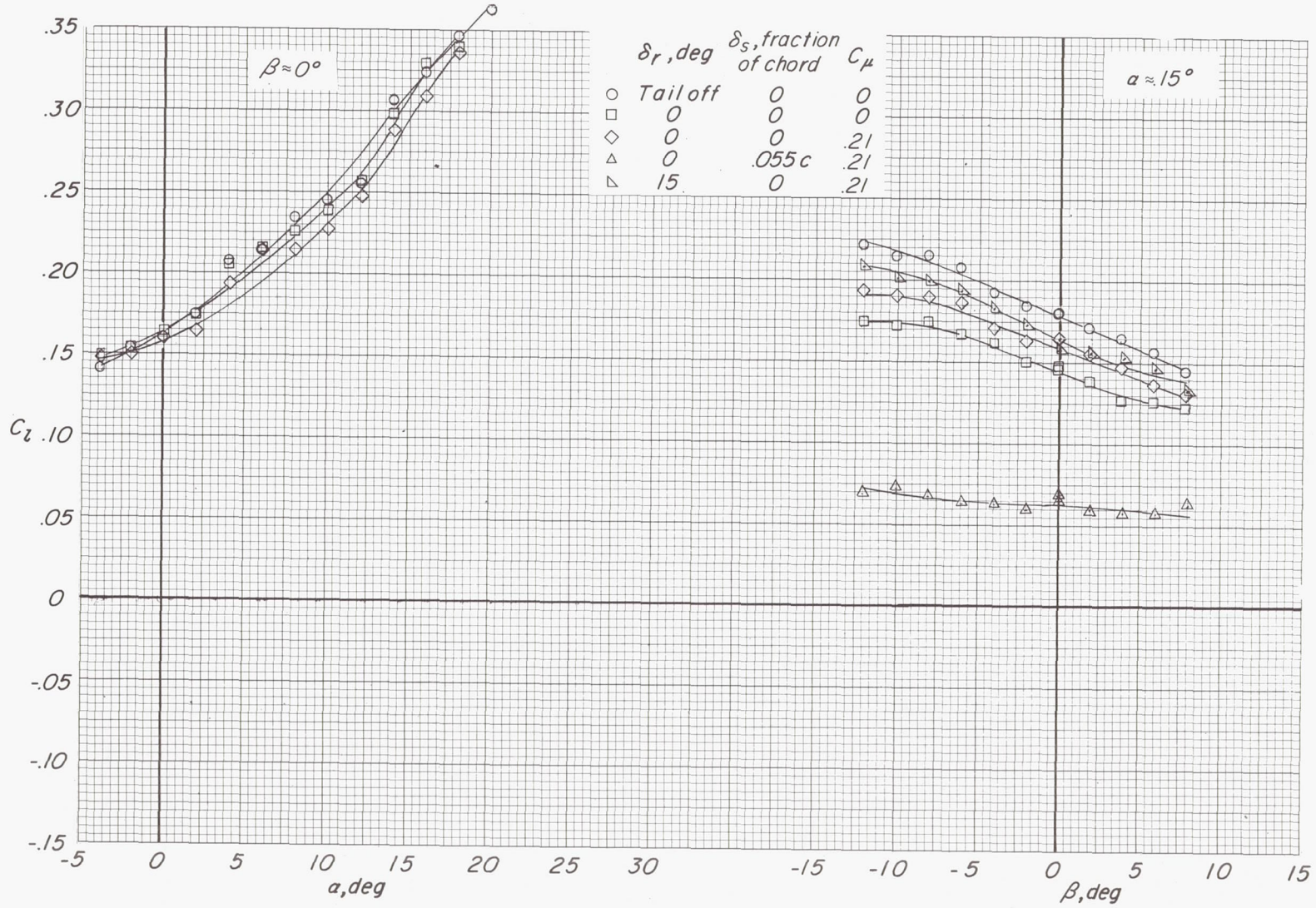

(d) Variation of C_l with α and β.

Figure 55.- Continued.

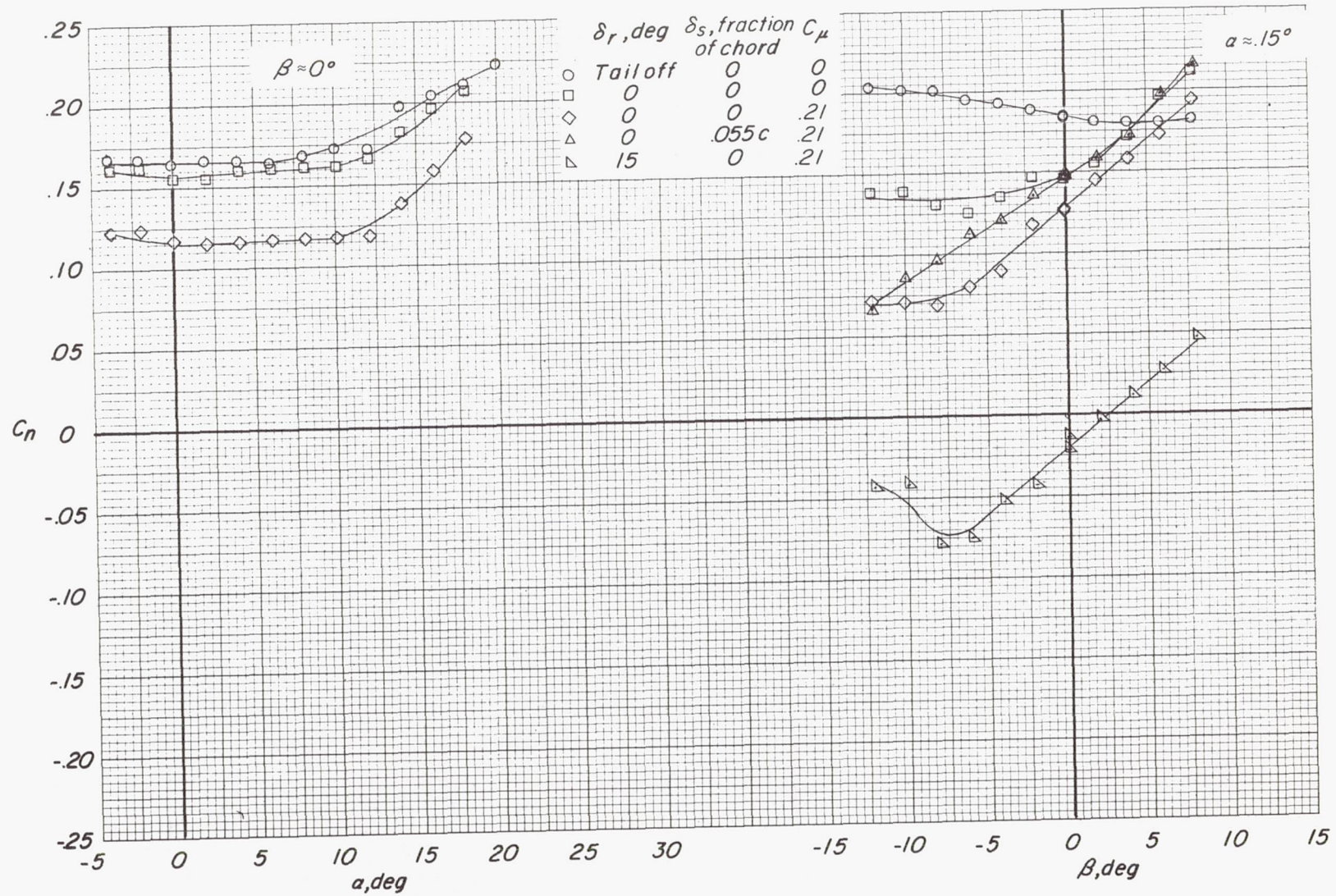

(e) Variation of C_n with α and β.

Figure 55.- Continued.

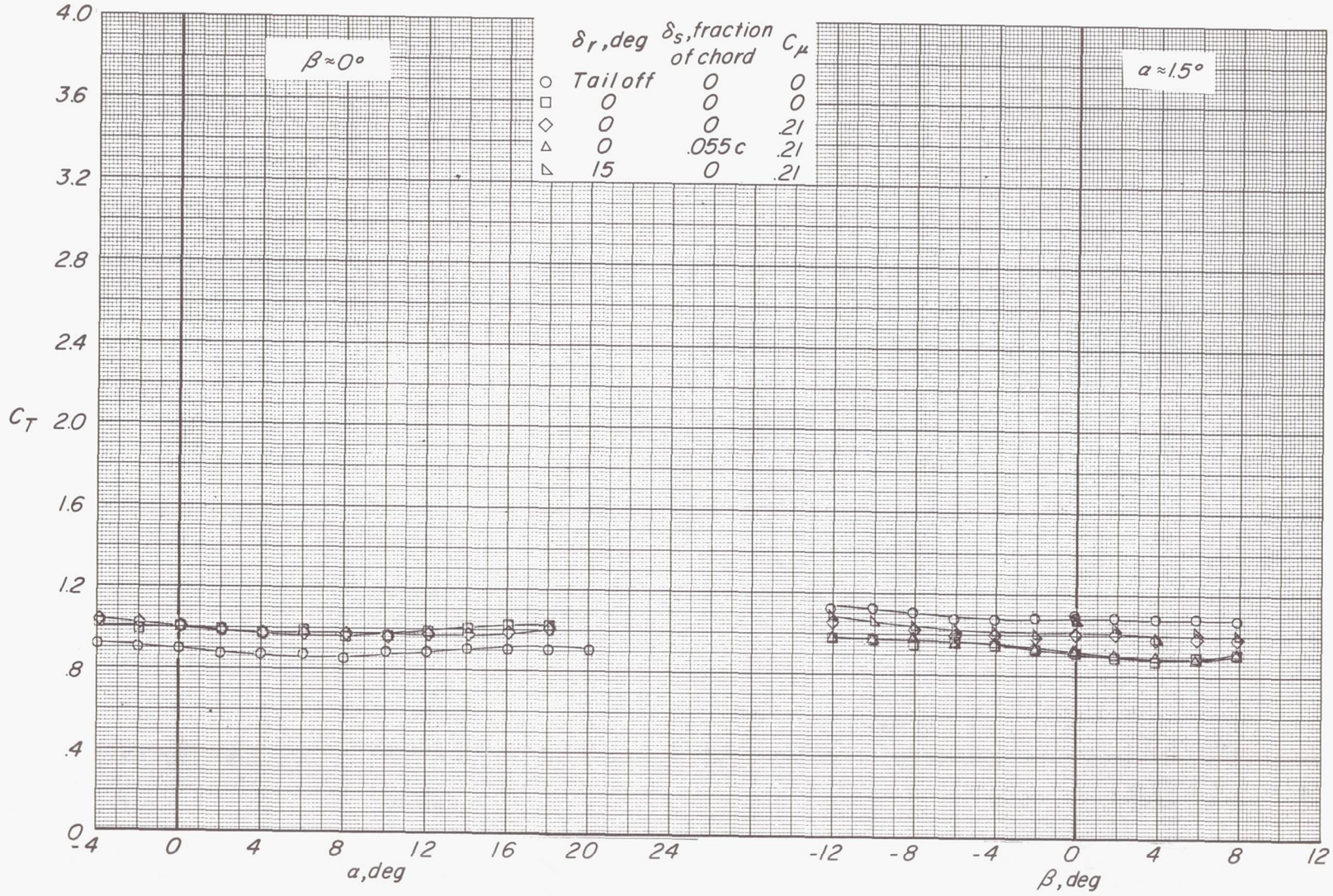

(f) Variation of C_T with α and β.

Figure 55.- Concluded.

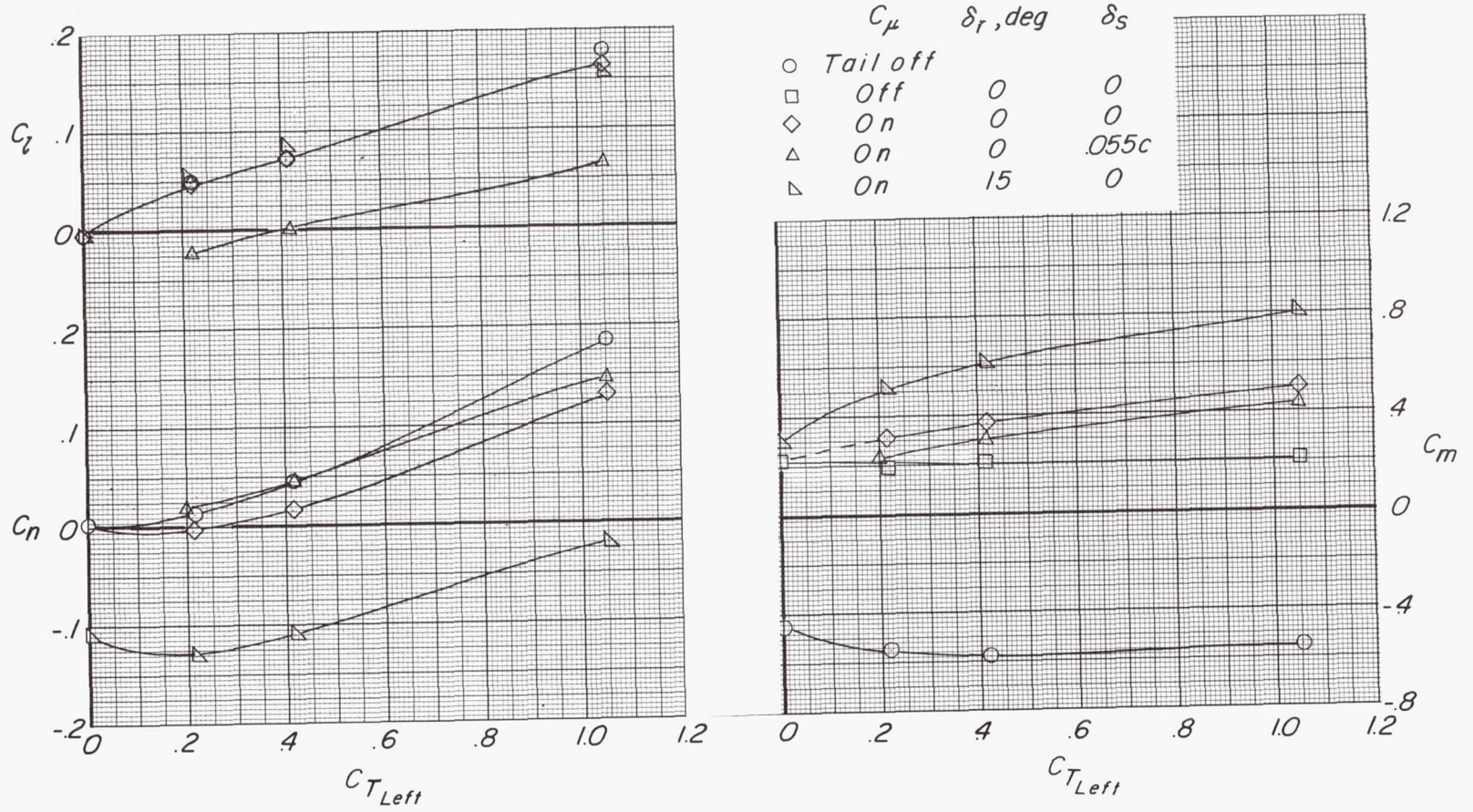

Figure 56.- Effect of left engine thrust coefficient when right engine is out. $\delta_f = 45^0$; $\alpha = 0^0$; $\beta = 0^0$; $i_t = 0^0$.

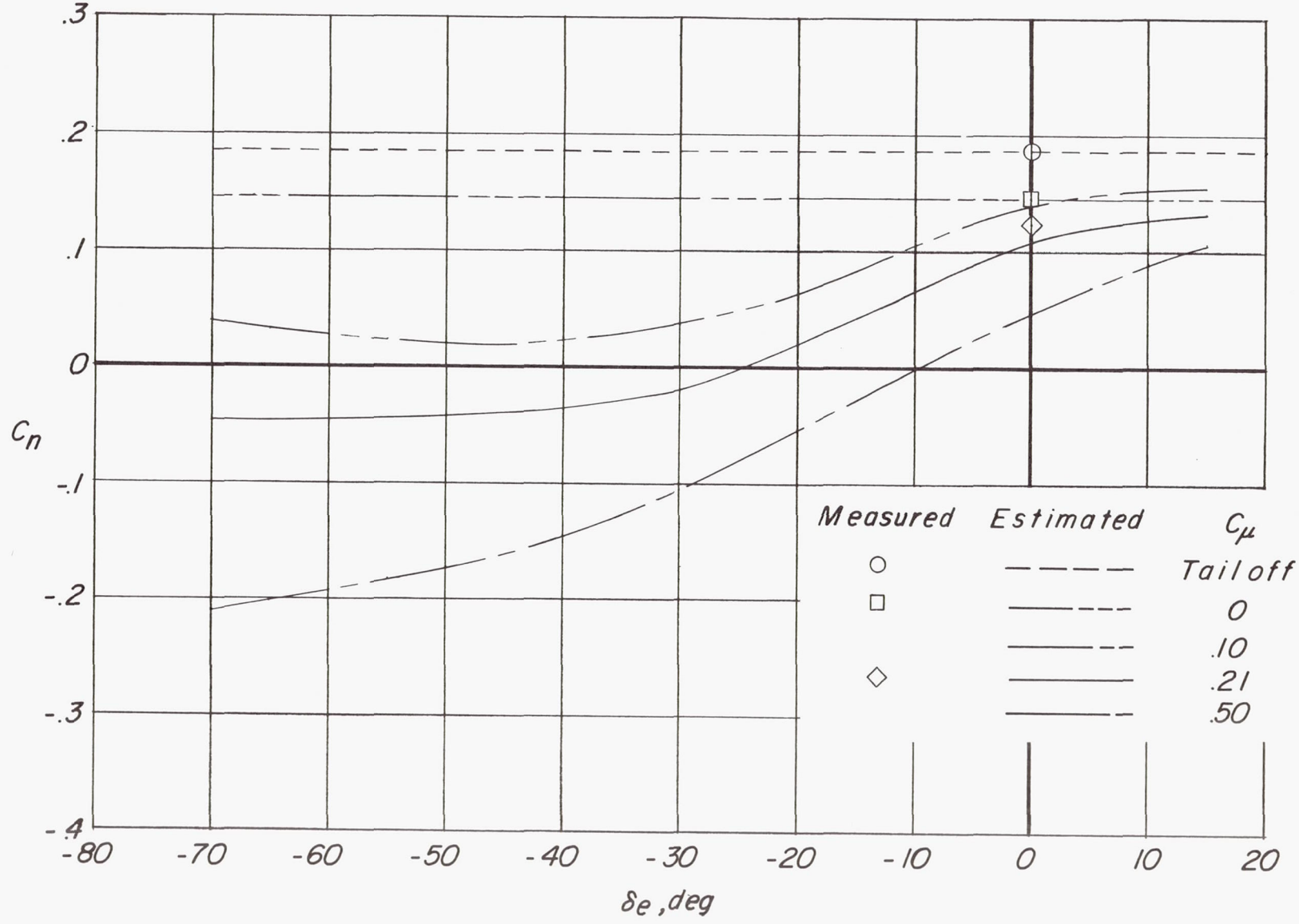

Figure 57.- Effect of elevator deflection and tail momentum coefficient on yawing-moment coefficient when right engine is out. $\delta_f = 45^0$; $C_{T_{Left}} \approx 2.10/2$; $\alpha = 0^0$; $\beta = 0^0$; $i_t = 0^0$.